Polyoxometalate-Supported Bioinspired Catalysts : Synthesis and Catalytic Activity

Weixian Wang

▶ **To cite this version:**

Weixian Wang. Polyoxometalate-Supported Bioinspired Catalysts : Synthesis and Catalytic Activity. Coordination chemistry. Sorbonne Université, 2022. English. NNT : 2022SORUS154 . tel-04162068

HAL Id: tel-04162068

https://theses.hal.science/tel-04162068

Submitted on 14 Jul 2023

HAL is a multi-disciplinary open access archive for the deposit and dissemination of scientific research documents, whether they are published or not. The documents may come from teaching and research institutions in France or abroad, or from public or private research centers.

L'archive ouverte pluridisciplinaire **HAL**, est destinée au dépôt et à la diffusion de documents scientifiques de niveau recherche, publiés ou non, émanant des établissements d'enseignement et de recherche français ou étrangers, des laboratoires publics ou privés.

THÈSE DE DOCTORAT DE SORBONNE UNIVERSITÉ

ÉCOLE DOCTORALE : Chimie Moléculaire de Paris Centre – ED 406

Institut Parisien de Chimie Moléculaire / Équipe Édifices PolyMétalliques

Polyoxometalate-Supported Bioinspired Catalysts: Synthesis and Catalytic Activity

Par M. Weixian WANG

Dirigée par Dr. Sébastien BLANCHARD

Prof. Anna PROUST

Présentée et soutenue publiquement le 13 juillet 2022

Pour obtenir le grade de

Docteur en Chimie de Sorbonne Université

Devant un jury composé de :

Pr. Desage-El Murr Marine	Université de Strabourg	Rapportrice
Pr. De Oliveira Pedro	Université de Paris-Sud	Rapporteur
DR CNRS Salmain Michèle	Sorbonne Université	Examinatrice
Dr. Sébastien BLANCHARD	Sorbonne Université	Directeur de thèse
Pr. Anna Proust	Sorbonne Université	Co-directrice

Abstract

In this thesis, the objective is to synthesize organic-inorganic hybrids based on POMs which work as the source of second-sphere interaction, coupled with bioinspired complexes mimicking active sites of metalloenzymes. First, we will synthesis the hybrid ligands, and then the coordination to metal ions. Once the hybrids are synthesized, we will then study the synergy between the POM and the metal complexes and the resulting catalytic activities.

The work carried out in this thesis led to the development of new hybrids that enrich this family of POMs. Firstly, a new alkyl-iodinated platform derived from $[PW_{11}O_{39}]^{7-}$ was obtained, but its use for functionalization with amino derivatives by nucleophilic substitution was unfortunately not successful. On the other hand, functionalization of polyanions with propargyl-DPA either by “Sonogashira” coupling or by “Click” reaction led to the obtention of two DPA-bearing POM ligands, $TBA_4[PW_{11}O_{39}SnC_6H_4CCCH_2DPA]$ (**K_{Sn}[DPA]**) and $TBA_3[PW_{11}O_{39}O\{SiCH_2CH_2CH_2N_3CHCCH_2DPA\}_2]$ (**K_{Si}[N_3DPA]-3**) . However, in the first case, no synergy between the POM and the grafted copper complex could be demonstrated. In the second case, the presence of triazole functions from the “Click” chemistry made the complexation studies a little bit more complicated and these will have to be further investigated. Finally, the direct approach from trialkoxo derivatives of DPA allowed the synthesis of a hybrid ligand $TBA_6[P_2V_3W_{15}O_{62}(TrisDPA)]$ (**D_{V3DPA}**), and furtherly being complexed with $Cu(OAc)_2$ to obtained **D_{V3DPA}Cu(OAc)**. The latter presents interesting photophysical properties that have been used for photocatalyzed trifluoromethylation reactions

Keywords：polyoxometalate functionalization; organic-inorganic hybrid; bioinspired complex; second-sphere interaction; catalyst; photoreduction

Acknowledgment

I appreciate the jury members, Desage-El Murr Marine, Pedro De Oliveira, and Michèle Salmain, for consenting to read my thesis and attend my defense. Your insightful criticism and recommendations enable me to raise the thesis' level of excellence.

Based on the "CSC/SU program," this thesis was initiated in October 2018 and be completed in July 2022 under the supervision of Dr. Sébastien BLANCHARD and Pr. Anna Proust. I appreciate CSC's financial assistance with my daily expenses.

I want to express my gratitude to Anna and Sebb for giving me the opportunity to study in Paris at the Sorbonne University and complete my PhD. This has been a very memorable learning experience for me, one that has helped me greatly and will be very beneficial for the rest of my life.

It is an honor for me to work with Sebb, who put a lot of effort into my four-year PhD, not only my theoretical and experimentation skills but also my life at Sorbonne. He has extensive expertise and makes a great teacher. We constantly ran across different problems while the project was being explored, but after talking about them, we were able to come up with answers. He can also constantly be upbeat and motivate me to keep going when I'm feeling down.

I would like to thank XRD unit, Lise-Marie Chamoreau, Geoffrey Gontard and Jérémy Forté for the solution of my crystal structures. I also want to thank Cédric Przybylski for the mass analysis. Besides, many thanks to the help from Clair Troufflard, Régina Maruchenko for the NMR analysis. In addition, I am grateful to Dr. Maylis Orio for the support of DFT calculations.

I would like to say many thanks to Dr. Guillaume Izzet, who is quite intelligent and kind, you could have a discussion with him at any time when he is available and shares his experience especially in POM synthesis. He has given a lot of suggestions to our project.

Séverine Renaudineau is one the most crucial women in E-POM team, who has helped me a lot with lab routine over the past four years, particularly with organizing and cleaning. She always treats you kindly and makes me feel welcome.

Many thanks to Dr. Teng Zhang for his kind guidance of my life in Paris and quite intelligent suggestions about my PhD career.

I really enjoy having Youssef Ben M'Barek, the Beard Man, as my lab partner. He has taught me a lot of lab skills that were very useful for me to finish my PhD. His optimism and intelligence make the lab a happy and lively place.

Many thanks to Kelly Trinh and Ludivine K/Bidi. We are always together to talk about our happiness and unhappiness not only about the research but also about our daily life to release our stress and to share our joy which makes me feel at home.

Many thanks to the entire E-POM team for being there for me throughout those four priceless years and for providing me with so many priceless memories. Special thanks go out to Kevin Mall Haidaraly, Dr. Matthieu Balas, and Dr. Richard Villanneau for their generous assistance.

I also want to thank Dr. Etienne Derat and Dr. Mickaël Ménand, who are my committees in “comite de suivi”, for their kind suggestions to my research.

Thanks to my Chinese friends, Haipeng Liu, Fang Liu, Enxu Liu, Zhonghang Wen, Na Li, Buqin Xu, Tingting Chen, Youwei Chen, Yupeng Fu and Jiaxu Zhang for their generous assistance during my PhD.

I am grateful for the support of my roommates Sunbin, Fen, Peipei, Peng Hao, Chao Wu, Liqiong, Kongkong, Yuhui Li, Xiao Liu, Yang Luo, and Zheng Han during the COVID pandemic.

Finally, I'd like to thank my parents, my big sister, and my girlfriend Meiting Li for their unconditional love and support throughout my PhD journey. When I am about to give up, they always encourage me!

Chapter 1

Introduction

Chapter 1 Introduction

Polyoxometalates (POMs) have been proved to have excellent redox properties and could be good candidates to work as electrons and protons reservoirs. The most interesting part to us is that the POMs could be functionalized with organic or organometallic moieties which could improve the physical and chemical properties and then expand the applications of POMs. Several examples have reported that these metal complexes functionalized POMs exist electron communication between the skeletons and the metal centers. The purpose of this thesis is to build hybrid structures of bioinspired metal complexes associated to POMs to mimic the metalloenzymes and to investigate the synergy between them.

In this chapter I will thus present shortly metalloenzymes, POMs and the functionalization of POMs in relation with my doctoral project "*Polyoxometalate-Supported Bioinspired Catalysts: Synthesis and Catalytic Activity".*

1.1 Metalloenzymes

Metalloenzymes are enzyme proteins containing meta ions (metal cofactors), which are directly bound to the protein or to enzyme-bound nonprotein components (prosthetic groups). About one-third of all enzymes known so far are metalloenzymes.[1] Metalloenzymes are a variety of important biocatalysts, involved in chemical transformations, often involving small molecule substrates and reagents such as molecular oxygen, hydrogen, nitrogen, and water.

1.1.1 Modeling metallic site

A large range of metallic cations or metal clusters are observed at the active-site cores in the crystal structures and proved to be the most essential part of metalloenzymes. Vanadium, molybdenum, tungsten, manganese, iron, cobalt, nickel, and copper metal centers have been characterized in some metalloenzymes so far, which can occur in mono-, di-, and multinuclear centers with nitrogen, oxygen, and sulfur atoms of the polypeptide chain as possible ligands.[2] In enzyme catalysis, transition metals are of special relevance due to their redox activity, and/or a high charge density, which allows the polarization of substrates and furtherly to activate them.

The behavior of metal ions in proteins cannot be divorced from their fundamental chemistry, thus investigation of the active-site through synthetic metal complexes is useful.[3,4] Despite inorganic models of metalloenzymes could not duplicate the natural properties, they help to elucidate the molecular structure, the spectroscopic, magnetic and electronic structures, the reactivity, and the chemical mechanisms providing insights that could not be easily attained from protein studies. For example, according to the high-resolution x-ray structure of Hemerythrin, a di-Fe^{II} deoxy structure was first proposed by Wieghardt and co-workers.[5] They indicated that it was possible to generate metastable peroxo di-Fe^{III}, (Fe_2-O_2) species through the reaction of O_2 and Fe^{II} complexes which was helpful for the understanding of the reactivity of the Fe^{II}-containing enzyme.

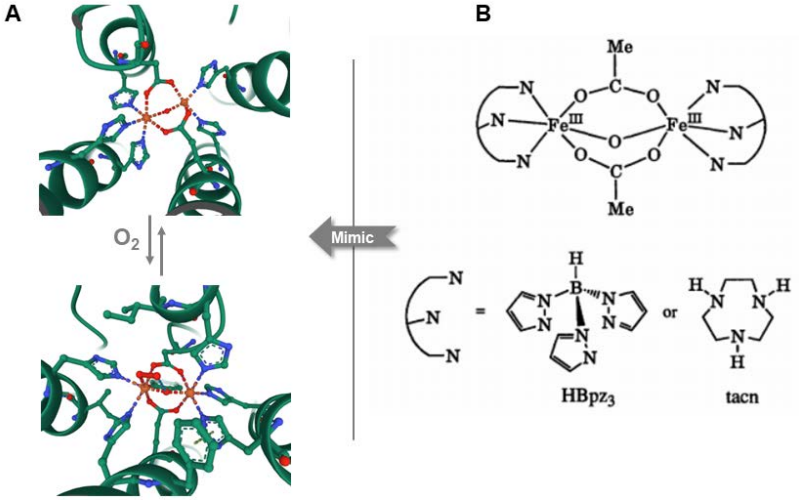

Figure 1-1 A) High-resolution x-ray structure of Deoxyhemerythrin and Oxyhemerythrin [Protein Data Bank ID: 1HMD & 1HMO],[6] B) the corresponding synthesized model complexes.[5,7]

1.1.2 Investigation of the environment of the metallic site

Although the reactions are based on metal centers, the protein matrix regulates the reactivity and the substrate and product delivering through internal pathways, specific ligation and dielectricity. For example, the dehydrogenases from prokaryotic organisms are members of the dimethyl sulfoxide reductase family of mononuclear molybdenum-containing and tungsten-containing metalloenzymes which catalyze the oxidation of the formate anion to CO_2.[8,9] Moura and coworkers,[10] proposed a possible catalytic mechanism according to

calculations with density functional theory (DFT) based on the crystal structure. In this oxidation reaction, there are two electrons being transferred from the substrate to the active site via iron-sulfur cluster, [4Fe-4S], as electron transfer carriers. In the meantime, the His-SeCys residue near the metallic site works as the proton relay which abstracts the proton from substrates. From the calculations of formate oxidation catalytic pathway, we could hypothesize that the high efficiency of the metalloenzyme must benefit from the environment which is so called secondary sphere of the metallic site(s), which works as relays of electrons and protons.

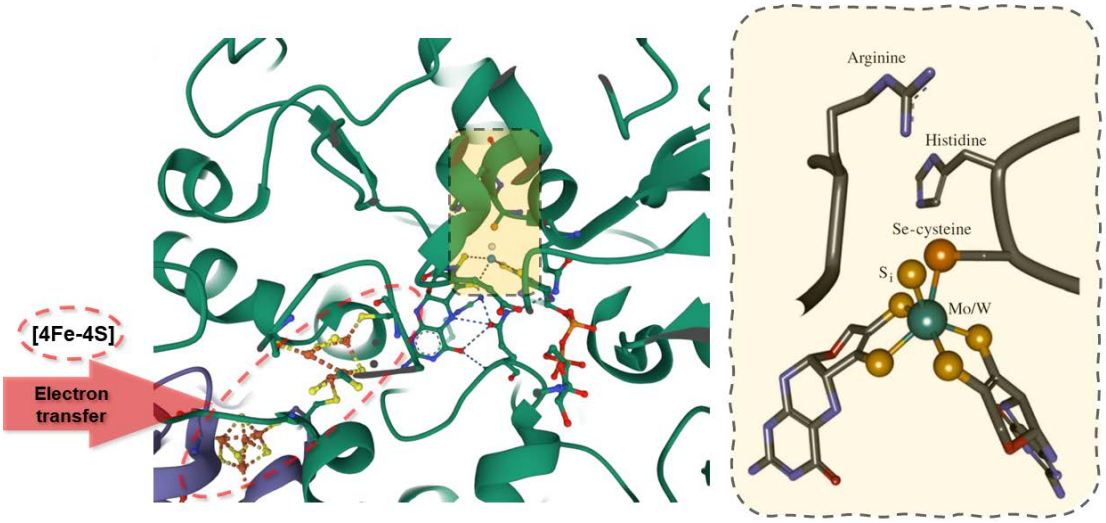

Figure1-2 Zoom of the crystal structure of oxidized molybdenum/tungsten containing formate dehydrogenase (Fdhs) [Protein Data Bank ID 1H0H];[11] coordination around the metal ion.[10]

1.1.3 Mimicking the environment and improving the catalytic property

In the last decades, thanks to development of protein crystallography and computational technologies, the structure and the mechanism of some metalloenzymes have been revealed.[12] Inspired by that, a huge number of synthetic metal complexes have been developed to mimic the metalloenzymes, not only the metallic sites but also the environment of them. Consequently, the bio-inspiration has largely improved the catalytic properties such as selectivity and efficiency and thus expanded the applications of metal complexes. Reversely, simple metal complex models could also help us to better understand and reveal the mechanisms of the catalytic processes of metalloenzymes. Further investigation of the

alteration of the ligand architecture offered the opportunity to tune the chelate rigidity, steric environment, and electronic properties to finally improve the catalytic performance.

Fe-Fe hydrogenases ([Fe-Fe]H_2ase) are one of the most efficient H_2 evolution metalloenzymes in nature with a catalytic activity of 6000-9000 molecules H_2 s^{-1} per site.[13] Inspired by their remarkable activity, many chemists are engaged in creating electro- and photochemical hydrogen production catalytic systems based on the diiron model complexes of the [Fe-Fe]H_2ase active site.[14,15]

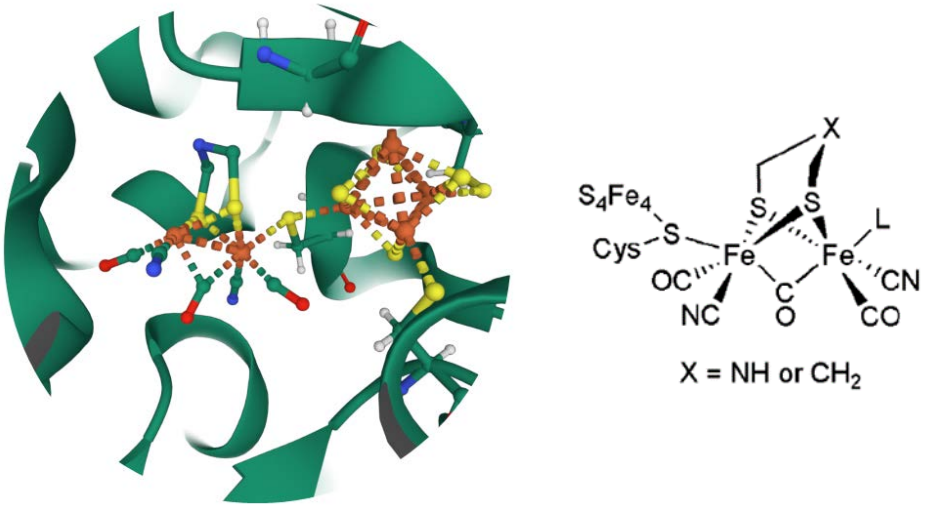

Figure 1-3 the [Fe-Fe]H_2ase and its active site, [Protein Data Bank ID: 6YF4].[13]

In 2008, Sun and coworkers,[16] synthesized a bioinspired [2Fe2S] complex, in which the weak electron donating phosphine ligand, tris(N-pyrrolyl)phosphine ($P(Pyr)_3$) was coordinated to the iron centers, with a small cathodic shift of reduction potential. It was applied as a catalyst combined with photosensitizer $[Ru(bpy)_3]^{2+}$ to photochemically produce hydrogen in the presence of a sacrificial electron donor, ascorbic acid which also worked as proton source. According to the photocatalysis results, the complex with one $P(Pyr)_3$ ligand has better photostability and photoactivity compared to the all-CO diiron complex and the complex with two $P(Pyr)_3$ ligands. In this process, the photosensitizer $[Ru(bpy)_3]^{2+}$ was excited by light and then abstracted an electron from ascorbic acid to produce $[Ru(bpy)_3]^{+}$ which was thermodynamically able to transfer an electron to the [2Fe2S] complexes. The reduced and protonated Fe^0Fe^I species then transferred the electrons to protons to release H_2. Although

the turnover number was low at this stage, the principle of mimicking not only the metallic site but also the electron transfer ability of the [Fe-Fe]H_2ase was validated.

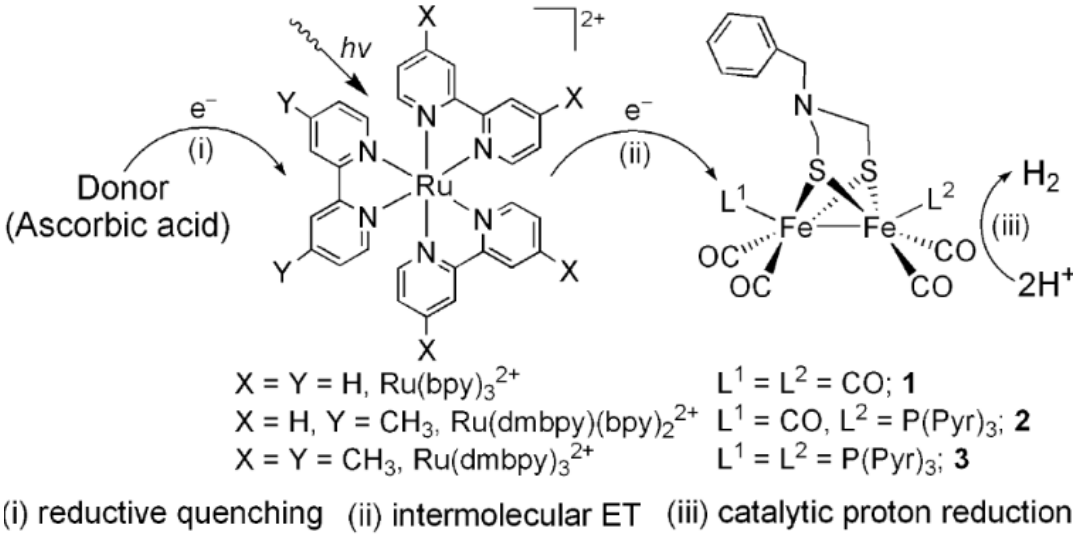

Figure 1-4 The Homogeneous Molecular Three-Component System for Photochemical H_2 Generation Catalyzed by [Fe-Fe]H_2ase Active Site Mimics.[16]

The copper-containing nitrite reductases (CuNIR) are among the metalloenzymes found in nature to perform the reduction of nitrite (NO_2^-) to nitric oxide (NO), and the reaction that they mediate is summarized in eq (1)

$$Cu\ (I) + NO_2^- + 2H^+ \rightarrow Cu\ (II) + NO + H_2O \quad (1)$$

Mimicking the relatively simple active site structure of CuNIR as indicated by crystallographic studies, plenty of copper complexes based on tripodal N-donor ligands have been synthesized. Recently, Symes and coworkers synthesized two copper complexes with two tripodal N-donor ligands, one bearing an ester and the other one containing an acetate.[17] Both of them were applied to the electroreduction of NO_2^-. From the electrocatalysis data, the nitrite reduction activity of the acetate containing complex was 2 times higher than the ester containing complex. According to the crystal structures of the NO_2^- and NO bound forms of CuNIR enzymes, Suzuki[18] and Hasnain[19] proposed that the H-bonding in the active site was essential to the catalytic reactions. In the previous example, once the NO_2^- coordinated to the Cu center, the carboxylic group di-coordinated to the Cu would be protonated in the present of acid to form carboxylic acid subsequently working as a proton-relay forming the H-bond with

the coordinated nitrite. This process is so called proton-coupled electron transfer which could largely increase the catalytic activity.

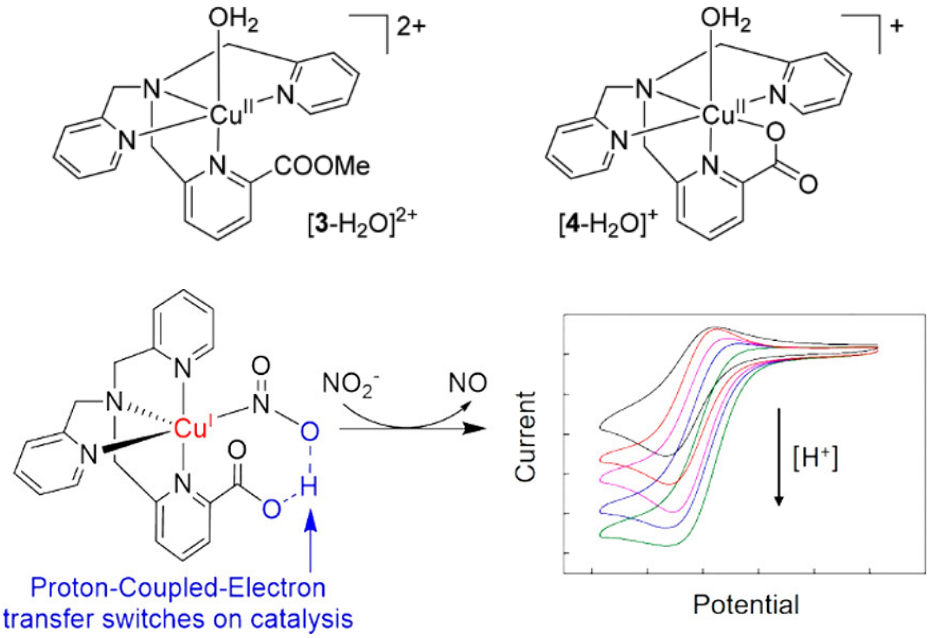

Figure 1-5 The two bioinspired tripodal N-donor Cu-complexes and the proposal Proton-Coupled-Electron transfer mechanism for the electrocatalytic reduction process of nitrite.[17]

1.2 Introduction of polyoxometalates

1.2.1 General introduction to polyoxometalates

Composition

Polyoxometalates (POMs) represent an important group of metal-oxo nanoclusters, typically constituted of early transition metals in high oxidation states (mainly V, Mo and W, less frequently Nb and Ta) and centered with p-block elements (such as B, Al, Si, Ge, P, S, As, Te, I). Commonly, POMs are formed in condensation processes of simple anions in solution (typically water) under various pH and temperature conditions. Owing to their all-inorganic nature and robust shell topologies, many POMs exhibit remarkable solution, redox and thermal stability, making them interesting to many actual and potential applications in catalysis,[20] molecular magnetism,[21] and life science.[22]

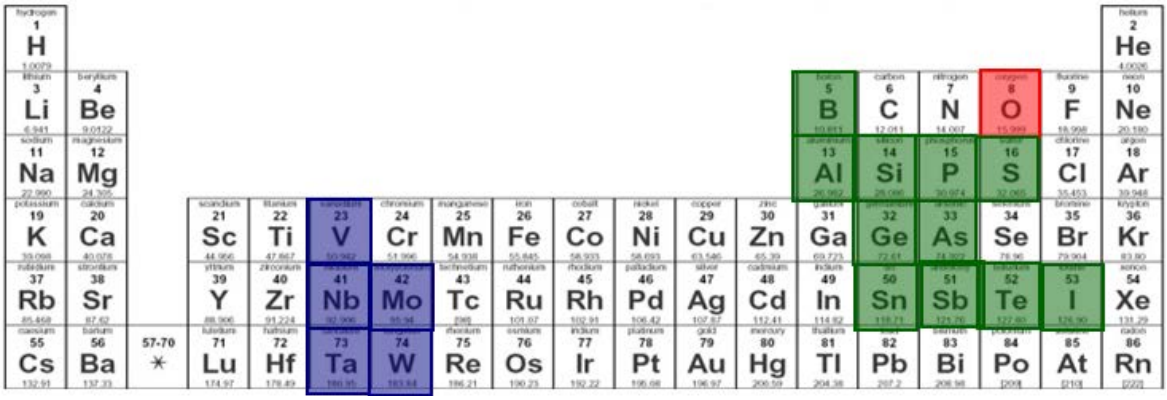

Figure 1-6 Polyoxoanion-forming elements.

Despite various types of POMs structure have been reported, the mostly investigated types are the Lindqvist $[M_6O_{19}]^{n-}$, Anderson-Evans $[XM_6O_{24}]^{n-}$, Keggin $[XM_{12}O_{40}]^{n-}$, and Well-Dawson $[X_2M_{18}O_{62}]^{n-}$ ones (Figure 1-6). In these POM structures, the metal atoms are in their highest oxidation states (d^0), and it is therefore clear that these complexes are in general capable of acting as oxidizing agents. It was very early noted that certain polyanions, especially the 12-molybdo Keggin-type anions were readily reduced to blue species.[23] The intensely colored reduced anions are due to intensity-enhanced d-d transitions and intervalence charge transfers.

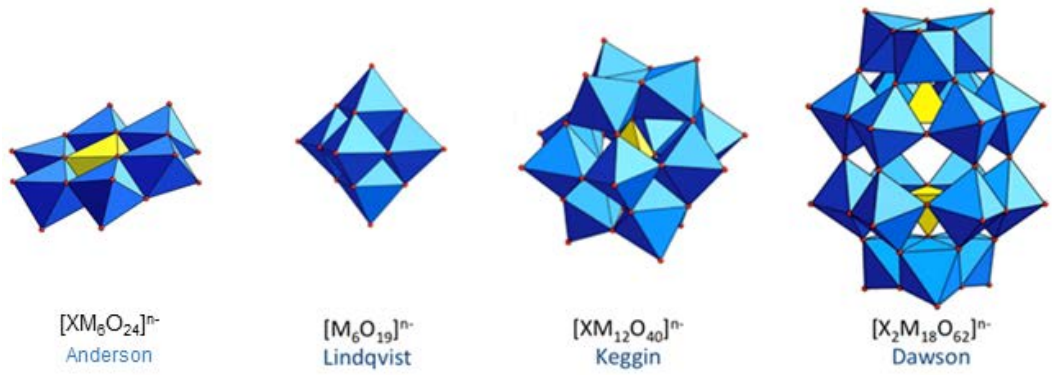

Figure 1-7 The most common types of Polyoxometalates.

Electrochemical properties

It has been proved that polyoxometalates have quite good redox properties by plenty of experiments. One of the most typical one is, in 2004, Alan M. Bond and co-workers[24] have studied the voltametric reduction of $[\alpha\text{-}S_2W_{18}O_{62}]^{4-}$, and they detected six well-defined reversible one-electron-transfer steps which indicated the Dawson skeleton could get and

release 6 electrons as the potential goes negative and revers. In the work of Himeno,[25] when they investigated the voltametric properties of the Keggin-type $[PW_{12}O_{40}]^{3-}$, they found that in the present of protons, the nice four one-electron reduction waves transformed into two two-electrons reversible reduction waves at higher potentials, protonation of the POM marking it much easier to get reduced. The investigations above demonstrate that the POM could be electrons and protons reservoir.

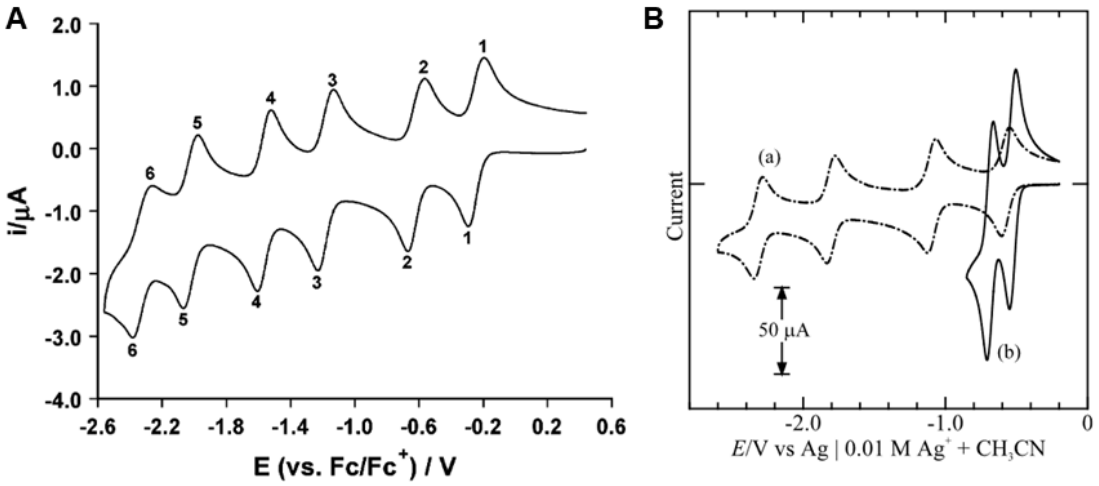

Figure 1-8 A) Cyclic voltammograms (v = 200 mV s^{-1}) for[25] $[\alpha\text{-}S_2W_{18}O_{62}]^{4-}$ (0.50 mM) in CH_3CN (0.1 M nBu_4NPF_6) at a GC macrodisc electrode (d = 1 mm);[24] B) Cyclic voltammograms for 0.50 mM $[PW_{12}O_{40}]^{3-}$ in CH_3CN containing 0.1 M n-Bu_4NClO_4. $[CF_3SO_3H]$/mM, (a) 0; (b) 5.0.[25]

Electrocatalytic activity

Multi-electron redox-processes of POMs make them ideal candidates for the development of multistep redox systems. These properties are quite interesting both in photocatalysis and electrocatalysis. In the work of Ronny Neumann and coworkers,[26] the phosphovanadomolybdate POM, $H_5PV_2Mo_{10}O_{40}$, was applied as a catalyst to oxidize methylarenes to benzaldehyde derivatives in aqueous sulfuric acid. In aqueous solution, H_2SO_4 reacts with $H_5PV^{V}_2Mo_{10}O_{40}$ to yield a protonated, cationic $[H_6PV^{V}_2Mo_{10}O_{40}]^+$ species which could get an electron from the substrate to form $[H_6PV^{IV}V^{V}Mo_{10}O_{40}]^{\bullet}$ and $PhCH_3^{\bullet+}$ respectively. Furtherly the formed $[H_6PV^{IV}V^{V}Mo_{10}O_{40}]^{\bullet}$ would abstract a proton from $PhCH_3^{\bullet+}$ resulting in $[H_7PV^{IV}V^{V}Mo_{10}O_{40}]^{\bullet+}$ and $PhCH_2^{\bullet}$. The $PhCH_2^{\bullet}$ radical couples to H_2O to form $PhCH_2OH$ with $H^{\bullet}$ transferred to the POM resulting in $[H_8PV^{IV}_2Mo_{10}O_{40}]^+$. $PhCH_2OH$ will be

further oxidized following almost the same process with another equivalent of $[H_6PV^{V}_2Mo_{10}O_{40}]^+$ to PhCHO. Finally, the 2-equivalent reduced $[H_8PV^{IV}_2Mo_{10}O_{40}]^+$ will release 2 equivalent H_2 with electrolysis. These multi-electrons/protons catalytic process clearly demonstrates the ability of POMs to act as electrons and protons reservoirs.

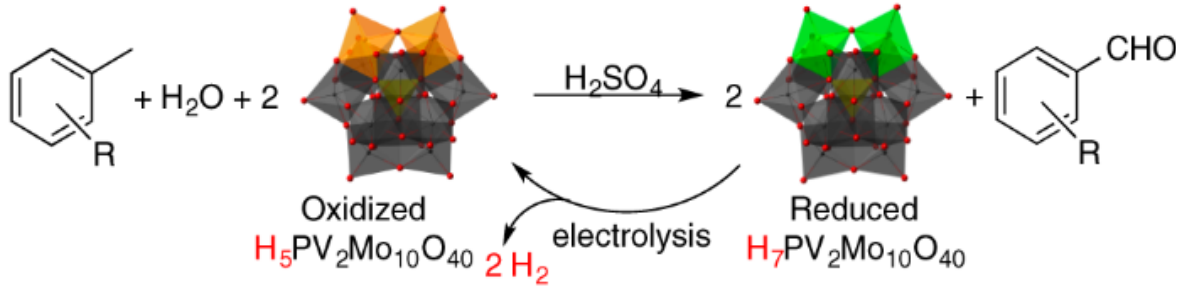

Figure 1-9 The oxidation of methylarenes to benzaldehyde derivatives in aqueous sulfuric acid with $H_5PV_2Mo_{10}O_{40}$ cycling with electrolysis.[26]

Photocatalytic activity

The photoactivity of POMs has been known for several decades. Indeed, in solution, due to the presence of LMCT absorption bands, strong absorption with a large molecular absorption coefficient ($\varepsilon > 1 \times 10^4$ M^{-1} L^{-1}) is often observed.[27] It is particularly well known that many molybdate-based salts containing organoammonium as counter ions easily undergo photoredox reactions in the solid state, resulting in the formation of intense blue-colored reduced molybdates, which is so-called heteropoly blues.[28]

Thanks to their terminal and bridged oxygens, especially in the lacunary forms, POMs could be applied as ligands to make complexes of transition metal cations. Making substituted POMs is one of the most investigated methodologies to improve the properties and expand the applications of POMs. With the transition metals, interactions between some small molecules such as CO_2, and POMs will be more favored through coordination. This concept was employed by Neumann and coworkers.[29] They synthesized a Ru-substituted Keggin anion, $[Ru^{III}(H_2O)SiW_{11}O_{39}]^{5-}$ which was applied as a homogeneous catalyst for the photochemical reduction of CO_2 by C=O bond activation in a toluene solution with triethyl amine as the sacrificial electron donor.

In order to expand the wavelength range for light-harvesting, hybrids base on POMs were developed, such as those associated with ruthenium-based photosensitizers which are quite good candidates for water oxidation. In Hill's work,[30] they applied three components containing $[Co_4(H_2O)_2(PW_9O_{34})_2]^{10-}$ (Co-POM), $[Ru(bpy)_3]^{2+}$ and peroxodisulphate ($S_2O_8^{2-}$) as a catalytic system for water oxidation. In this photocatalytic process, light induced oxidation of $[Ru(bpy)_3]^{2+}$ in the presence of $S_2O_8^{2-}$ to form $[Ru(bpy)_3]^{3+}$, in the meantime, water was oxidized by the Co-POM and electrons transferred to the oxidized $[Ru(bpy)_3]^{3+}$ to reform the $[Ru(bpy)_3]^{2+}$ to finish the cycle.

1.2.2 organic-inorganic covalent hybrid POMs

Organic-inorganic covalent hybrid POMs are an extremely important branch in POMs chemistry which has largely expanded the actual or protentional applications in catalysis, bioinorganic chemistry and materials science.

In the past decades, since the structure of the first organic hybrid POM, $[(CH_3)_2AsMo_4O_{13}H]^{2-}$, figured out through X-ray diffraction by Pope and coworkers in 1975,[31] organic–inorganic POM-based hybrid platforms through covalently grafting have been developed a lot. The "lacunary" POMs mentioned before are synthesized through pH-controlled treatment of the complete polyoxo species. They are formally lacking one or several MO_6 octahedral units, giving rise to mono- or poly-lacunary POMs. The lacunary POMs are the mostly used precursors to prepare organic-inorganic POM hybrids. In terms of the bridge units between the POMs core and the organic moieties, the most investigated could be defined as organosilyl, organotin, organophosphorus and tris alkoxy derivatives. Here we would like to introduce the first example of each type of hybrid:

1. The first organosilyl functionalized polyoxometalates was reported by Knoth,[32] who obtained anions of the composition $[SiW_{11}O_{39}\{O(SiR)_2\}]^{4-}$, (-R = -Et, -Ph, $-C_3H_5$, $-(CH_2)_3$ NC), by reacting $RSiCl_3$ with $[SiW_{11}O_{39}]^{8-}$ in unbuffered solution. In 1991, three similar organosilyl groups were also attached to the trivacant Keggin α-A-$[PW_9O_{34}]^{9-}$ to give rise to α-A-$[PW_9O_{34}(SiR_2)_3]^{3-}$under phase-transfer conditions with R_2SiCl_2.

2. Organotin derivatives were first synthesized by Knoth[32] with several Keggin type POMs such as $[SiW_{11}O_{39}]^{8-}$: functionalization with R_2SnCl_3 gives $[SiW_{11}O_{39}(SnR)]^{4-}$ (R= $-CH_3$, $-C_6H_5$, $-C_3H_5$, $-CH_2CH_2COOH$)
3. Organophosphonoyl derivatives were synthesized by Hill and co-workers[33] by reaction between the monovacant species α-$[SiW_{11}O_{39}]^{8-}$ or α-$[PW_{11}O_{34}]^{7-}$ and $PhPOCl_2$, resulting in the formation of the hybrids α-$[(PhPO)_2SiW_{11}O_{39}]^{4-}$ and α-$[(PhPO)_2PW_{11}O_{39}]^{3-}$ respectively.
4. Another very frequent bridge is tris alkoxy which could be covalently grafted onto Anderson, and also trisvanadate substituted Dawson type POMs. In 1993, Hill and coworkers,[34] described the reaction between tris(hydroxyethyl) and $[V_3P_2W_{15}O_{59}]^{9-}$ to form the tester bonds resulting in the $[RC(CH_2O)_3HV_3P_2W_{15}O_{59}]^{5-}$ (R= $-CH_3$, $-NO_2$ and $-CH_2OH$) derivatives. In 2002, Pierre Gouzerh and coworkers,[35] successfully prepared the Anderson $[MMo_6O_{18}\{(OCH_2)_3CR\}_2]^{3-}$ ($M=Fe^{III}$, Mn^{III}, Ni^{II}, Zn^{II}, R=CH_3, NO_2, CH_2OH, functionalized on both sides.

Inspired by these initial functionalization methodologies, a great number of organic-inorganic covalently connected hybrids based on POMs were developed in the past decades, with various functional groups depending on the sought applications.

To achieve that, two different strategies are developed according to the functional groups: direct-functionalization and post-functionalization. In the former case, the functional groups or the organometal moieties are covalently bonded with the bridge units, which are then grafted onto the POMs core directly. For the post-functionalized one, special functional groups modified bridge units are first introduced onto the POMs core to form POM platforms displaying reactive groups or ligand-like sites which can be further coupled with other organic molecules or coordinated to metal cations or metal-containing clusters. The direct organic functionalization of POMs is normally performed under acidic conditions or high temperature, which could be too harsh for the aimed functional groups especially to the organometal moieties. If we would like to functionalize with some fragile groups, it is better to use post-functionalization methods. The usual mild conditions of the post-functionalization would not

only protect the aimed functional groups but also be much easier for the following purification process due to the less degradation.

1.2.3 Methodologies of Post-functionalization:

For post-functionalization of POM hybrids, the first step is to synthesize proper platforms. In the last decades, plenty of precursors with special groups have been synthesized which could be involved in subsequent reactions such as condensation reaction, “Sonogashira” coupling, “click” reaction and the more recently developed metal free nucleophilic substitution.

Condensation reaction

Condensation reaction is one of the most common methods to functionalize POMs with organic moieties. Depending on the terminal groups, this kind of reaction could be defined as amidation,[36–38] thioether formation,[39] sulfonamidation,[40,41] and imine bond formation.[42] These kind of reactions have been applied to modify functionalized POMs with peptides or proteins[43] and oligonucleotides.[44] In 2003, Bareyt and coworkers,[45] synthesized two mono-organotin functionalized Dawson POMs, α_1- and α_2-$[P_2W_{17}O_{61}\{Sn(CH_2)_2COOH\}]^{7-}$ with a terminal acetic acid group which could furtherly react with other organic moieties bearing amine or alcohol group through amidation or esterification in mild conditions.

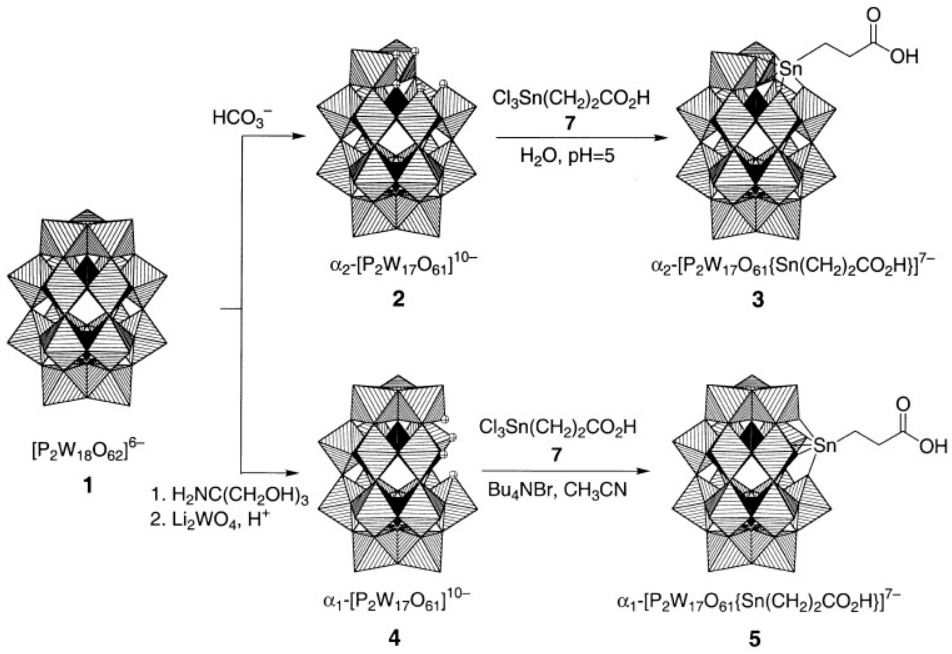

Figure 1-10 Preparation of terminal acetatic acid group functionalized Well-Dawson platforms: α_1- and α_2-$[P_2W_{17}O_{61}\{Sn(CH_2)_2COOH\}]^{7-}$.[45]

The terminal groups of the organic moieties grafted onto the POMs could also be amine, hydroxyl or sulfhydryl which could also react with other groups such as carboxylic acid through condensation reactions. In 2014, Song and coworkers,[38] expanded the $[(SiW_{11}O_{39})O\{Si(CH_2)_3\text{-}NH_2\}_2]^{4-}$ POM by hybridization with an azobenzene derivative, thus opening a pathway to fabricate thermotropic liquid-crystalline nanomaterials.

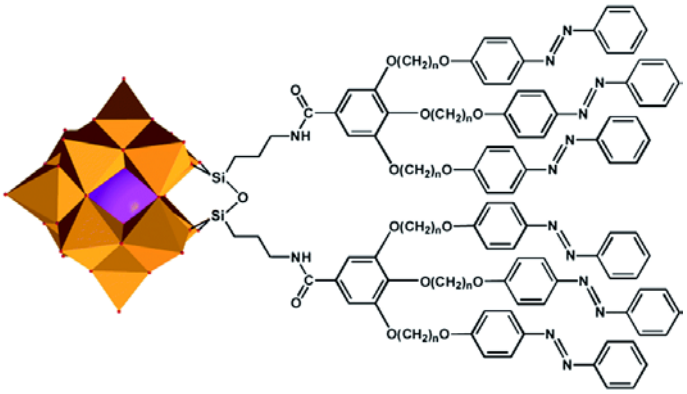

Figure 1-11 A schematic presentation of liquid-crystalline polyoxometalate hybrids with WO_6 indicated by gold octahedron and SiO_4 indicated by pink sphere.[38]

The sulfonamidation of an alternative NH_2-terminated hybrid $[\gamma\text{-}SiW_{10}O_{36}\{O(Si(CH_2)_3\text{-}NH_2)_2\}]^{4-}$ POM was demonstrated by Bonchio and co-workers[40] by reaction with dansyl chloride in the presence of triethylamine. The resulting hybrid could work as a selective fluorescence sensor for Cu^{2+} and Pb^{2+} ions in quenching and enhancing mode respectively.

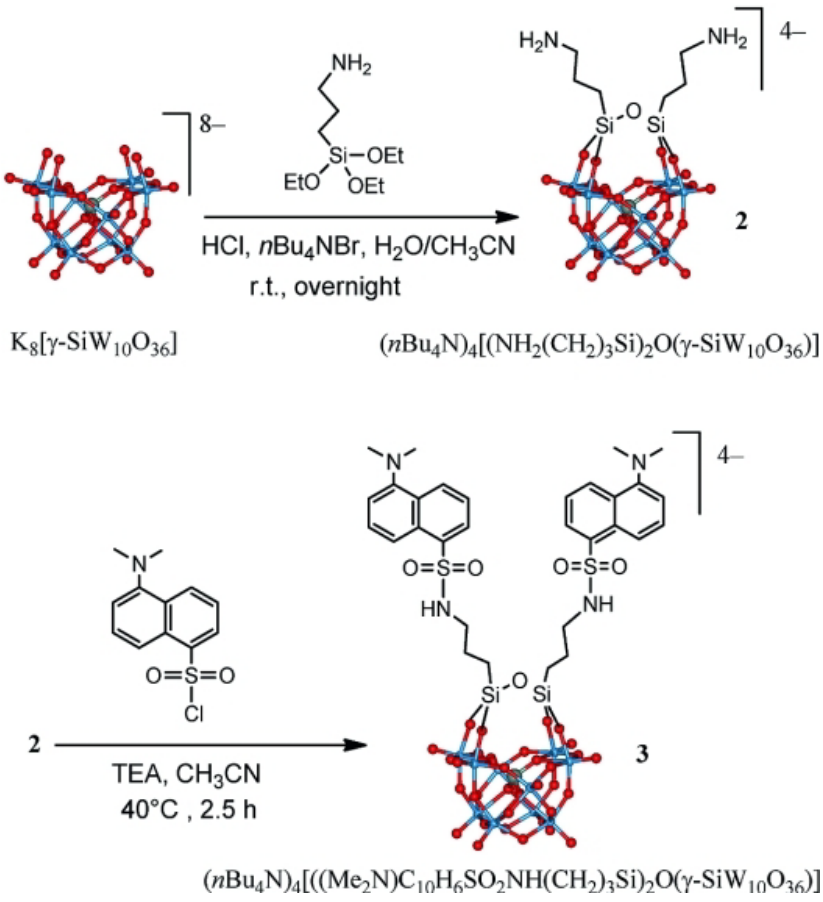

Figure 1-12 The synthesis route of NH_2-terminated hybrid [γ-$SiW_{10}O_{36}${$O(Si(CH_2)_3$-$NH_2)_2$}]$^{4-}$ and its psot-sulfonamidation.[40]

"Sonogashira" coupling

The "Sonogashira" reaction is a cross-coupling reaction used in organic synthesis to form carbon–carbon bonds. It employs a palladium catalyst as well as copper co-catalyst to form a carbon–carbon bond between a terminal alkyne and an aryl or vinyl halide.[46] In 2001, Peng and coworkers,[47] built an hybrid organoimido functionalized POM containing phenyliodo group which was applied to perform the "Sonogashira" coupling with aromatic alkynes. This demonstrated that functionalized organoimido derivatives of POMs could be furtherly post-functionalized with organic moieties for the first time.

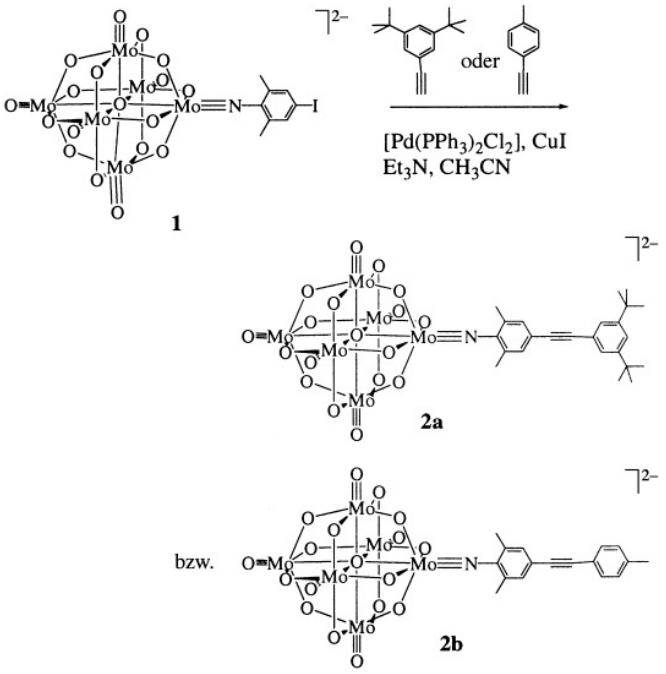

Figure 1-13 Pd-catalyzed coupling of the iodo-functionalized hexamolybdate anion with alkynes.[47]

As we mentioned before, organo-silyl, organo-phosphonyl and organotin derivatives of POMs, allow to address the functionalization of electronically more interesting Keggin or Dawson series and to provide a very simple path to multi-functionalization. In 2009, Izzet, Proust and co-workers,[48] built a di-functionalized POM platform by the reaction between the mono lacunary Keggin type $[PW_{11}O_{39}]^{7-}$ and 1-iodo-4-(triethoxysilyl)benzene in acidic conditions. The resulting di-iodophenyl functionalized hybrid could perform "sonogashira" reaction with alkynes, using $Pd(PPh_3)_2Cl_2$ and CuI as co-catalysts in the presence of triethylamine. And they extended the reaction to a terminal alkyne bearing a terpyridine which was an excellent remote ligand to coordinate transition metal cations.

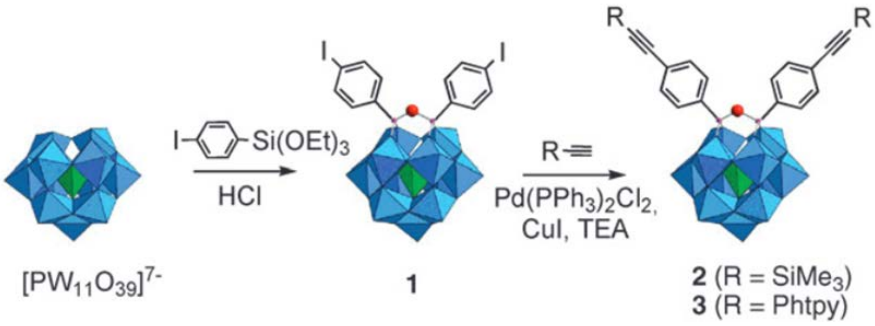

Figure 1-14 Synthetic route to the organo-silyl POM-based hybrids from $[PW_{11}O_{39}]^{7-}$.[48]

"Click" reaction

Copper(I)-catalyzed azide-alkyne cycloaddition (CuAAC) has become a commonly employed method for the synthesis of complex molecular architectures under challenging conditions. The huge success of this reaction in organic chemistry relies on its selective nature, fast reaction kinetics and high yields, the absence of side-reactions, widely applicable substrates and reaction conditions and the formation of a stable 1,2,3-triazole bond which is insensitive towards hydrolysis or redox reactions.[49] In 2007, Lacôte and coworkers,[50] for the first time applied "Click" reaction in the investigation of organic-inorganic hybrid POMs in mixture of acetonitrile and water solvent with $CuSO_4$/Na ascorbate as catalyst. The precursors they used were azido/alkynyl organotin functionalized POMs which were water compatible. In 2009, Odobel and co-workers,[51] described a family of Dawson-type POMs di-functionalized with organo-silyl or organo-phosphonyl azido moieties which were engaged in "Click" reactions in dry DMF with $CuSO_4$/ascorbic acid as catalyst to attach organic chromophores with >80% yield.

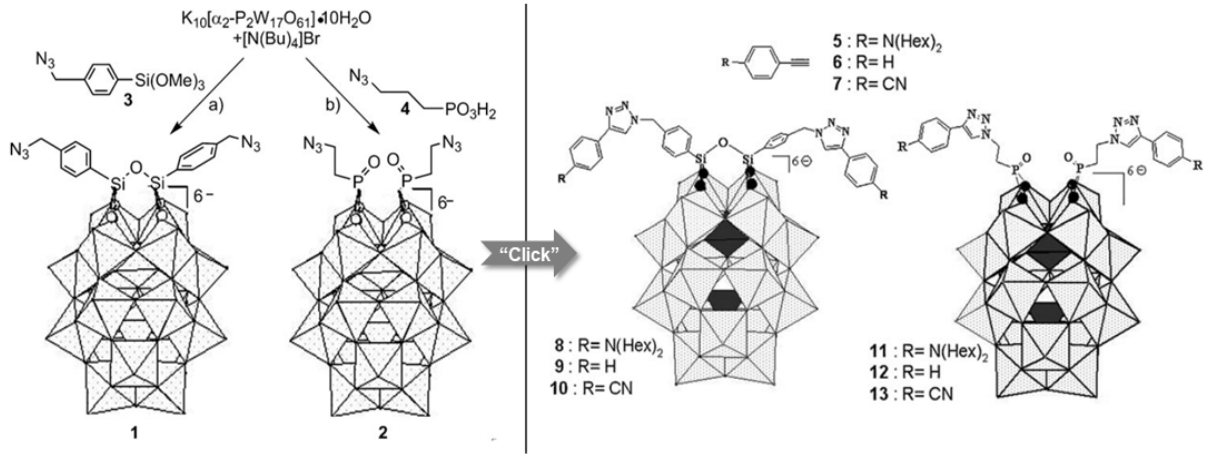

Figure 1-15 The route for the preparation of the di-azido functionalized Well-Dawson platforms and the furtherly "Click" reaction with alkyne terminal organic moieties.[51]

In 2015, Parac-Vogt and coworkers,[52] synthesized a new azido functionalized Anderson polyoxometalate which was subsequently used as building block for further post-functionalization through CuAAC with $Cu(CH_3CN)_4PF_6$/diisopropylethylamine (DIPEA) or $CuSO_4$/Na ascorbate as catalyst in acetonitrile or DMF. After optimization of the temperature and the amount of catalyst, this resulted in an efficient, fast and convenient POM coupling

method. In the same year, Cronin and coworkers[53] synthesized several terminal alkyne and azido groups functionalized Mn Anderson POMs to be used as building blocks. Then the formation of hybrid oligomers and polymers was controlled by CuAAC coupling reaction, playing with the coupling conditions such as the ratio of the symmetric and asymmetric azido and alkyne functionalized building blocks.

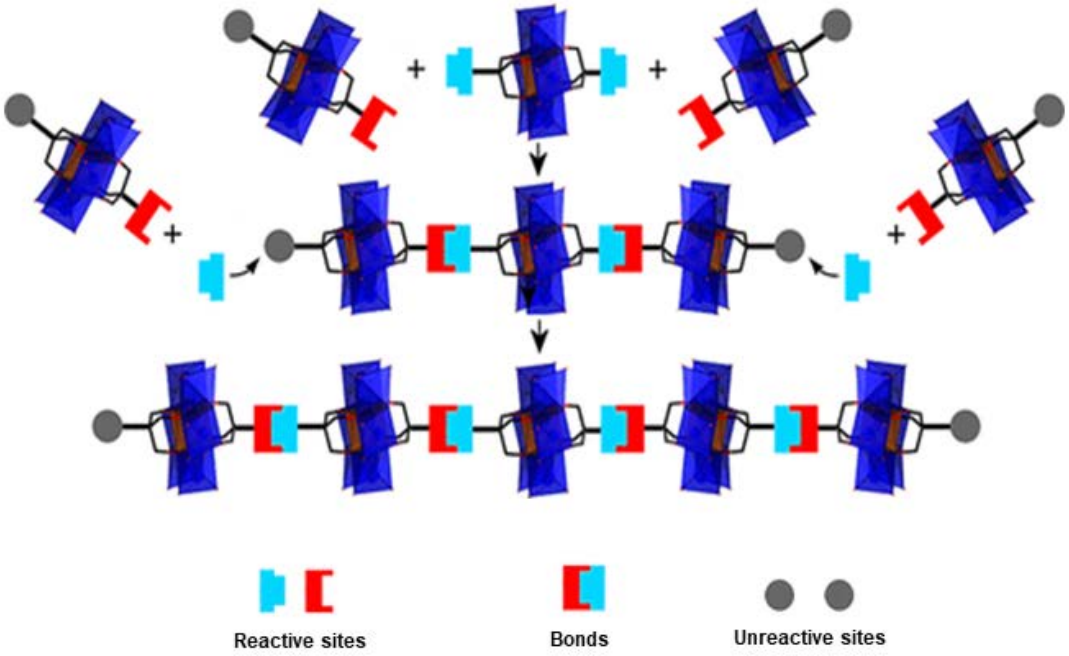

Figure 1-16 Combinations possible with AA couplings (between two identical functional groups) and AB couplings (between two different functional groups) shown for Anderson POMs.[53]

Nucleophilic substitution

The nucleophilic substitution is one of the oldest and most simple reactions of organic chemistry, but it is quite fresh in organic-inorganic POMs synthesis. In 2016, Wei and coworkers[54] performed nucleophilic substitution on the chloropropyl-imido derivatives of the hexamolybdate with sodium iodide and silver nitrate. It was the first time that nucleophilic substitution was applied to in the post-functionalization of POMs, but they could only be achieved with some simple and unfunctional groups.

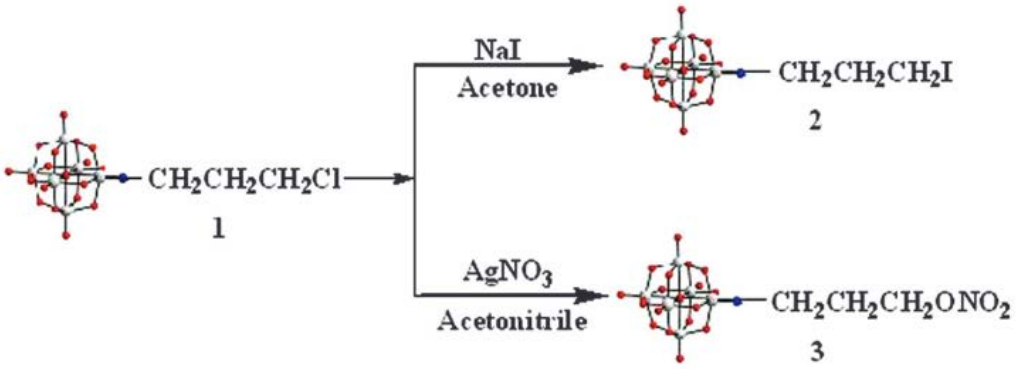

Figure 1-17 Nucleophilic substitution of chloropropyl functionalized hexamolydate.[54]

In the following year, Parac-Vogt and coworkers,[55] expanded the methodology on a chloro acetamide-functionalized Anderson POM which was substituted with amines and thiols in the present of sodium carbonate as a base. The same year, they extended the reaction to the trivanadate cap substituted Dawson type POM:[56] nucleophilic substitution of an azido group to the chloro group opened the way to subsequent "Click" reaction for post-functionalization with other organic moieties.

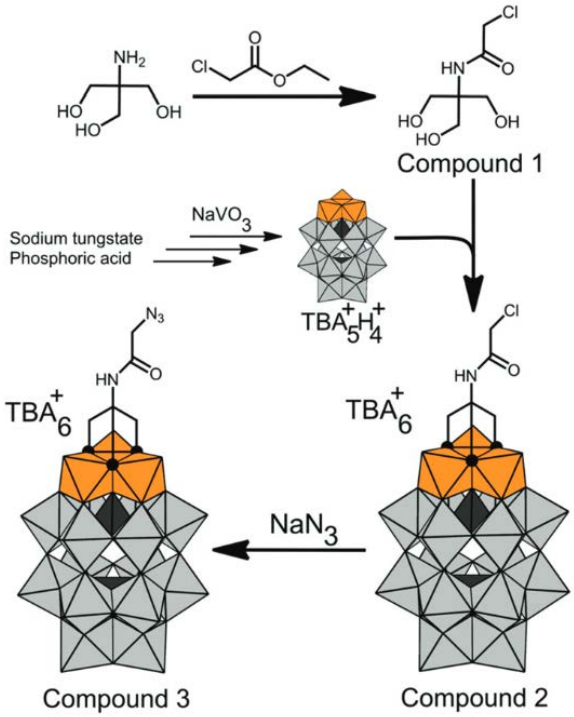

Figure 1-18 The synthesis route to terminal azido functionalized trivanadate substituted Dawson POM, following a with nucleophilic substitution reaction.[55]

1.2.4 Applications of POM based organic-inorganic hybrids

The emerging class of post-functionalized hybrid-POMs permit the coupling of multi-electron redox responsive POMs with different organic and metal cation functionalities, thereby expanding the key physicochemical properties that are relevant for applications such as in catalysis and materials science.

Supramolecular self-assembly

Peng and coworkers[57] successfully introduced one or two iodophenylimido ligands onto the hexamolybdate core prior to their post-functionalization with alkynes modified bis(terpyridine) through “Sonogashira” coupling. The resulting POM ligands were applied to the coordination of Fe^{2+} and formation of transition-metal complexes of POM hybrids. The mono-functionalized one resulted in a dimer, while the di-functionalized one resulted in the formation of oligomers/polymers. This method could allow the rational design of catalysts or building blocks to prepare supramolecular structures. In 2016, Izzet and coworkers, reported a bis(terpyridine) post functionalized Dawson-type POMs building-block. Fe^{2+} coordination driven could self-assembly results in the formation of discrete supramolecular triangles in a dissociating solvent like DMSO and dense monodisperse aggregates in less dissociating solvents like acetonitrile. The density of the self-assembly is controlled by adjusting the DMSO to acetonitrile ratio.[58]

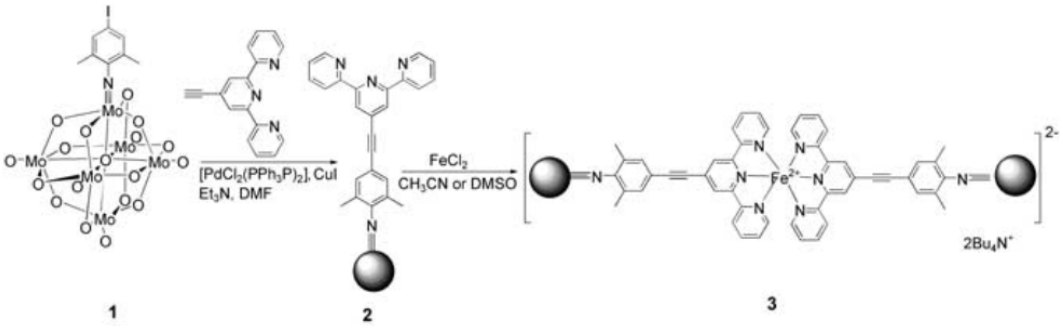

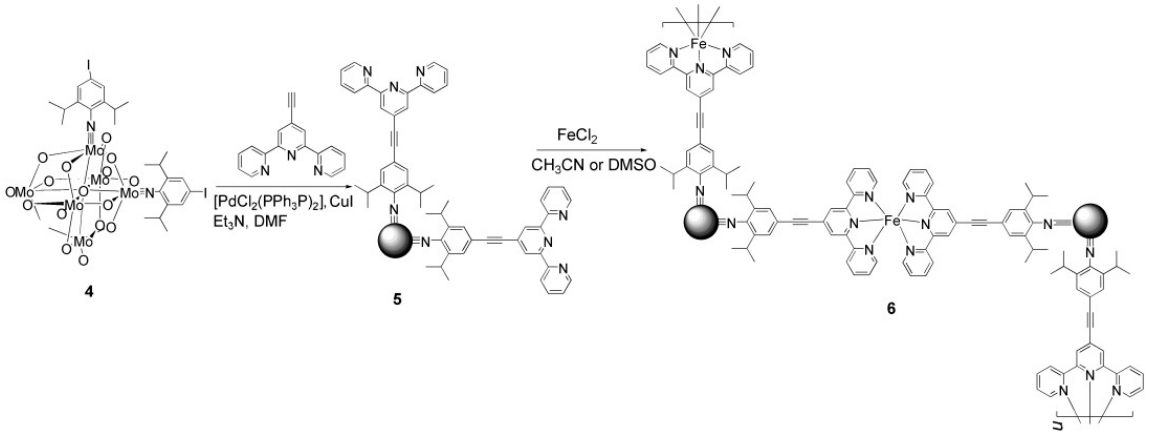

Figure 1-19 Synthesis of transition-metal complexes of POM hybrid-based ligands: dimer and polymer. [57]

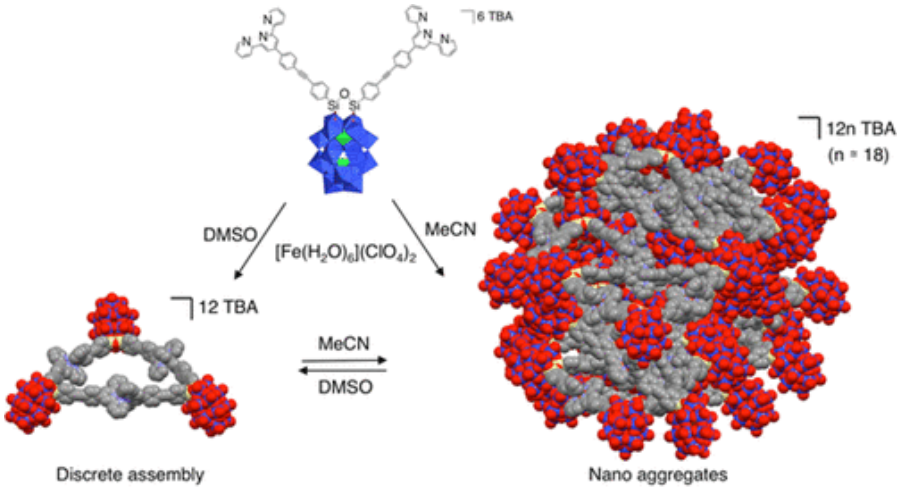

Figure1-20 Representation of the formation of the nanosized aggregates by hierarchical self-assembly of $\boldsymbol{D_{si}}$***[tpy]*** *upon complexation with* Fe^{2+}*.* [58]

Organometallic catalysts tethered to POMs

Neumann and coworkers,[42] grafted triethoxypropylamine onto the lacunary POMs to form di-amines functionalized POM precursors, which were post-functionalized with salicylaldehyde to form salen-modified POMs. Coordination to the metal cations yielded metallosalen POM complexes. These hybrids are generally described as being more active and/or selective than the related organometallic precursor complexes. The main role of the POM is to tune the steric and electronic properties of the catalyst. In the meantime, the charge transfer between the metallo-salen donor and the POM acceptor has been observed, with stabilization of unusual oxidation state of the coordinated metal M and/or oxidation of the salen

ligand. Interestingly, this is an intramolecular phenomenon, not observed for the mixtures of the parent POM and free metallo-salen complexes. This underlines the beneficial effect of covalent tethering compared to an electrostatic association. The Pd-salen-POM was applied as a heterogeneous catalyst for the Suzuki cross-coupling of various aryl halides and arylboronic acids in 2014 by Lei,[59] showing greatly improved activity compared to the Pd-salen and the POMs skeleton alone which proved the synergistic effect of metal complex-POM hybrids. And in the work of Neumann,[60] they applied the Rh hybrid POM, $\{SiW_{11}O_{39}[O\text{-}(SiCH_2CH_2CH_2PPh_2)_2(PPh_3)Rh(I)Cl]\}^{4-}$, in the hydrogenation of alkenes. The higher catalytic activity of the Rh-POM complex compared to the complex alone was proposed to the grafted alkyl chains in the phosphine ligands improving stabilization of intermediate Rh^{III}.

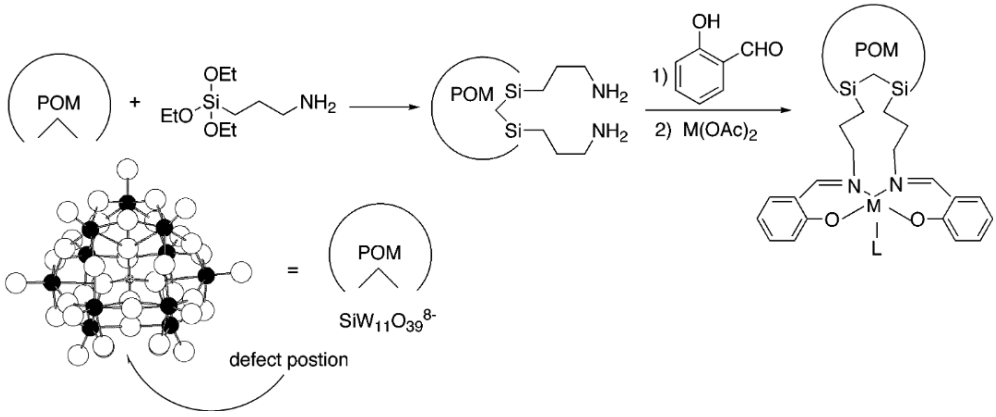

Figure 1-21 Synthetic Pathway for the preparation of the M-Salen-POM Compounds, M= Mn, Co, Ni and Pd.[42]

Intramolecular Electron Transfers

In 2009, Harriman and Odobel built an series of hybrids combining Dawson-type POM and metallo-porphyrin residues through CuAAC “Click” reaction allowing the redoxactive units to approach within close contact to the POM.[61] They demonstrated that the choice of the anchoring group has a significant effect on the reduction potential of the POM that could be utilized to design highly specific catalysts. Among the hybrids they synthesized the cyclic votammetry indicates that two electrons could be added to the POM before reduction of the porphyrin takes place. So that the porphyrin π-radical anion formed by photolysis should be able to reduce the POM. For the rigid linkage, the rate of electron transfer interaction was remarkably slow no matter from the photoexicted Zn porphrin to the POM or from the one

electron reduced POM to Zn porphrin. In the flexible linkage case, the electron transfer is much faster for both direction and the one electron reduced POM would transfer electron to the singlet-excited-state of the porphyrin. But these systems could still not acculate electrons onto a single POM residue even by attaching two porphrins onto the POM.

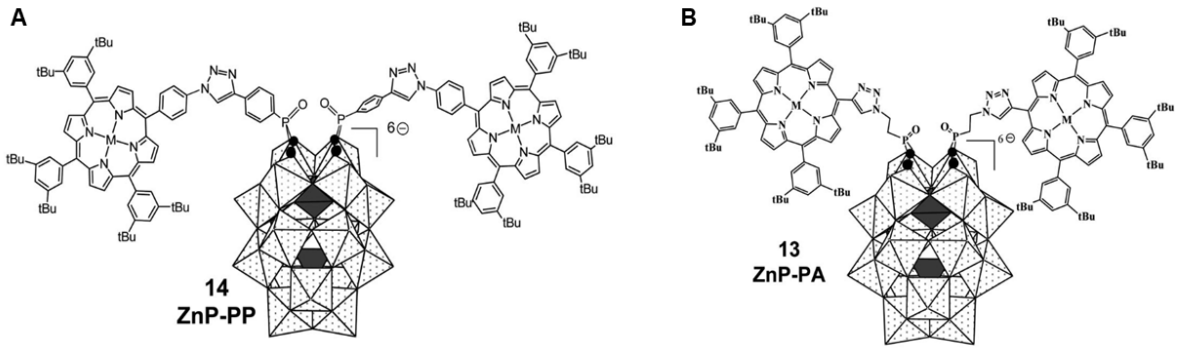

Figure 1-22 Zinc porphyrin functionalized Well-Dawson POMs through A) rigid and B) flexible spacers.[61]

In 2013, Izzet and coworkers successfully grafted iridium(III) complex photosensitizer to various POM precursors which were pre-functionalized with mono- or bi-phenyliodo organotin or organosilyl bridges through “Sonogashira” coupling.[62–64] In this series of photosensitizer covalently grafted to Keggin or Dawson POMs, the transient absorption spectroscopy and spectroelecrochemical measurements revealed a photoinduced electron transfer from the excited photosensitizer to the POM skeletons. Taking into consideration of the efficiency of charge-separation and the lifetime of the charge-separated states, the organosilyl grafted Dawson hybrid complex has the most balanced photophysical properties.[63] It was thus applied in further investigation, as we could see in Figure 1-23 in the present of triethylamine as an electron sacrificial donor, there were two electrons accumulated onto the POM skeleton under visible-light irradiation. The process was monitored by the UV-vis spectroscopy which showed the two characteristic absorptions due the one electron and two electrons reduction of the Dawson POM skeleton. This Dawson POM iridium complex was applied as H_2-evolving catalyst in the presence of acetic acid with turn-over numbers up to 41 within 7 days, which paves the way to functional photosynthetic devices using sunlight as a source of clean, renewable energy.

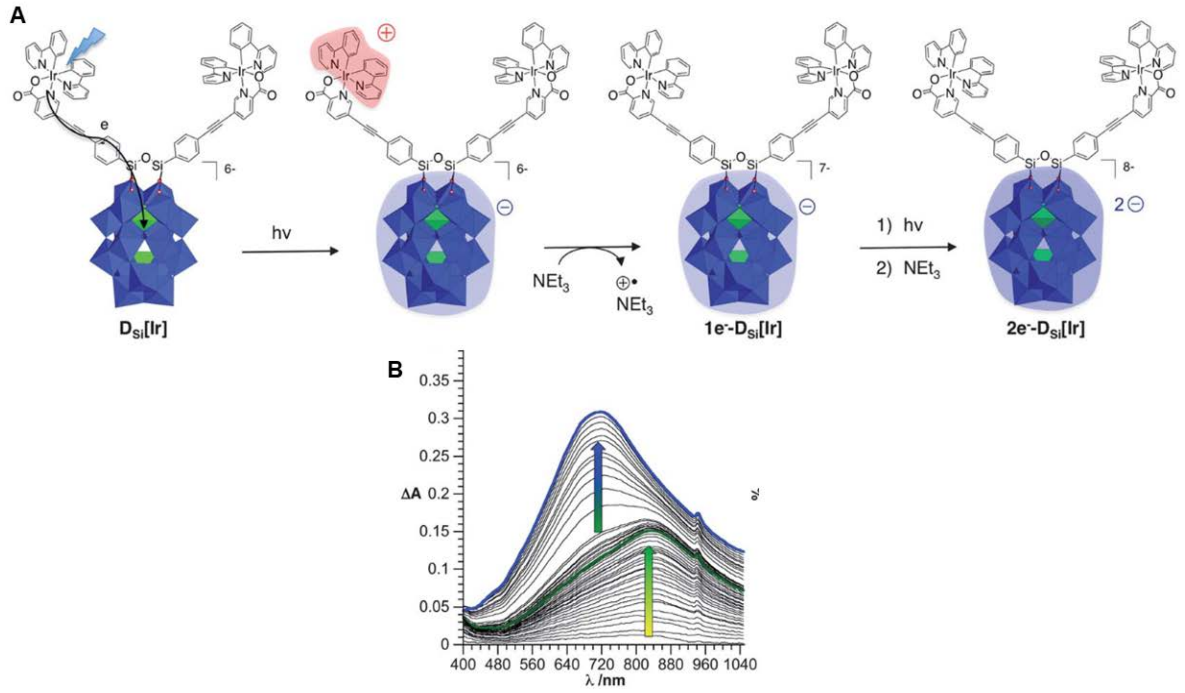

Figure 1-23 Iridium (III) complex photosensor functionalized Well-Dawson and its photoactivity in the hydrogen evolution. A) Charge photo-accumulation occurring in the ***D_{Si}[Ir]*** *dyad; B) evolution of the differential visible absorption spectrum of a solution of* ***D_{Si}[Ir]*** *(0.2 mM) in DMF containing Et_3N (1 M) during photoirradiation under visible light.*[64]

1.3 Perspective and description of the project

In order to enhance the communication between the POMs and the metal complexes, the strategy here is to covalently graft the ligand onto the POMs skeleton and then to coordinate metal ions, such as Cu^{2+}, $Fe^{2+/3+}$ and Co^{2+}, to mimic the metalloenzymes expecting the enhancement of catalytic properties. We will then investigate the synergy between the skeletons and the metal complexes as well as the resulting catalytic activities.

Firstly, proper POM skeletons, such as lacunary Keggin and Well-Dawson types, are chose to covalently functionalize with the ligands using direct-functionalization or post-functionalization strategies, such as “Sonogashira” coupling, “click” reaction and the most recent nucleophilic substitution method. Another purpose here is to expand the methodology of POMs functionalization of with some more valuable groups. And then we would like to coordinate them to proper metal ions to form POM metal complexes and monitor the process with NMR or UV-vis spectroscopy. At each step, we will pay special attention to the purification

procedures and the full characterization by NMR, IR, Mass spectrum, UV-vis, elemental analysis and cyclic voltammetry. The synergy between the skeletons and the metal centers will be analyzed as well as its catalytic activity.

In Chapter 2, I will present the exploration of nucleophilic substitution to function polyoxometalates based on $(TBA)_3[PW_{11}O_{39}\{O(SiCH_2I)_2\}]$ (**K_{Si}[I]-1)** with bis(pyridine-2-ylmethyl) (**DPA**).

Chapter 3 is devoted to the synthesis of two kind of post-functionalized Keggin hybrid, $(TBA)_4[PW_{11}O_{39}(SnC_6H_4CCCH_2N(CH_2C_5H_4N)_2)]$ (**K_{Sn}[DPA]**) and $(TBA)_3[PW_{11}O_{39}\{O(SiCH_2CH_2\ CH_2N_3CCHCH_2NCH_2C_5H_4N)_2\}]$ (**K_{Si}[N_3DPA]-3**) through "Sonogashira" coupling and "Click" reaction respectively and the complexation of them. For **K_{Sn}[DPA]**, we also investigated the electrochemical properties of its complex as electrocatalytic properties to nitrite reduction.

In Chapter 4, I will describe the synthesis and characterization of direct-functionalized $TBA_4H_5[P_2V_3W_{15}O_{62}]$ with Tris-modified DPA, as well as the complexation of the POM hybrid (**D_{V3DPA}**) with $Cu(OAc)_2$, **D_{V3DPA}**@Cu(OAc). The photoactivity was observed with ^1H NMR and ^{31}P NMR variation. Furtherly, the photo-induced reduction of the **D_{V3DPA}**@Cu(OAc) was confirmed with EPR spectrum. The UV-vis absorption evolution, there are three electrons accumulated onto the POM which could be applied to reduce CF_3^+ to CF_3 radical.

.

References:

(1) Holm, R. H.; Kennepohl, P.; Solomon, E. I. Structural and Functional Aspects of Metal Sites in Biology. *Chem. Rev.* **1996**, *96* (7), 2239–2314.

(2) Degtyarenko, K. Bioinorganic Motifs: Towards Functional Classification of Metalloproteins. *Bioinformatics* **2000**, *16* (10), 851–864.

(3) Hill, H. A. O. Metals, Models, Mechanisms, Microbes and Medicine. *Chem. Br.* **1976**, *12* (4), 119–123.

(4) Ibers, J. A.; Holm, R. H. Modeling Coordination Sites in Metallobiomolecules. *Science* **1980**, *209* (4453), 223–235.

(5) Chaudhury, P.; Wieghardt, K.; Nuber, B.; Weiss, J. $[L_2Fe(\mu\text{-}OH)(\mu\text{-}CH_3CO_2)_2](ClO_4)\cdot H_2O$, a Model Compound for the Diiron Centers in Deoxyhemerythrin. *Angew. Chem. Int. Ed. Engl.* **1985**, *24* (9), 778–779.

(6) Holmes, M. A.; Le Trong, I.; Turley, S.; Sieker, L. C.; Stenkamp, R. E. Structures of Deoxy and Oxy Hemerythrin at 2.0 Å Resolution. *J. Mol. Biol.* **1991**, *218* (3), 583–593.

(7) Karlin, K. D. Metalloenzymes, Structural Motifs, and Inorganic Models. *Sci. New Ser.* **1993**, *261* (5122), 701–708.

(8) Boyington, J. C.; Gladyshev, V. N.; Khangulov, S. V.; Stadtman, T. C.; Sun, P. D. Crystal Structure of Formate Dehydrogenase H: Catalysis Involving Mo, Molybdopterin, Selenocysteine, and an $[Fe_4S_4]$ Cluster. *Sci. New Ser.* **1997**, *275* (5304), 1305–1308.

(9) Raaijmakers, H. C. A.; Romão, M. J. Formate-Reduced E. Coli Formate Dehydrogenase H: The Reinterpretation of the Crystal Structure Suggests a New Reaction Mechanism. *JBIC J. Biol. Inorg. Chem.* **2006**, *11* (7), 849–854.

(10) Mota, C. S.; Rivas, M. G.; Brondino, C. D.; Moura, I.; Moura, J. J. G.; González, P. J.; Cerqueira, N. M. F. S. A. The Mechanism of Formate Oxidation by Metal-Dependent Formate Dehydrogenases. *JBIC J. Biol. Inorg. Chem.* **2011**, *16* (8), 1255–1268.

(11) Raaijmakers, H.; Macieira, S.; Dias, J. M.; Teixeira, S.; Bursakov, S.; Huber, R.; Moura, J. J. G.; Moura, I.; Romão, M. J. Gene Sequence and the 1.8 Å Crystal Structure of the Tungsten-Containing Formate Dehydrogenase from Desulfovibrio Gigas. *Structure* **2002**, *10* (9), 1261–1272.

(12) Fontecilla-Camps, J. C.; Amara, P.; Cavazza, C.; Nicolet, Y.; Volbeda, A. Structure–Function Relationships of Anaerobic Gas-Processing Metalloenzymes. *Nature* **2009**, *460* (7257), 814–822.

(13) Lampret, O.; Duan, J.; Hofmann, E.; Winkler, M.; Armstrong, F. A.; Happe, T. The Roles of Long-Range Proton-Coupled Electron Transfer in the Directionality and Efficiency of [FeFe]-Hydrogenases. *Proc. Natl. Acad. Sci.* **2020**, *117* (34), 20520–20529.

(14) Gloaguen, F.; Lawrence, J. D.; Rauchfuss, T. B. Biomimetic Hydrogen Evolution Catalyzed by an Iron Carbonyl Thiolate. *J. Am. Chem. Soc.* **2001**, *123* (38), 9476–9477.

(15) Mejia-Rodriguez, R.; Chong, D.; Reibenspies, J. H.; Soriaga, M. P.; Darensbourg, M. Y. The Hydrophilic Phosphatriazaadamantane Ligand in the Development of H2 Production Electrocatalysts: Iron Hydrogenase Model Complexes. *J. Am. Chem. Soc.* **2004**, *126* (38), 12004–12014.

(16) Na, Y.; Wang, M.; Pan, J.; Zhang, P.; Åkermark, B.; Sun, L. Visible Light-Driven Electron Transfer and Hydrogen Generation Catalyzed by Bioinspired [2Fe2S] Complexes. *Inorg. Chem.* **2008**, *47* (7), 2805–2810.

(17) Cioncoloni, G.; Roger, I.; Wheatley, P. S.; Wilson, C.; Morris, R. E.; Sproules, S.; Symes, M. D. Proton-Coupled Electron Transfer Enhances the Electrocatalytic Reduction of Nitrite to NO in a Bioinspired Copper Complex. *ACS Catal.* **2018**, *8* (6), 5070–5084.

(18) Kataoka, K.; Furusawa, H.; Takagi, K.; Yamaguchi, K.; Suzuki, S. Functional Analysis of Conserved Aspartate and Histidine Residues Located Around the Type 2 Copper Site of Copper-Containing Nitrite Reductase. *J Biochem* **2000**, *127* (2), 6.

(19) Antonyuk, S. V.; Strange, R. W.; Sawers, G.; Eady, R. R.; Hasnain, S. S. Atomic Resolution Structures of Resting-State, Substrate- and Product-Complexed Cu-Nitrite Reductase Provide Insight into Catalytic Mechanism. *Proceedings of the National Academy of Sciences* **2005**, *102* (34), 12041–12046.

(20) Weinstock, I. A.; Schreiber, R. E.; Neumann, R. Dioxygen in Polyoxometalate Mediated Reactions. *Chem. Rev.* **2018**, *118* (5), 2680–2717.

(21) Clemente-Juan, J. M.; Coronado, E.; Gaita-Ariño, A. Magnetic Polyoxometalates: From Molecular Magnetism to Molecular Spintronics and Quantum Computing. *Chem. Soc. Rev.* **2012**, *41* (22), 7464–7478.

(22) Bijelic, A.; Aureliano, M.; Rompel, A. Polyoxometalates as Potential Next-Generation Metallodrugs in the Combat Against Cancer. *Angew. Chem. Int. Ed.* **2019**, *58* (10), 2980–2999.

(23) *Polyoxometalate Molecular Science*; Borrás-Almenar, J. J., Coronado, E., Müller, A., Pope, M., Eds.; Springer Netherlands: Dordrecht, 2003.

(24) Zhang, J.; Bond, A. M.; Richardt, P. J. S.; Wedd, A. G. Voltammetric Reduction of α- and Γ*-[S2W18O62]4- and α-, β-, and γ-[SiW12O40]4-: Isomeric Dependence of Reversible Potentials of Polyoxometalate Anions Using Data Obtained by Novel Dissolution and Conventional Solution-Phase Processes. *Inorg. Chem.* **2004**, *43* (26), 8263–8271.

(25) Himeno, S.; Takamoto, M. Difference in Voltammetric Properties between the Keggin-Type [XW12O40]N− and [XMo12O40]N− Complexes. *J. Electroanal. Chem.* **2002**, *528* (1), 170–174.

(26) Sarma, B. B.; Efremenko, I.; Neumann, R. Oxygenation of Methylarenes to Benzaldehyde Derivatives by a Polyoxometalate Mediated Electron Transfer–Oxygen Transfer Reaction in Aqueous Sulfuric Acid. *J. Am. Chem. Soc.* **2015**, *137* (18), 5916–5922.

(27) Streb, C. New Trends in Polyoxometalate Photoredox Chemistry: From Photosensitisation to Water Oxidation Catalysis. *Dalton Trans* **2012**, *41* (6), 1651–1659.

(28) Yamase, T. Photo- and Electrochromism of Polyoxometalates and Related Materials. *Chem. Rev.* **1998**, *98* (1), 307–326.

(29) Khenkin, A. M.; Efremenko, I.; Weiner, L.; Martin, J. M. L.; Neumann, R. Photochemical Reduction of Carbon Dioxide Catalyzed by a Ruthenium-Substituted Polyoxometalate. *Chem. – Eur. J.* **2010**, *16* (4), 1356–1364.

(30) Huang, Z.; Luo, Z.; Geletii, Y. V.; Vickers, J. W.; Yin, Q.; Wu, D.; Hou, Y.; Ding, Y.; Song, J.; Musaev, D. G.; Hill, C. L.; Lian, T. Efficient Light-Driven Carbon-Free Cobalt-Based Molecular Catalyst for Water Oxidation. *J. Am. Chem. Soc.* **2011**, *133* (7), 2068–2071.

(31) Barkigia, K. M.; Rajkovic, L. M.; Pope, M. T.; Quicksall, C. O. New Type of Heteropoly Anion. Tetramolybdo Complexes of Dialkyl- and Diarylarsinates. *J. Am. Chem. Soc.* **1975**, *97* (14), 4146–4147.

(32) Knoth, W. H. Derivatives of Heteropolyanions. 1. Organic Derivatives of $W_{12}SiO_{40}^{4-}$, $W_{12}PO_{40}^{3-}$, and $Mo_{12}SiO_{40}^{4-}$. *J. Am. Chem. Soc.* **1979**, *101* (3), 759–760.

(33) Kim, G. S.; Hagen, K. S.; Hill, C. L. Synthesis, Structure, Spectroscopic Properties, and Hydrolytic Chemistry of Organophosphonoyl Polyoxotungstates of Formula $[C_6H_5P(O)]_2X^{n+}W_{11}O_{39}^{(8-n)-}$ ($X^{n+} = P^{5+}$, Si^{4+}). *Inorg. Chem.* **1992**, *31* (25), 5316–5324.

(34) Hou, Y.; Hill, C. L. Hydrolytically Stable Organic Triester Capped Polyoxometalates with Catalytic Oxygenation Activity of Formula $[RC(CH_2O)_3V_3P_2W_{15}O_{59}]^{6-}$ (R = CH_3, NO_2, CH_2OH). *J. Am. Chem. Soc.* **1993**, *115* (25), 11823–11830.

(35) Hasenknopf, B.; Delmont, R.; Herson, P.; Gouzerh, P. Anderson-Type Heteropolymolybdates Containing Tris(Alkoxo) Ligands: Synthesis and Structural Characterization. *Eur. J. Inorg. Chem.* **2002**, *2002* (5), 1081–1087.

(36) Chen, W.; Huang, L.; Hu, J.; Li, T.; Jia, F.; Song, Y.-F. Connecting Carbon Nanotubes to Polyoxometalate Clusters for Engineering High-Performance Anode Materials. *Phys. Chem. Chem. Phys.* **2014**, *16* (36), 19668–19673.

(37) Wang, J.; Lin, C.-G.; Zhang, J.; Wei, J.; Song, Y.-F.; Guo, J. Polyoxometalate-Based Organic–Inorganic Hybrids for Stabilization and Optical Switching of the Liquid Crystal Blue Phase. *J. Mater. Chem. C* **2015**, *3* (16), 4179–4187.

(38) Lin, C.-G.; Chen, W.; Omwoma, S.; Song, Y.-F. Covalently Grafting Nonmesogenic Moieties onto Polyoxometalate for Fabrication of Thermotropic Liquid-Crystalline Nanomaterials. *J. Mater. Chem. C* **2014**, *3* (1), 15–18.

(39) Cannizzo, C.; Mayer, C. R.; Sécheresse, F.; Larpent, C. Covalent Hybrid Materials Based on Nanolatex Particles and Dawson Polyoxometalates. *Adv. Mater.* **2005**, *17* (23), 2888–2892.

(40) Carraro, M.; Modugno, G.; Fiorani, G.; Maccato, C.; Sartorel, A.; Bonchio, M. Organic-Inorganic Molecular Nano-Sensors: A Bis-Dansylated Tweezer-Like Fluoroionophore Integrating a Polyoxometalate Core. *Eur. J. Org. Chem.* **2012**, *2012* (2), 281–289.

(41) Modugno, G.; Syrgiannis, Z.; Bonasera, A.; Carraro, M.; Giancane, G.; Valli, L.; Bonchio, M.; Prato, M. The Supramolecular Design of Low-Dimensional Carbon Nano-Hybrids Encoding a Polyoxometalate-Bis-Pyrene Tweezer. *Chem. Commun.* **2014**, *50* (38), 4881–4883.

(42) Bar-Nahum, I.; Cohen, H.; Neumann, R. Organometallic−Polyoxometalate Hybrid Compounds: Metallosalen Compounds Modified by Keggin Type Polyoxometalates. *Inorg. Chem.* **2003**, *42* (11), 3677–3684.

(43) Yvon, C.; Surman, A. J.; Hutin, M.; Alex, J.; Smith, B. O.; Long, D.-L.; Cronin, L. Polyoxometalate Clusters Integrated into Peptide Chains and as Inorganic Amino Acids: Solution- and Solid-Phase Approaches. *Angew. Chem.* **2014**, *126* (13), 3404–3409.

(44) Debela, A. M.; Ortiz, M.; Beni, V.; Thorimbert, S.; Lesage, D.; Cole, R. B.; O'Sullivan, C. K.; Hasenknopf, B. Biofunctionalization of Polyoxometalates with DNA Primers, Their Use in the Polymerase Chain Reaction (PCR) and Electrochemical Detection of PCR Products. *Chem. – Eur. J.* **2015**, *21* (49), 17721–17727.

(45) Bareyt, S.; Piligkos, S.; Hasenknopf, B.; Gouzerh, P.; Lacôte, E.; Thorimbert, S.; Malacria, M. Highly Efficient Peptide Bond Formation to Functionalized Wells-Dawson-Type Polyoxotungstates. *Angew. Chem.* **2003**, *115* (29), 3526–3528.

(46) Chinchilla, R.; Nájera, C. Recent Advances in Sonogashira Reactions. *Chem. Soc. Rev.* **2011**, *40* (10), 5084.

(47) Xu, B.; Wei, Y.; Barnes, C. L.; Peng, Z. Molekulare Hybridmaterialien Durch Kovalente Verknüpfung Anorganischer Polyoxometallate Und Organischer Konjugierter Systeme. *Angew. Chem.* **2001**, *113* (12), 2353–2356.

(48) Duffort, V.; Thouvenot, R.; Afonso, C.; Izzet, G.; Proust, A. Straightforward Synthesis of New Polyoxometalate-Based Hybrids Exemplified by the Covalent Bonding of a Polypyridyl Ligand. *Chem. Commun.* **2009**, *0* (40), 6062–6064.

(49) Meldal, M.; Tornøe, C. W. Cu-Catalyzed Azide−Alkyne Cycloaddition. *Chem. Rev.* **2008**, *108* (8), 2952–3015.

(50) Micoine, K.; Hasenknopf, B.; Thorimbert, S.; Lacôte, E.; Malacria, M. A General Strategy for Ligation of Organic and Biological Molecules to Dawson and Keggin Polyoxotungstates. *Org. Lett.* **2007**, *9* (20), 3981–3984.

(51) Odobel, F.; Séverac, M.; Pellegrin, Y.; Blart, E.; Fosse, C.; Cannizzo, C.; Mayer, C. R.; Elliott, K. J.; Harriman, A. Coupled Sensitizer–Catalyst Dyads: Electron-Transfer Reactions in a Perylene–Polyoxometalate Conjugate. *Chem. – Eur. J.* **2009**, *15* (13), 3130–3138.

(52) Vanhaecht, S.; Jacobs, J.; Meervelt, L. V.; N. Parac-Vogt, T. A Versatile and Highly Efficient Post-Functionalization Method for Grafting Organic Molecules onto Anderson-Type Polyoxometalates. *Dalton Trans.* **2015**, *44* (44), 19059–19062.

(53) Macdonell, A.; Johnson, N. A. B.; Surman, A. J.; Cronin, L. Configurable Nanosized Metal Oxide Oligomers via Precise “Click” Coupling Control of Hybrid Polyoxometalates. *J. Am. Chem. Soc.* **2015**, *137* (17), 5662–5665.

(54) Li, Q.; Zhang, J.; Wang, L.; Hao, J.; Yin, P.; Wei, Y. Nucleophilic Substitution Reaction for Rational Post-Functionalization of Polyoxometalates. *New J. Chem.* **2016**, *40* (2), 906–909.

(55) Vanhaecht, S.; Quanten, T.; Parac-Vogt, T. N. A Simple Nucleophilic Substitution as a Versatile Postfunctionalization Method for the Coupling of Nucleophiles to an Anderson-Type Polyoxometalate. *Inorg. Chem.* **2017**, *56* (5), 3095–3101.

(56) Vanhaecht, S.; Quanten, T.; Parac-Vogt, T. N. A Mild Post-Functionalization Method for the Vanadium Substituted P2W15V3 Wells–Dawson Polyoxometalate Based on a Copper Catalyzed Azide–Alkyne Cycloaddition. *Dalton Trans.* **2017**, *46* (31), 10215–10219.

(57) Kang, J.; Xu, B.; Peng, Z.; Zhu, X.; Wei, Y.; Powell, D. R. Molecular and Polymeric Hybrids Based on Covalently Linked Polyoxometalates and Transition-Metal Complexes. *Angew. Chem.* **2005**, *117* (42), 7062–7065.

(58) Izzet, G.; Abécassis, B.; Brouri, D.; Piot, M.; Matt, B.; Serapian, S. A.; Bo, C.; Proust, A. Hierarchical Self-Assembly of Polyoxometalate-Based Hybrids Driven by Metal Coordination and Electrostatic Interactions: From Discrete Supramolecular Species to Dense Monodisperse Nanoparticles. *J. Am. Chem. Soc.* **2016**, *138* (15), 5093–5099.

(59) Tong, J.; Wang, H.; Cai, X.; Zhang, Q.; Ma, H.; Lei, Z. Suzuki Coupling Reaction Catalyzed Heterogeneously by Pd(Salen)/Polyoxometalate Compound: Another Example

for Synergistic Effect of Organic/Inorganic Hybrid. *Appl. Organomet. Chem.* **2014**, *28* (2), 95–100.

(60) Bar-Nahum, I.; Neumann, R. Synthesis, Characterization and Catalytic Activity of a Wilkinson's Type Metal-Organic–Polyoxometalate Hybrid Compound. *Chem. Commun.* **2003**, *0* (21), 2690–2691.

(61) Harriman, A.; Elliott, K. J.; Alamiry, M. A. H.; Pleux, L. L.; Séverac, M.; Pellegrin, Y.; Blart, E.; Fosse, C.; Cannizzo, C.; Mayer, C. R.; Odobel, F. Intramolecular Electron Transfer Reactions Observed for Dawson-Type Polyoxometalates Covalently Linked to Porphyrin Residues. *J. Phys. Chem. C* **2009**, *113* (14), 5834–5842.

(62) Matt, B.; Moussa, J.; Chamoreau, L.-M.; Afonso, C.; Proust, A.; Amouri, H.; Izzet, G. Elegant Approach to the Synthesis of a Unique Heteroleptic Cyclometalated Iridium(III)-Polyoxometalate Conjugate. *Organometallics* **2012**, *31* (1), 35–38.

(63) Matt, B.; Xiang, X.; L. Kaledin, A.; Han, N.; Moussa, J.; Amouri, H.; Alves, S.; L. Hill, C.; Lian, T.; G. Musaev, D.; Izzet, G.; Proust, A. Long Lived Charge Separation in Iridium(Iii)-Photosensitized Polyoxometalates: Synthesis, Photophysical and Computational Studies of Organometallic–Redox Tunable Oxide Assemblies. *Chem. Sci.* **2013**, *4* (4), 1737–1745.

(64) Matt, B.; Fize, J.; Moussa, J.; Amouri, H.; Pereira, A.; Artero, V.; Izzet, G.; Proust, A. Charge Photo-Accumulation and Photocatalytic Hydrogen Evolution under Visible Light at an Iridium(Iii)-Photosensitized Polyoxotungstate. *Energy Environ. Sci.* **2013**, *6* (5), 1504

Chapter 2

Nucleophilic substitution's route

Chapter 2 Nucleophilic substitution's route

As described in the introduction, over the past decades, many post-functionalization routes have been developed to diversify the function of polyoxometalates through attaching various organic groups to their scaffolds, such as amidation, esterification, imine bond formation, "Sonogashira" coupling, "Click" reaction and Diels-Alder reaction. Recently, Parac-Vogt and co-workers[1] successfully grafted primary/secondary amines onto pre-synthesized chloroacetamide functionalized Anderson type POM through nucleophilic substitution reaction in the presence of sodium carbonate and tetrabutylammonium iodide (TBAI) (Scheme 2-1). The mild, metal free conditions in this new approach are quite interesting to us: as we want to graft coordination sites onto the POM surface, avoiding parasitic coordination of metal ions involved in the coupling process is a clear advantage. Based on their work, we would like to extend the nucleophilic substitution on other type of polyoxometalates with more complex organic moieties than simple amines.

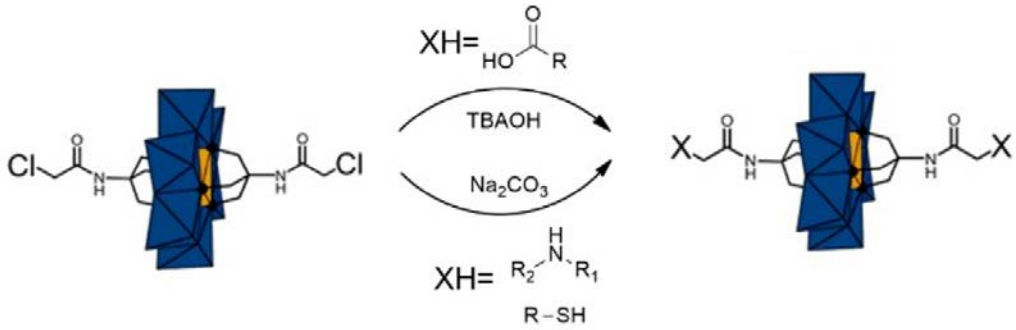

Scheme 2-1 Nucleophilic substitution reaction for the post-functionalization of Anderson type polyoxometalates.[1]

Our initial target is to mimic the bimetallic oxo-complexes with so-called "diamond" core $[M_2(\mu\text{-}O)_2]^{n+}$, M=Mn, Cu, Fe, which are stabilized by polyamine ligands.[2] In the case of iron and copper complexes, such compounds are capable of oxidizing various organic functionalities in reactions of biological inspiration. In order to achieve the bimetallic complex, the Anderson type polyoxometalates are not ideal scaffolds as the two functions are directed in two opposite directions. To the contrary, lacunary Keggin and Dawson polyoxometalates appear as better candidates. The first organo-functionalized hybrid POM[3] which was based

on a $[SiW_{11}O_{39}]^{8-}$ POM, was reported by Knoth in 1979 and represented the beginning of a large series of derivatives of monolacunary Keggin hybrid POMs. These organosilyl derivatives of polyoxometalates have two arms in the lacuna and thus could be functionalized with two ligands, in line with the synthesis of bimetallic sites with oxo bridges on a single polyoxometalate.

Thus, we envisioned the synthetic route proposed in Scheme 2-2: first, the lacunary polyoxometalates are functionalized with two haloalkyltriethoxylsilane (X= Cl, I), moieties bridged by an Si-O-Si link. Then, the two halogens will be substituted by the desired nucleophiles bearing the coordination site, followed by the complexations of some metals such as Cu, Fe and Mn, which could form oxo bridges. Finally, the catalytic properties of these hybrids' complexes would be investigated.

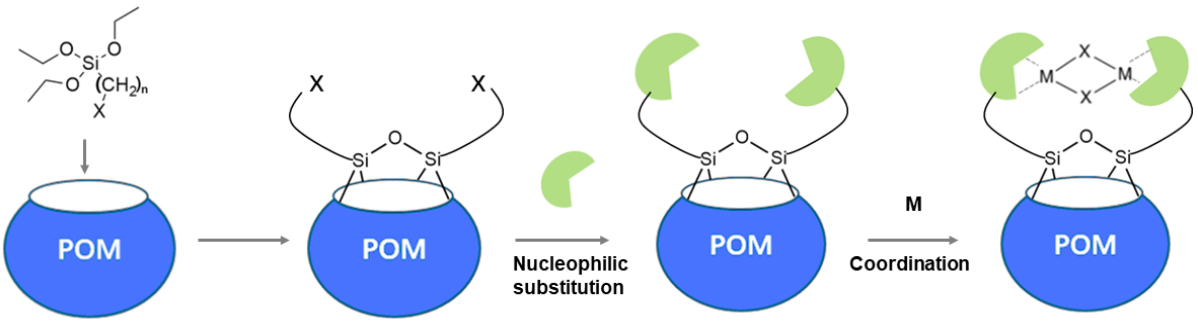

Scheme 2-2 The strategy toward polyoxometalate's based bimetallic complexes.

Besides the metal free conditions, another advantage of this nucleophilic substitution route relies in the possibility, which is hard to achieve in the "Sonogashira" coupling and "Click" reaction, to adjust the length of the link, and notably to have a shorter distance between the POM surface and the grafted complex. A shorter linker could, in particular, enhance the communication between the polyoxometalates and the complexes, and thus enhance the synergy between them and make the catalytic process more efficient. To start with, the mono-lacunary polyoxometalate $[PW_{11}O_{39}]^{7-}$ was chosen as scaffold as the reactions could conveniently be monitored with ^{31}P NMR.

2.1 Nucleophilic substitution of K_{Si}[Cl]-1

Some preliminary work on this project has been done by Julia Struwe (Erasmus internship, 2017) and Nikos Kostopoulos (M2 internship, 2018). A chloromethyl functionalized

$[PW_{11}O_{39}]^{7-}$ was synthesized using classical methods:[4–6] hydrolysis, in acidic conditions, of commercially available chloromethyltriethoxylsilane in the presence of the lacunary POM lead to the expected product in good yields as a white powder, which was characterized by various techniques. A shift of the (halogeno)methyl protons of the organic part from 2.86 ppm of chloromethyltriethoxylsilane to 2.99 ppm in ^{1}H NMR while a single peak in ^{31}P NMR at -13.28 ppm for the final product is in favor of a successful and clean grafting. This is further confirmed by the detection, in IR, of the characteristic band at 1110 cm^{-1} of the Si-O-Si bridge. Finally, slow diffusion of ether into an acetonitrile solution allowed for the growth of single crystal of sufficient quality for X-ray structure determination.

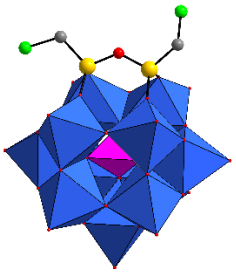

*Scheme2-3 Synthesis of $TBA_3[PW_{11}O_{39}\{O(SiCH_2Cl)_2\}]$ (**K_{Si}[Cl]-1**) with its X-ray structure*

Nucleophilic substitution of the chloride in **K_{Si}[Cl]-1** with some simple amine such as diethylamine and benzylamine was then explored. The reactions were carried out under the condition described in the work of Parac-Vogt, with sodium carbonate as base and TBAI as catalyst in acetonitrile. In the case of diethylamine, both at high temperature and room temperature, the degradation of the grafted silyl, in particular with a diminution of the Si-O-Si stretch in IR, was observed.

Scheme 2-4 The nucleophilic substitution of ***K_{Si}[Cl]-1*** *with diethylamine and benzylamine.*

As Wei and co-workers[7] had successfully displaced by nucleophilic substitution a chloride on an hexamolybdate-based hybrid ($TBA_2[Mo_6O_{18}NCH_2CH_2CH_2Cl]$) with iodo using sodium iodide and considering that the iodo could be a better leaving group, the nucleophilic substitution of chloro with TBAI was also carried out. But even after 7 days refluxing at 80℃, almost no iodo derivative was observed from NMR. The difficulty of the substitution of chloro with iodo in this case would suggest that the chloride in this case is not a good enough leaving group and hampers any substitution reaction.

2.2 Nucleophilic substitution of K_{Si}[I]-1

As the iodo derivative could not be easily synthesized via substitution on the chloro derivative **K_{Si}[Cl]-1**, we wonder if the direct synthesis of $(TBA)_3[PW_{11}O_{39}\{O(SiCH_2I)_2\}]$ (**K_{Si}[I]-1**) could be performed, thus allowing for a better leaving group on the POM and possibly facilitating the substitution reaction.

2.2.1 Synthesis of triethoxy(iodomethyl)silane

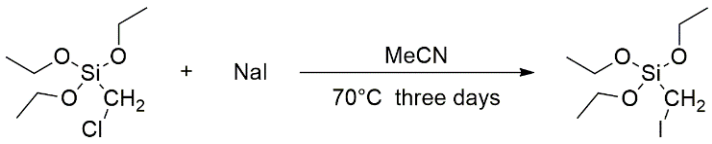

Scheme 2-5 The synthesis of the triethoxy(iodomethyl)silane

First, the triethoxy(iodomethyl)silane was synthesized according to a slightly modified published procedure,[8] where triethoxy(chloromethyl)silane was reacted with sodium iodide in

acetonitrile refluxing under inert atmosphere. In order to get full conversion, optimizations of the reaction conditions were explored, as indicated in *table 2-1* with 4.0 eq. of NaI at reflux for 3 days being an optimum.

*Table 2-1 Optimization runs of the **I** vs **Cl** exchange*

entry	***NaI (eq.)***	***reflux time (h)***	***Conversion (%)***
1	1.05	15	20
2	2.00	72	86
3	1.05	86	98
4	4.00	72	100

After filtration of insoluble sodium salt, the resulting bright yellow solution was concentrated to 1/5 and poured into diethyl ether to finish removing the residual sodium salt. The large chemical shift of Si-CH_2X in ^1H NMR from 2.89 ppm (X= Cl) to 2.01 ppm (X=I) confirmed the successful transformation.

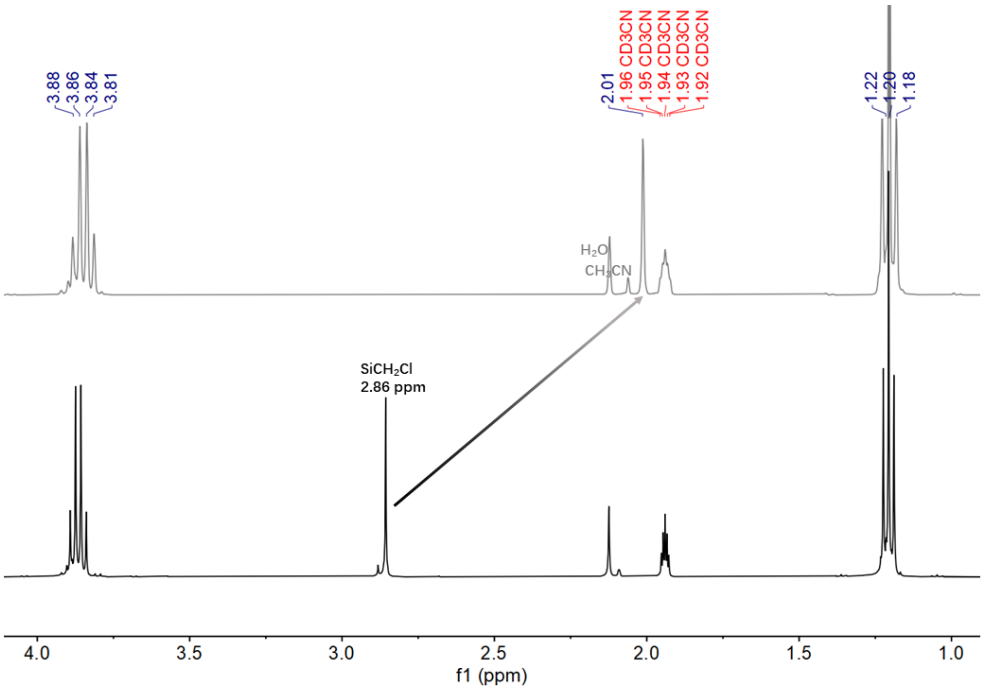

Figure 2-1 ^1H NMR spectrum of triethoxy(iodomethyl)silane (gray) and triethoxy(chloromethyl)silane (black) in CD_3CN.

2.2.2 Synthesis of K_{Si}[I]-1

Scheme 2-5 Synthesis of ***K_{Si}[I]-1****.*

K_{Si}[I]-1 was synthesized following the same procedure as for **K_{Si}[Cl]-1**. Iodomethyltriethoxysilane was added to an acetonitrile suspension of lacunary Keggin K_7[α-$PW_{11}O_{39}$] and TBABr. After being stirred at room temperature for half an hour, the hydrochloric acid was added at 0℃ and stirred overnight at room temperature. A single peak at -13.00 ppm in ^{31}P NMR confirmed the full conversion into a single product. Formation of the Si-O-Si bridge which was confirmed by the band at 1111 cm^{-1} in the IR spectrum, where the classical bands of the POM skeleton) with strong vibrations at 1067 and 1038 cm^{-1} (P-O), 964 and 874 cm^{-1} (W-O) and 825 cm^{-1} (W-O-W) are also present (Figure 2-5).[4] The tungsten isotopic distribution pattern of the ESI-Mass was in agreement with the calculated signature of $\{TBA[PW_{11}O_{39}\{O(SiCH_2I)_2\}]\}^{2-}$ at m/z= 1637.14 (Figure 2-3). The peak around 2.1 ppm in the ^{1}H NMR is attributed to the $SiCH_2$ moiety. Interestingly, and contrary to the "expected" singlet observed for the triethoxysilyl precursor, it is now a doublet of doublet with a strong "roof" effect: this probably results from hampered rotation of the CH_2I due to the bulk of the iodo and the short distance to the POM surface, leading to the nonequivalence of the two protons of the methylene group and thus diastereotopic differentiation.

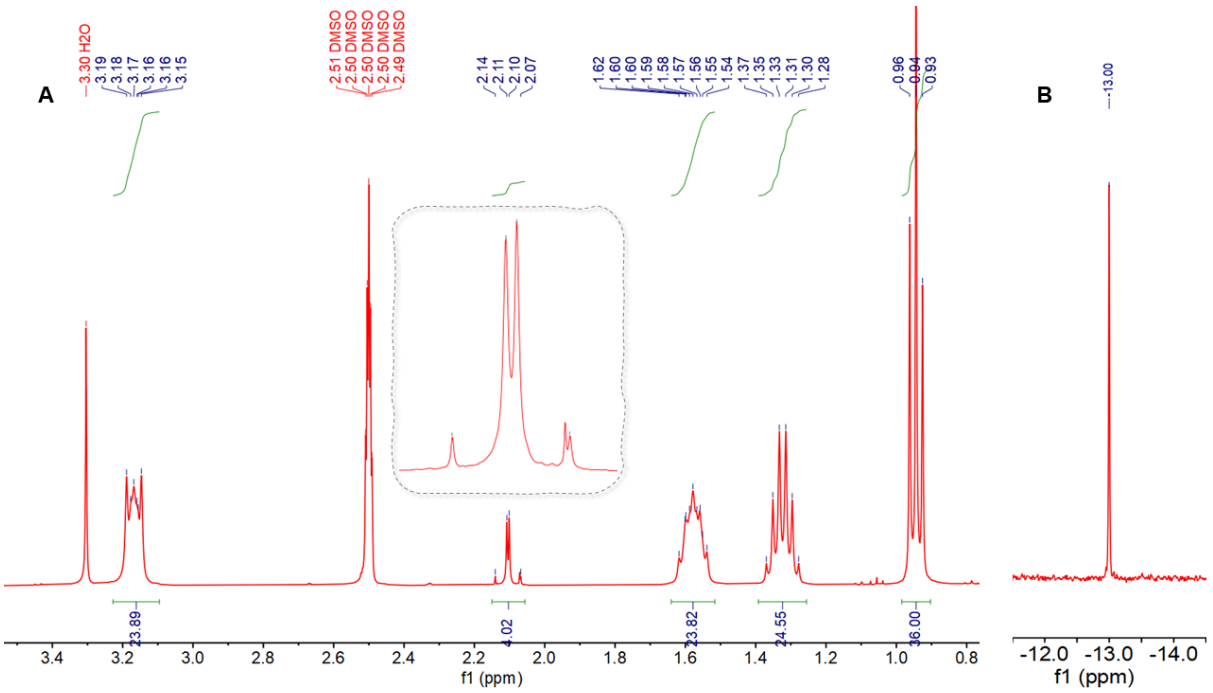

*Figure 2-2 A) ^{1}H NMR and B)^{31}P NMR of **K_{Si}[I]-1** in DMSO-d_6*

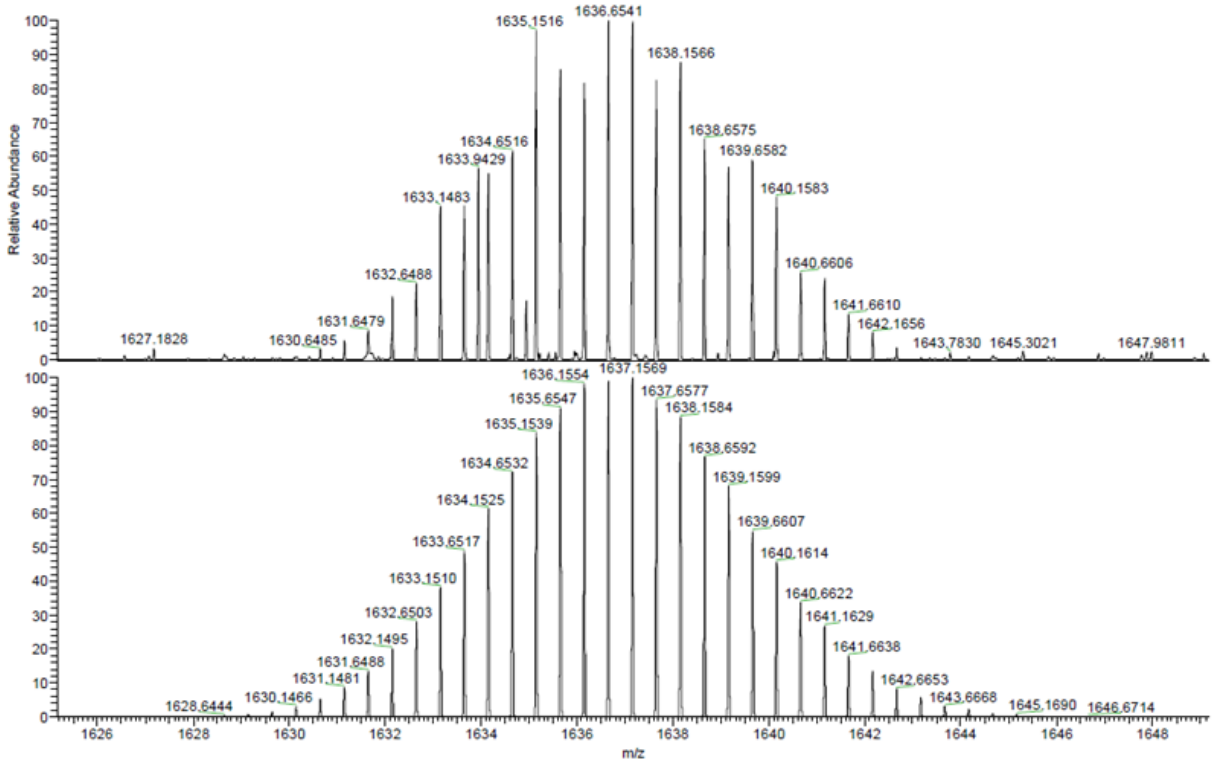

*Figure 2-3 ESI-mass spectrum of **K_{Si}[I]-1** and its simulation give the formular {TBA[$PW_{11}O_{39}${$O(SiCH_2I)_2$}]}$^{2-}$.*

2.2.3 Nucleophilic substitution of K_{Si}[I]-1 with DPA

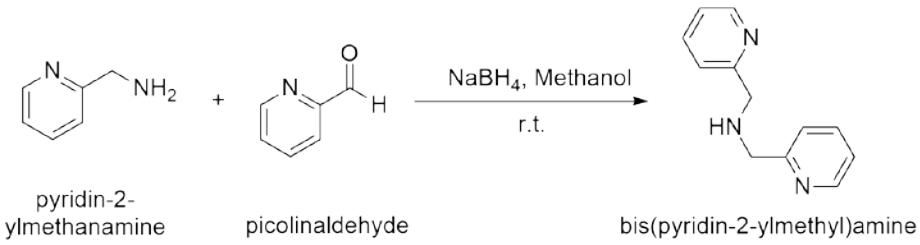

*Scheme 2-7 Synthesis of bis(pyridin-2-ylmethyl)amine (**DPA**)*

The tripodal ligand, DPA ,has been used in bioinspired complexes with various metals such as Cu and Co.[9,10] It was synthesized according to a modified procedure published by Arnold.[11]

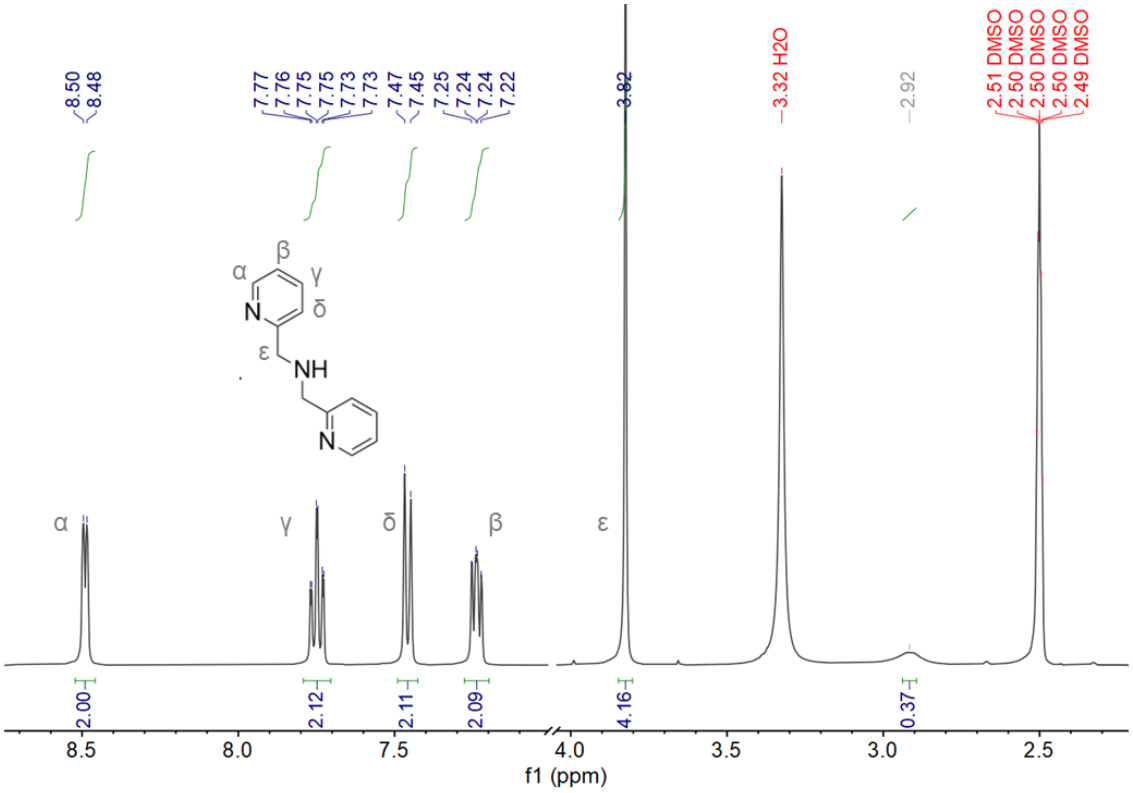

Figure 2-4 ^{1}H NMR of DPA in DMSO

It was also selected as Parac-Vogt has shown in her work that secondary amine could be successfully used as nucleophile for the substitution of the halogen group on the polyoxometalates.[1] However, the use of polyfunctional systems, especially polyamines, has not been tested so far.

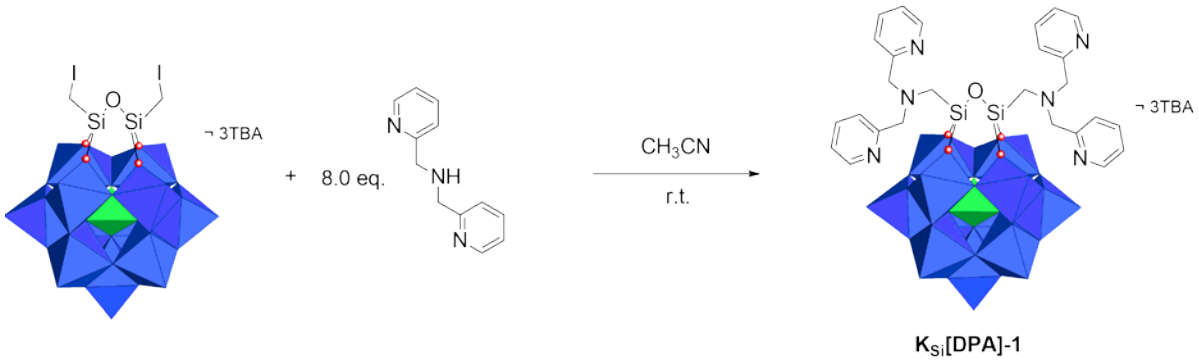

Scheme 2-8 Nucleophilic substitution of ***K_{Si}[I]-1*** *with DPA to form* $(TBA)_3[PW_{11}O_{39}\{O(SiCH_2DPA)_2\}]$ (***K_{Si}[DPA]-1***)

In the exploration of nucleophilic substitution of **K_{Si}[Cl]-1**, as decomposition of the polyoxometalates skeleton was observed, we tried to simplify the system and choose to use DPA both as a nucleophile and a base, removing Na_2CO_3 from the reaction medium. Thus, an excess of DPA was added in anhydrous acetonitrile under argon to avoid potential formation of OH^- that could degrade the POM. When stirring a yellow acetonitrile solution containing 1.0 eq. **K_{Si}[I]-1** and 8.0 eq. of DPA at room temperature, a color change from yellow to green and finally to dark green was observed over 1 hour, even we covered the flask with alumina paper, together with a somewhat abundant precipitate which was proved to be the protonated H-DPA$^+$ cation by ^{1}H NMR in DMSO. The precipitation of protonated DPA indicated that a reaction occurred which released protons, as would be expected if the nucleophilic substitution did take place.

The reaction was monitored by ^{1}H NMR on aliquots precipitated with ethanol (typical spectrum on figure 2-6), which clearly showed the chemical shifts at 8.62 ppm, 7.86 ppm, 7.52 ppm and 7.4 ppm that belonging to pyridine of DPA, but significantly different from the pyridine peaks of the free DPA. In the meantime, the chemical shift of $SiCH_2$ at 2.10 ppm of the polyoxometalate precursor diminished, with a new peak growing at 1.85 ppm as the reaction continued. In parallel, the ^{31}P NMR spectrum was also carried out with a gradual disappearance of the starting material at -12.99 ppm and two main peaks at -13.21 ppm and -15.05 ppm appearing. While the latter suggest some degradation of the POM to form the complete $[PW_{12}O_{40}]^{3-}$ anion, but the singlet at -13.21 ppm could belong to the aimed product with a shift compared to the starting **K_{Si}[I]-1** at -12.99 ppm in CD_3CN. Some minor evolutions

are also observed on the IR spectrum of the powder, but the latter still present the main bands expected for the post functionalized POM (Figure 2-5).

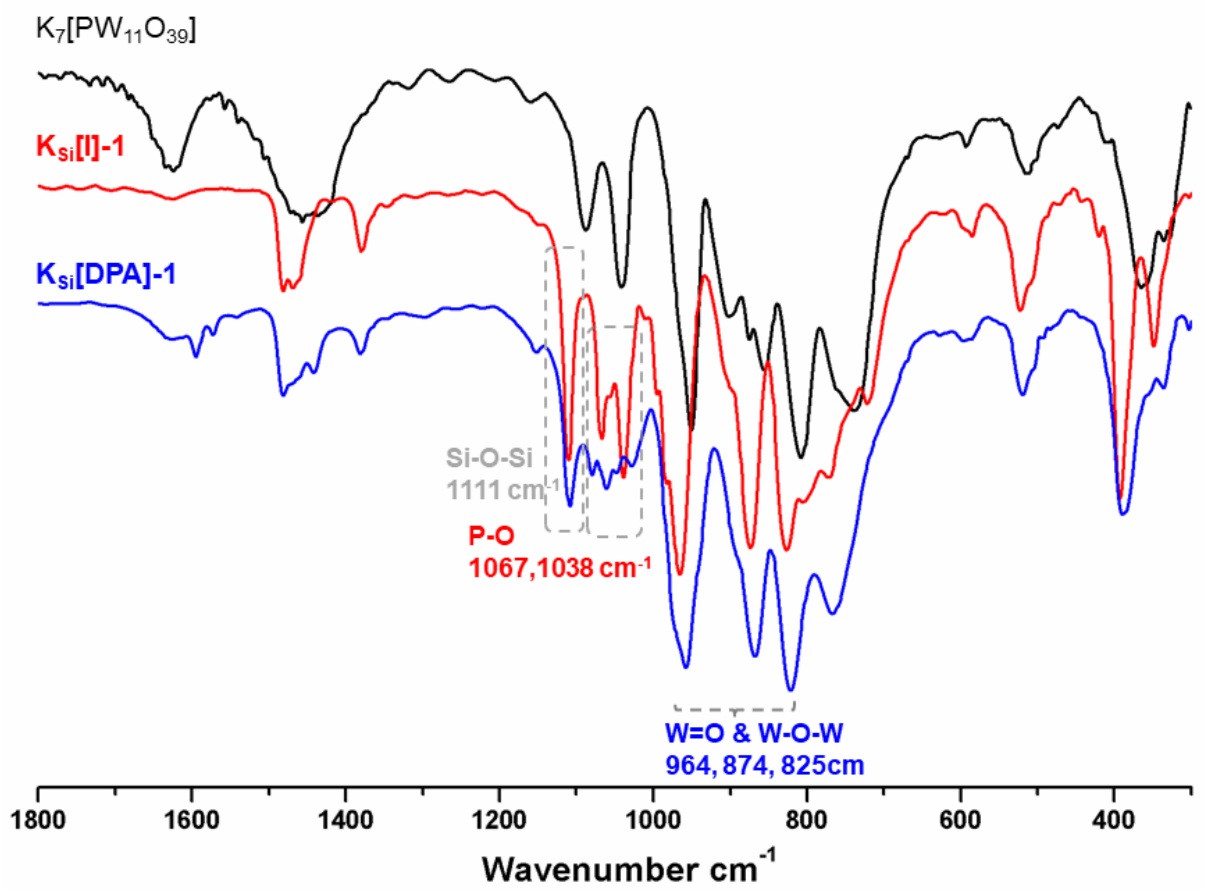

*Figure 2-5 IR spectrum (KBr) of the $K_7[PW_{11}O_{39}]$ (black), **K_{Si}[I]-1** (red), and the synthesized **K_{Si}[DPA]-1** (blue).*

Despite all these very encouraging evidences, some unexpected data call for caution: in particular, the integration of the ^{1}H NMR signal attributed to the methylene spacers $SiCH_2$ was quite small compared to that of the DPA and TBA^+ peaks, the integration indicated there was only around 0.2 eq. of $SiCH_2$ (based on DPA).

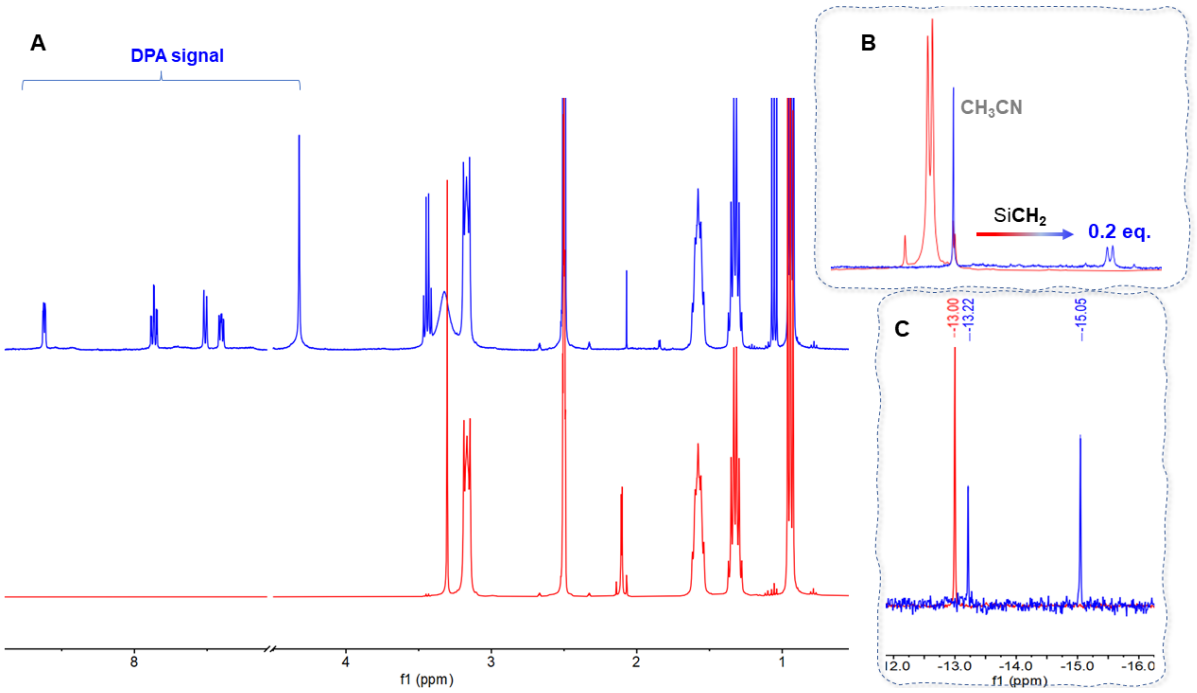

Figure 2-6 The Full range (A) and zoom of the $SiCH_2$ (B) of the ^{1}H NMR and ^{31}P NMR(C) spectrum of precursor ***K_{Si}[I]-1*** *(red) and the synthesized* ***K_{Si}[DPA]-1****(blue).*

Despite trying to work as anhydrous as possible, the ^{31}P NMR of the product always displays the peak at -15.05 ppm. However, we noticed that its relative intensity could be reduced when air exposure of the crude solution during the treatment of the reaction was kept as short as possible. This might suggest that the presence of basic group on the POM may favor, in the open, the formation of hydroxide from the water in the air and thus favor degradation of the POM skeleton during the treatment and not the reaction by itself.

Obviously, optimization of the synthesis was required in order to improve the purity and efficiency of this reaction.

2.2.4 Exploration of the nucleophilic substitution conditions

Changing the base

In this reaction, the DPA work not only as the nucleophile but also as the base to remove the HI produced during the substitution process. During the reaction, we observed that the solution turned from slightly yellow to green and finally to dark blue after one to two hours stirring under inert atmosphere, coupled with some dark precipitate. In the POM chemistry, the blue color is usually associated with POM reduction. The DPA is a secondary

amine which could work as the electron donor for the reduction of the polyoxometalates.[12] Thus, the excess of DPA could facilitate the reduction and thus induce the color change. Indeed, when we reduced the amount of the DPA from 8.0 eq. to 4.0 eq., the color of the solution changed much slower and from yellow to dark blue only. However, this change in DPA/POM ratio did not induce any changes in the ^{1}H NMR spectrum as the position and the ratio of the peaks attributed to $SiCH_2$ and to DPA didn't have a significant change. Moreover, there was still some degradation with multiple peaks in the ^{31}P NMR.

We thus try to use a more classical base and tired triethylamine which is a strong organic base with a high pKa frequently used in POM chemistry.[13] It is usually used in excess of triethylamine (here ~10 eq.). In the presence of Et_3N *a*nd 2.2 eq DPA, after overnight stirring, the ^{1}H NMR spectrum of the isolated product did not display any DPA signals around 8 ppm, but there was still a tiny signal at 1.87 ppm: the latter was previously attributed to $SiCH_2$ moiety after successful substitution of I by DPA on the POM surface, which is obviously an error. We did detect some triethylammonium peaks, that could not be washed away, suggesting that some Et_3N has been protonated and attracted by the POM surface. As we observed some reduction (blue color) of the POM skeleton, we wondered if the signal at 1.85 ppm could correspond to $SiCH_2$ after the reduction of the POM skeleton. The association of the oxidation with the NMR signals was verified by the treatment of oxidizer, tetrabutylammonium tribromide ($TBABr_3$), during the treatment.

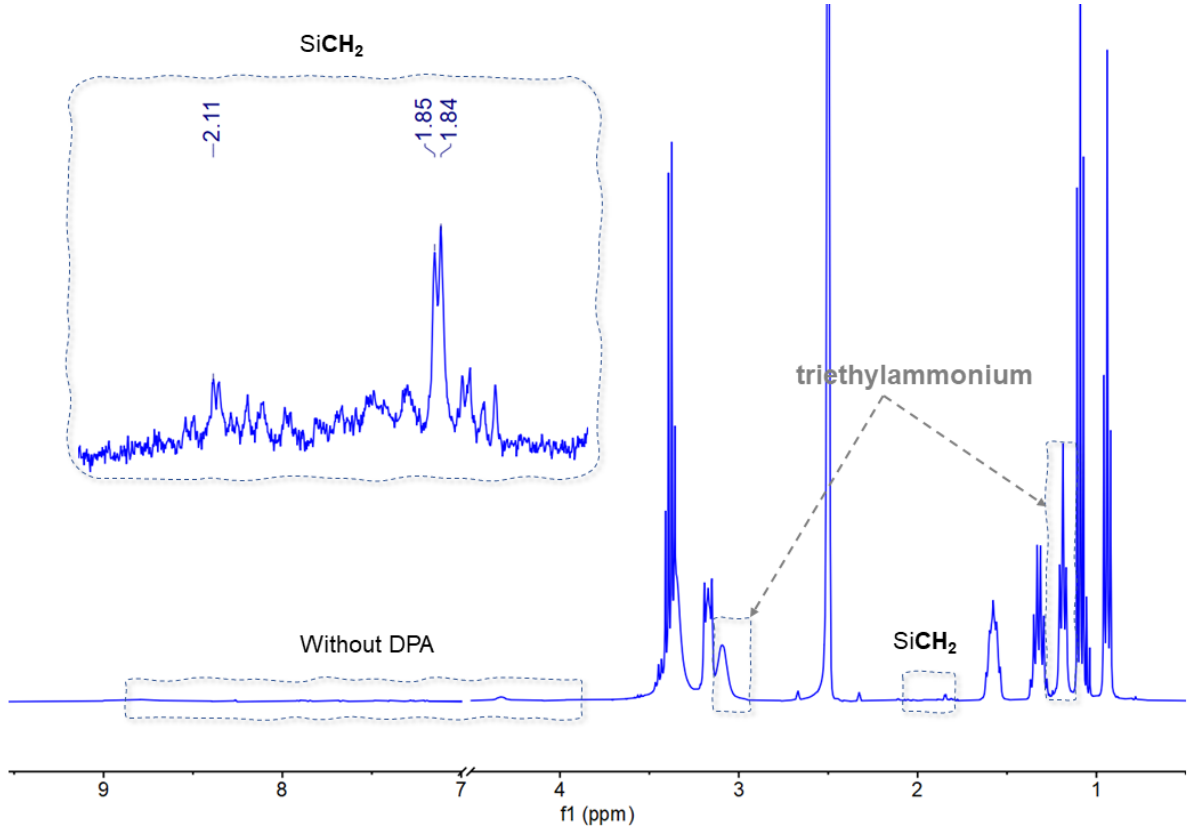

Figure 2-7 the ^{1}H NMR of the resulting product with the addition of Et_3N as the base

Treating with $TBABr_3$ at the end of the reaction

As the $TBABr_3$ solution was added gradually, the dark blue solution was turned to yellow under argon. In ^{1}H NMR, the ratio of "$SiCH_2$" signal at the position around 2.10 ppm was increasing compared to the 1.85 ppm peak (Figure 2-8, insert, blue to pale blue). In the meantime, the ratio of peak at -13.0 ppm was increased in ^{31}P NMR (Figure 2-9, blue to pale blue). But, as the solution in the NMR tube turned from yellow to blue after overnight, the peak at -13.0 ppm was most gone, mainly -13.2 ppm coupled with some degradation signal at -15.0 ppm (Figure 2-9, pale blue to navy blue).

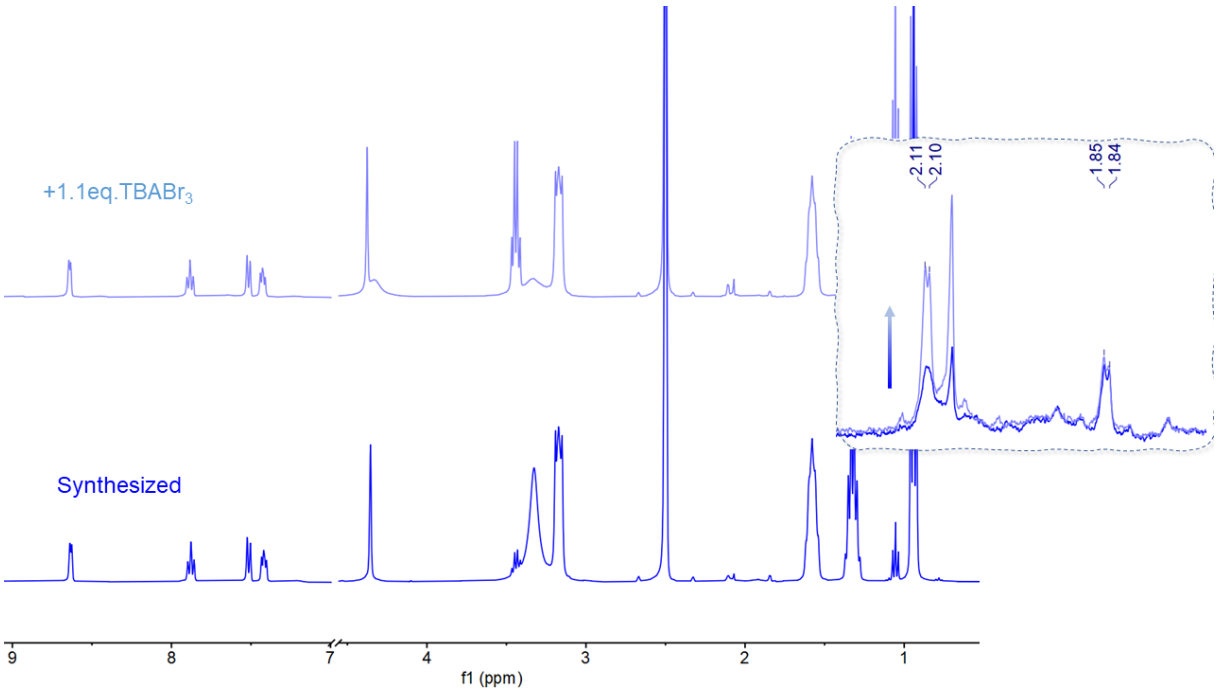

Figure 2-8 the ^{1}H NMR (in DMSO-d6) of the resulting product before (navy) and after (red) the treatment with $TBABr_3$, insert: zoom

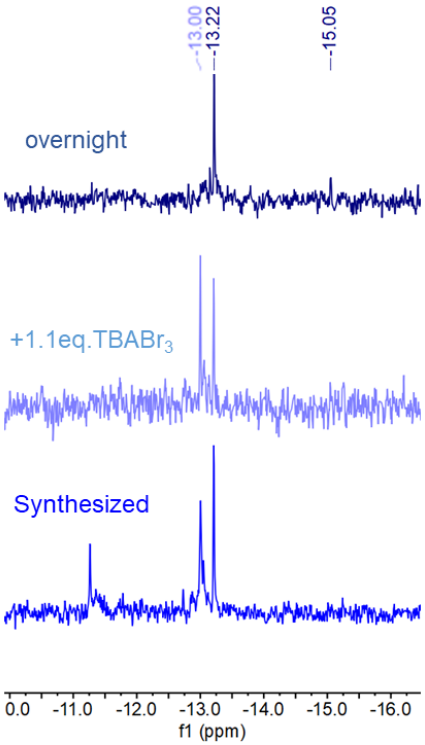

Figure 2-9 the ^{1}H NMR (in DMSO) of the resulting product before (blue) and after (pale blue) the treatment with $TBABr_3$, overnight in the NMR tube (navy blue).

Upon the results above, we could conclude from the results above that no matter the chemical shift of the $SiCH_2$ or the phosphate were just caused by the reduction or the oxidation of the POM skeletons. Overnight, the oxidized POM solution in NMR tube, turned back to blue could be due to the existence of the DPA in the solution resulting the reductio of the POM skeleton.

Adding $TBABr_3$ during the reaction

The reoxidation of the final dark blue solution to yellow, always coupled with some white precipitate which was proved to be $HDPA^+$ by ^1H NMR. It indicated that some electrostatically associated $HDPA^+$ could be released upon reoxidation and diminution of the charge of the POM. We hypothesis that the reduced POM could strongly abstract the $HDPA^+$ electrostatically to its surface resulting in no nucleophilic substitution process. In order to verify that we try to add $TBABr_3$ into the solution during the reaction:

1. Add 0.5 eq. of $TBABr_3$ (based on POM) at the beginning of the reaction. But the solution still changed from yellow to green after about half an hour. ^1H NMR experiments indicate that the $SiCH_2$ signal belonging to the starting material was still present even after three days of reaction, without the appearance of any new $SiCH_2$ signals that could be associated with the targeted product. Moreover, we could still observe quite amount of DPA. Finally, there were still several peaks in the ^{31}P NMR which indicated some degradation of the POM during the course of the reaction.
2. We also tried to add the $TBABr_3$ gradually during the reaction to keep the solution yellow, however no improvement was observed. From the results we obtained above, the treatment with $TBABr_3$ can't help improving the nucleophilic substitution.

2.2.5 DOSY

From the results above, one key question arose : can we definitely prove that the modification observed in the ^1H NMR upon reaction with DPA correspond to a covalent grafting or not. This is even more relevant as we have clearly identified the formation of $HDPA^+$ in the reaction. The latter could just associate to the POM as a counter ion.

We thus turned toward diffusion ordered spectroscopy (DOSY) NMR. Indeed, DOSY experiments resolve different compounds spectroscopically in a mixture based on their respective diffusion coefficients, which depends on the size and shape of the molecules. If the DPA was covalently grafted onto the POM, it must have the same diffusion coefficient as the proton of the platform (**K_{Si}[I]-1**), otherwise it just connects to the POM through electrostatic interaction or coordinate interaction.

From the DOSY spectrum (Figure 2-11), the diffusion coefficient of the DPA (~$2.50\times10^{-10}m^2/s$) is almost the same as that of TBA^+ (~$2.40\times10^{-10}m^2/s$) and quite different from the possible "$SiCH_2$" (~$1.20\times10^{-10}m^2/s$). It indicated the DPA was not covalently grafted onto the POM at all and just acted like the cation as the TBA^+.

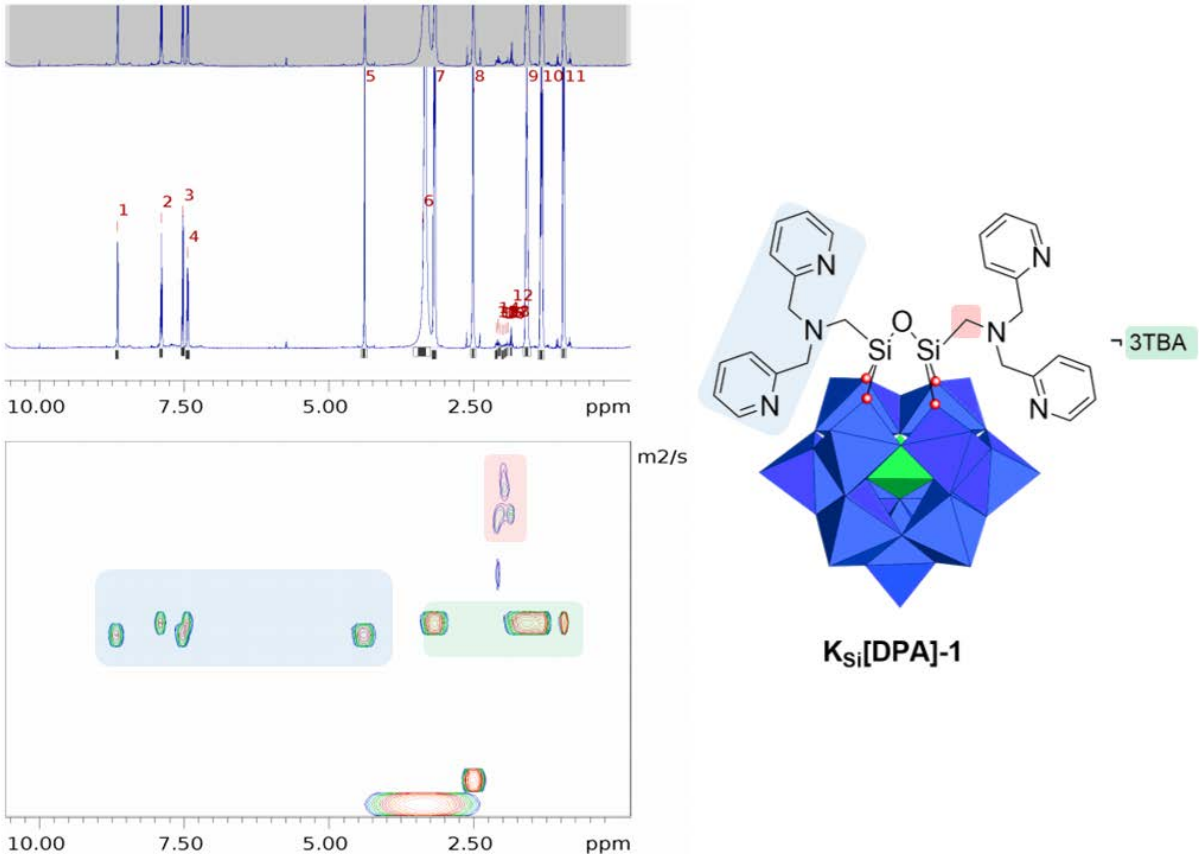

*Figure 2-10 The DOSY NMR (in DMSO-d6) of the synthesized **K_{Si}[DPA]-1**.*

Table 2-2 The of diffusion coefficient of the synthesized ***K_{Si}[DPA]-1***

Peaks	Species	F2(ppm)	D($\times10^{-10}$ m²/s)	error$\times10^{-11}$
1	DPA	8.656	**2.49**	0.136
2		7.893	**2.47**	0.141
3		7.519	**2.52**	0.074
4		7.436	**2.48**	0.145
5		4.391	**2.57**	0.060
6		3.386	8.78	0.589
7	TBA^+	3.182	**2.47**	0.221
9		1.584	**2.41**	0.038
10		1.333	**2.41**	0.120
11		0.947	**2.42**	0.077
12	Possible "$SiCH_2$"	1.852	**1.11**	0.333
13		2.112	**1.17**	0.465
14		2.085	**1.64**	2.142
15		2.049	**1.04**	0.663
16		1.996	0.84	1.151
17		1.951	0.94	0.645
18		1.917	1.12	0.260

2.2.6 intermediate conclusion

We have tried to covalently graft the bioinspired ligand DPA onto **K_{Si}[I]-1** surface through a nucleophilic substitution reaction. But the results above suggest that this reaction failed using rather mild conditions. While we have tried to play with the base and control the oxidation state of the POM during the reaction, there was always degradation of the polyoxometalates skeleton, notably with formation of the complete $[PW_{12}O_{40}]^{3-}$ anion. Another potential reason of this failure could be steric hindrance, which is one of the main difficulties faced in nucleophilic substitution,[14] in the reaction between the bulk POM and the entering group, with a short linker as $SiCH_2$.

2.3 Direct-functionalization to graft $[PW_{11}O_{39}]^{7-}$

As the nucleophilic substitution on the functionalized POM appeared somewhat compromised, an alternative route was sought direct-functionalization with the DPA-substituted triethoxysilane derivative. For the triethoxyhalogenoalkyl silane amination, there are not so many cases in the literatures. In order to lower any steric hindrance, we choose the

(3-chloropropyl)triethoxysilane to study this reaction, in order to, if we successfully synthesized the 3-DPA-(propyl)triethoxysilane, try to shorten the alkyl chain.

2.3.1 Synthesis of organic precursors

1-(tri-ethoxy-silyl-propyl)-3-methyl-imidazolium chloride

The DPA coupling with this type of silane is not described in the literature. However, we found an amination reaction of this kind using imidazole as a nucleophile. Thus, we synthesized 1-(tri-ethoxy-silyl-propyl)-3-methyl-imidazolium chloride according to the protocol published by Sun.[15]

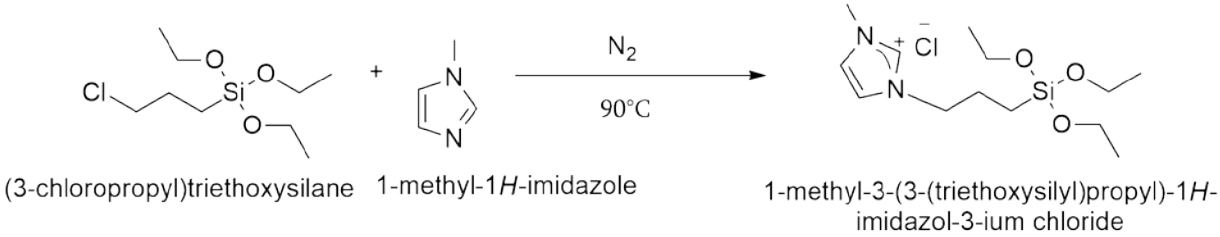

(3-chloropropyl)triethoxysilane 1-methyl-1*H*-imidazole 1-methyl-3-(3-(triethoxysilyl)propyl)-1*H*-imidazol-3-ium chloride

Scheme 2-9 The synthesis of 1-(tri-ethoxy-silyl-propyl)-3-methyl-imidazolium chloride

1:1 of (3-chloropropyl)triethoxysilane and 1-methyl-1H-imidazole (**NMI**) was stirred at 90℃ without any solvent. After about 3 days, the resulting liquid was washed with diethyl ether. As can be seen in the ^{1}H NMR (Figure 2-11), the clear chemical shift of the propyl from 0.68 ppm, 1.75 ppm and 3.60 ppm to 0.51 ppm,1.82 ppm and 4.14ppm, together with the new peaks of the imidazolium moiety above 7 ppm, indicated the successful coupling.

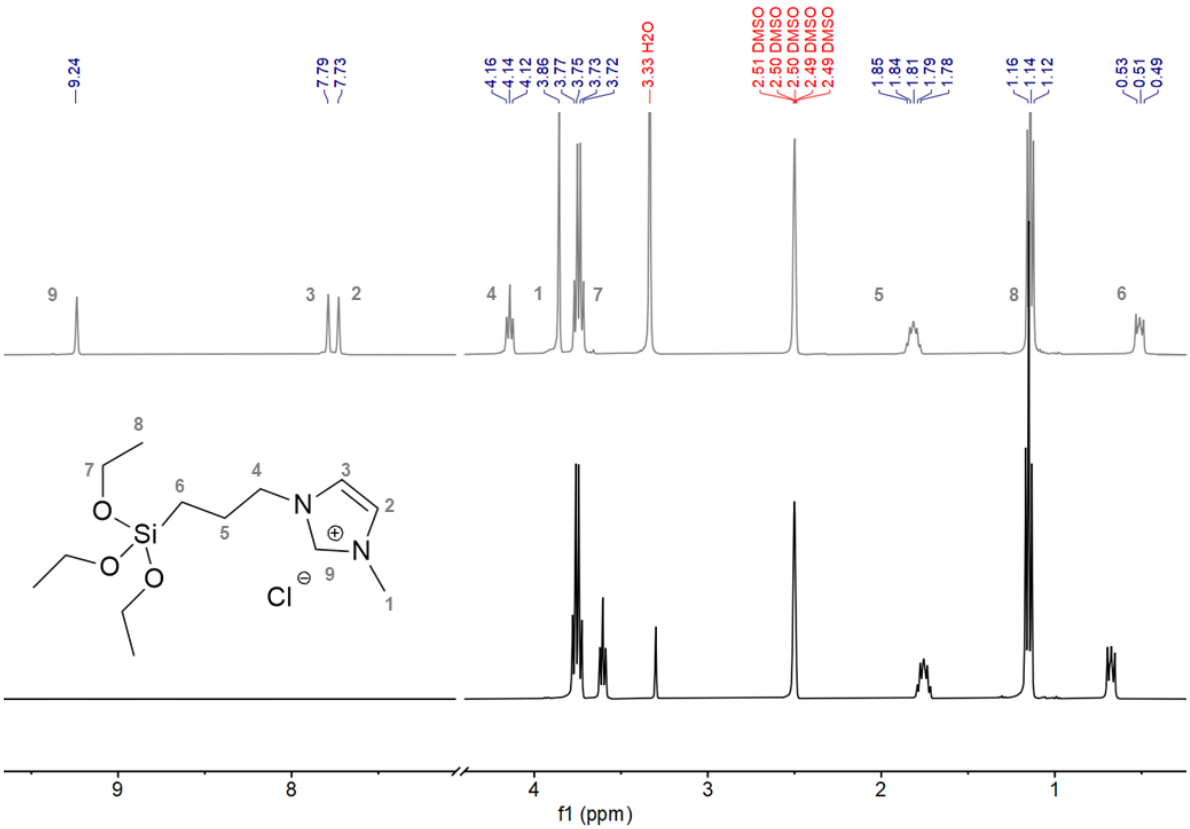

*Figure 2-11 The evolution in ^{1}H NMR of synthesis of 1-(tri-ethoxy-silyl-propyl)-3-methyl-imidazolium chloride (gray) from the solvent-free reaction of (3-chloropropyl)triethoxysilane (black) and 1-methyl-1H-imidazole (**NMI**).*

N,N-bis(pyridin-2-ylmethyl)-3-(triethoxysilyl)propan-1-amine

Once we successfully synthesized 1-(tri-ethoxy-silyl-propyl)-3-methyl-imidazolium chloride, we tried the same procedure to couple DPA with (3-chloropropyl)triethoxysilane in a solvent free system.

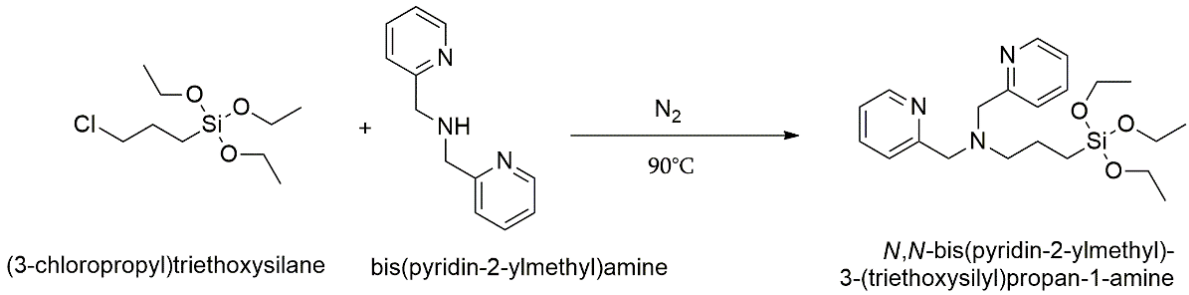

(3-chloropropyl)triethoxysilane bis(pyridin-2-ylmethyl)amine *N,N*-bis(pyridin-2-ylmethyl)-3-(triethoxysilyl)propan-1-amine

Scheme 2-9 The synthesis of N,N-bis(pyridin-2-ylmethyl)-3-(triethoxysilyl)propan-1-amine.

From the proton NMR in DMSO, we could again observe significant chemical shift of the three peaks of the propyl chain, from 3.60 ppm,1.75 ppm and 0.67ppm to 2.43 ppm,1.49 ppm and 0.46 ppm. It indicated that the coupling did occur. However, peaks between 7-9 ppm indicates that the isolated product does contain a little bit of free DPA. Nevertheless, we considered it was pure enough to firstly test the grafting onto the POM surface, before to optimize this synthesis if needed.

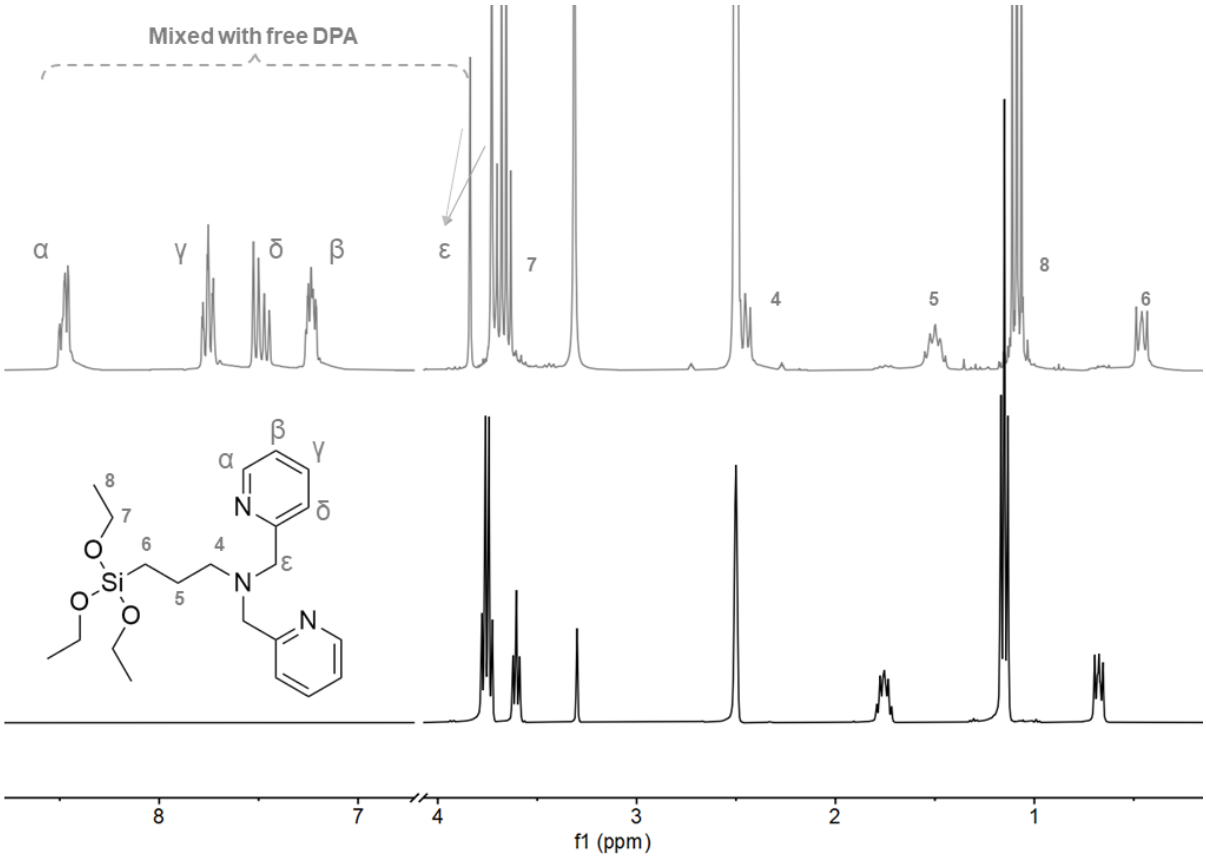

Firgure 2-12 The evolution in ^{1}H NMR of N,N-bis(pyridin-2-ylmethyl)-3-(triethoxysilyl)propan-1-amine (gray) from the reaction of (3-chloropropyl)triethoxysilane (black) and DPA.

2.3.2 Direct-functionalization

$(TBA)_3[PW_{11}O_{39}\{O(SiCH_2CH_2CH_2NMI)_2\}]$ (K_{Si}[NMI]-3)

Scheme 2-10 The direct-functionalization of ***K_{Si}[NMI]-3***

To the lacunary $K_7[PW_{11}O_{39}]$ in H_2O was added a solution of TBABr and 1-(tri-ethoxy-silyl-propyl)-3-methyl-imidazolium chloride in acetonitrile resulting a suspension. After about half an hour, 2.4 M HCl was added gradually with some bulk precipitate produced. The suspension was stirred overnight at room temperature, the sticky white precipitate was separated which was proved to be the right product by the following analysis, yield 60%. In the meantime, the liquid phase was rotary evaporated to remove most part of the solvent and precipitated in ethanol to yield just about 10%.

The significant chemical shift of the silane chain from (0.51 ppm,1.82 ppm and 4.14 ppm to 0.75 ppm, 2.04 ppm and 4.28 ppm) and the imidazole from (7.76 ppm and 9.23 ppm to 7.72 and 9.07 ppm) in ^{1}H NMR spectrum coupled with the characteristic stretch vibration at 1110 cm^{-1} in IR strongly indicate the successful covalent grafting. However, for the bulk gel product, there is just 1.5 eq. of TBA^+ which should be 3.0 eq. compared to the grafted organic group. As we known, the imidazolium was 1^+ charged that could result in the whole of the functionalized POM being less charged so that surrounding less TBA^+ which could explain why the bulk gel product is not soluble in acetonitrile. From the ^{31}P NMR, the only one single peak -13.2 ppm with a tiny side peak at 13.6 ppm.

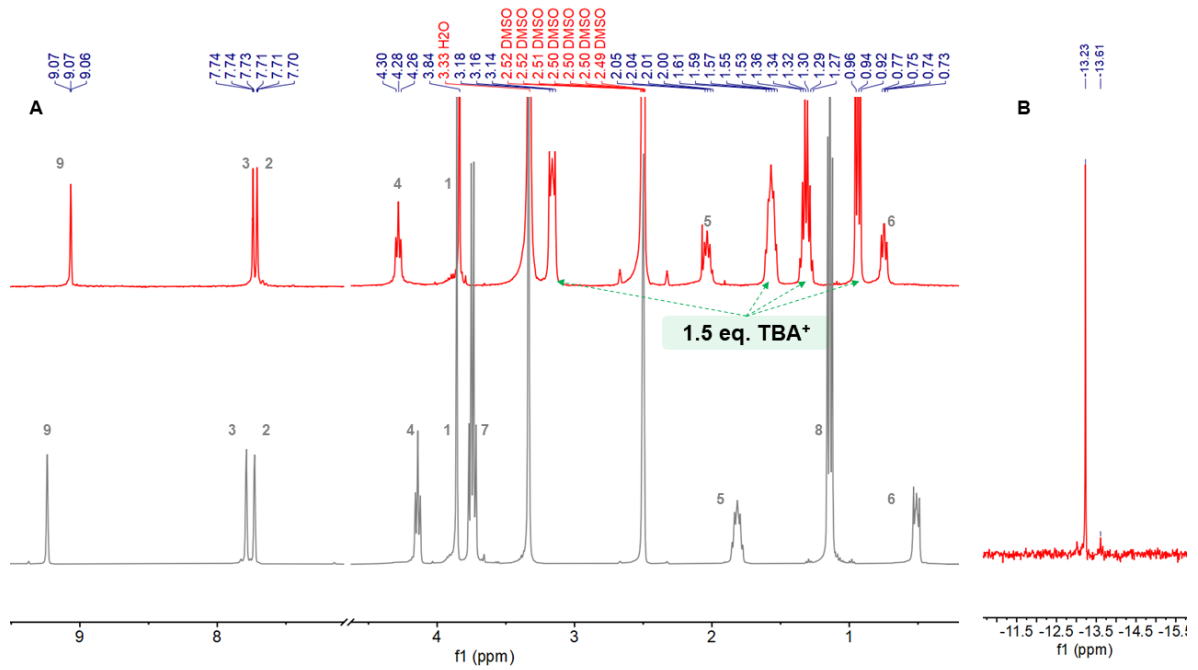

Figure 2-13 The ^{1}H NMR (A) ^{31}P NMR (B) of the direct-functionalization of ***K_{Si}[NMI]-3*** *(red) in DMSO.*

$(TBA)_3[PW_{11}O_{39}\{O(SiCH_2CH_2CH_2DPA)_2\}]$ (K_{Si}[DPA]-3)

Once the imidazolium was grafted, we tried N,N-bis(pyridin-2-ylmethyl)-3-(triethoxysilyl)propan-1-amine to directly graft onto the POM surface with the same grafting procedure.

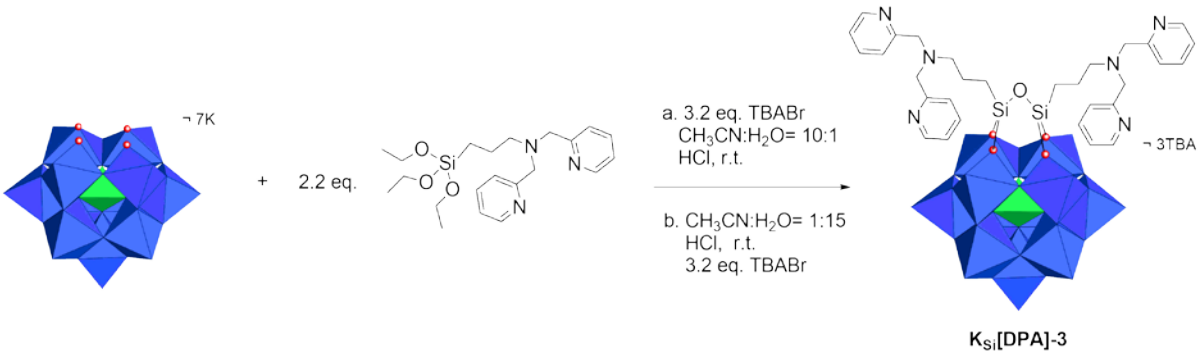

Scheme 2-11 The direct-functionalization of ***K_{Si}[DPA]-3****.*

Applying the same procedure as before, we observed a large amount of brown precipitate with the gradual addition of HCl. In ^{1}H NMR spectrum in DMSO of the precipitate, the aromatic region signals around 8.0 ppm companying with the barely visible phosphate signal in ^{31}P NMR indicated the precipitate was mainly DPA. But in the IR spectrum, as we

could observe in Figure 2-14 (red), the stretch at 957, 864, 809 and 768 cm^{-1} indicated POM skeleton was remained. The only one broad absorption at 1080 cm^{-1} was unlike the organosilyl functionalized polyoxometalates with an Si-O-Si bridge (~1110 cm^{-1}). Thus, it is likely that this isolated powder contains mainly $HDPA^+$, with a little bit of lacunary $[PW_{11}O_{39}]^{7-}$ as counter ion.

As we had observed before, the $HDPA^+$ is not soluble in acetonitrile, and this precipitation very likely hampers any reaction with the lacunary POM. We thus tried to increase the water proportion, as both the lacunary $K_7[PW_{11}O_{39}]$ and $HDPA^+$ are soluble in H_2O. To a mixture of $K_7[PW_{11}O_{39}]$ in H_2O and N,N-bis(pyridin-2-ylmethyl)-3-(triethoxysilyl)propan-1-amine dissolved in a minimum of acetonitrile, we added gradually 2.4 M HCl to adjust the pH to 1. Although this procedure also led to large amount of brown precipitate, interestingly, in IR (figure 2-14, black) of the precipitate, a clear Si-O-Si vibration at 1110 cm^{-1} can be observed together with the characteristic features of the POM skeleton around 900 cm^{-1}, suggesting at least partial grafting.

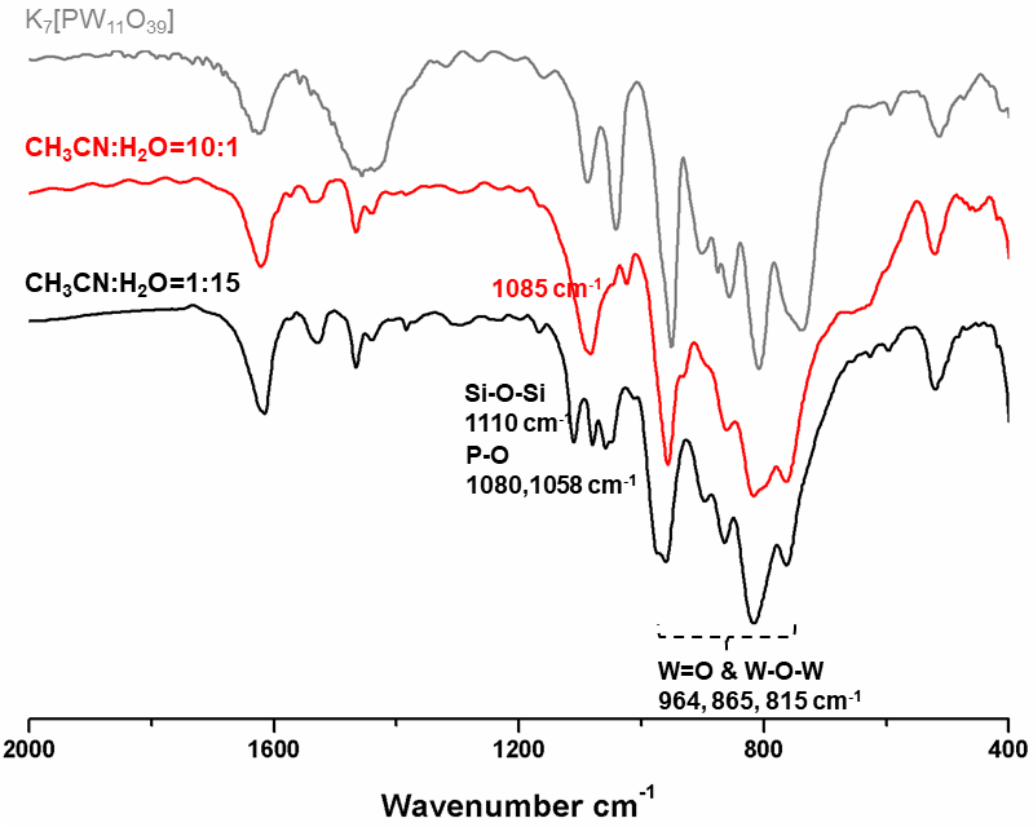

Figure 2-14 IR of the direct-functionalization of ***K_{Si}[DPA]-3*** *in solvent $CH_3CN:H_2O=10:1$ (red) and $CH_3CN:H_2O=1:15$ (black) compared to the $K_7[PW_{11}O_{39}]$(gray).*

Moreover, on the ^{1}H NMR, some broad signals at 3.2 ppm, 1.9 ppm and 0.6 ppm that could belong to the propylchain of the target product, are present (Figure 2-15), together with the DPA peaks. Unfortunately, we failed to purify this product no matter what approach we used, either by re-precipitation with aqueous TBABr solution or using cation exchange chromatography with TBA^{+} resin.

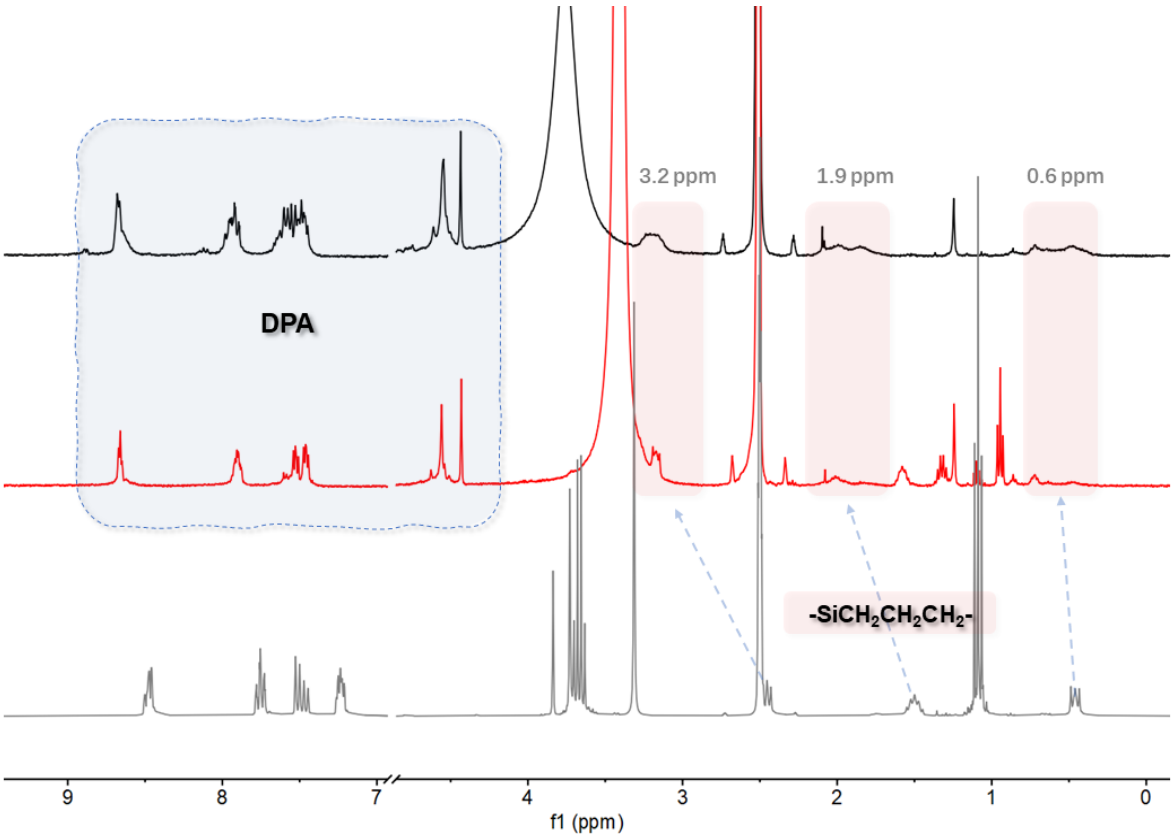

*Figure 2-15 The ^{1}H NMR of the direct-functionalization of **K_{Si}[DPA]-3** in solvent $CH_3CN:H_2O$=10:1 (red) and $CH_3CN:H_2O$=1:15 (black) compared to the organic precursor N,N-bis(pyridin-2-ylmethyl)-3-(triethoxysilyl)propan-1-amine (gray).*

2.4 Conclusion and perspective

In this section, we tried to expand the methodology of nucleophilic substitution to covalently graft polyamine onto the POM surface based on a newly synthesized a Keggin type platform, **K_{Si}[I]-1** through the substitution of iodo. Indeed, there are some variations upon the reaction no matter the color of the solution or the characterization with NMR or the IR. Unfortunately, it was proved to be the reduction or the degradation of the platform probably due to the polyamine, DPA. And also, we have tried to optimize the conditions trough modifying

the amount of DPA, change the base or tuning the oxidation states of the POM skeleton during the course of the reaction or treatment. But there was not improvement at all.

There are several hypotheses for the failure of the nucleophilic substation and the corresponding improvements: 1) One of the reasons could be the steric hindrance. The short methylene spacers result in the substitution sites quite near to the POM framework, that lead to the DPA could not get close to the sites. To overcome the steric hindrance, we need to prolong the spacers to ethylene or propylene or change it to other types of linkers that may sacrifice the communication of the POM with the anchoring terminals. 2) Another reason could be the protonation of DPA, which results in a decrease of the nucleophilic capability and being electrostatically attracted by the reduced POM. 3) Another improving approach is to find another suitable base without forming the cations, such as *tert*-butylimino-tri(pyrrolidino)phosphorane (BTPP).[16]

In the very recent work of parav-vogt,[17] they successfully performed substitution reaction with the doubly iodide-functionalized Wells−Dawson-type $[P_2W_{17}O_{62}]^{10-}$. They have proved that organosilyl-inserted $[\alpha_2\text{-}P_2W_{17}O_{61}]^{10-}$ could be stable in the nucleophilic substitution reaction. It encourages us to do further investigation on the nucleophilic substitution methodology of POM post-functionalization.

Experimental section

Synthesis of (Iodomethyl) triethoxysilane

4.2 g (28.2 mmol) of sodium iodide was dried under vacuum at 120℃ for 1 hour followed by the addition of 10 mL anhydrous acetonitrile. 2.1 g (9.4 mmol) (chloromethyl) triethoxysilane were slowly added into the resulting suspension. After being refluxing for 3 days, the resulting yellow suspension was filtered, and the filtrate was evaporated to until 2 mL followed by the addition of 10 mL diethyl ether to remove the sodium salt residue. The filtrate was rotary evaporated after the filtration. The resulting yellow liquid was significantly pure for the subsequent synthesis. Yield 85%. ^{1}H NMR (300 MHz, CD_3CN) δ 3.85 (q, *J* = 7.0 Hz, 6H), 2.01 (s, 2H), 1.21 (t, *J* = 7.0 Hz, 9H).

Synthesis of **K_{Si}[I]-1**:

$K_7[PW_{11}O_{39}]$ 2.0 g and 0.67 g TBABr were weighed and dissolved in 120 mL acetonitrile. Keep the solution at 0℃ and stir it for about 30 mins followed by adding 420 mg triethoxyl(iodomethyl)siline. Then adding 5 mL, 2.4 M HCl into the solution under 0℃ and keeping it at room temperature overnight. Filter the solution to remove the white solid and rotary evaporate the filtrate until about 5 mL and then precipitate the solution in 80mL ethanol. Wash the solid with 2*20 mL ethanol and 2*20 mL ether. And we get about 2.16 g light yellow powder. Yield 97.5%. ^{1}H NMR (400 MHz, DMSO) δ 3.23 – 3.10 (m, 24H), 2.15 – 2.06 (m, 4H), 1.64 – 1.52 (m, 24H), 1.32 (h, *J* = 7.4 Hz, 25H), 0.94 (t, *J* = 7.3 Hz, 36H). ESI-MS, detected: $\{TBA[PW_{11}O_{39}\{O(SiCH_2I)_2\}]\}^{2-}$ at m/z= 1637.14, calculated m/z= 1637.15

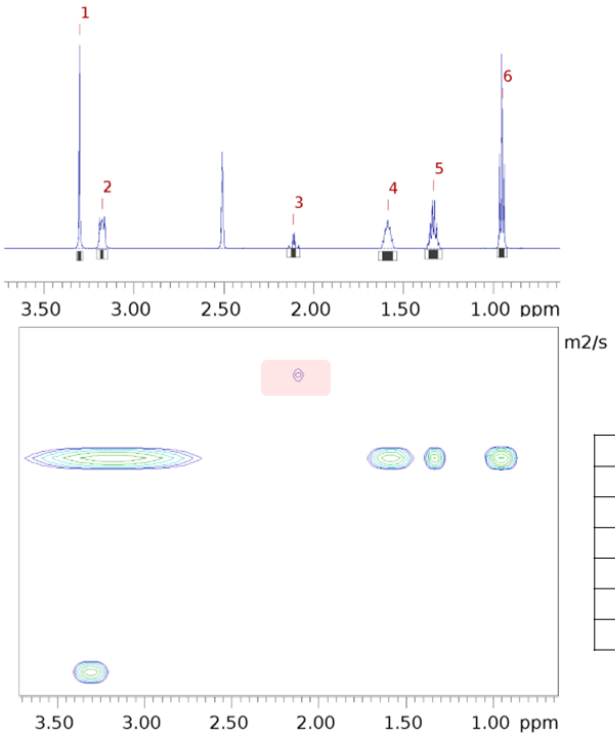

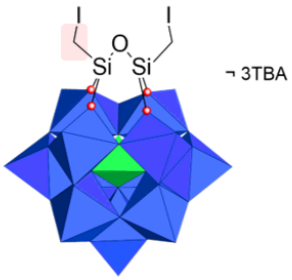

$K_{Si}[I]$-1

Peaks	Species	F2(ppm)	D(×10^{-10} m^2/s)	error×10^{-11}
1	H_2O	3.303	**10.30**	0.474
2	TBA	3.177	**2.75**	0.084
3	$SiCH_2$	2.112	**1.63**	0.031
4	TBA	1.588	**2.74**	0.022
5	TBA	1.333	**2.75**	0.072
6	TBA	0.953	**2.75**	0.069

Synthesis of bis(pyridin-2-ylmethyl)amine (DPA)

The bis(pyridin-2-ylmethyl)amine (DPA) was prepared by reductive amination reaction according to the modified procedure published by Lee.[18] 2-aminomethylpyridine (2,00 g, 18.5mmol, 1.0 equiv) was dissolved in 36mL methanol followed by dropwise addition 2-pyridylcarboxaldehyde (1.98 g, 18.5mmol, 1.0 eq.). After stirring the solution for 30 minutes, $NaBH_4$ (1.40g, 37.0mmol, 2.0 eq.) was added into the yellow solution and kept at room temperature overnight. HCl (48mL, 5.0M, 13.0 equiv) was then added into the yellow solution. After stirring for about 1 hour, 10M NaOH was poured into the solution to adjust the pH to 12. The yellow solution was extracted with 3*50mL dichloromethane, then the organic phase was evaporated to give a slightly yellow oil. For further purification, the yellow oil was dissolved into 25mL ethanol followed by the addition of HCl (12.5mL, 5M, 3.5 equiv). The solution was added into 500mL acetonitrile resulting in a large amount of white crystal. The white crystal was redissolved into 20mL H_2O followed by the addition of 10M NaOH to adjust the pH to 12-14. Then the resulting solution was extracted with 3*40mL dichloromethane. The organic solvent was evaporated after being dried with anhydrous $NaSO_4$ and resulting in a slight yellow oil (3.29g, yield 83%). ^{1}H NMR (400 MHz, DMSO) δ 8.49 (d, *J* = 4.5 Hz, 2H), 7.75 (td, *J* = 7.6, 1.9 Hz, 2H), 7.46 (d, *J* = 7.8 Hz, 2H), 7.24 (dd, *J* = 7.0, 5.3 Hz, 2H), 3.82 (s, 4H).

Synthesis of 1-(tri-ethoxy-silyl-propyl)-3-methyl-imidazolium chloride

The procedure was following the publish of Sun 1.62 g, 0.02 mol1-methyl-1H-imidazole (NMI) and 4.82 g, 0.02 mol (chloropropyl) triethoxysilane was mixed under N_2. The resulting a slightly brown liquid was stirred at 90℃ for 54 hours, followed by the extraction of diethyl ether for 3 times (3*20 mL) and the residue was dried at room temperature. ^{1}H NMR (400 MHz, DMSO) δ 9.24 (s, 1H), 7.79 (t, *J* = 1.8 Hz, 1H), 7.75 – 7.70 (m, 1H), 4.14 (t, *J* = 7.2 Hz, 2H), 3.86 (s, 3H), 3.79 – 3.69 (m, 6H), 1.88 – 1.75 (m, 2H), 1.14 (t, *J* = 7.1 Hz, 9H), 0.55 – 0.47 (m, 2H).

Synthesis of N,N-bis(pyridin-2-ylmethyl)-3-(triethoxysilyl)propan-1-amine

428.6 mg, 2.0 mmol DPA and 361.2 mg, 1.5 mmol (chloropropyl) triethoxysilane was put in a well dried round-bottomed flask. The resulting a slightly brown liquid was stirred at 90℃ for 66 hours, followed by washing with diethyl ether for 3 times (3*20 mL), the precipitate was discarded while the organic phase was rotary evaporated and distillated to remove unreacted the (chloropropyl) triethoxysilane. The resulting dark gel was used without further purification.

Synthesis of K_{Si}[NMI]-3

600 mg 0.187 mmol $K_7[PW_{11}O_{39}]$ and 192 mg 0.598 mmol TBABr were dissolved in 7.5 mL acetonitrile followed by the addition of 118.5 mg 0.412 mmol which was dissolved in 2.5 mL acetonitrile. The resulting solution was stirred for about 30 mins followed by adding 1.6 mL, 2.4 M HCl at room temperature resulting bulk precipitate. The resulting suspension was kept at room temperature for overnight followed by the centrifuge to separate the white gel solid and solution. The solid was washed with water for 3 times resulting 377 mg white powder (yield 60%, A_1). While the filtrate was rotary evaporated to until 5 mL and then precipitated in 80mL ethanol resulting 63 mg white powder (yield 10%, A_2). A_1: ^{1}H NMR (400 MHz, DMSO) δ 9.07 (d, *J* = 1.7 Hz, 2H), 7.72 (dt, *J* = 12.1, 1.9 Hz, 4H), 4.28 (t, *J* = 7.3 Hz, 4H), 3.84 (s, 6H), 3.21 – 3.12 (m, 11H), 2.04 (dd, *J* = 15.1, 7.7 Hz, 4H), 1.57 (p, *J* = 7.8 Hz, 12H), 1.31 (h, *J* = 7.4 Hz, 11H), 0.94 (t, *J* = 7.3 Hz, 16H), 0.75 (dd, *J* = 9.2, 6.6 Hz, 4H). ^{1}P NMR (162 MHz, DMSO) δ -13.23, -13.61(tiny).

Reference:

(1) Vanhaecht, S.; Quanten, T.; Parac-Vogt, T. N. A Simple Nucleophilic Substitution as a Versatile Postfunctionalization Method for the Coupling of Nucleophiles to an Anderson-Type Polyoxometalate. *Inorg. Chem.* **2017**, *56* (5), 3095–3101.

(2) Que, L., Jr.; Tolman, W. B. Bis(μ-Oxo)Dimetal "Diamond" Cores in Copper and Iron Complexes Relevant to Biocatalysis. *Angewandte Chemie International Edition* **2002**, *41* (7), 1114–1137.

(3) Knoth, W. H. Derivatives of Heteropolyanions. 1. Organic Derivatives of $W_{12}SiO_{40}^{4-}$, $W_{12}PO_{40}^{3-}$, and $Mo_{12}SiO_{40}^{4-}$. *J. Am. Chem. Soc.* **1979**, *101* (3), 759–760.

(4) Duffort, V.; Thouvenot, R.; Afonso, C.; Izzet, G.; Proust, A. Straightforward Synthesis of New Polyoxometalate-Based Hybrids Exemplified by the Covalent Bonding of a Polypyridyl Ligand. *Chemical Communications* **2009**, *0* (40), 6062–6064.

(5) Matt, B.; Coudret, C.; Viala, C.; Jouvenot, D.; Loiseau, F.; Izzet, G.; Proust, A. Elaboration of Covalently Linked Polyoxometalates with Ruthenium and Pyrene Chromophores and Characteriation of Their Photophysical Properties. *Inorg. Chem.* **2011**, *50* (16), 7761–7768.

(6) Matt, B.; Renaudineau, S.; Chamoreau, L.-M.; Afonso, C.; Izzet, G.; Proust, A. Hybrid Polyoxometalates: Keggin and Dawson Silyl Derivatives as Versatile Platforms. *The Journal of Organic Chemistry* **2011**, *76* (9), 3107–3112.

(7) Li, Q.; Zhang, J.; Wang, L.; Hao, J.; Yin, P.; Wei, Y. Nucleophilic Substitution Reaction for Rational Post-Functionalization of Polyoxometalates. *New Journal of Chemistry* **2016**, *40* (2), 906–909.

(8) Sorokin, M. S.; Lopyrev, V. A.; Chipanina, N. N.; Sherstyannikova, L. V.; Voronkov, M. G. S-(Trimethoxysilylmethyl)- and S-(Silatranylmethyl)Isothiuronium Halides and Their N-Substituted Derivatives. *Russian Journal of General Chemistry* **2004**, *74* (4), 551–558.

(9) Li, Q.; Peng, Y.; Qian, J.; Yan, T.; Du, L.; Zhao, Q. A Family of Planar Hexanuclear $Co^{III}_4Ln^{III}_2$ Clusters with Lucanidae-like Arrangement and Single-Molecule Magnet Behavior. *Dalton Trans.* **2019**, *48* (34), 12880–12887.

(10) Silva, A. C.; Fernández, T. L.; Carvalho, N. M. F.; Herbst, M. H.; Bordinhão, J.; Jr, A. H.; Wardell, J. L.; Oestreicher, E. G.; Antunes, O. A. C. Oxidation of Cyclohexane Catalyzed by Bis-(2-Pyridylmethyl)Amine Cu(II) Complexes. *Applied Catalysis A: General* **2007**, *317* (2), 154–160.

(11) Chomitz, W. A.; Minasian, S. G.; Sutton, A. D.; Arnold, J. Synthesis and Reactivity of Metal Complexes Supported by the Tetradentate Monoanionic Ligand Bis(2-Picolyl)(2-Hydroxy-3,5-Di- *Tert* -Butylbenzyl)Amide (BPPA). *Inorg. Chem.* **2007**, *46* (17), 7199–7209.

(12) Pellegrin, Y.; Odobel, F. Sacrificial Electron Donor Reagents for Solar Fuel Production. *Comptes Rendus Chimie* **2017**, *20* (3), 283–295.

(13) Matt, B.; Moussa, J.; Chamoreau, L.-M.; Afonso, C.; Proust, A.; Amouri, H.; Izzet, G. Elegant Approach to the Synthesis of a Unique Heteroleptic Cyclometalated Iridium(III)-Polyoxometalate Conjugate. *Organometallics* **2012**, *31* (1), 35–38.

(14) Fu, G. C. Transition-Metal Catalysis of Nucleophilic Substitution Reactions: A Radical Alternative to S_N1 and S_N2 Processes. *ACS Central Science* **2017**, *3* (7), 692–700.

(15) Zhou, Y.; Liu, J.; Huang, R.; Zhang, M.; Xiao, M.; Meng, Y.; Sun, L. Covalently Immobilized Ionic Liquids on Single Layer Nanosheets for Heterogeneous Catalysis Applications. *Dalton Trans.* **2017**, *46* (38), 13126–13134.

(16) Matier, C. D.; Schwaben, J.; Peters, J. C.; Fu, G. C. Copper-Catalyzed Alkylation of Aliphatic Amines Induced by Visible Light. *Journal of the American Chemical Society* **2017**, *139* (49), 17707–17710.

(17) Anyushin, A. V.; Vanhaecht, S.; Parac-Vogt, T. N. A Bis-Organosilyl-Functionalized Wells–Dawson Polyoxometalate as a Platform for Facile Amine Postfunctionalization. *Inorganic Chemistry* **2020**, *59* (14), 10146–10152.

(18) Wong, Y.-L.; Mak, C.-Y.; Kwan, H. S.; Lee, H. K. Mononuclear Iron(III) Complexes Supported by Tripodal N3O Ligands: Synthesis, Structure and Reactivity towards DNA Cleavage. *Inorganica Chimica Acta* **2010**, *363* (6), 1246–1253.

Chapter 3

Post-functionalization of Keggin-type and the complexation

Chapter 3 Post-functionalization of Keggin-type polyoxometalates and the complexation

To perform covalent post-functionalization of POMs, first, appropriate organic functional group need to be grafted on the polyoxometalates skeleton. Among them, iodo aryl, terminal alkyne, azido groups appear to be promising candidates as they have already been used for post-functionalization of POMs in mild conditions .[1–9]

3.1 Mono functionalization of Keggin $[PW_{11}O_{39}]^{7-}$ through "Sonogashira" coupling

Iodo aryl groups can be involved in palladium-catalyzed C-C coupling reactions.[10] particular, "Sonogashira" couplings are attractive since they allow the grafting of organic moieties under mild conditions which could be employed in the functionalization of the polyoxometalates. In the past decade, many successful cases have been achieved [1,3–5,11] to graft organic moieties onto POMs. In this section, we would like to introduce the exploration of the grafting of alkyne modified DPA on the iodo phenyl grafted Keggin precursor through "Sonogashira" coupling. And then make the complex of the synthesized POM ligand followed by the investigation of the redox properties and catalytic activities of it.

3.1.1 Synthesis of I-iodo-4-(trichlorotin) Benzene

The precursor, I-iodo-4-(trichlorotin) Benzene was synthesized according to the procedure published by Proust.[12] First, 1,4-diiodobenzene was activated by Grignard reagent, iPrMgCl in freshly distilled THF at -30℃, leading to the substitution of one of the iodide. Then, the resulting 4-iodophenylmagnesium chloride solution was canulated into trimethyltin chloride resulting in the substituted product 1-Iodo-4-(trimethyltin)benzene. Finally, the three methyl of 1-Iodo-4-(trimethyltin)benzene were replaced by chloride with large excess of tin(IV) chloride resulting I-iodo-4-(trichlorotin) Benzene. As we can observe in the ^{1}H NMR, after the substitution of methyl with chloride, there are two clean aromatic peaks around 7.98 ppm and 7.37 ppm that belong to the monomer I-iodo-4-(trichlorotin) Benzene according to the literature. Then we tried to distill out the excess of $SnCl_4$ and the side-products tin methyl derivatives

$SnCl_x(CH3)_{4-x}$ at 110℃ under reduce pressure, monitoring the advancement of the reaction with ^1H NMR. The decrease of the methyl signals indicated the $SnCl_x(CH_3)_{4-x}$ was distilled out and there should not be any $SnCl_4$ due to the lower boiling point compared to the methyl derivatives. But to our surprise, a new set of aromatic signals appeared at 7.89 ppm and 7.40 ppm (Figure 3-1 & 3-2). Our hypothesis is that the I-iodo-4-(trichlorotin) Benzene could substitute each other to form the dimer once the $SnCl_4$ was distilled out at high temperature.

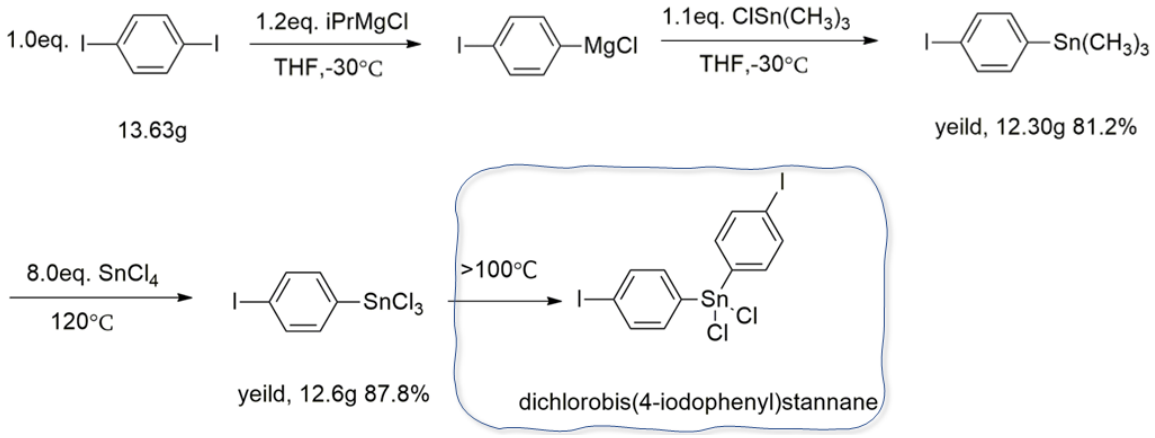

Scheme 3-1 The synthesis route of I-iodo-4-(trichlorotin) Benzene and the proposal dimerization.

This hypothesis was substantiated by the fact that the signals at 7.89 ppm and 7.40 ppm increased when raising the temperature at 120℃. To reverse this equilibrium, we added more $SnCl_4$, in order to shift the reaction back toward the monomer: once the methyl derivative was completely distilled out, another 8 equivalents of $SnCl_4$ were added into the remaining gray solid. The resulting suspension was heated at 70℃ for 3 hours followed by the distillation at 70℃ to remove the excess of $SnCl_4$ and traces of the methyl derivative. The remaining residue was then used without further purification, as it was quite clean from the proton NMR.

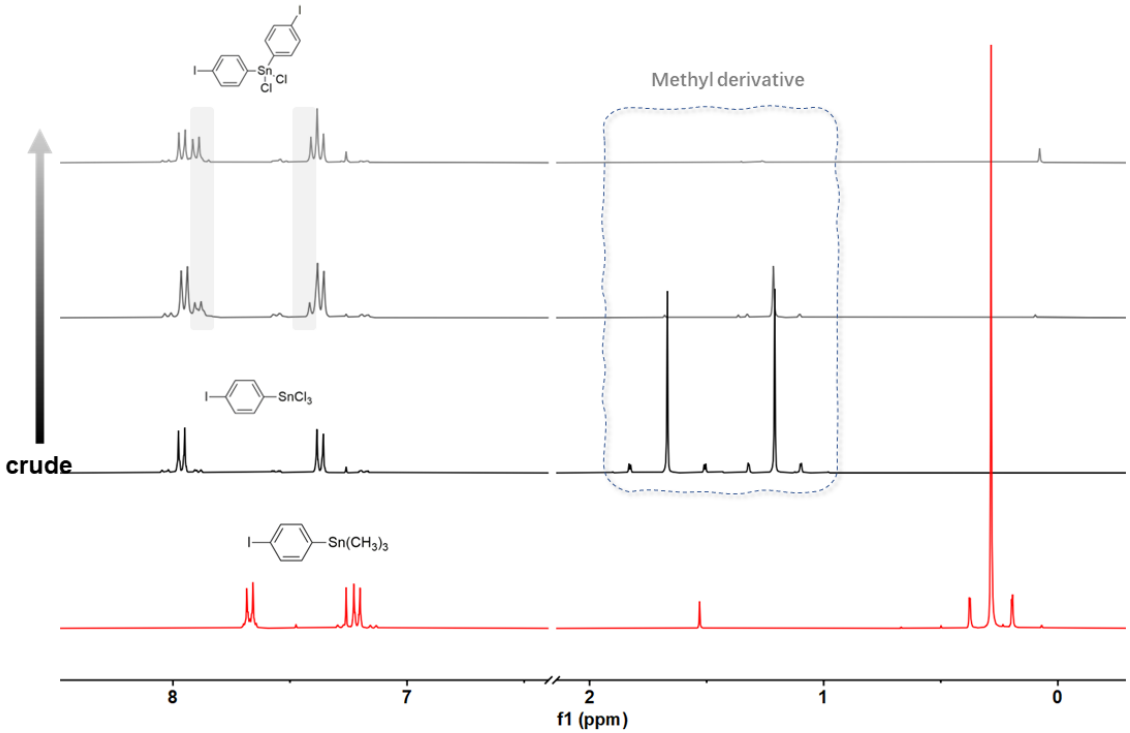

Figure 3-1 ^{1}H NMR monitor of the synthesis of I-iodo-4-(trichlorotin) Benzene from1-Iodo-4-(trimethyltin)benzene; and the distillation to remove the methyl derivatives.

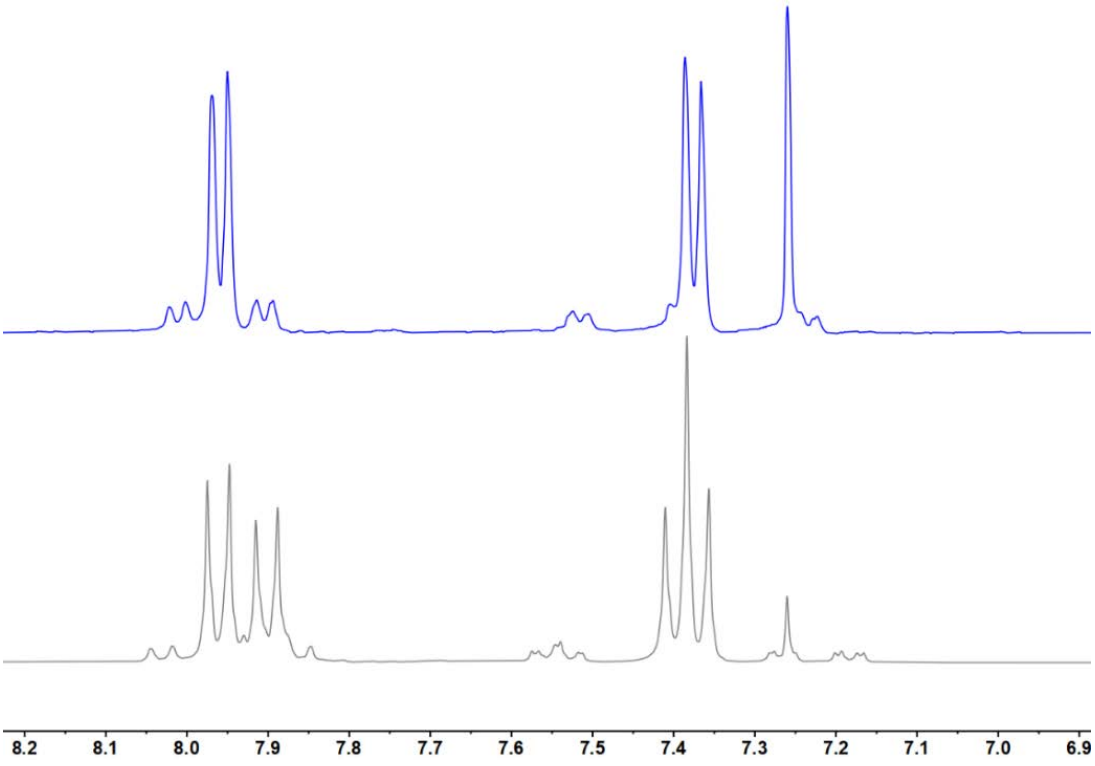

Figure 3-2 Zoom of the aromatic region of ^{1}H NMR of the de-dimerization process. Bottom before and top after reaction with $SnCl_4$.

3.1.2 Synthesis of propargyl DPA

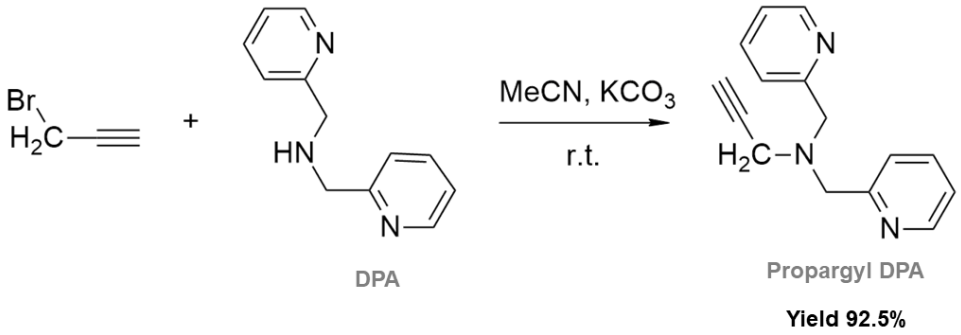

Scheme 3-2 The terminal alkyne modification of DPA to form N,N-bis(pyridin-2-ylmethyl)prop-2-yn1-amine (propargyl DPA)

In order to perform “Sonogashira” or Huisgen couplings, we need to functionalize our ligand with a terminal alkyne moiety.[13,14]Thus, DPA-H was dissolved in dry acetonitrile followed by the additon of anhydrous K_2CO_3, and then 3-bromoprop-1-yne was added dropwise into the resulting yellow solution under N_2 atmosphere and kept at room temperature for three days. Dichloromethane was added into the resulting suspension to precipitate the excess of K_2CO_3. The solvent of the resulting yellow filtrate was evaporated until getting a dark brown oil which was chromatographied with basic alumina eluting with dichloromethane. Upon evaporation of the solvent, a brown oil was isolated in almost quantitative yield.

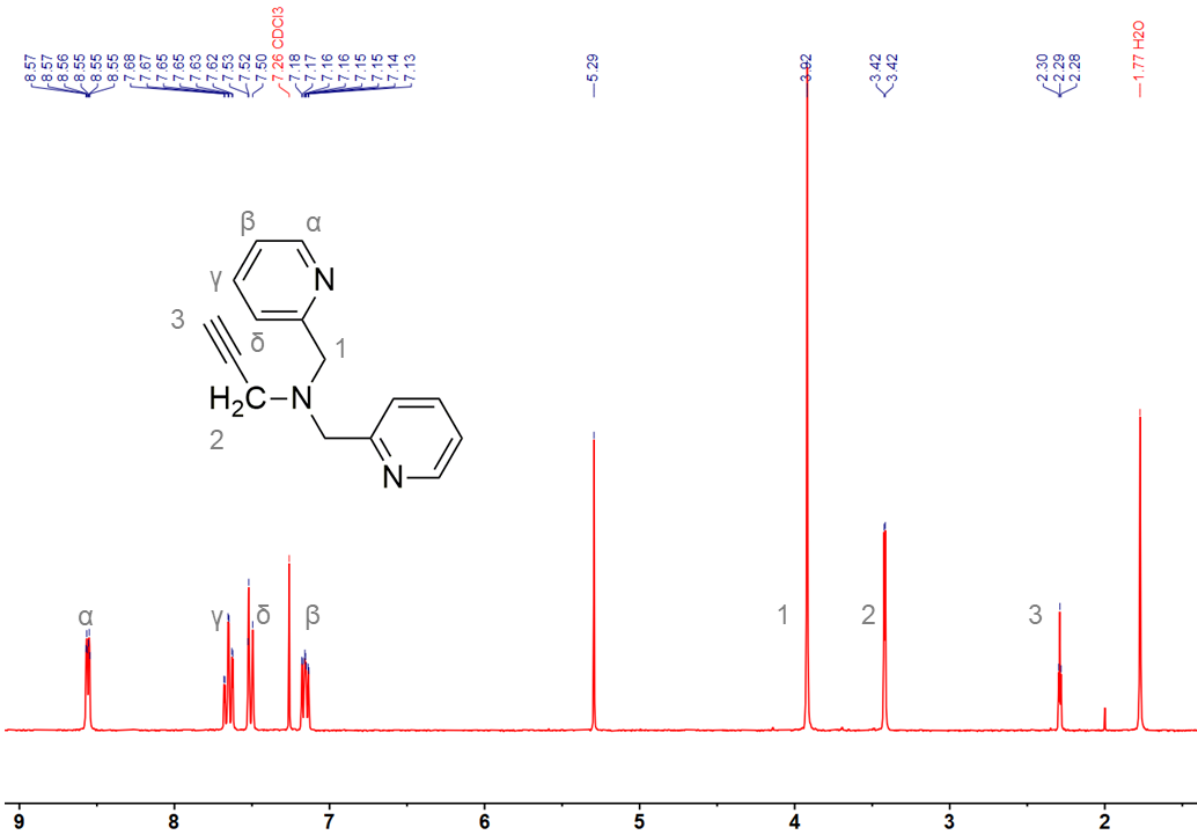

Figure 3-3 ^{1}H NMR of propargyl DPA

3.1.3 Synthesis of K_{Sn}[I]

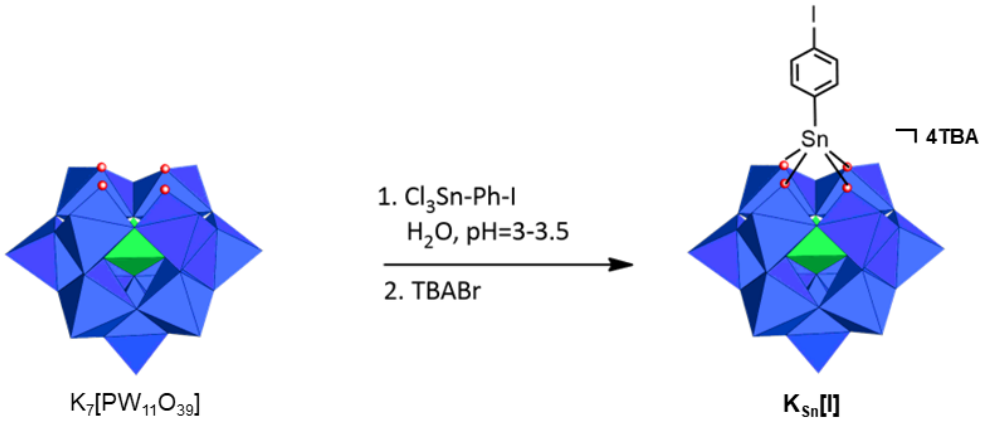

*Scheme 3-3 The synthesis of **K_{Sn}[I]***

Synthesis of the Keggin POM-based platform $TBA_4[PW_{11}O_{39}\{Sn(C_6H_4I)\}]$ (named **K_{Sn}[I]**) was performed following a general procedure,[15–17] through the reaction between the monovacant $[PW_{11}O_{39}]^{7-}$ and a slight excess of 1-iodo-4-(trichlorotin)benzene in water.

Increasing the pH from ~1 to 3 by addition of aliquots of a KOH solution prevented the competitive formation of the complete $[PW_{12}O_{40}]^{3-}$. After filtration of the solution, the addition of tetrabutylammonium bromide (TBABr) led to the precipitation of the POM as a TBA salt. Its purity was attested by ^{1}H and ^{31}P NMR spectroscopy. The obvious coupling between the phosphate and tin in the ^{31}P NMR indicates the successful grafting of the tin moiety onto the Keggin POM skeleton and the unique phosphate peak at 11.63 ppm means there is only one kind of POM skeleton without any degradation. Moreover, the ^{1}H NMR spectrum of **K_{Sn}[I]** presents only one set of resonances for the aryl group at 7.85 and 7.46 ppm together with the TBA^{+} signature in the proton NMR, which further confirms the successful grafting and the purity of the grafted **K_{Sn}[I]**.

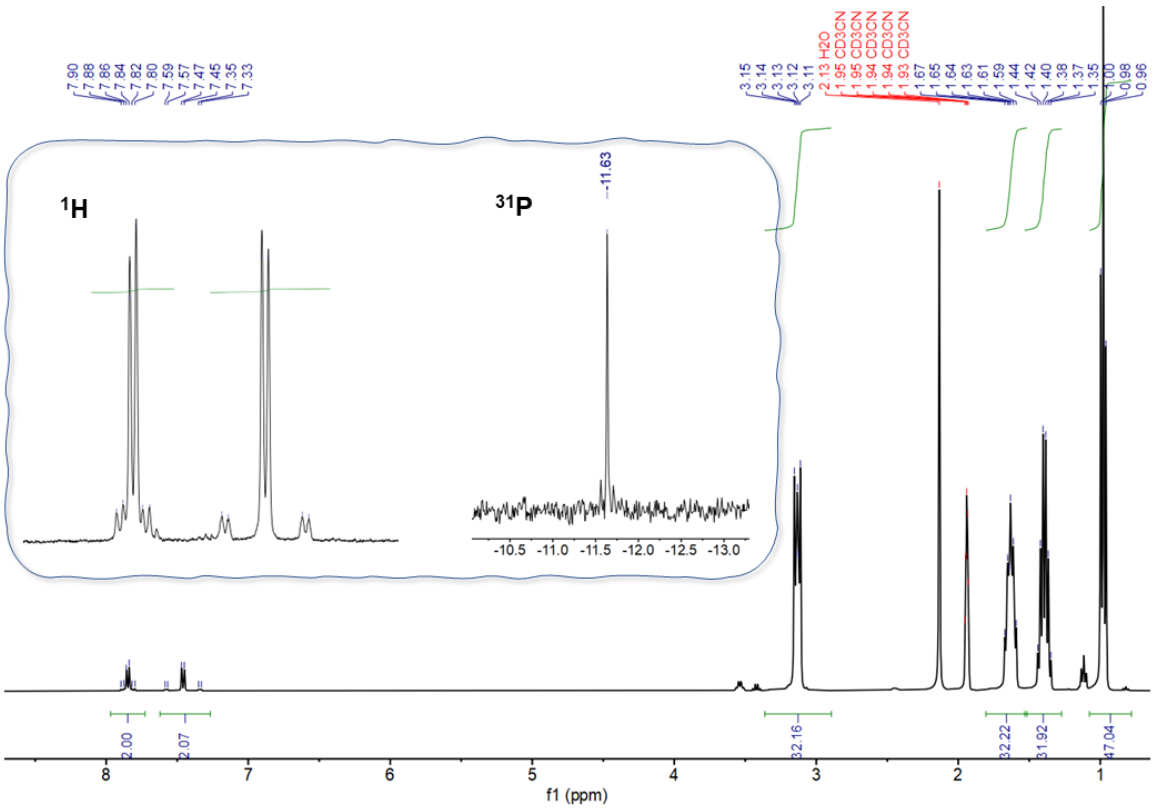

*Figure 3-4 ^{1}H NMR and ^{31}P NMR (insert) of **K_{Sn}[I]** in CD_3CN.*

3.1.4 Synthesis of K_{Sn}[DPA]

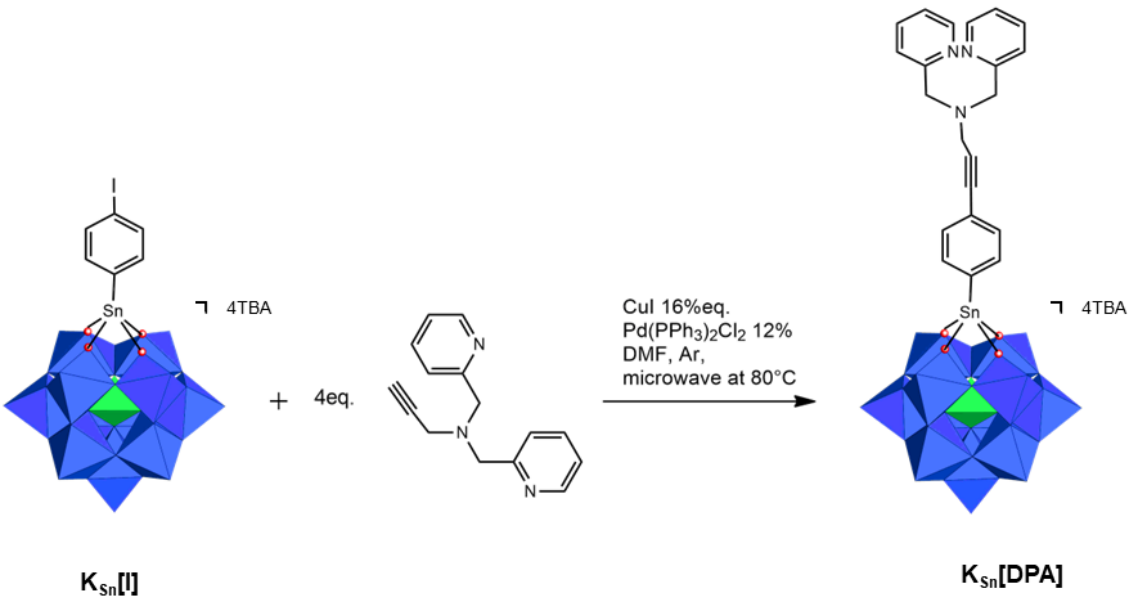

*Scheme 3-4 The synthesis of $TBA_4[PW_{11}O_{39}SnC_6H_4CCCH_2DPA]$ (**K_{Sn}[DPA]**)*

The “Sonogashira” couplings are attractive since they allow the grafting of organic moieties under relatively mild conditions. We started our exploration according to the literature, which was published by our group.[13,18] First, we applied 16% CuI and 12% $Pd(PPh_3)_2Cl_2$ as the co-catalysts to launch the reaction with the presence of 20 eq. triethylamine, which works as base to activate the alkyne, under argon atmosphere at room temperature in DMF. After being stirred for 16 hours, the reaction was analyzed with ^{1}H NMR after precipitation with diethyl ether.

As can be seen on the ^{1}H NMR (Figure 3-5), the signals of the organic moiety are quiet broad which makes it hard to analyze. This may come from the coordination of Cu or Pd to the DPA or protonation of the organic moieties.

To check if protonation is indeed at stake, TBAOH was added as the base. Thus, the crude dark brown solid was redissolved in CD_3CN, and then 0.1 M TBAOH was gradually added into it which was monitored with ^{1}H NMR after precipitate with diethyl ether (Figure 3-5). Indeed, the profile of the aromatic region became more and more sharp. After a total of 1.5 eq. TBAOH was added. The high resolution of NMR profile indicates the deprotonation could a pathway to purify the product.

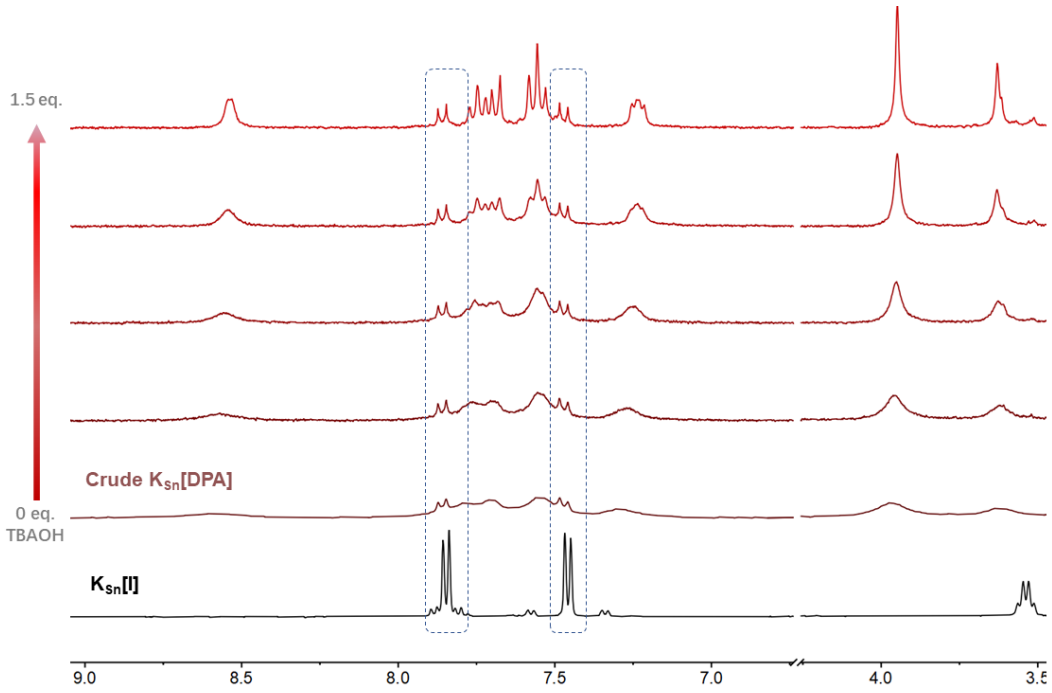

*Figure 3-5 The deprotonation of synthesized crude **K_{Sn}[DPA]** with TBAOH.*

It also clearly showed us two peaks, 7.85 ppm and 7.53 ppm, which belongs the starting **K_{Sn}[I].** As the starting material and the DPA grafted product have very similar physicochemical properties and difficult to separate, we thus tried to push the reaction to full conversion, by optimizing the conditions. As there was barely any influence on the conversion when we increased the amount CuI, which indicated that the catalyst was not the key factor for the conversion, we focused on the ratio of the reactants and the temperature (Table 3-1).

Table 3-1 The optimizing conditions

entry	Propargyl DPA	CuI, $Pd(PPh_3)_2Cl_2$	T	t
1	2 eq.	16%, 12%	r.t.	42 h
2	4 eq.	16%, 12%	r.t.	42 h
3	4 eq.	16%, 12%	70℃	2 h
4	4 eq.	16%, 12%	80℃	1 h

In the ^{1}H NMR of the products after being deprotonated with TBAOH (Figure 3-6), a diminution of the residual starting POM is observed, with a complete disappearance once 4 equivalents of propargyl DPA are added. This ratio has been kept for further optimization.

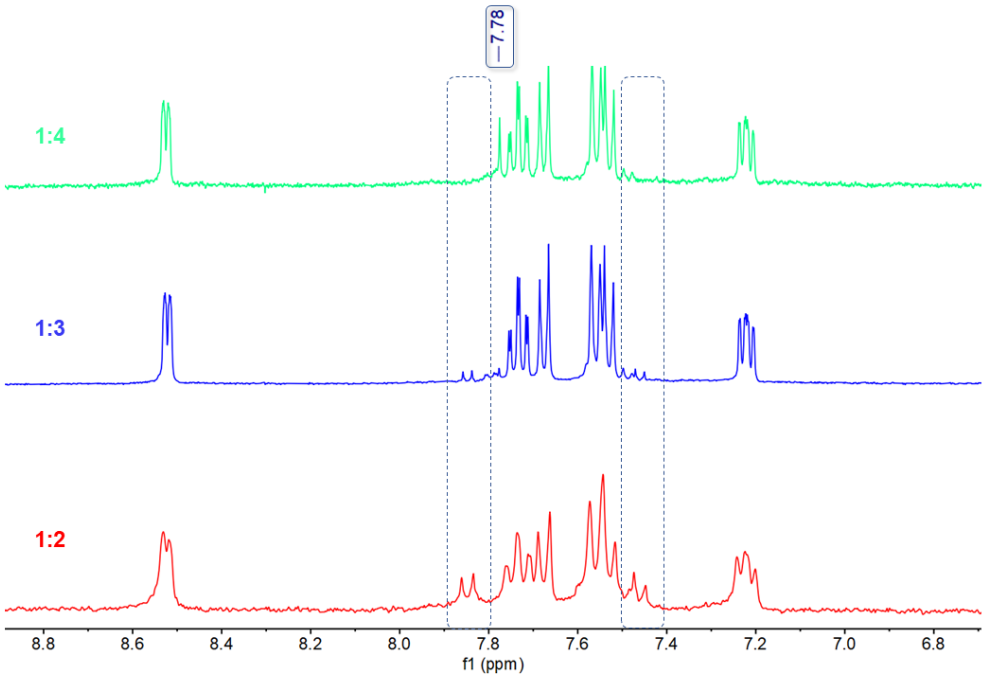

*Figure 3-6 ^{1}H NMR (in CD_3CN) of **K_{Sn}[DPA]** after the treatment with TBAOH, produced with different ratio of **K_{Sn}[I]** and propargyl DPA 1:2, 1:3 and 1:4 in presence of 16% CuI, 12% $Pd(PPh_3)_2Cl_2$ and 20 eq. TEA in DMF.*

In order to speed up the reaction, we checked microwave heating as we know from the literature, microwave heating could dramatically speed up the "sonogashira" reaction in POM functionalization.[1] We launched the coupling reaction at 70 ℃ and 80 ℃ with microwave irradiation, monitoring the evolution via proton NMR after precipitating the crude dark red solution in diethyl ether. Compared to the room temperature experiment, which lasted for 2 days, there was less starting material attested by the peaks at 7.85 ppm and 7.53 ppm at 70℃, while we observed almost full conversion at 80 ℃ after one hour heating with microwave irradiation. Thus one hour microwave irradiation at 80℃ was applied in the following synthesis.

In the dark brown obtained via these optimized conditions after the treatment with TBAOH, there is an additional singlet at 7.78 ppm in ^{1}H NMR which we failed to identify. According to Proust and coworkers[12,18], impurity in hybrid POMs can be removed through playing on the solubility in different solvents. Ethyl acetate, as a bad solvent, was thus added gradually into the hybrid-POM acetonitrile solution. Interestingly, impurities precipitated out

first while the solution turned to colorless. The dark precipitate was discarded, and the resulting colorless supernatant was precipitate in diethyl ether, as a slightly yellow powder in reasonable yields (about 35%).

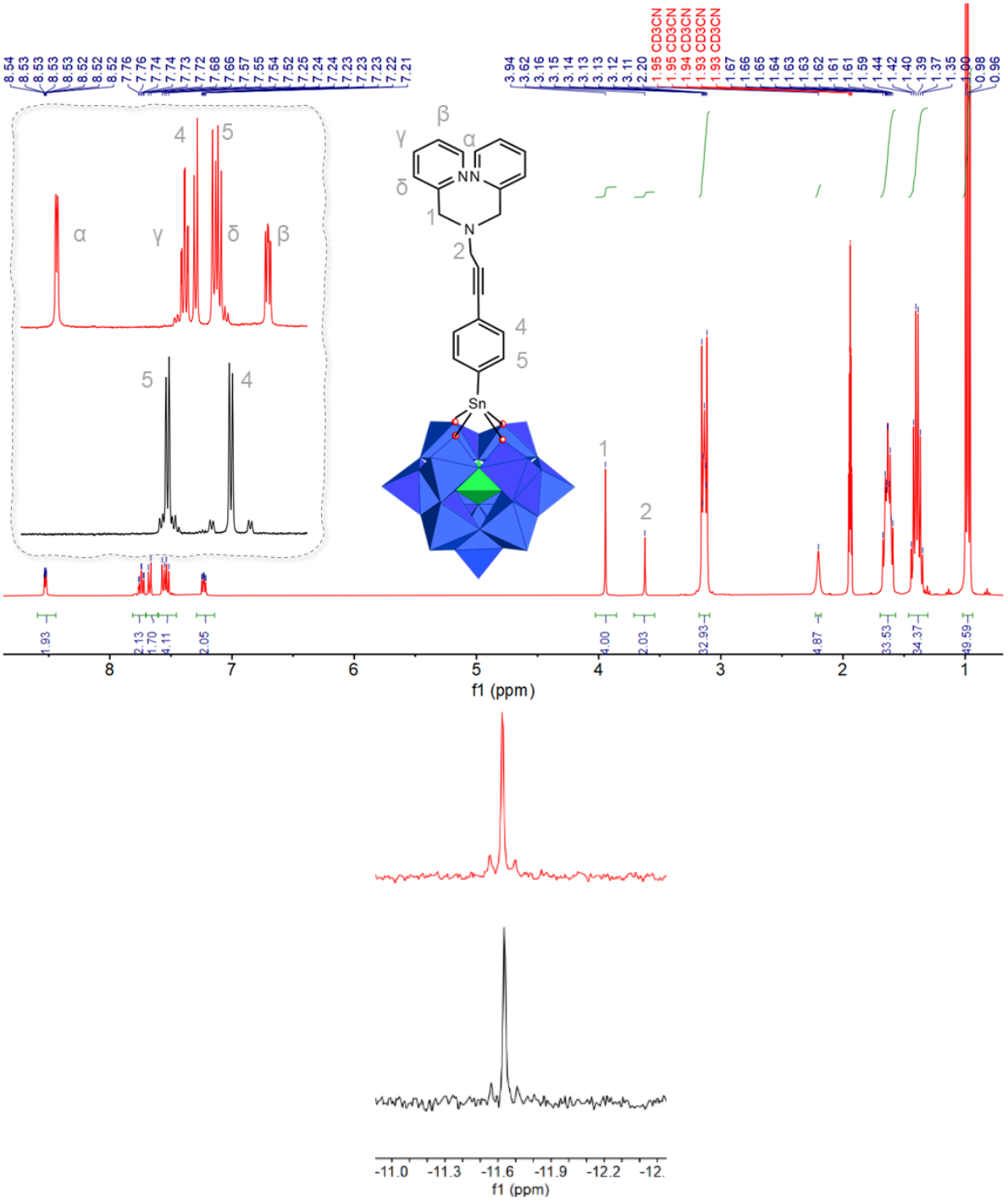

*Figure 3-7 ^{1}H NMR and ^{31}P NMR of **K_{Sn}[DPA]** after purification in CD_3CN.*

At this stage, a very satisfying ^{1}H NMR, especially around the aromatic peaks, is obtained (Figure 3-7). In ^{31}P NMR, the unique peak presents a slight chemical shift to -11.62

ppm compared to -11.63 ppm for the starting materiel, thus confirming a clean product without POM skeleton degradation during the synthesis. This is also confirmed by the infrared spectrum (Figure 3-15, red), where the POM skeleton characteristic bands at 1071, 963, 885, and 813 cm^{-1} remained compared to the precursor **K_{Sn}[I]** (Figure 3-15, black), while the two new features at 1593 and 1570 cm^{-1} could be the absorption of the grafted pyridines. The successful synthesis was further confirmed by the ESI-mass spectrum, which shows a nice tungstate isotopic distribution pattern of a tri-anionic species at m/z=1037.09, corresponding to **{HK_{Sn}[DPA]}$^{3-}$**, and ultimately by elemental analysis.

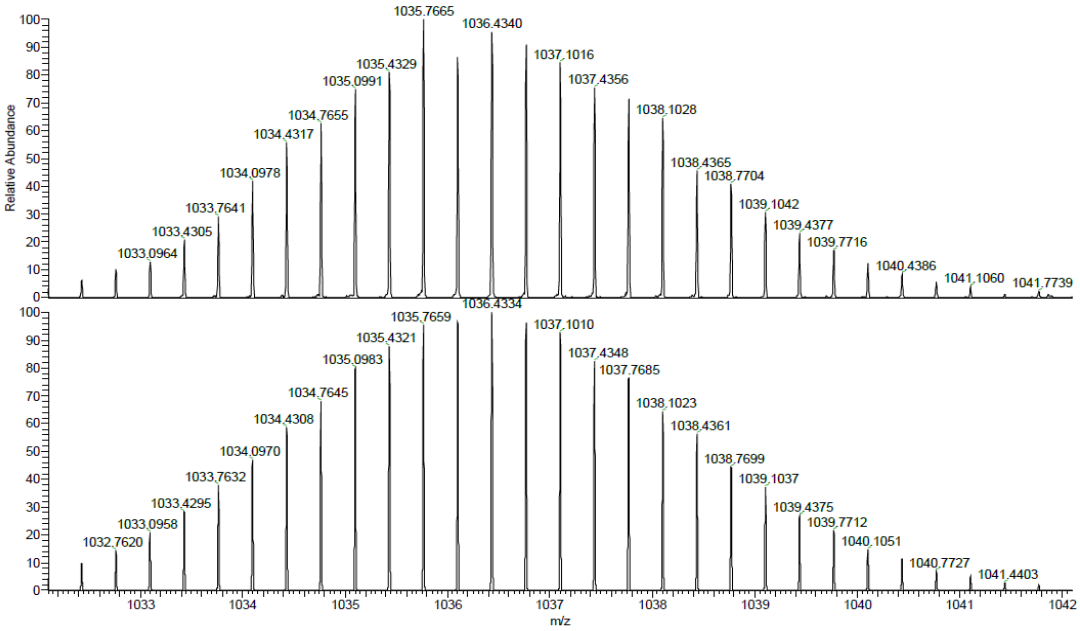

*Figure 3-8 The ESI-MS of **K_{Sn}[DPA]** which gives the formular **{HK_{Sn}[DPA]}$^{3-}$**.*

Attempts to grow crystal of the synthesized organic moiety functionalized Keggin polyoxometalates through diethyl ether diffusion into concentrated acetonitrile solution, led to quite nice cube crystals, but they were not suitable for the single crystal X-ray diffraction.

3.1.5 Complexation investigation of K_{Sn}[DPA]

Complexation of $ZnCl_2$ with K_{Sn}[DPA]

In order to test the coordination ability of the **K_{Sn}[DPA]**, we started with the diamagnetic metal salt $ZnCl_2$, so that we could monitor the complexation process through NMR. As can be seen (Figure 3-9), the group of pyridine peaks (α, 8.59 ppm, β, 7.32 ppm, δ, 7.57 ppm, γ, 7.82

ppm) were significantly shifted to (α, 8.91 ppm, β, 7.65 ppm, δ, 7.64 ppm, γ, 8.10 ppm) after the 1:1 complexation, while the phenyl peaks did almost not evolve (4, 7.67 ppm to 7.70 ppm; 5, 7.50 ppm to 7.52 ppm) which confirmed the coordination of zinc to the pyridines. In the meantime, there is a splitting of the CH_2 (1, 4.03ppm) connecting the nitrogen to the pyridine in the DPA ligand into a doublet of doublet (4.37 ppm and 4.16 ppm, J = 83.0 Hz). This indicates that the two diastereotopic hydrogens have been differentiated upon coordination of Zn^{2+}.[19]

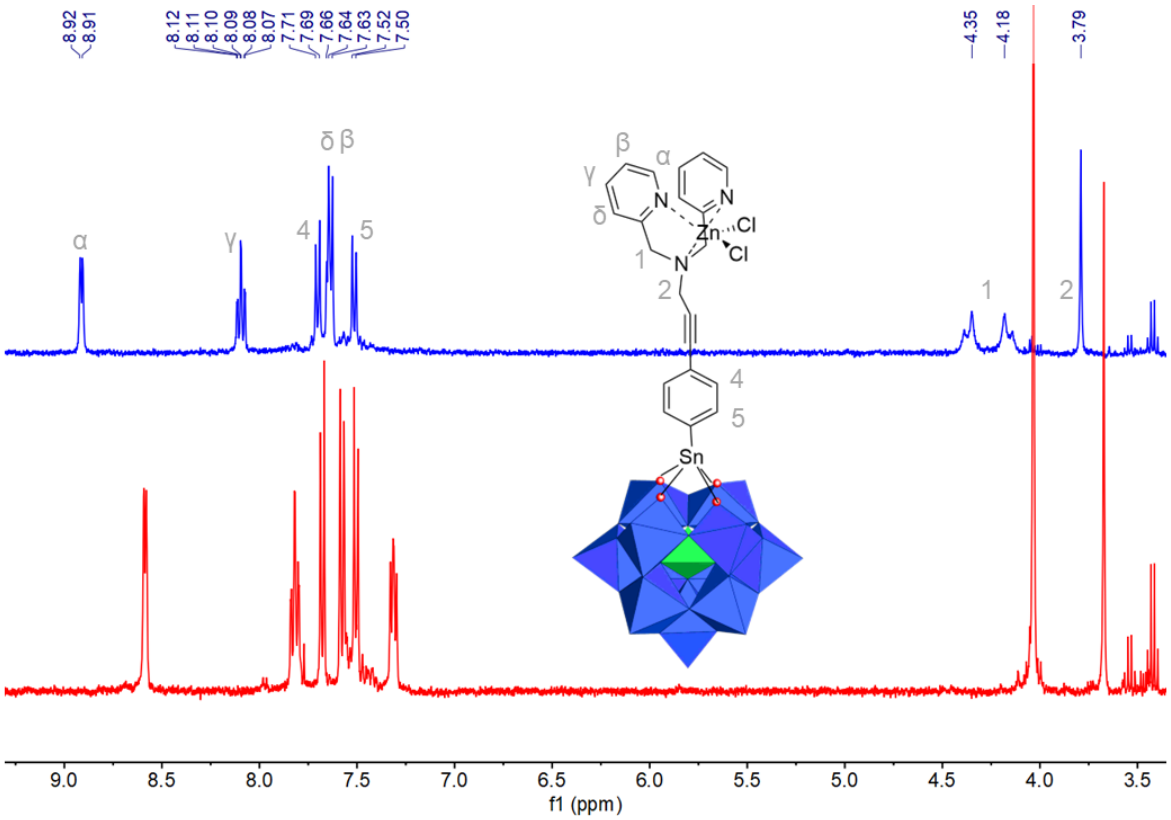

*Figure 3-9 The 1H NMR variation of the **K_{Sn}[DPA]** complexation process with $ZnCl_2$.*

Complexation of $CuCl_2$ with K_{Sn}[DPA]

While Zn(II) afforded an easy detection of coordination by NMR, interaction with copper, a metal that plays an important role in the activation of dioxygen in enzymatic systems[20,21], would allow to mimic the biological action of copper monooxygenases.

First, study of the coordination of copper chloride with **K_{Sn}[DPA]** was performed. As the paramagnetic Cu(II) complex couldn't be detected by NMR, the stoichiometry of ligand binding to Cu(II) was followed by UV−vis titrations. A 2 mL 1.0 mM $CuCl_2$ acetonitrile solution

was titrated by a 20mM **K_{Sn}[DPA]** acetonitrile solution directly into the UV-vis cuvette. As can be seen in Figure 3-10, there were two processes upon addition of the POM solution. Up to 0.6 eq. of the addition of **K_{Sn}[DPA]**, the absorption at 460 nm and 607 nm grew, while the absorption at 400 nm and 820 nm decreased with two isosbestic points at 439 nm and 739nm. With further addition of the POM solution, a second process with a new isosbestic point at 561 nm took place. Upon the addition ~ 2.0 eq. of the POM, the absorption peak at 460 nm did completely vanish while the peak at 745 nm reached its maximum. The UV-vis titration indicated that 1.0 eq. $CuCl_2$ could be coordinated with 2.0 eq. **K_{Sn}[DPA]** maximum. The fact that we didn't first fully complex the Cu(II) with one ligand suggested that the second complexation constant is either very close or may be even bigger than the first one. Upon the addition of more **K_{Sn}[DPA]** (from 0.6 eq. to 2.0 eq.)**,** the dimer coordination process occurred.

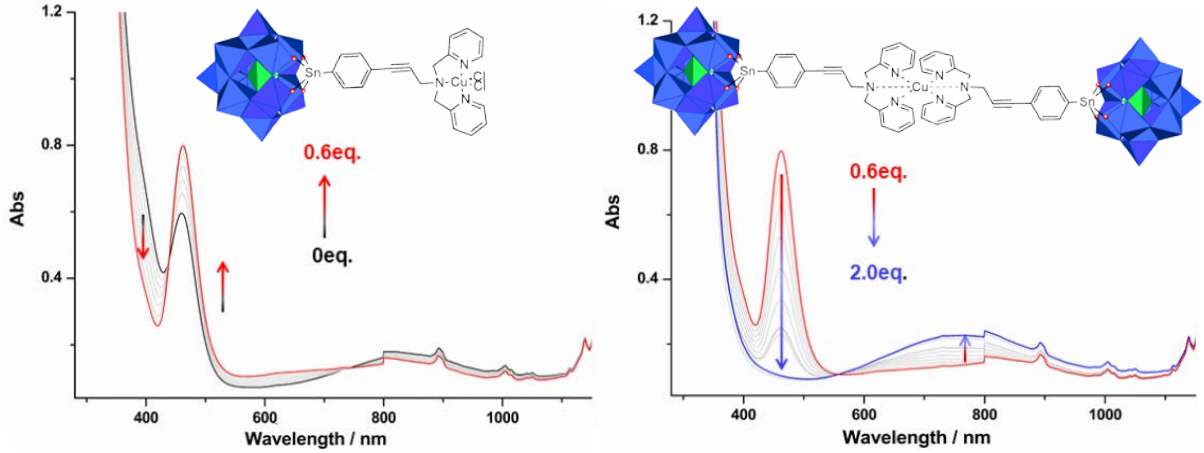

*Figure 3-10 The UV-vis titration of 1.0 mM $CuCl_2$ with **K_{Sn}[DPA]**.*

The coordination environment around the copper (II) ion is essential for the access of an external ligand which is the keynote for the catalyst. Isolating to form 1**K_{Sn}[DPA]**: 1**Cu(II)** complex seems difficult to achieve in this case. Thus, we tried another copper salt, copper acetate, where the acetate might be somewhat harder to substitute, to perform the coordination.

Complexation of $Cu(OAc)_2$ with K_{Sn}[DPA]

Addition of aliquots of a 20 mM **K_{Sn}[DPA]** solution into the 1.0 mM copper acetate acetonitrile solution led to a decrease of the absorption at 674 nm together with a slight blue shift to 664 nm with an isosbestic point at 592 nm which remains until 1.0 eq was added. As

more POM solution was added, there is new evolution which probably arise from the added absorbance of the free ligand. The slop of the titration (Figure 3-11 insert) indicated this is 1:1 complexation.

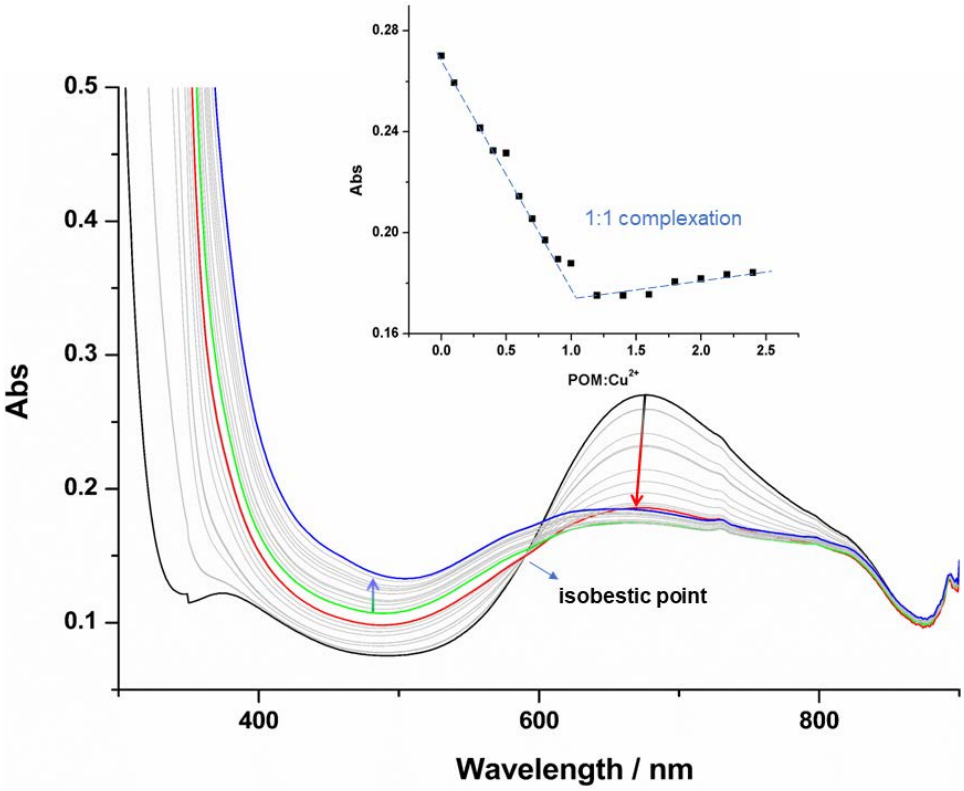

Figure 3-11 The UV-vis titration of the complexation of 1.0 mM $Cu(OAc)_2$ with ***K_{Sn}[DPA]****.*
Insert : evolution of the absorbance at 664 nm as a function of POM/Cu ratio

This led us to perform the 1:1 complexation reaction on a preparative scale in acetonitrile. The resulting pale blue solution was precipitated in ethanol. The pale blue solid was tested with UV-vis spectrum in acetonitrile. Surprisingly, the d-d transition in the isolated product, which was precipitated with ethanol, was blue shifted to 624 nm, compared to the corresponding peak at 664 nm in the titration.

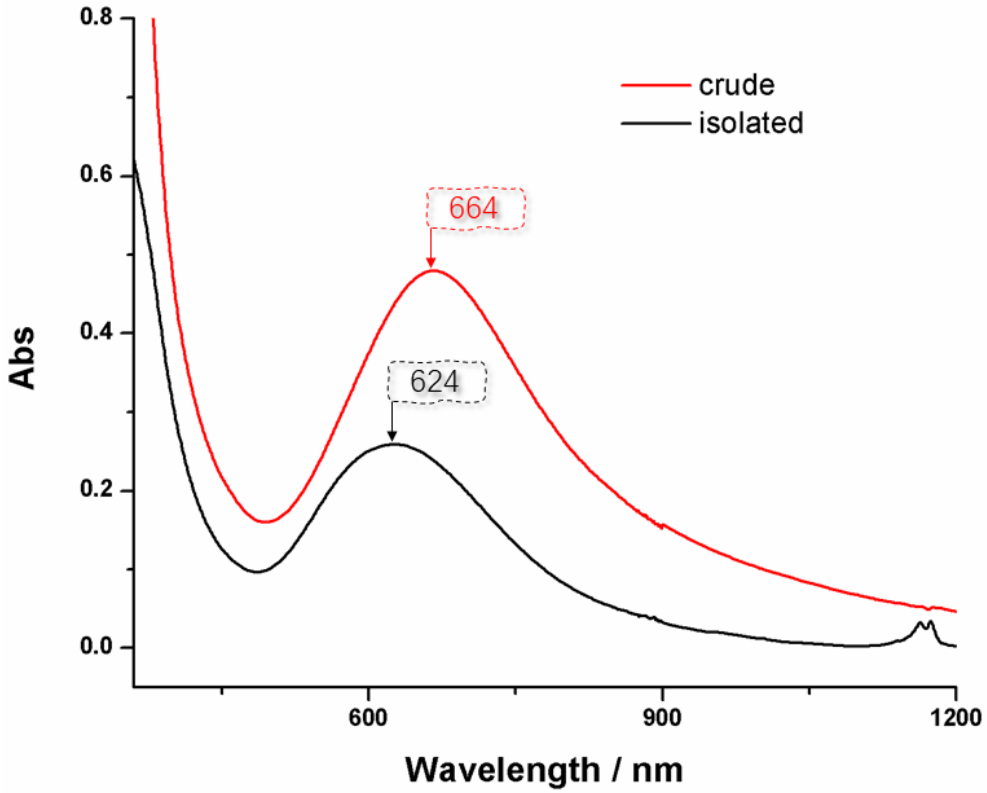

Figure 3-12 UV-vis spectrum of the crude complex (black) and after being isolating with ethanol (red).

Additional insight was given by ^{31}P NMR : as can be observed on spectrum, after the ligand was coordinated to the copper, the main signal turned from a singlet at -11.62 ppm to a main broad one at -11.51 ppm together with some less intense peaks (-11.6 ppm and -12.0 ppm). The crude product obviously requires purification by fractional crystallization using a "bad solvent"

Isolated crude complex was redissolved in acetonitrile and then we tried several "bad" solvents such as and THF to precipitate it. There was not significant improvement in ^{31}P NMR when treated with ethyl acetate or dichloromethane. Whereas, after being treated with THF, the peak at -12.0 ppm totally vanished (Figure 3-13, blue). Indeed, there was the impurity in the supernatant, together with some free ligand $\mathbf{K_{Sn}[DPA]}$ at -11.62 ppm. (Figure 3-13, blue dash). After the purification with THF, there seems still some free ligand left, indeed, as a side peak at -11.62 ppm remains and seemed to decrease when another 0.5 eq. copper acetate (Figure 3-13, purple) was added.

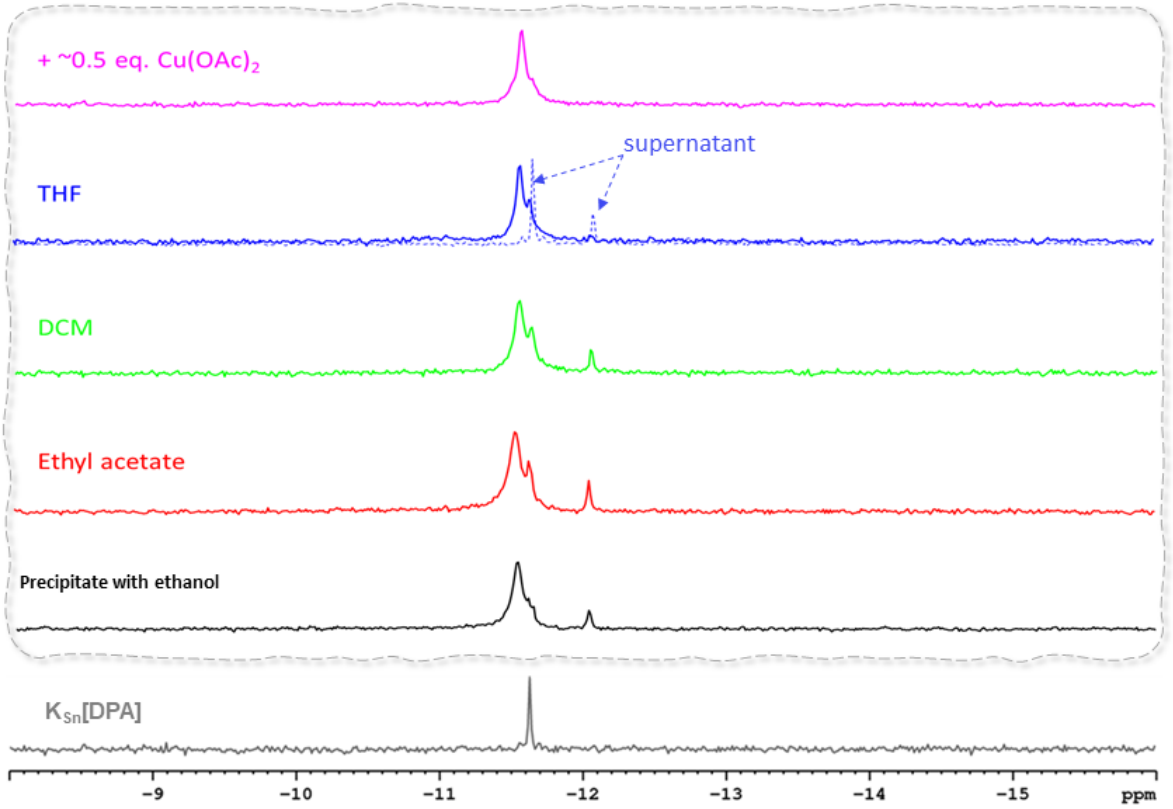

Figure 3-13 The 31P NMR of ***K_{Sn}[DPA]****@$Cu(OAc)_2$ after the treatment with ethanol (black), ethyl acetate (red), dichloromethane (green) and THF (blue); add ~0.5 eq. $Cu(OAc)_2$ based on the THF treatment (purple).*

The presence of this side peak is reproducible, as shown in a second experiment treated with THF. However, in this case, no further improvement was observed, when $Cu(OAc)_2$ was added (Figure 3-14). Interestingly, in this experiment, when we added some tetrabutylammonium nitrite salt ($TBANO_2$), the resulting ^{31}P NMR signal turned to a single singlet at -11.64 ppm with no side peak. It suggests strongly that the obtained complex, **K_{Sn}[DPA]**@$Cu(OAC)_2$ is pure without any POM degradation. Thus, we propose that the side peak could be somewhat related to the coordination modes of acetate or the number of acetates on the copper. This is also confirmed when changing the deuterated solvent, as only one singlet with tiny tin coupling is observed in deuterated DMSO.

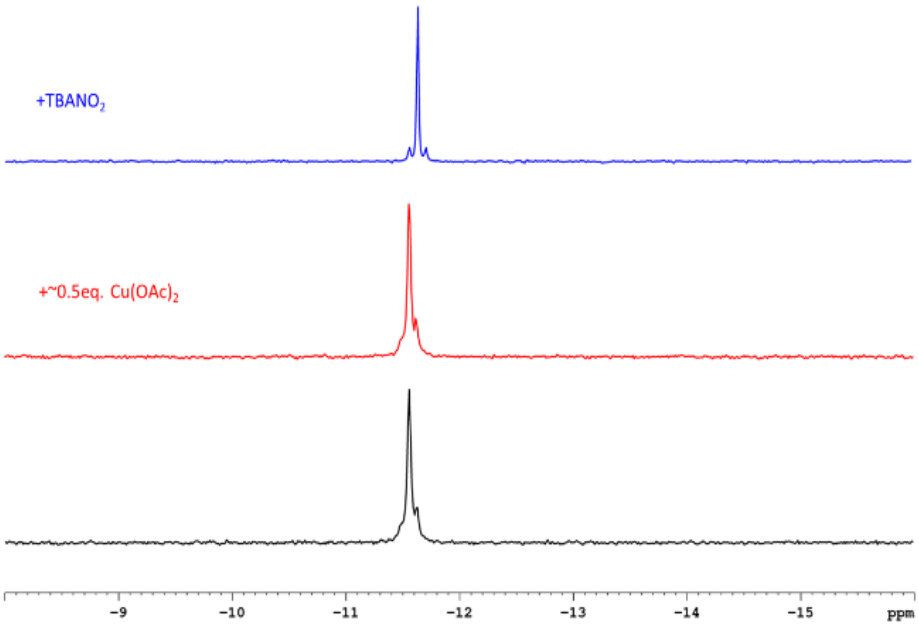

Figure 3-14 The ^{31}P NMR of the complex precipitated with THF (black); after the addition another 0.5 eq. $Cu(OAc)_2$ (red); and $TBANO_2$ (blue).

In order to further characterize the prepared complexes, infrared spectrum was carried out, in order to detect the specific signature of the acetate ligand and may be identify its coordination mode (unidented, bidented or bridged) through the difference of some specific absorption peaks.[22] Although the absorptions of DPA and the cation TBA are also at this region, and all the signals seem overlapped, compared to the **K_{Sn}[DPA]** starting material, there are two new peaks at 1613 and 1444 cm^{-1} respectively (Δ =169 cm^{-1}), which might be identified to the coordinated acetate.[23] In the meantime, a small decrease of the peaks of pyridine at 1593 and 1570 cm^{-1} could be attributed to the coordination. The remained characteristic bands at 1071, 963, 885, and 813 cm^{-1} confirmed that no degradation of the polyoxometalates did occur, in line with the ^{31}P NMR spectrum.

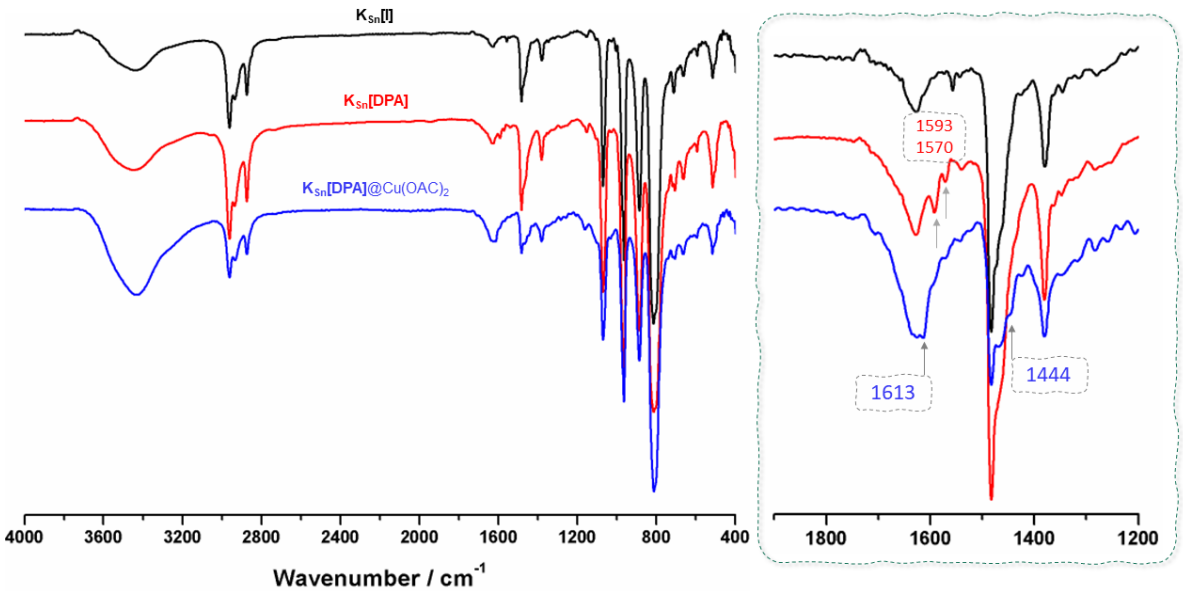

Figure 3-15 The normalized infrared spectrum of precursor platform ***K_{Sn}[I]*** *(black), the ligand* ***K_{Sn}[DPA]*** *(red) and the complex* ***K_{Sn}[DPA]****@Cu(OAc) (blue).*

3.1.6 Redox properties of K_{Sn}[DPA]@$(Cu(OAc)_2$

Cyclic voltammetry

The redox properties were investigated by cyclic voltammetry in deoxygenated acetonitrile with $TBAPF_6$ as supporting electrolyte in a standard three electrode cell, composed of a glassy carbon working electrode, a platinum counter electrode, and a saturated calomel reference electrode (SCE). All following potentials, unless otherwise specified, are given toward the SCE electrode. Figure 3-16 shows the behavior of **K_{Sn}[DPA]**@$Cu(OAc)_2$. There are three one-electron reduction waves. The first broad and quasi-reversible reduction wave around -0.27 V is assigned to the reduction of the copper ion with two reoxidation waves at -0.11 V and 0.082 V (Figure 3-16 blue), which is somewhat classical for Cu(II)/Cu(I) processes:[24] since Cu(I) prefers to be four coordinate, the irreversibility of the Cu(II/I) couple may be due to the rearrangement of the symmetry. If more negative sweeps are investigated (Figure 3-16 red), a quasi-reversible reduction wave is detected at – 1.01 V, which is attributed to the first tungstate reduction processes.[18] However, an unexpected re-oxidation wave appears at -0.33 V which is not so clear to attribute . The current intensity of this oxidation wave increases dramatically with a slight negatively shift to -0.41V, once we swept down an

even more negative potential (Figure 3-16 black) with the appearance of a second reversible reduction wave at -1.47 V, again W -centered by analogy with former work.

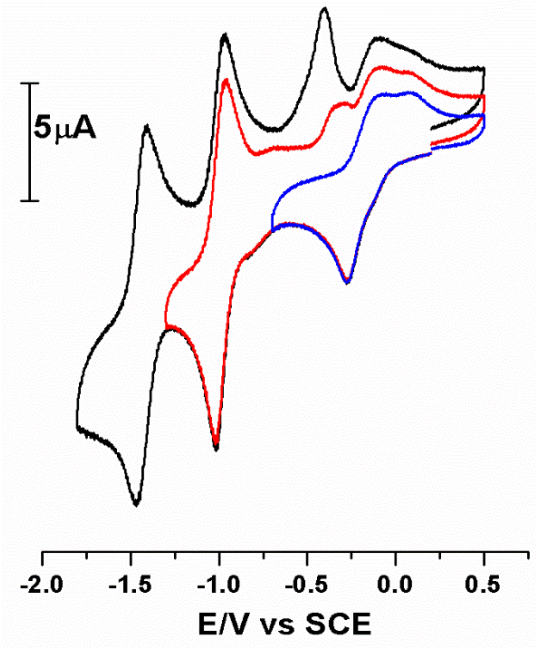

Figure 3-16 Cyclic voltammogram of 1.0 mg/mL solution of ***K_{Sn}[DPA]*** *@$Cu(OAc)_2$ with different scan windows:1) 0.5 to -0.7 V (blue); 2) 0.5 to -1.3 V (red); 3) 0.5 to -1.8 V (black) in MeCN containing 0.1 M of $TBAPF_6$, scan rate: 100 mV/s, working electrode: glassy carbon, reference electrode: SCE.*

Table 3-2: Potentials of the waves in V vs SCE. Half-wave potentials $E_{1/2} = (E_p^{ox} + E_p^{red})/2$. In brackets: $\Delta Ep = E_p^{ox} - E_p^{red}$, in mV.

Scale	Cu(II)/Cu(I)			W(VI)/W(V)						Unattributed oxidation wave		
				1st			2nd					
	E_p^{ox}	E_p^{red}	$E_{1/2}$	E_p^{ox}	E_p^{red}	$E_{1/2}$	E_p^{ox}	E_p^{red}	$E_{1/2}$	E_p^{ox}	E_p^{red}	$E_{1/2}$
(0.5 - 1.8)	-0.11 0.082	-0.27	*	-0.96	-1.01	-0.99 (64)	-1.41	-1.47	-1.44 (64)	-0.41	/	/
(0.5 - 1.3)	-0.11 0.082	-0.27	*	-0.96	-1.01	-0.99 (64)	/	/	/	- 0.332	/	/
(0.5 - 0.7)	-0.11 0.082	-0.27	*	/	/	/	/	/	/	/	/	/

For electrochemically reversible electron transfer processes involving freely diffusing redox species, the Randles−Sevcik equation (eq 1) describes how the peak current i_p (A)

increases linearly with the square root of the scan rate ν (V/s), where n is the number of electrons transferred in the redox event, *A* (cm^2) is the electrode surface area, D_o (cm^2 s^{-1}) is the diffusion coefficient of the oxidized analyte, and C^0 (mol cm^{-3}) is the bulk concentration of the analyte.

$$i_p = 0.446nFAC^0\left(\frac{nF\nu D_o}{RT}\right)^{1/2} \quad \text{eq (1)}$$

For an electrode-adsorbed species, the current response is described by eq (2), where $\Gamma^*$is the concentration of adsorbed species in mol cm^{-2}.[25]

$$i_p = \frac{n^2F^2}{4RT}\nu A\Gamma^* \quad \text{eq (2)}$$

As we could observe, sequential scan rates, 50, 100, 200, 400 mV/s were carried out resulting in a gradient intensity of the reduction and oxidation waves (Figure 3-17 A). The current of every wave in function of the square root of the scan rate, and the fitting slops are linear (Figure 3-17 B), which indicates every species is freely diffusion controlled. Thus, the re-oxidation wave at -0.41 V cannot be due to some electrode deposition of a Cu(I/0) reduction product, and thus is probably associated with some reorganization of the hybrid-POM structure upon reduction.

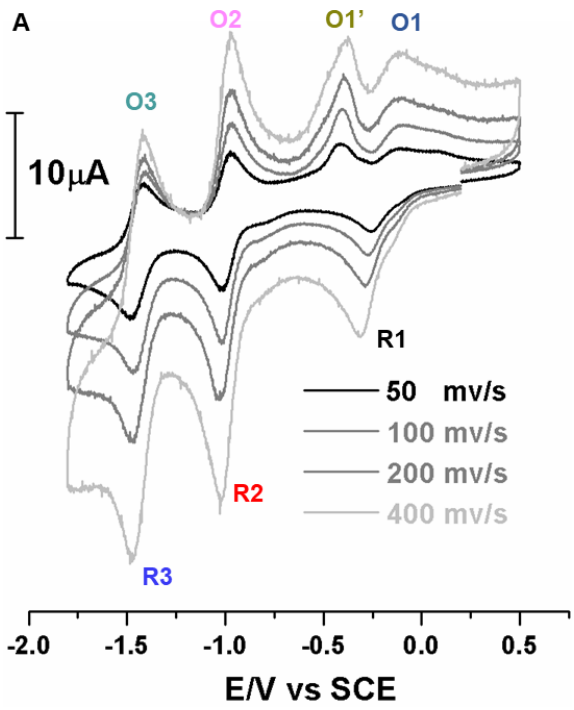

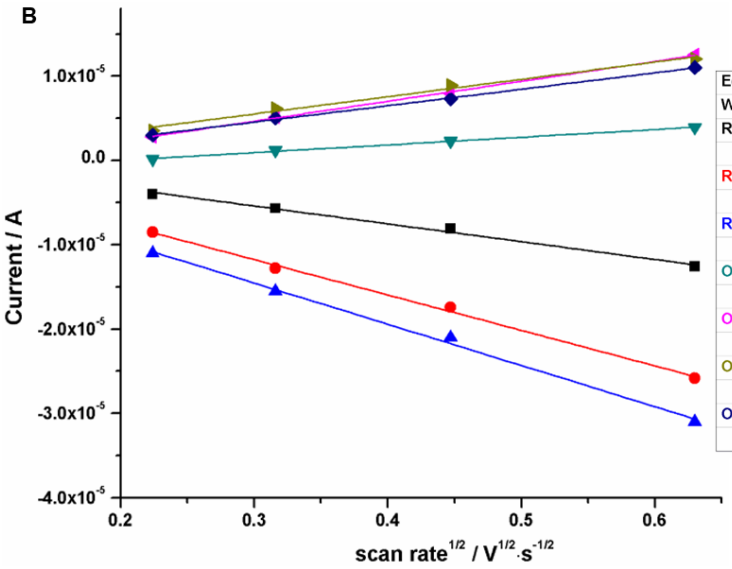

Equation	y = a + b*x			
Waves		Value	Standard Err	Adj. R-Square
R1	Intercept	9.42486E-7	5.10951E-7	0.99066
	Slope	-2.11317E-5	1.18256E-6	
R2	Intercept	8.43021E-7	6.76873E-7	0.99583
	Slope	-4.19741E-5	1.56658E-6	
R3	Intercept	1.18124E-7	8.35735E-7	0.99531
	Slope	-4.88389E-5	1.93425E-6	
O3	Intercept	-1.81567E-6	1.43742E-7	0.99603
	Slope	9.13585E-6	3.32681E-7	
O2	Intercept	-2.44021E-6	2.24804E-7	0.99855
	Slope	2.36369E-5	5.20293E-7	
O1'	Intercept	-6.42175E-7	7.38402E-7	0.97947
	Slope	2.05187E-5	1.70898E-6	
O1	Intercept	-1.30129E-6	1.93137E-7	0.99842
	Slope	1.94837E-5	4.47003E-7	

Figure 3-17 A) Cyclic voltammogram of 1.0 mg/mL solution of ***K_{Sn}[DPA]***@Cu(OAc)$_2$ *in MeCN containing 0.1 M of TBAPF$_6$, scan rate: 50, 100, 200, 400 mV/s, working electrode: glassy carbon, reference electrode: SCE; B) the slop of current in function of square root of scan rate.*

Electrocatalytic reduction of nitrite with K_{Sn}[DPA]@Cu(OAc)2

The selective and efficient electrocatalytic reduction of nitrite to nitric oxide (NO) is of tremendous importance, both for the development of NO-release systems for biomedical applications[26] and for the removal of nitrogen oxide pollutants from the environment.[27] In nature, this transformation is mediated by enzymes, one of it known as the copper-containing nitrite reductases (CuNIR).[28] Cu sites are ligated to a methionine, a cysteine and two histidines in either a distorted or flattened tetrahedral geometry.

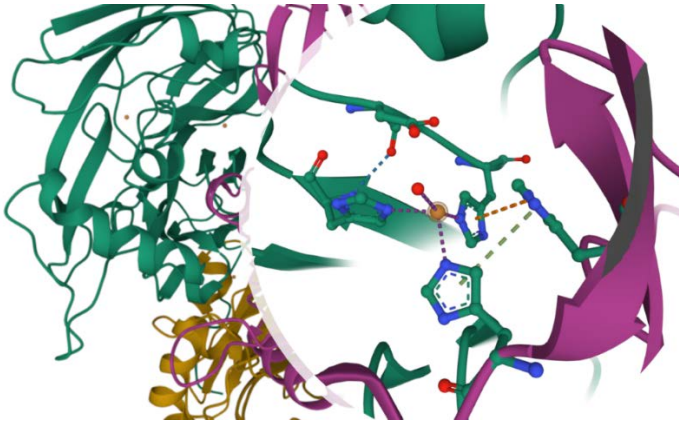

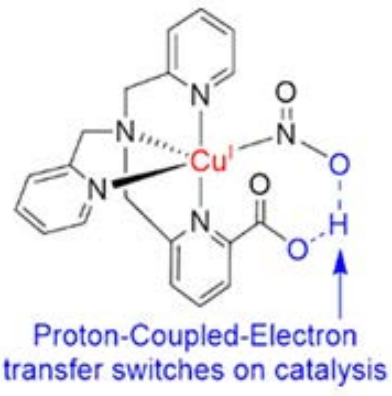

Scheme 3-5 left):The crystal structure of the blue nitrite reductase from Alcaligenes xylosoxidans GIFU 1051. PDB: 1BQ5.[28] right) the mimic of the Cu site.[29]

Inspired by the active site of the CuNIR, many model complexes were synthesized to mimic the nitrite reduction process. Recently, Symes and coworkers[29] have developed a tetradentate tris(2-methylpyridyl)amine (TMPA) ligand that are competent for the electrocatalytic reduction of nitrite to NO in nonaqueous solvent. They highlight that the proton-relaying groups are essential to the efficiency of the nitrite reduction (Figure 1-4).

The POM skeleton could work not only the electron relay but also the proton relay. Herein, we would like to test the effect of the POM presence or absence on the electrocatalytic reduction of nitrite to see if there were any synergy via covalent grafting.

Coordination

Substitution of acetate by nitrite was followed using various techniques. The addition of 0 to 20 eq. $TBANO_2$ to $\mathbf{K_{Sn}[DPA]}$@$Cu(OAc)_2$ initially shows a shift on the absorption spectrum from 624 nm to 742 nm of the main absorption peak with an isosbestic point at 647 nm (Figure 3-18 A) which is associate with nitrite coordination to the copper center. But the large excess nitrite needed indicates that the copper prefers to coordinate with acetate. Further addition of $TBANO_2$ to 100 eq. resulted in another new species forming according to the growing absorption at 559 nm with an isosbestic point 631 nm, probably introducing a second nitrite in the coordination sphere of the copper.

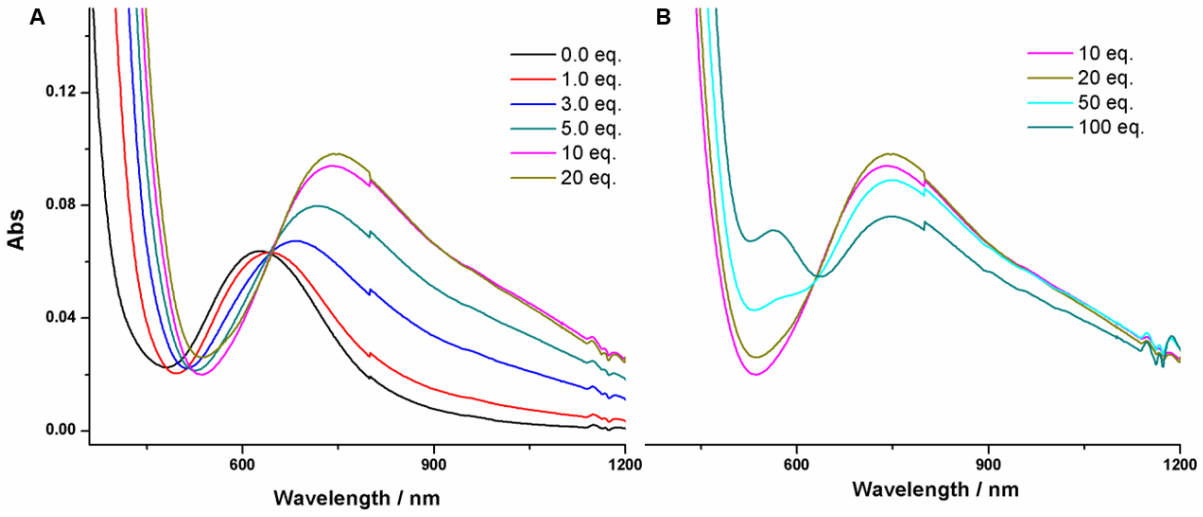

Figure 3-18 the UV-vis spectrum of 0.5 mM ***K_{Sn}[DPA]***@*$Cu(OAc)_2$ in the present of A) 1, 3, 5, 10, 20 eq. and B) 10, 20, 50 and 100 eq. $TBANO_2$.*

In parallel, this experiment was followed by X-band EPR spectroscopy in frozen acetonitrile at 30K. Figure 3-19 (black) shows the spectrum of isolated **K_{Sn}[DPA]**@$Cu(OAc)_2$ anion which can be reasonably simulated with an almost axial g-matrix (g_x=2.23, g_y=2.07, g_z=2.05) with hyperfine coupling of A_x= 550 MHz only detectable on the highest g-value, which is in agreement with a four or five coordinated Cu(II) ion in a geometry close to square planar or square pyramidal (two acetate coordinated).[30,31] Upon the addition of the $TBANO_2$, a clear evolution of the spectrum occurred toward a more rhombic system. The significant shift of the g-value (g_x=2.25, g_y=2.18, g_z=2.035) and A-values (450 MHz), together with the detection of some superhyperfine structure on the z-line (A estimated to 60MHz) clearly indicated substitution of acetate by nitrite on the copper (II) center.

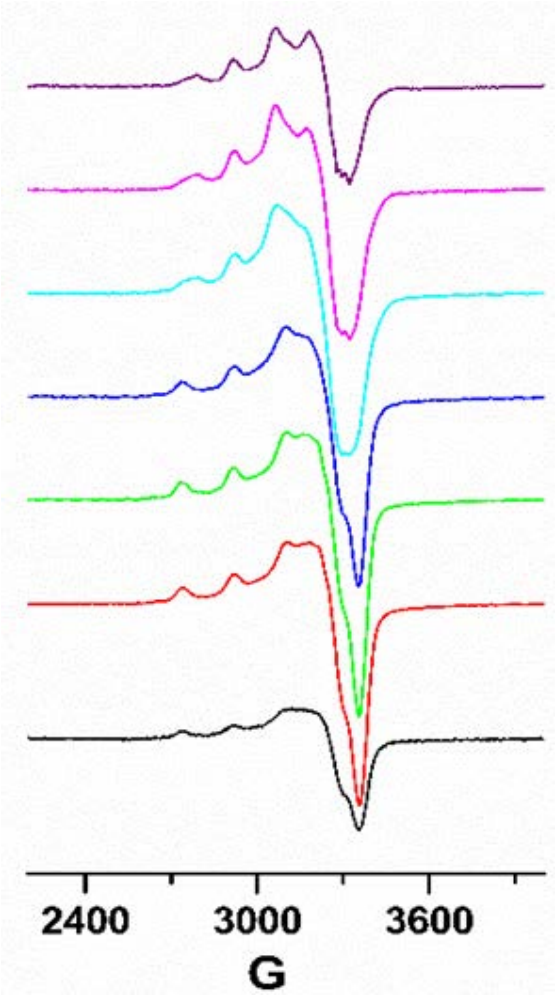

Figure 3-19 The EPR spectrum of 0.5 mM ***K_{Sn}[DPA]***@$Cu(OAc)_2$ *in the presence of 0, 1, 3, 5, 10, 20 and 50 of* $TBANO_2$

As seen previously, the ^{31}P NMR spectrum the POM in presence of $TBANO_2$ presents a single peak at -11.64 ppm (Figure 3-14). This is in contrast with the isolated **K_{Sn}[DPA]**@$Cu(OAc)_2$, where the peak at - 11.55 ppm seemed to be more composite, suggesting the presence of different environment around the copper. Thus, this latter experiment first proves that substitution of acetate by nitrite did occur, but also clearly confirm that the initial product was rather pure.

Finally, the infrared spectrum of **K_{Sn}[DPA]**@$Cu(OAc)_2$ was also carried out before and after a 1:1 reaction with $TBANO_2$. Upon substitution with nitrite, two peaks at 1575 cm^{-1} and 1445 cm^{-1}, that could be attributed to coordinated acetate, seems disappear while a new feature at 1270 cm^{-1}, corresponding to coordinated nitrite, appeared.

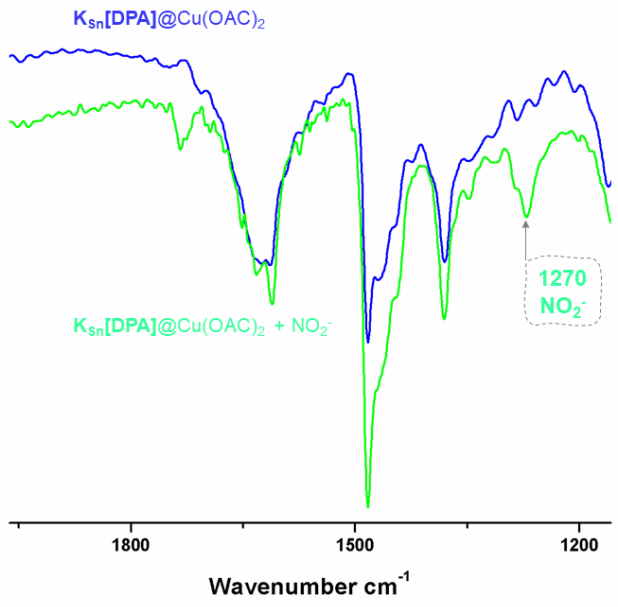

Figure 3-20 IR of the isolated titration product of ***K_{Sn}[DPA]***@$Cu(OAc)_2$ *(green) with* $TBANO_2$.

Electrocatalytic reduction

First, we tested the electrocatalytic behavior of the **K_{Sn}[DPA]**@$Cu(OAc)_2$ in the presence of the $TBANO_2$. We synthesized the complex propargyl-DPA@$Cu(OAc)_2$ as a reference.

Table 3-3: Potentials of the waves in V vs SCE. Half-wave potentials $E_{1/2}$ = (E_p^{ox} + E_p^{red})/2. In brackets: ΔEp= E_p^{ox} - E_p^{red}, in mV.

K_{Sn}[DPA]@Cu(OAc)$_2$	Cu(II)/Cu(I)			W(VI)/W(V)					
	E_p^{ox}	E_p^{red}	$E_{1/2}$	1st			2nd		
				E_p^{ox}	E_p^{red}	$E_{1/2}$	E_p^{ox}	E_p^{red}	$E_{1/2}$
	-0.27	-0.37	-0.32 (100)	-1.08	-1.14	-1.11 (60)	-1.56	-1.64	-1.60 (80)

Propargyl-DPA@Cu(OAc)$_2$	E_{p1}^{ox}	E_{p2}^{ox}	E_{p1}^{red}	E_{p2}^{red}
	-0.04	-0.18	-0.29	-0.72

As the propargyl-DPA@Cu(OAc)$_2$ is not well soluble in acetonitrile, here, we performed the cyclic voltammetry in DMF (Table 3-3). The first reduction wave of **K_{Sn}[DPA]**@Cu(OAc)$_2$, **E_p^{red}** = -0.37 V, which belongs to the copper complex moiety variated with the addition of $TBANO_2$. Although the variation seems random, it shifts positively from - 0.36 V to - 0.25 V all of whole which means it was easier to get the complex reduced once the nitrite was bonded to the copper. No obvious catalytic reduction wave was observed until 20 eq. of $TBANO_2$ was added, but then the second reduction wave of the POM skeleton started being shifted from -1.64 V to -1.38 V and increased. As more $TBANO_2$ was added, from 20 eq. to 100 eq., there was a big irreversible reduction wave at -1.6 V, in the meantime, both of two W-based reduction waves increased.

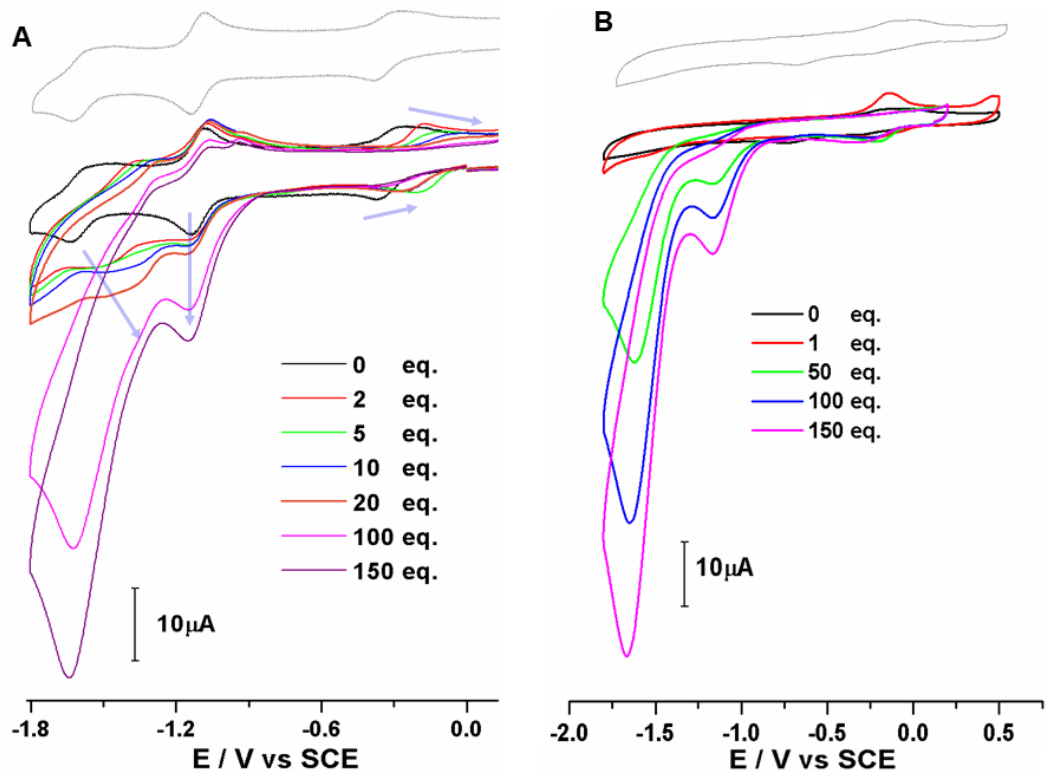

Figure 3-21 Cyclic voltammogram of A) 0.45 mM solution of ***K_{Sn}[DPA]***@$Cu(OAc)_2$ *in the presence of (0, 2, 5, 10, 20, 100, 150 eq.) $TBANO_2$; B) 0.45 mM solution of propargyl DPA@$Cu(OAc)_2$ in the presence of (0, 1, 50, 100, 150 eq.) $TBANO_2$ in degassed DMF containing 0.1 M of $TBAPF_6$, scan rate: 100 mV/s, working electrode: glassy carbon, reference electrode: SCE.*

In order to figure out whether the POM hybrid complex could have higher efficiency or not, the same electrocatalytic reduction was carried out with the POM free propargyl copper complex. Unfortunately, the almost same "catalytic like" reduction waves at -1.14 V and – 1.60 V were obtained with the addition of $TBANO_2$ up to 50 eq. We also tried to electrocatalytically reduce nitrite in the presence of benzoic acid (PhCOOH) with both **K_{Sn}[DPA]**@$Cu(OAc)_2$ and propargyl-DPA@$Cu(OAc)_2$. The cyclic voltammetry curves are almost the same with or without POM, and thus no synergetic effect could be observed in this case.

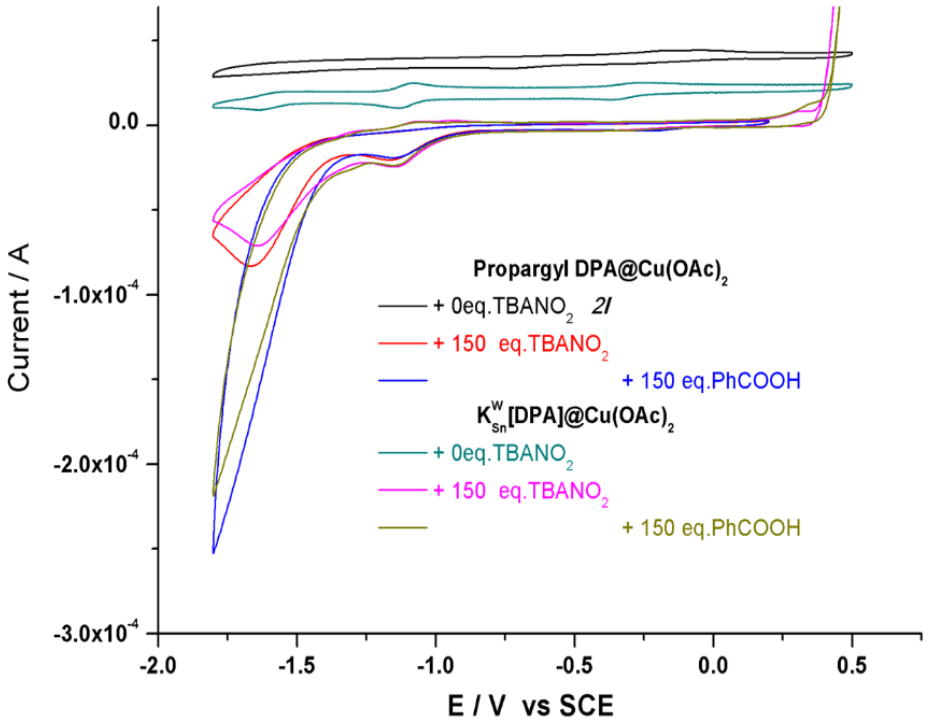

Figure 3-22 Cyclic voltammogram of 0.45 mM solution of ***K_{Sn}[DPA]***@Cu(OAc)$_2$ *and propargyl DPA@Cu(OAc)$_2$ respectively, with or without the presence of 150 eq. TBANO$_2$ and 150 eq. PhCOOH, in degassed DMF containing 0.1 M of TBAPF$_6$, scan rate: 100 mV/s, working electrode: glassy carbon, reference electrode: SCE.*

3.2 Di-functionalization Keggin $[PW_{11}O_{39}]^{7-}$ through "Click" reaction

Over the past years, "click" reactions[32] have been gaining increasing interest as they can be applied under relatively mild conditions allowing coupling of the POM hybrid platform with various organic molecules with suitable functional groups. The Cu(I) catalyzed azide–alkyne cycloaddition (CuAAC) is a very popular reaction that has motivated the design of specific hybrid POMs.[8,33]

3.2.1 Synthesis of $K_{Si}[N_3]$-3

For the exploration of the "click", a propyl-azido precursor Keggin platform, $TBA_3[PW_{11}O_{39}O\{SiCH_2CH_2CH_2N_3\}_2]$ (abbreviated as **$K_{Si}[N_3]$-3**), was built according to the synthesis protocol of the **K_{Si}[I]** in chapter 2. First, an azido substitute triethoxysilane, 3-azidopropyl triethoxysilane, was synthesized with the nucleophilic substitution reaction of 3-

chloropropyl triethylsilane with sodium azido in the presence of TBABr, as presented in scheme 3-6.

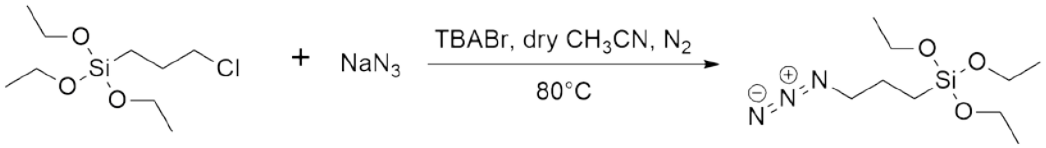

Scheme 3-6 The synthesis of 3-azidopropyl triethoxysilane.

Conversion to the azido derivatives result in a large shift of the protons of the propyl group in ^{1}H NMR from 3.53 ppm, 1.88 ppm and 0.75 ppm in the chloro derivative to 3.26 ppm, 1.71 ppm and 0.66 ppm in the azido one, confirming full conversion toward the expected product (Figure 3-23).

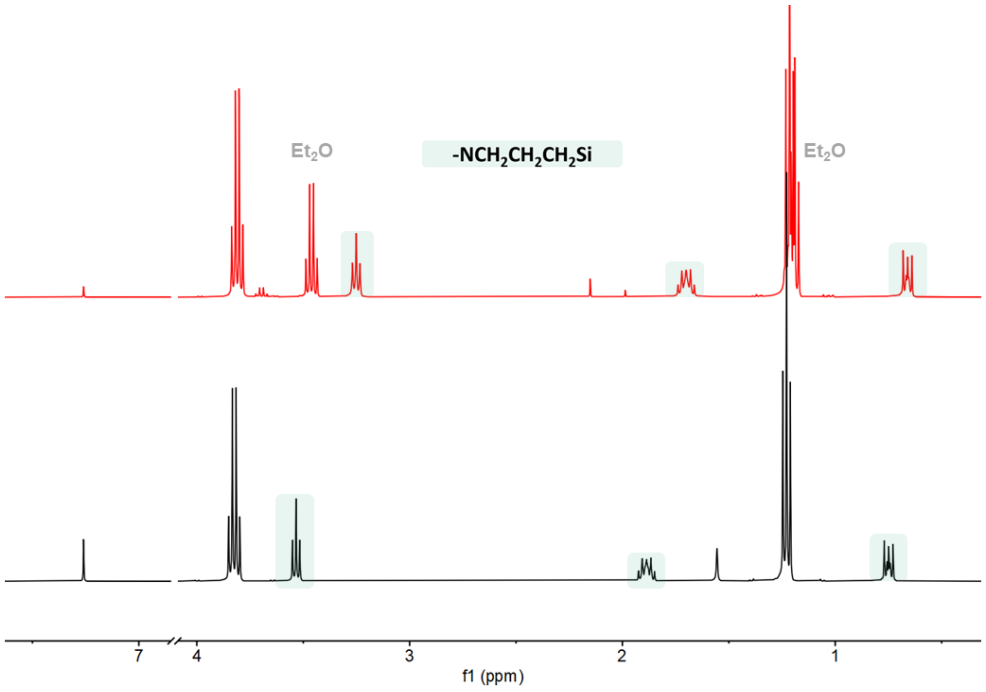

Figure 3-23 the ^{1}H NMR of the 3-azidopropyl triethoxysilane (red) and the precursor 3-chloropropyl triethoxysilane ($CDCl_3$)

Then the 3-azidopropyl triethoxysilane was grafted onto the lacunary Keggin $[PW_{11}O_{39}]^{7-}$.

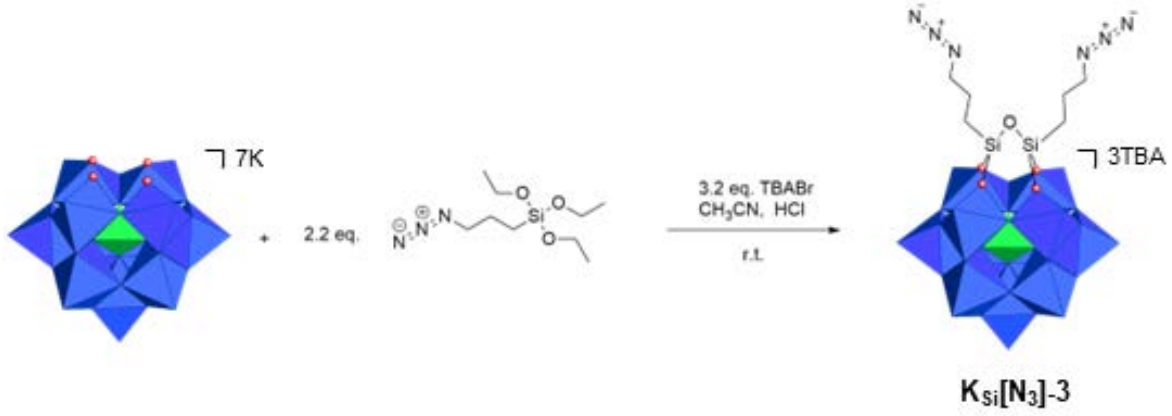

Scheme 3-7 the synthesis of the azido precursor Kiggin platform ***$K_{Si}[N_3]$-3****.*

A mixture of $K_7[PW_{11}O_{39}]$ and TBABr was dissolved in acetonitrile followed by the addition of 3-azidopropyl triethoxysilane. After the addition of 2.4 M HCl at 0 ℃, the resulting colorless solution was stirred overnight at room temperature. Precipitation with ethanol gave a white powder with a 95.7% yield. From the ^{1}H NMR spectrum in deuterated DMSO, we could clearly observe three propyl peaks now at 3.42 ppm, 1.77 ppm and 0.78 ppm together with the TBA peaks. A single peak at -13.24 ppm in the ^{31}P NMR confirmed a clean product.

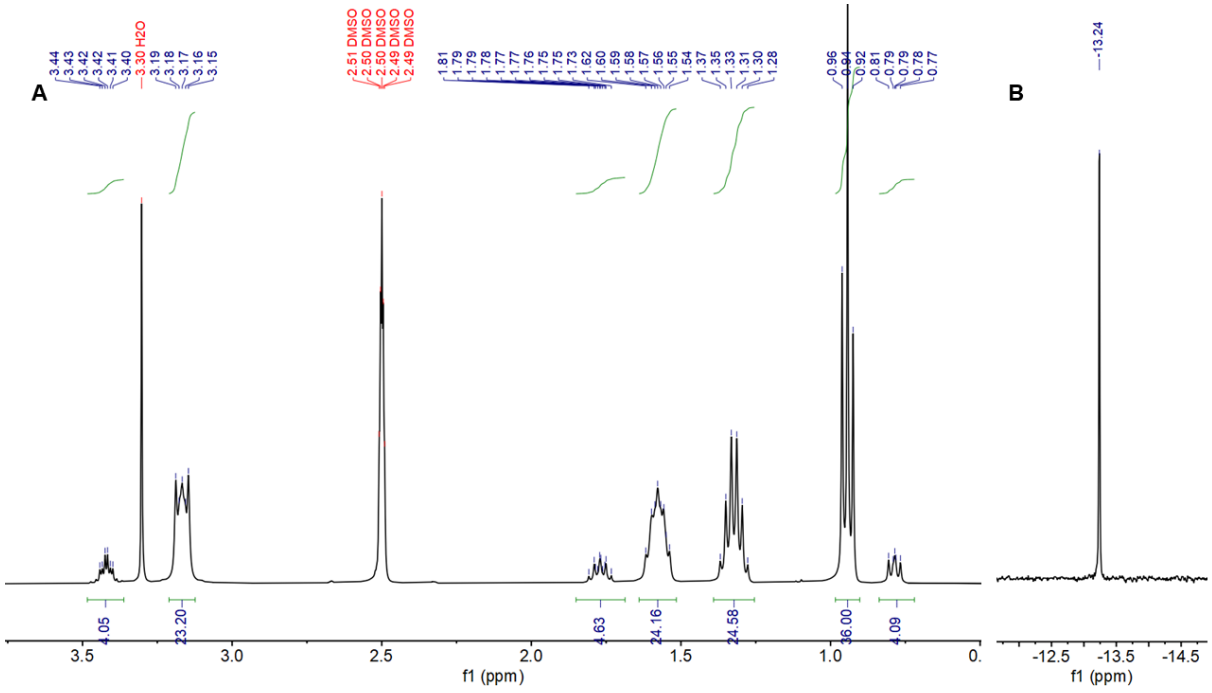

Figure 3-24 the ^{1}H NMR of ***$K_{Si}[N_3]$-3*** *in DMSO and the ^{31}P NMR.*

The characteristic absorption peak of azido group at 2096 cm^{-1} (Figure 3-25, black) was also observed in the infrared spectrum, alongside the characteristic peaks of the mono-lacunary Keggin structure. Finally, the molecular peak of $[PW_{11}O_{40}Si_2C_6H_{12}N_6]^{3-}$ at m/z = 972.76 (z=3) was detected in ESI-Mass.

3.2.2 Synthesis of $K_{Si}[N_3DPA]$-3

Classical conditions

To the best of our knowledge, in 2007, Lacôte and co-workers[7] used CuAAC reaction for the first time in polyoxometalate chemistry to graft organics to organotin Keggin and Dawson polyoxotungstates to generate hybrids. The initial reactions were carried out following the typical $CuSO_4$/sodium ascorbate modified procedure in which they applied 1 full equivalent of $CuSO_4$ to overcome the low reactivity because of possible ion-pairing of POM with the copper cations. Following this study, several other works with minor modifications on the synthetic protocols have been reported. Odobel and co-workers[8,34] successfully covalently connected porphyrin and Dawson POM through the “click” reaction to study the intramolecular electron transfer systems and artificial photosynthesis.

Inspired by these successful cases, we have tried to graft the DPA to the Keggin POM through the “click” reaction using the $CuSO_4$/sodium ascorbate protocol to form $(TBA)_3[PW_{11}O_{39}O\{SiCH_2CH_2CH_2N_3CCHCH_2N(CH_2Py)_2\}_2]$ (abbreviated as **$K_{Si}[N_3DPA]$-3**) from **$K_{Si}[N_3]$-3**. First, 2.0 eq. $CuSO_4$ and 8.0 eq. propargyl DPA were dissolved in DMF resulting in blue suspension and then mixed with colorless POM DMF solution. Upon addition of sodium ascorbate aqueous solution, the mixed blue suspension turned from slightly blue to green and finally to dark brown solution. The resulting dark brown solution was precipitated in ethanol after overnight stirring at room temperature and dark brown gel was obtained which was characterized by IR. Indeed, the proportion of the characteristic azido absorption around 2096 cm^{-1} (Figure 3-25, blue) got smaller, compared to the precursor (Figure 3-25, black). It indicated the “click” reaction did occur. But unfortunately, the ^1H NMR spectrum showed us broad and weak signals around 8 ppm, so that the characteristic triazole peak around 8 ppm could not be identified, which could be resulted by the coordination to the paramagnetic Cu^{2+}.

Therefore, less amount of $CuSO_4$, 0.2 eq. to the POM precursor, was added, with 2.0 eq. of sodium ascorbate.

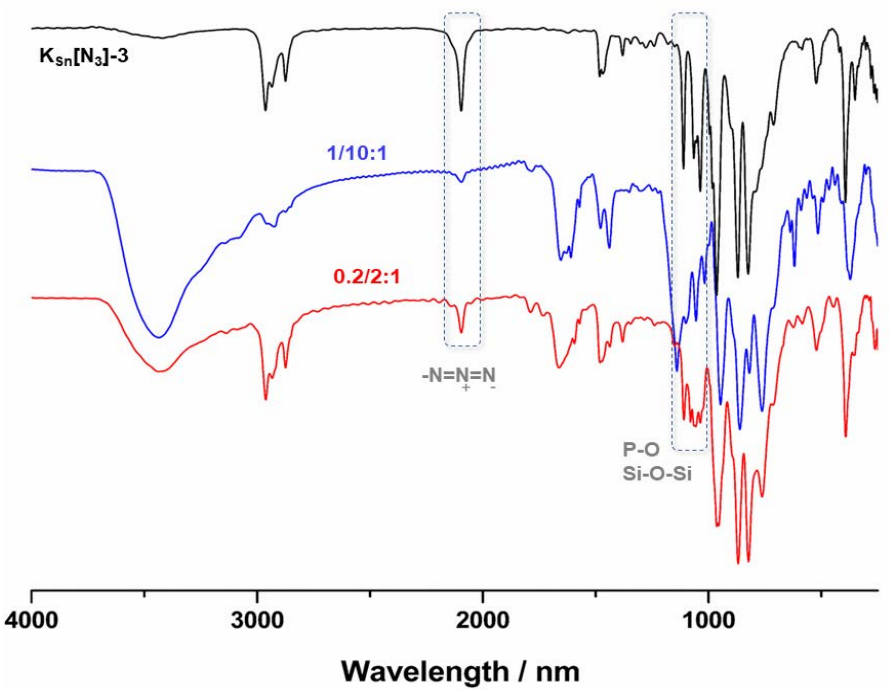

Figure 3-25 The IR of the resulting product with the ratio of $CuSO_4$ /sodium ascorbate to ***$K_{Si}[N_3]$-3****= 1/10:1(blue)and 0.2/2:1(red) in mixture solvent DMF/H_2O.*

From the IR spectrum, the “click” did again happen although much less azido was converted at the end of the reaction (Figure 3-25, red). The aromatic signals in ^{1}H NMR of the resulting crude product showed not only pyridine but also tiny broad peak around 8.1 ppm which could be identified to triazole. The product was furtherly treated with NaS_2NEt_2 which is a strong ligand to coordinate to the copper. Interestingly, the resulting product shows a clear singlet peak at 8.12 ppm verifying that “click” coupling could be achieved in our system.

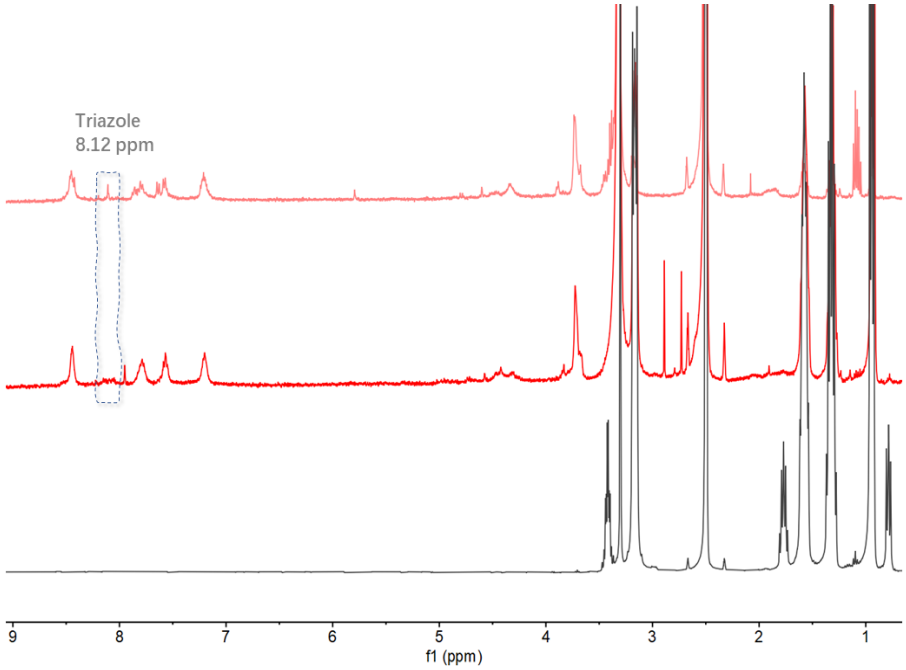

*Figure 3-26 The ^{1}H NMR of the crude product with $CuSO_4$/sodium ascorbate: **$K_{Si}[N_3]$-3** = 0.2/2.0:1 catalytic system (red) and the treated with NaS_2NEt_2 (pale red).*

Although we could achieve the coupling, the reaction clearly needs some more optimization. Moreover, it is difficult to isolate pure product even though we could remove part of Cu^{2+} with NaS_2NEt_2. Although the IR spectrum shows us the W-O and W=O stretch at 966, 866 and 821 cm^{-1} almost unchanged, the P-O and Si-O-Si stretch at 1111 and 1038 cm^{-1} moved a lot. We have also carried out the reaction with anhydrous DMF, the resulting product did not improve too much even heating at 50℃, excluding the effects of the water which could hydrolysis the silane functionalized POM. All the results above indicate us the classical condition might not be suitable for our system. Therefore, we need to find another “cleaner” condition to make this “click” coupling.

CuI/diisopropylamine

In 2015, Cronin and co-workers[33] successfully applied CuI as the catalyst in an anhydrous condition to “click” the Mn Anderson hybrid blocks together in a modular fashion without decomposition of the POMs in the presence of diisopropylethylamine as the base. The mild conditions of this approach should also permit to form the organic-inorganic hybrids of a range of other POMs.

Methyl propiolate

First, a simple alkynyl compound as a model, methyl propiolate (MP) is applied to perform the “click” coupling to test the feasibility of this CuI mild condition in our silane functionalized Keggin system.

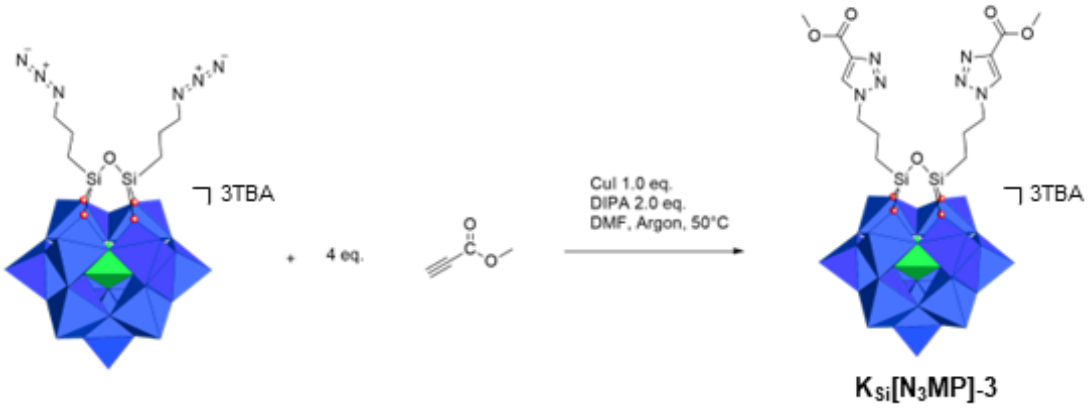

Scheme 3-8 The synthesis of ***K$_{Si}$[N$_3$MP]-3*** *in with CuI as catalyst.*

For the first bench reaction, diisopropylamine (DIPA), instead of diisopropylethylamine (DIPEA), was added by mistake as the base. Here, 1.0 eq. of **K$_{Si}$[N$_3$]-3**, 4.0 eq. methyl propiolate (MP) and 4.0 eq. DIPA were mixed under argon atmosphere and dissolved with anhydrous DMF followed by the addition of 1.0 eq. of CuI. After overnight stirring at room temperature, the resulting yellow solution was precipitated in ethanol. The IR spectrum of the yellow-greenish solid clearly displayed barely variated W-O and W=O stretches at 966, 866 and 821 cm^{-1} and P-O and Si-O-Si stretches at 1111 and 1038 cm^{-1}, in the meantime, the azido band at 2092 cm^{-1} diminished. The additional new absorption peaks at 1722 cm^{-1}(C=O), 1654 cm^{-1}(C=N) and 1225 cm^{-1} (might be attributed to C-N breathing) were identified to the characteristic stretch of the ester moiety.[35] Thus, we decided to keep working with DIPA as the base.

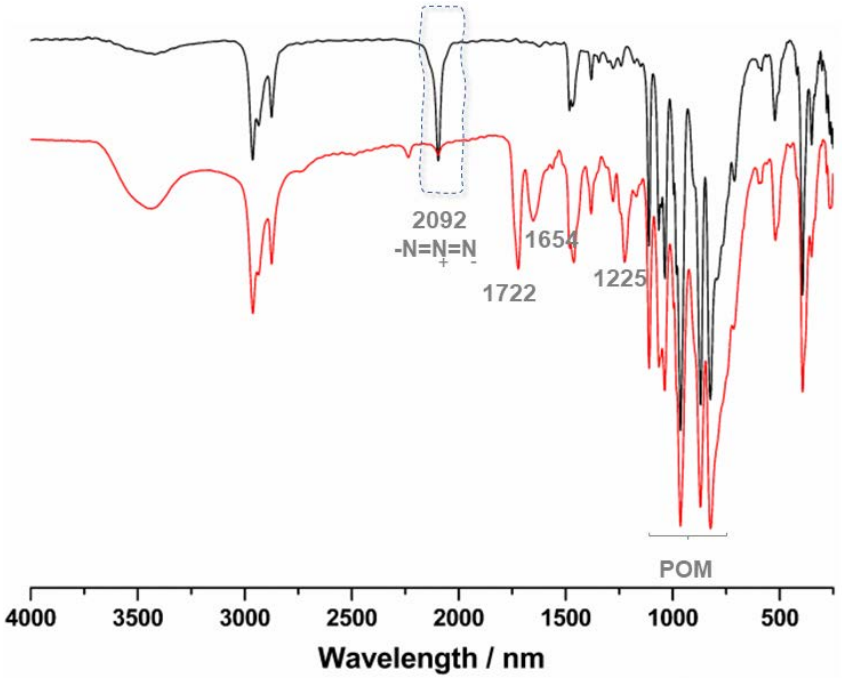

Figure 3-27 Comparison of the IR spectrum of the isolated product ***K_{Si}[MP]-3*** *and the starting* ***$K_{Si}[N_3]$-3****.*

In order to optimize the condition to push the reaction to the end, several parameters were studied, such as the amount of the DIPA and the temperature. First, three benches reaction were launched at room temperature for overnight with different amount of DIPA 2.0, 4.0, and 8.0 eq.

Table 3-4 The optimization of "click" of ***$K_{Si}[N_3]$-3*** *and methyl propiolate*

Entry	$K_{Si}[N_3]$-3	MP	CuI	DIPA	T
1	1eq.	4eq.	1eq.	8eq.	r.t.
2	1eq.	4eq.	1eq.	4eq.	r.t.
3	1eq.	4eq.	1eq.	2eq.	r.t. / 50℃

The reactions were monitored with IR spectrum which showed 4.0 eq was the most efficient: too much or too less base seem deleterious to the reaction (Figure 3-28). Based on the 2.0 eq. DIPA bench reaction which barely reacted, we heated it at 50℃ for overnight, in which case the azido was fully converted (Figure 3-29). For the following exploration of "click" reaction between **$K_{Si}[N_3]$-3** and propargyl-DAP, the condition of 4.0 eq propargyl-DPA and 2.0 eq. DIPA at 50℃ were thus chosen.

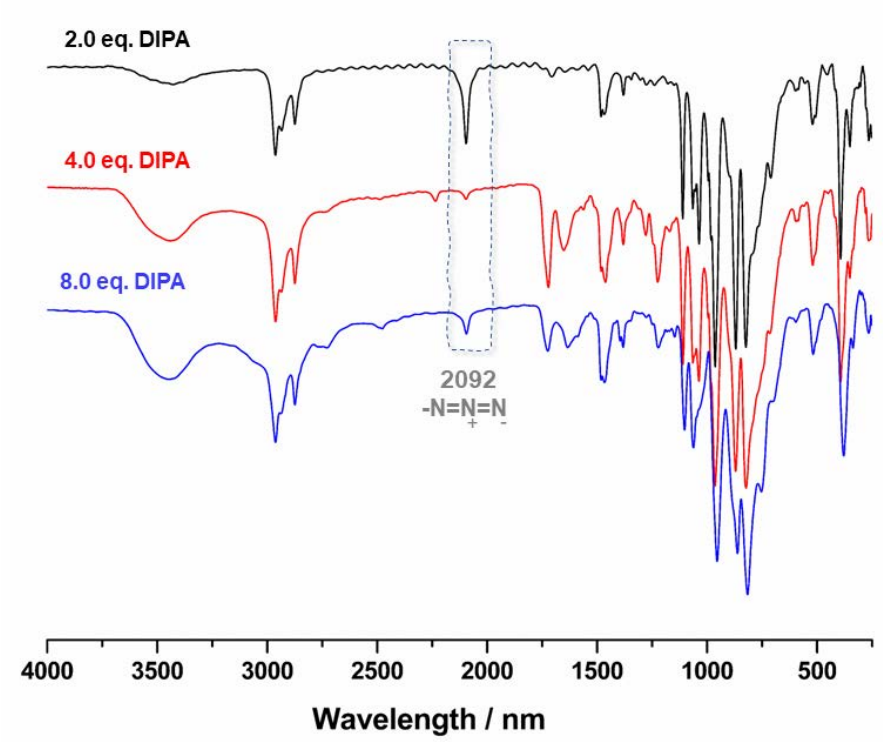

Figure 3-28 IR monitor of the "click" between ***$K_{Si}[N_3]$-3*** *and methyl propiolate in the presence of different amount of DIPA 2.0 eq. (black), 4.0 eq. (red) and 8.0 eq (blue) at room temperature.*

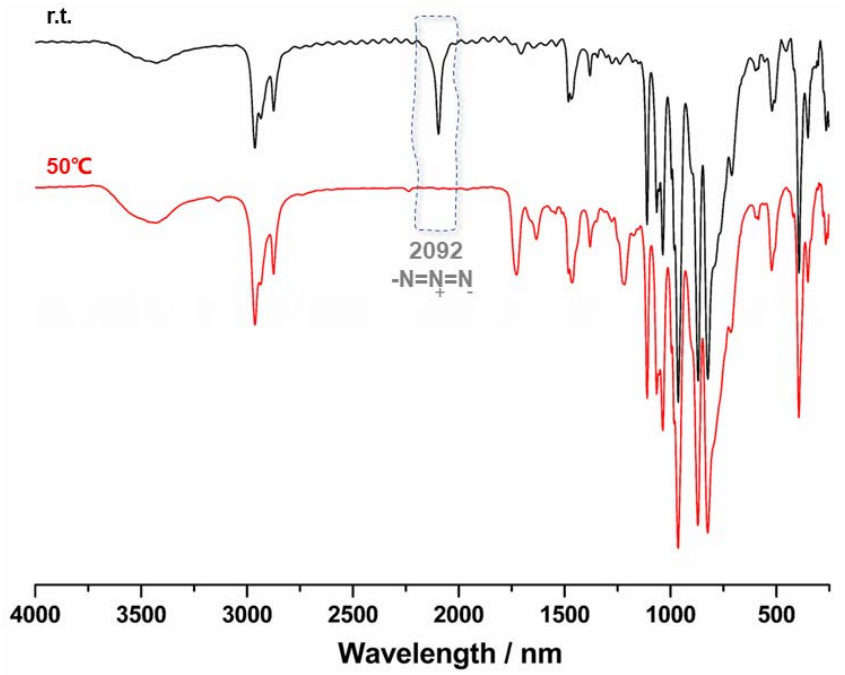

Figure 3-29 IR monitor of the "click" between ***$K_{Si}[N_3]$-3*** *and methyl propiolate in the presence of 2.0 eq. DIPA at room temperature (black) and 50℃ (red).*

Propargyl-DPA

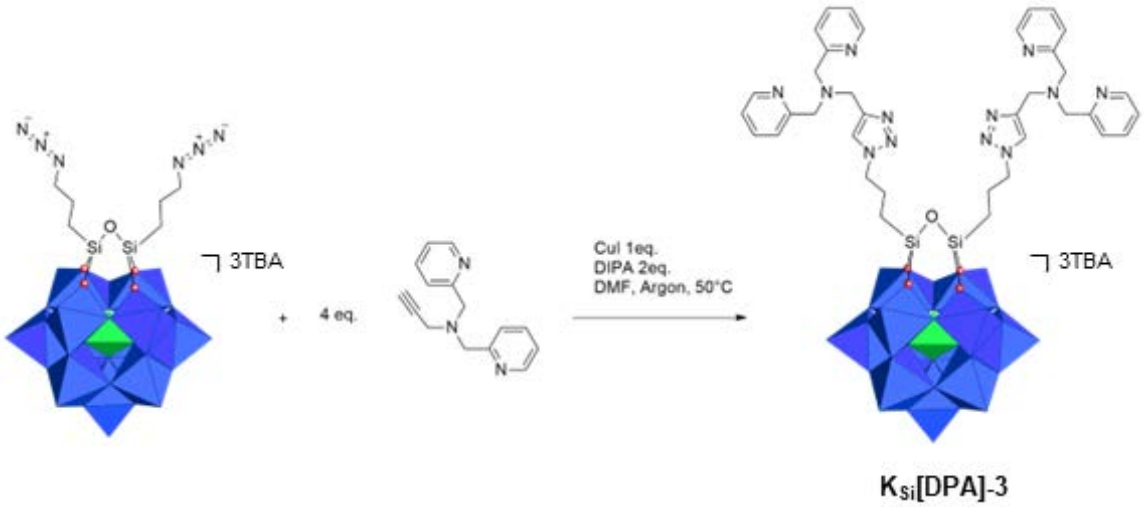

Scheme 3-9 The synthesis of ***$K_{Si}[N_3DPA]$-3*** *with CuI as catalyst.*

We applied the conditions optimized above to the coupling of propargyl DPA with **$K_{Si}[N_3]$-3**. 2.0 eq. of DIPA were mixed with 1.0 eq. **$K_{Si}[N_3]$-3** and 4.0 eq. propargyl DPA followed by the addition of DMF under argon and degassed before the addition of 1.0 eq. CuI. After overnight stirring at 50 ℃, the resulting olive solution was precipitated in ether and a green powder was obtained. Disappearance of the azido stretch in IR (Figure 3-30), coupled with the detection in ^{1}H NMR of the characteristic triazole peak at 8.12 ppm suggested the successful “click” reaction.

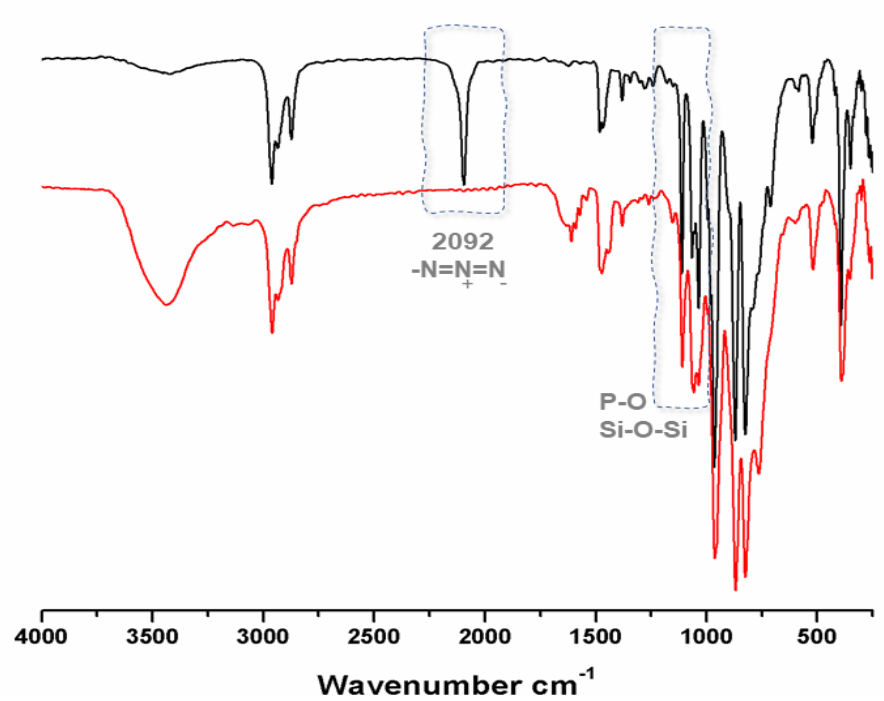

Figure 3-30 The IR spectrum of the synthesis of ***K_{Si}[N_3DPA]-3*** *with 1.0 eq. of CuI and 2.0 eq. DIPA heated at 50℃.*

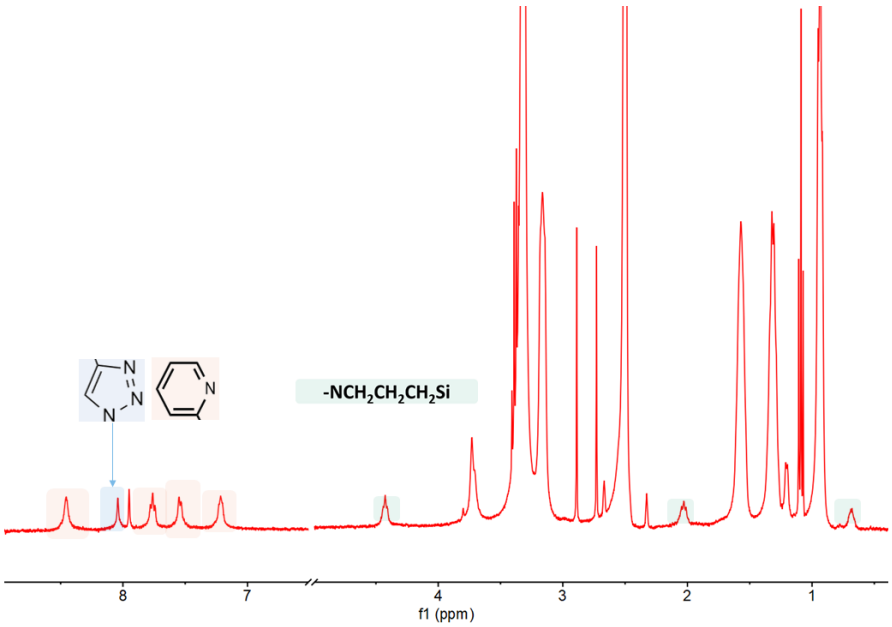

Figure 3-31 the ^{1}H NMR of the synthesis ***K_{Si}[N_3DPA]-3*** *with 1.0 eq. of CuI and 2.0 eq. DIPA heated at 50℃, inset: the ^{31}P NMR.*

This was further confirmed by DOSY NMR. The result showed us the propylene and pyridine have similar diffusion coefficients, ~1.1 ×10^{-10} m^2/s and ~1.2 ×10^{-10} m^2/s respectively, moreover in line with the methylene peaks of **K_{Si}[I]**. The diffusion coefficients of the TBA^+, ~2.5 ×10^{-10} are somewhat larger.

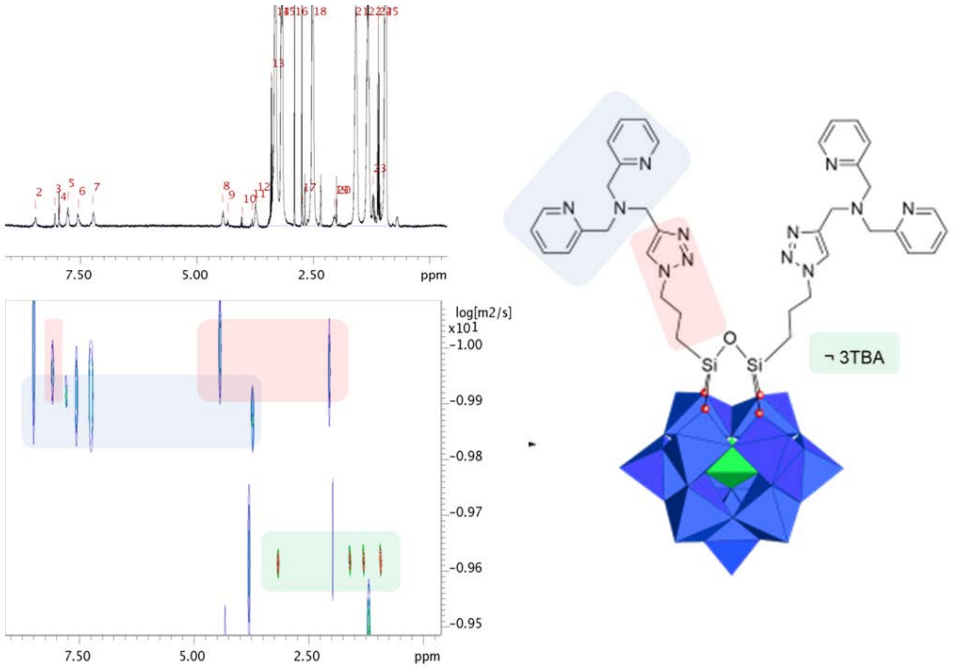

*Figure 3-32 the DOSY NMR of the crude **K_{Si}[DPA]-3**.*

*Table3-6 The of diffusion coefficient of the synthesized **K_{Si}[N_3DPA]-3***

Peaks	Species	F2(ppm)	D(×10^{-10} m^2/s)	error×10^{-11}
2	DPA	8.468	**0.99**	3.525
5		7.770	**1.17**	0.523
6		7.541	**1.27**	2.148
7		7.229	**1.18**	2.146
12		3.175	**1.33**	1.482
3	triazole	8.049	**1.08**	1.078
8	-$SiCH_2CH_2CH_2$-	4.441	**1.04**	1.987
19		2.048	**1.09**	2.350
11		3.808	**2.54**	8.307
15	TBA^+	3.170	**2.55**	0.330
21		1.603	**2.46**	0.502
22		1.326	**2.51**	0.370
25		0.951	**2.45**	0.195

This clearly confirm that the organic moiety was covalently grafted onto the POM skeleton. Finally, a signal at m/z=1696.78 (z= -2), with the expected tungstate isotopic pattern, corresponding to the molecular ion $\{H[PW_{11}O_{62}Si_2C_{30}H_{30}N_{12})]\}^{2-}$ was detected in ESI-MS.

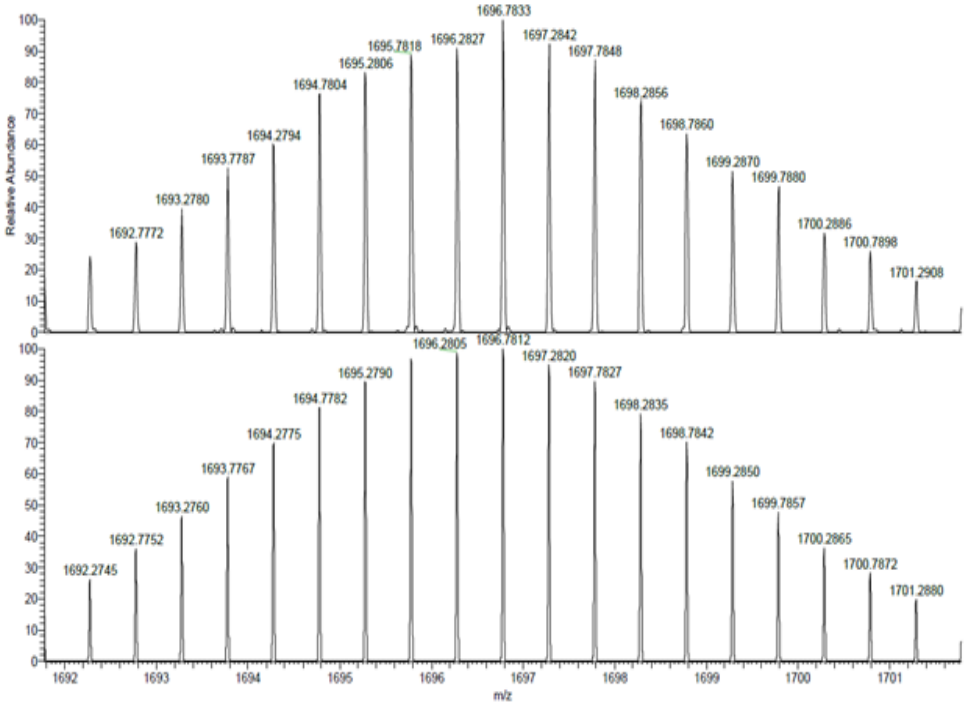

Figure 3-33 the ESI-Mass of ***K_{Si}[DPA]-3****.*

However, the blue-greenish color of the powder, together with somewhat broad NMR peaks, suggest presence of copper impurities: thus, the crude powder was redissolved in minimum of acetonitrile and precipitated slowly with ethyl acetate. The resulting dark precipitate was discarded via centrifugation and the slightly yellow solution was precipitated with diethyl ether. A slightly yellow powder with sharp pyridine and triazole peaks in ^{1}H NMR was obtained, with a single peak in ^{31}P NMR, however with less than 20% final yield.

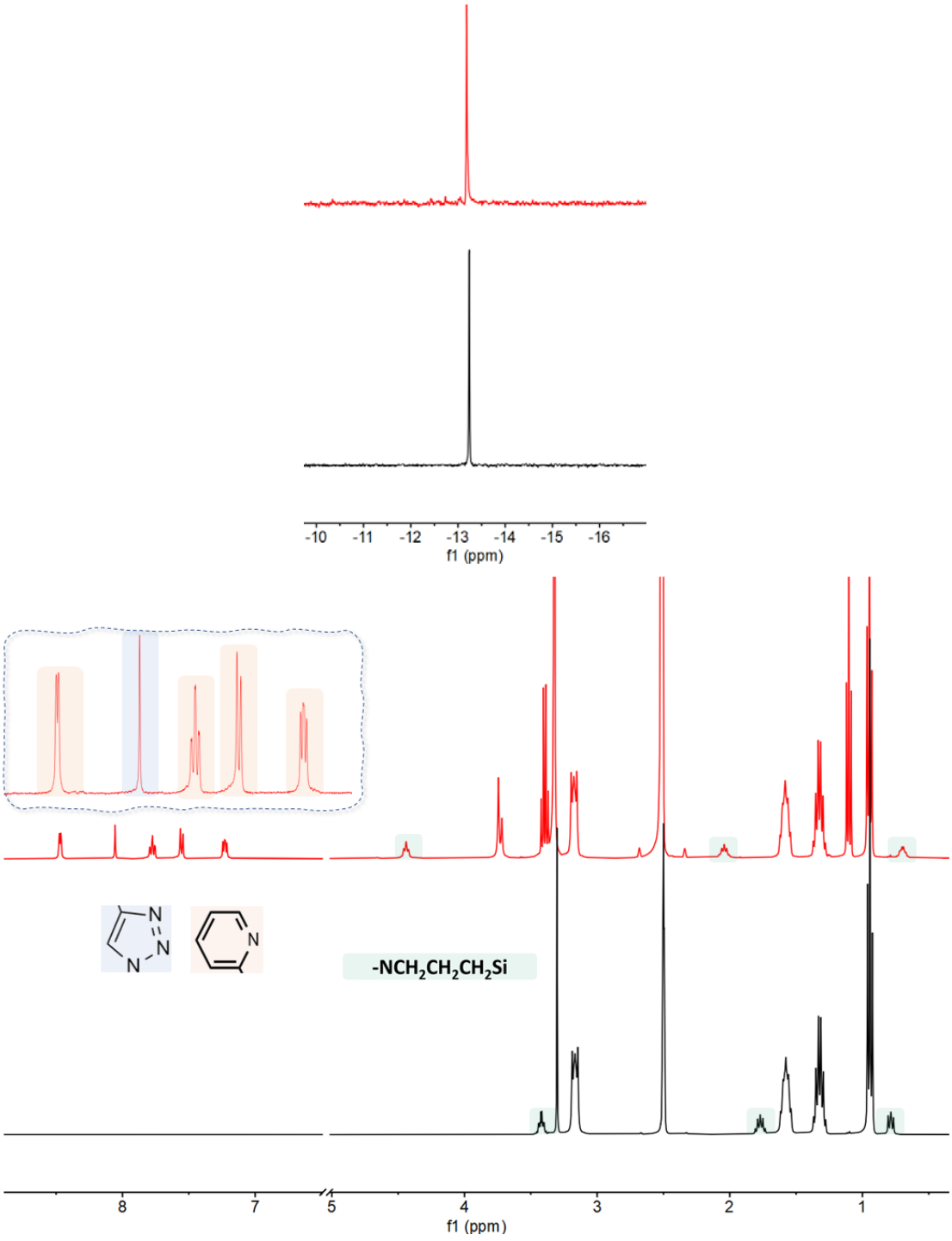

Figure 3-34 Comparison of the ^{1}H NMR and ^{31}P NMR of the purified ***K_{Si}[N_3DPA]-3*** *(black)and* ***K_{Si}[N_3]-3*** *(red).*

In order to improve the yield of the reaction, we tried to reduce the amount of CuI to get rid of its coordination as much as possible. Another three reactions were carried out with 0.25 eq., 0.35 eq. and 0.50 eq. of CuI, which were monitored with IR spectrum: 0.50 eq. of CuI are enough to fully consume the azido, while improving the global yield to 49.2%.

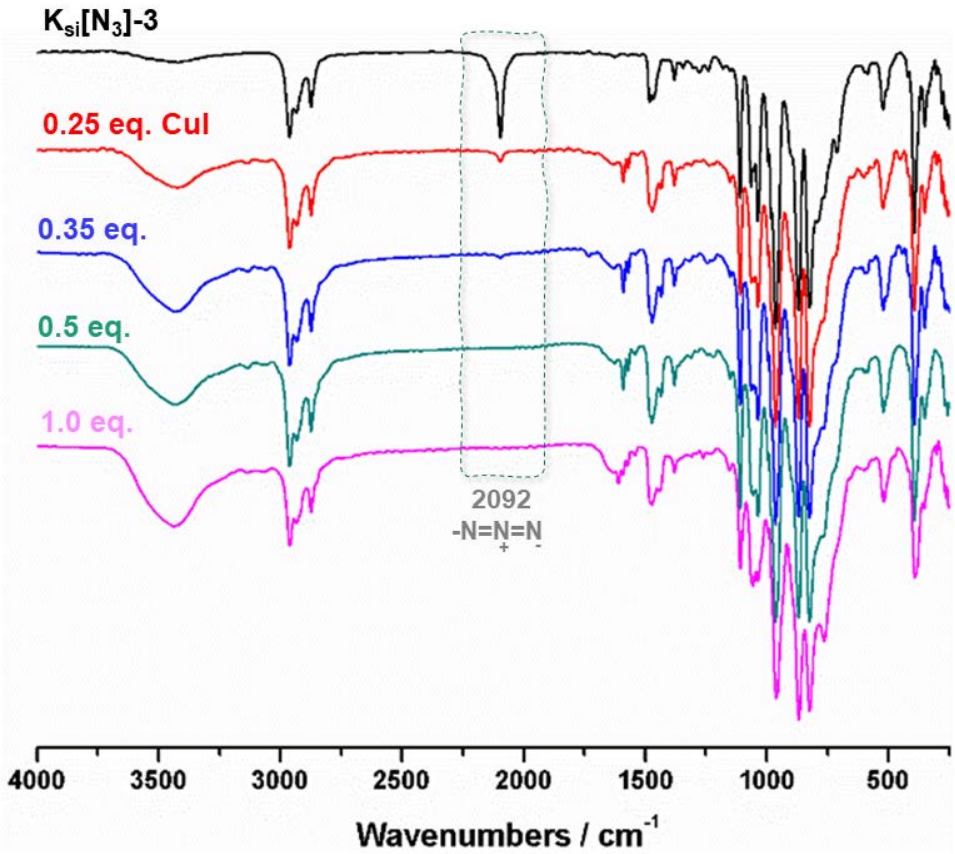

Figure 3-35 the optimization of the amount of CuI in the "click" reaction of ***$K_{Si}[N_3]$-3*** *and propargyl-DPA.*

3.2.3 Complexation of $K_{Si}[N_3DPA]$-3

The complexation of copper acetate was carried out with **$K_{Si}[N_3DPA]$-3**. A copper acetate acetonitrile solution was titrated with **$K_{Si}[N_3DPA]$-3** and monitored using UV-vis spectroscopy. A diminution of the characteristic absorption of copper acetate in acetonitrile at 670 nm upon the gradual addition of **$K_{Si}[N_3DPA]$-3** was observed, with a new band growing at 847 nm. Four isosbestic points at 376, 471, 566 and 803 nm are present from the addition of 0 eq. to 0.60 eq. of **$K_{Si}[N_3DPA]$-3**. However, the slope (Figure 3-36 B) shows the complexation process is finished upon 0.35 eq. of **$K_{Si}[N_3DPA]$-3** added which indicates one **$K_{Si}[N_3DPA]$-3** ligand could coordinate 3 copper ions. It is quite unexpected, as this suggests additional coordination sites besides the two DPA moieties.

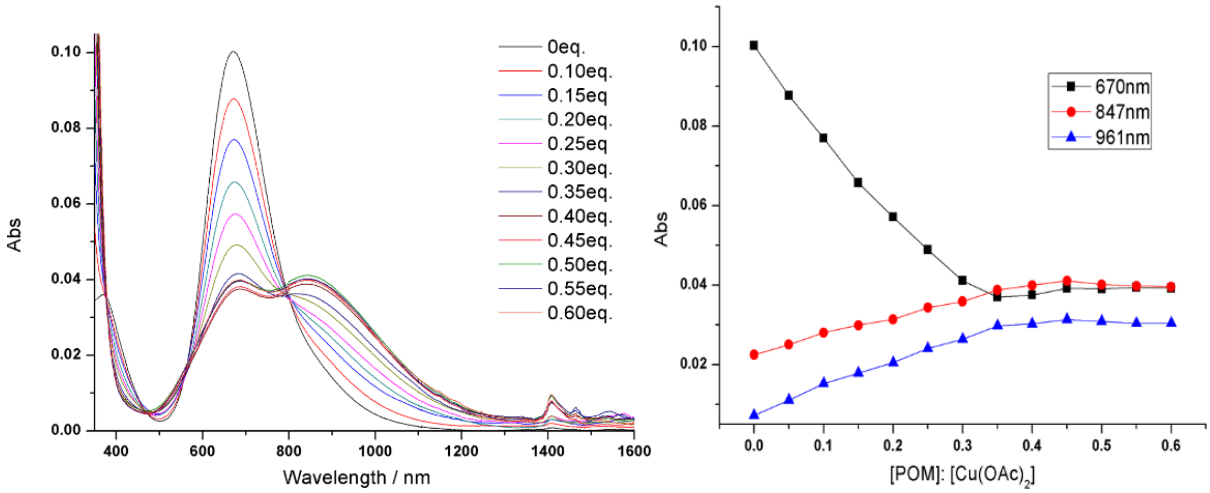

*Figure 3-36 The UV-vis titration of 0.50 mM $Cu(OAc)_2$ with **K_{Si}[N_3DPA]-3** in acetonitrile and the slope at 670, 847 and 961nm.*

It is plausible that the triazole rings could also play a ligand role,[36] and a putative structure for a complex is given below. This will require further investigations into the nature of the complex formed, and the properties of this ligand and its coordination mode.

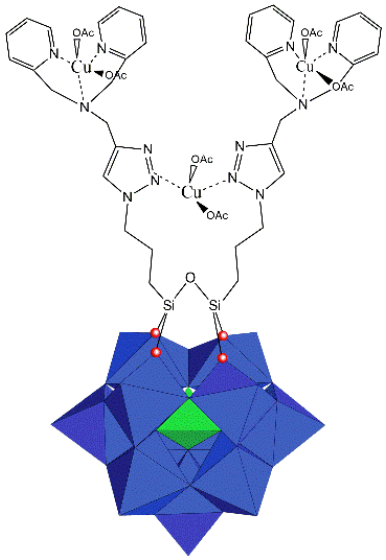

*Figure 3-37 A possible coordination structure of **K_{Si}[N_3DPA]-3**@$Cu(OAc)_2$.*

3.3 Conclusion and perspective

In this chapter we have used two different coupling reactions to perform the post-functionalization of Keggin polyoxometalates with the tripodal organic ligand propargyl-DPA.

The first ligand relies on well-known “Sonogashira” coupling and has afforded POM ligand (**K_{Sn}[DPA]**) successfully. It has been fully characterized, and a corresponding Cu

complex (**K_{Sn}[DPA]**@$Cu(OAc)_2$) has been prepared. This route can be easily extended with the “propargyl approach” to numerous N based ligands. Unfortunately, the first reactivity trial, nitrite reduction, has not given the expected results, but this exploration of preparation of POM complex and reactivity has opened a lot of perspectives.

In order to investigate the “click” reaction on POM functionalization, we have prepared a new azido-functionalized precursor, **$K_{Si}[N_3]$-3**. Through optimizing the “click” conditions, we have successfully obtained a bi-DPA functionalized POM ligand, **$K_{Si}[N_3$DPA]-3**. First complexation studies suggest that the triazole ring might interfere with the coordination process. The multi-potential coordinate sites could be applied to mimic multi-metal sites enzymes. Thus, using this reactivity, we could open the road to the grafting of two similar polyamine ligands onto POM skeletons in a controlled manner.

Experimental section

Synthesis of 1-Iodo-4-(trimethyltin)benzene

1,4-diiodobenzene (13.63 g, 41 mmol, 1.0 eq.) was dissolved in 80 mL freshly distilled THF under argon followed by the drop wisely addition of a solution of iPrMgCl (25 ml, 2 M, 50 mmol, 1.2 eq.) at -30°C. After being stirred at -30°C for 5 h, the resulting solution of 4-iodophenylmagnesium chloride was slowly canulated to a 50 mL freshly distilled THF solution of trimethyltin chloride (9.06 g, 45.5 mmol, 1.1 eq.) at -30°C. The resulting solution was stirred at -30°C for 1 h and then at room temperature overnight. The solvent was removed under vacuum and the residue was dissolved in diethyl ether followed by washing 3 times with saturated NH_4Cl aqueous and 2 times with water, the organic phase was dried with anhydrous Na_2SO_4, filtered and concentrated to get a crude that was purified by distillation under reduced pressure at 120°C. The compound was obtained as a colorless oil. Yield :12.30g, 81.2 %. ^1H NMR (300 MHz, $CDCl_3$) δ 7.73 – 7.61 (m, 2H), 7.33 – 7.10 (m, 2H), 0.29 (s, 9H)

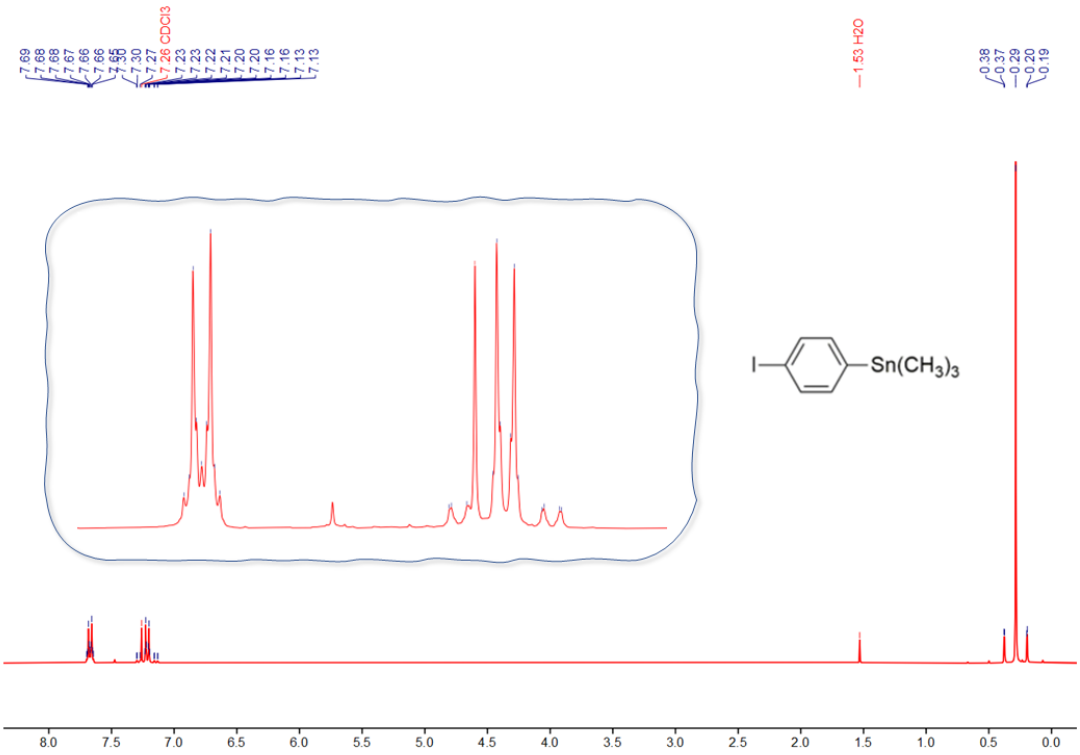

1-Iodo-4-(trimethyltin)benzene (12.30 g, 33.5 mmol, 1.0 eq.) was put in a sealed reactor in presence of tin(IV) chloride (31.5 mL, 131 mmol, 8 eq.) under argon atmosphere. The resulting solution was heated at 120°C for 2 hours. The crude was directly evaporated

under vacuum at 70-90℃ to remove all side products based on tin methyl derivatives produced during the reaction. The remaining residue was used without further purification. Yield 12.60 g, 87.6%. ^{1}H NMR (400 MHz, $CDCl_3$) δ 8.04 – 7.87 (m, 2H), 7.56 – 7.30 (m, 2H).

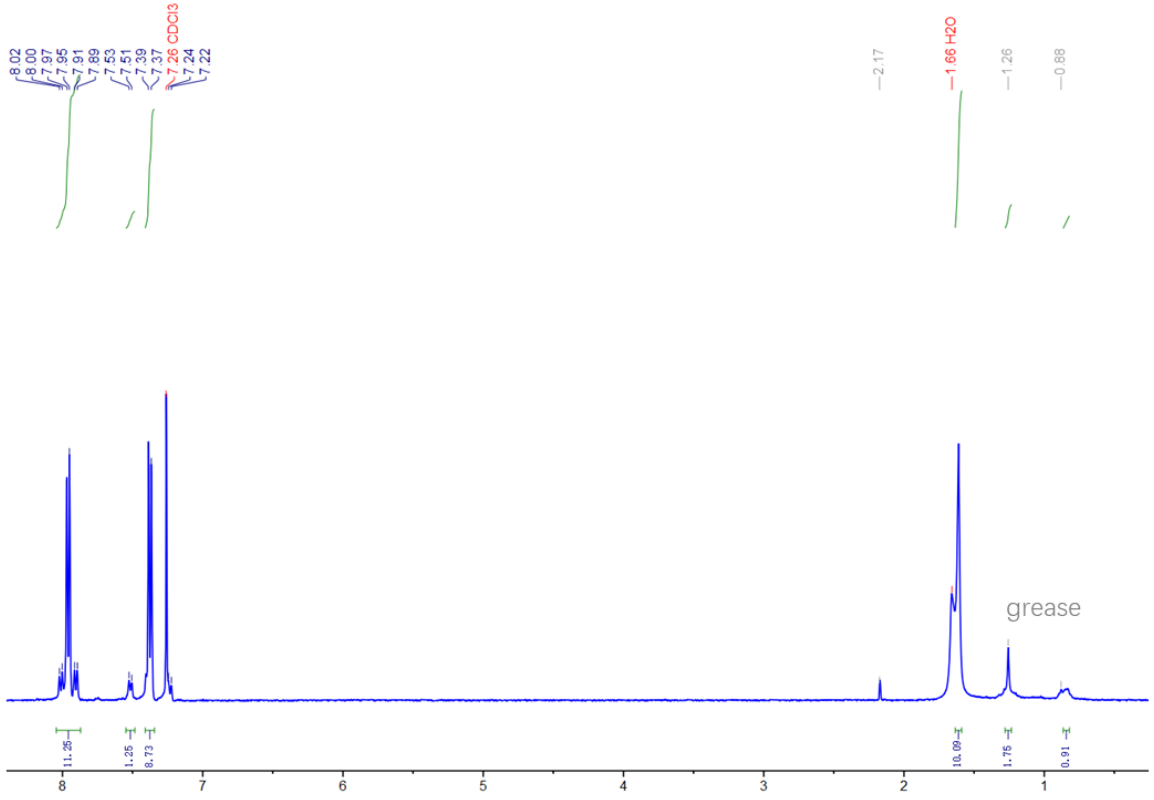

Synthesis of N,N-bis(pyridin-2-ylmethyl)prop-2-yn1-amine (propargyl-DPA)

DPA (2.14 g,10 mmol) was dissolved in 20 mL dry acetonitrile followed by the addition of anhydrous K_2CO_3 (5.40 g, 39 mmol, 4.0 eq.). Then 3-bromoprop-1-yne(1.52 g, 97%, 12.4 mmol, 1.2 eq.) was dropwise added into the yellow solution under N_2 atmosphere and kept at room temperature for three days. 20 mL dichloromethane was added into the resulting suspension to precipitate the dissolved redidue K_2CO_3. The solvent of the resulting yellow filtrate was evaporated until getting a dark brown oil. The latter was purified by basic alumina column eluting with dichloromethane. Upon evaporation of the solvent, a brown oil was isolated (2.37g, yield 92.5%).^{1}H NMR ($CDCl_3$): δ(ppm) 8.56 (d, J= 4.9 Hz, 2H), 7.65 (td, J_1= 7.8 Hz, J_2= 1.7 Hz, 2H), 7.50 (d, J= 7.8 Hz, 2H), 7.16 (dd, J_1= 7.8Hz, J_2= 4.9Hz, 2H), 3.92 (s, 4H),3.42 (d, J=2.3Hz, 2H), 2.29 (t, J=2.3Hz, 1H).

Synthesis of **K_{Sn}[I]**

The precursor **K_{Sn}[I]** was synthesised according to the work by G. Izzet *et al*..[13] $K_7[PW_{11}O_{39}]$ •$14H_2O$ (2.00 g, 0.62 mmol) was dissolved in 27 mL H_2O, followed by the addition of trichloro(4-iodophenyl) stannane (0.44 g, 1.03 mmol, 1.65 eq.) resulting in a gray suspension. Then 1M KOH was added into the suspension to adjust the pH to 3.5. The resulting suspention was stirred at room temperature for 15 minutes, then centrifuged to remove the solide. Tetrabutulammonium bromide aqueous solution (1.55 mM, 2.6 mL, 6.4 eq.) was added into the supernatante resulting in a large amount of white precipitate pure enough for further use (2.36 g, yield 95.2%). ^{1}H NMR (CD_3CN): δ(ppm) 7.85 (d+dd, J= 8.0 Hz, J_{SnH}= 30.5Hz, 2H), 7.53 (d+dd, J= 8.0 Hz, J_{SnH}=94.9 Hz, 2H), 3.12 (m, 32H), 1.62 (m, 32H), 1.39 (h, J= 7.3 Hz, 32H), 0.98 (t, J= 7.3 Hz, 52H).^{31}P (CD3CN): δ(ppm) -11.64 (s+d, J_{SnP}=23.5Hz).

Synthesis of **K_{Sn}[DPA]**

The **K_{Sn}[DPA]** was prepared according to an adaptation of the procedure of G.Izzet et al[37]: A mixture of **K_{Sn}[I]** (400 mg, 0.108 mmol), CuI (0.31 mg, 0.016 mmol, 0.16 eq.) and $[PdCl_2(PPh_3)_2]$ (8.5 mg, 0.012 mmol, 0.12 eq.) in 6 mL of dry DMF was prepared in a Schlenk tube under argon atmosphere followed the addition of the Propargyl-DPA (95.6 mg, 0.432 mmol, 4.0 eq.). After careful freeze-pump-thaw degassing with argon for 3 times, freshly distilled under inert atmosphere triethylamine (TEA) (280 mL, 2.16 mmol, 20 eq.) was added. The mixture was heated at 80°C for 1 hour, under microwave irradiation. The resulting dark red solution was precipitated with diethyl ether. The dark precipitate was filtered and redissolved in 2 mL acetonitrile under ultrasonicating for 10 minutes. The resulting dark brown solution was filtered followed the addition of 8 mL ethyl acetate. A dark precipitate was discarded from the colorless supernatant, which was again precipitated using a large excess of diethyl ether, then wash with ethanol, yielding after drying a slight yellow powder (130.0 mg, Yield: 31.5%).^{1}H NMR (CD_3CN): δ(ppm) 8.53 (d, J= 4.9 Hz, 2H), 7.74 (td, J_1= 7.8 Hz, J_2= 1.8 Hz, 2H), 7.68 (d+dd, J= 8.1 Hz, J_{SnH}= 95.6 Hz, 2H), 7.56 (d, J= 7.8 Hz, 2H), 7.53 (d+d, J= 8.1 Hz, J_{SnH}=33.4 Hz, 2H), 7.23 (dd, J_1= 7.8 Hz, J_2= 4.9 Hz, 2H), 3.94 (s, 4H), 3.62 (s, 2H), 3.12 (m, 32H), 1.62 (m, 32H), 1.39 (h, J= 7.3 Hz, 32H), 0.98 (t, J= 7.3 Hz, 52H).^{31}P (CD3CN): δ(ppm) -11.63(s+dd, J_{SnP}=23.5 Hz). HRMS (ESI-): m/z {**HK_{Sn}[DPA]**}$^{3-}$ 1036.43, calculated for

$[PW_{11}O_{39}SnC_{21}H_{19}N_3]^{3-}$: 1036.43. Elemental analysis calculated for **K_{Sn}[DPA]**•EtOH (%): C 25.34; H 4.11; N 2.38; found C 25.52; H 3.81; N 2.53.

Synthesis of 3-azidopropyl triethoxysilane

20 mL dry acetonitrile was added into the flask which contained 0.50 g, 7.5 mmol NaN_3 and 0.35 g, 1.0 mmol TBABr under argon followed by the addition of 1.21g, 5mmol 3-chloropropyl triethoxysilane. The resulting slightly yellow solution was filtered following being precipitated with diethyl ether after refluxing at 80℃ for 48 hours. The filtrate was rotary evaporated resulting 1.22 g slightly brown oil with a yield 93.1%. ^{1}H NMR (400 MHz, $CDCl_3$) δ 3.81 (q, *J* = 7.0 Hz, 6H), 3.25 (t, *J* = 7.0 Hz, 2H), 1.76 – 1.64 (m, 2H), 1.22 (t, *J* = 7.0 Hz, 12H), 0.72 – 0.62 (m, 2H).

Synthesis of **K_{Si}[N_3]-3**

A mixture of $K_7[PW_{11}O_{39}]$ •$14H_2O$ (300.0 mg, 0.094 mmol) and TBABr (96.6 mg, 0.3 mmol, 3.2 eq.) was dissolved with 18 mL acetonitrile followed by the addition of (azidopropyl)triethoxysilane (51.0 mg, 0.21 mmol, 2.2 eq.). Following the gradual addition of HCl (0.75 mL, 2.4 M, 19 eq.) at 0℃, the colorless solution was stirred at room temperature overnight. The resulting suspension was filtered to remove the white solid. The filtrate was concentrated to 3 mL, poured in 20 mL absolute ethanol. After filtration, the resulting white precipitate was recrystallized through the diffusion of ethanol into an acetonitrile solution to yield white crystal (230.0 mg, yield 67.4%). ^{1}H NMR (DMSO): δ(ppm) 3.42 (m, 4H), 3.16 (m, 24H), 1.77 (m, 4H, H_4), 1.57 (m, 32H), 1.32 (h, J= 7.3 Hz, 24H), 0.94 (t, J= 7.3 Hz, 36H), 0.78 (t, 8.1 Hz, 4H).^{31}P (DMSO): δ(ppm) -13.24 (s). IR (KBr, cm^{-1}): 2963(s), 2932 (m), 2874(m), 2092(s, -N=N=N), 1109 (s, Si-O-Si), 1062, 1036(s, P-O), 963 (W=O), 869 (W=O), 823 (W-O-W). HRMS (ESI-Mass): m/z **{K_{Si}[N_3]-3}$^{3-}$** 972.76, calculated for $[PW_{11}O_{40}Si_2C_6H_{12}N_{60.}]^{3-}$: 972.76.

Synthesis of **K_{Si}[N_3DPA]-3**

K_{Si}[N_3DPA]-3 was prepared according to a modified procedure of that published by Cronin, L and co-wokers[33]. **K_{Si}[N_3]-3** (300.0 mg, 0.08 mmol) was dissolved in 10 mL dry DMF

in a Schlenk tube under argon followed by the addition of propargyl DPA (76.0 mg, 0.32 mmol, 4.0 eq.) and DIPA (20.0 mg, 0.20 mmol, 2.0 eq.). After careful freeze-pump-thaw degassing with argon for 3 times, CuI (7.6 mg, 0.04 mmol, 0.5 eq.) was added. The mixture was heated at 50°C for 5 hours. The resulting dark green solution was precipitated with diethyl ether. The dark precipitate was centrifugated, the precipitate redissolved in 2 mL acetonitrile, which was ultrasonicated for 10 minutes, the resulting dark brown suspension was filtered, and 8 mL ethyl acetate wad gradually added into the filtrate. A dark precipitate was removed from the colorless supernatant which was poured into a large excess of diethyl ether, yielding a slightly yellow powder (167 mg, Yield: 49.2%). ^{1}H NMR (DMSO-d6): δ(ppm) 8.45 (d, J= 4.8 Hz, 4H), 8.05 (s,2H), 7.75 (t, J= 7.7 Hz, 4H), 7.54 (d, J= 7.7 Hz, 4H), 7.21 (td, J_1= 7.7 Hz J_2= 4.8 Hz, 4H), 4.42 (t, J=6.9 Hz, 4H), 3.73 (s, 8H), 3.70 (s, 2H), 3.16 (m, 24H), 2.03 (m, 4H), 1.57 (m, 32H), 1.31 (h, J= 7.3 Hz, 24H), 0.93 (t, J= 7.3 Hz, 36H), 0.68 (m, 4H).^{31}P (DMSO): δ(ppm) -13.19(s). IR (KBr, cm^{-1}): 2963(s), 2932 (m), 2874(m), 1109 (s, Si-O-Si), 1062, 1036 (s, P-O), 963 (s, W=O), 869 (s, W=O), 823 (W-O-W). HRMS (ESI-MS): m/z {**HK_{Si}[N_3DPA]-3**}$^{2-}$ 1696.78, calculated for $[PW_{11}O_{40}Si_2C_{36}H_{44}N_{12}]^{2-}$: 1696.78.

IR of the complexation process of **K_{Si}[N_3DPA]-3** with $Cu(OAc)_2$

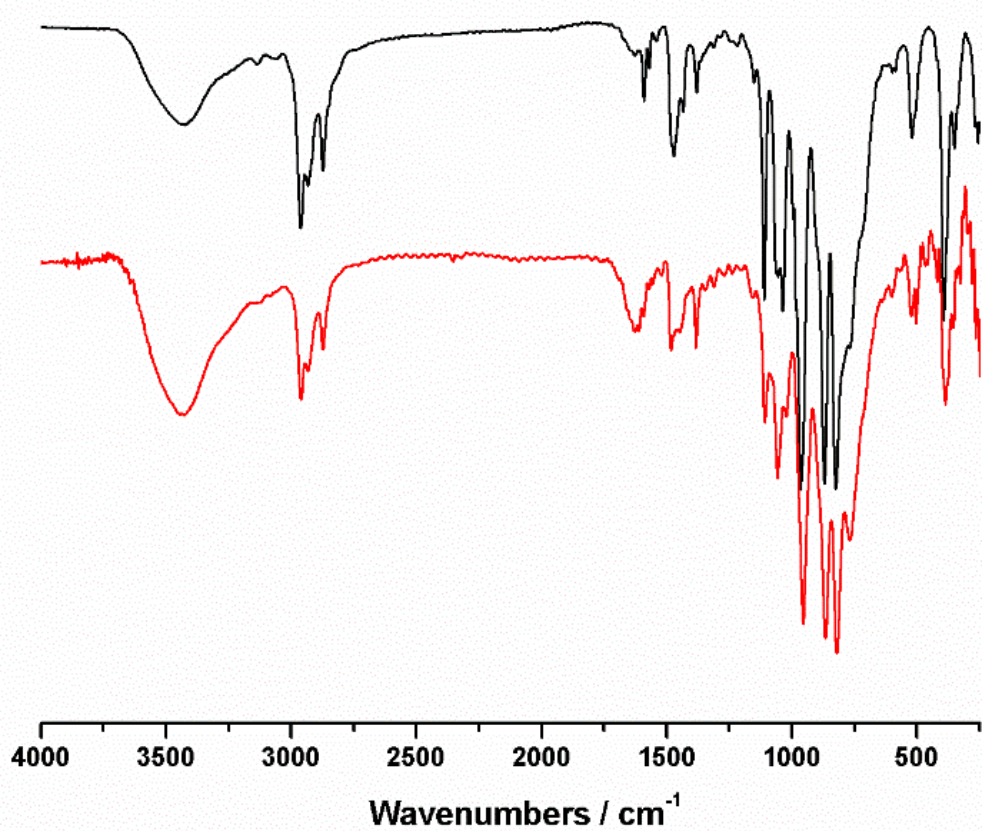

*Figure 3-38 the IR spectrum of the isolated **K_{Si}[N_3DPA]-3**@$Cu(OAc)_2$*

Synthesis of 2-azidoethyl triethoxysilane

Scheme 3-10 The synthesis of 2-azidoethyl triethoxysilane.

20 mL dry acetonitrile was added into the flask which contained 0.65 g, 1.0 mmol NaN_3 and 0.35 g, 1.0 mmol TBABr under argon followed by the addition of 1.13 g, 5 mmol 2-chloropropyl triethoxysilane. The resulting slightly yellow solution was filtered following being precipitated with diethyl ether after refluxing for 72 hours. The filtrate was rotary evaporated resulting 0.96 g slightly brown oil with a yield 77.3%. ^{1}H NMR (300 MHz, CD_3CN) δ 3.81 (q, *J* = 7.0 Hz, 6H), 3.41 – 3.29 (m, 2H), 1.19 (t, *J* = 7.0 Hz, 9H), 1.10 – 0.95 (m, 2H).

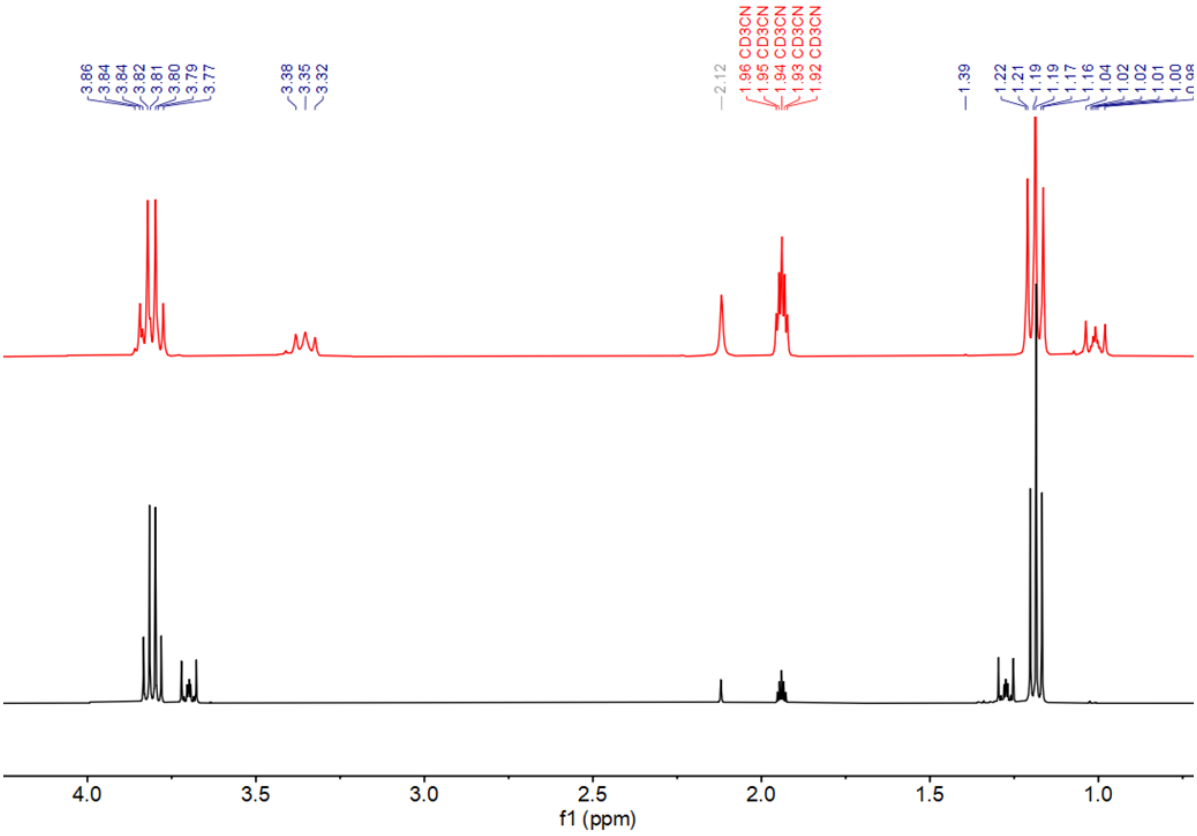

Figure 3-39 The ^{1}H NMR of 2-azidoethyl triethoxysilan (red) and the precursor 2-chloroethyl triethoxysilan (black) in CD_3CN .

Synthesis of $(TBA)_3[PW_{11}O_{39}O\{SiCH_2CH_2\text{-}N_3\}_2]$ (**K_{Si}[N_3]-2**)

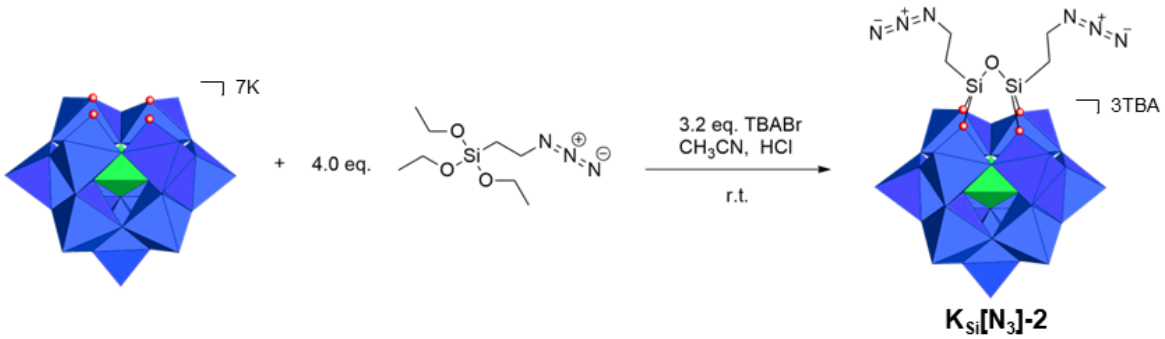

Scheme 3-11 The synthesis of KSi[N3]-2

A mixture of $K_7[PW_{11}O_{39}]$ •$14H_2O$ (300.0 mg, 0.094 mmol) and TBABr (96.6 mg, 0.3 mmol, 3.2 eq.) was dissolved with 18 mL acetonitrile followed by the addition of (azidoethyl)triethoxysilane (87.7 mg, 0.376 mmol, 4.0 eq.). Following the gradual addition of HCl (0.75 mL, 2.4 M, 19 eq.) at 0℃， the colorless solution was stirred at 0℃ for 0.5 hour and then room temperature overnight. The resulting suspension was filtered to remove the white

solid. The filtrate was concentrated to 2 mL, poured in 25 mL absolute ethanol. After filtration, the resulting 220mg white precipitate was recrystallized through the diffusion of ethanol into an acetonitrile solution to yield 170 mg white crystal, yield 64.7%. ^{1}H NMR (DMSO): δ(ppm) 3.5 (m, 4H), 3.18 (m, 24H), 1.59 (m, 32H), 1.33 (h, 24H), 1.16 (t, 4H), 0.95 (t, 36H).^{31}P (DMSO): δ(ppm) -13.19 (s). IR (KBr, cm^{-1}): 2963 (s), 2932 (m), 2874 (m), 2090 (s, -N=N=N), 1110 (s, Si-O-Si), 1065, 1040 (s, P-O), 965 (W=O), 870 (W=O), 825 (W-O-W). HRMS (ESI-Mass): m/z **{$K_{Si}[N_3]$-2}$^{3-}$** 963.09, calculated for $[PW_{11}O_{40}Si_2C_6H_{12}N_{60.}]^{3-}$: 973.40.

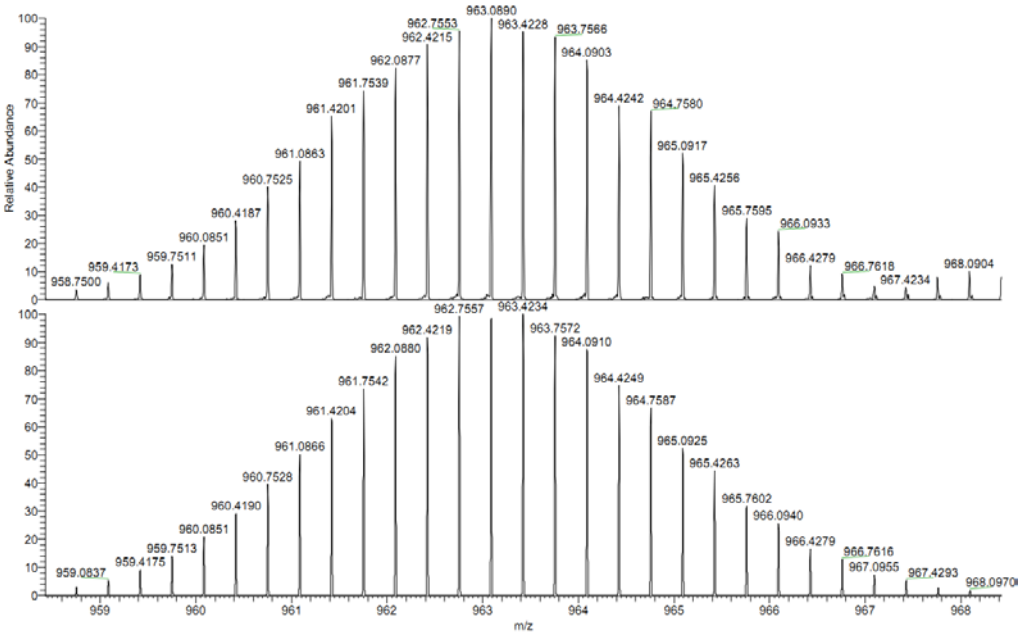

Figure 3-40 ESI-MS of ***$K_{Si}[N_3]$-2***

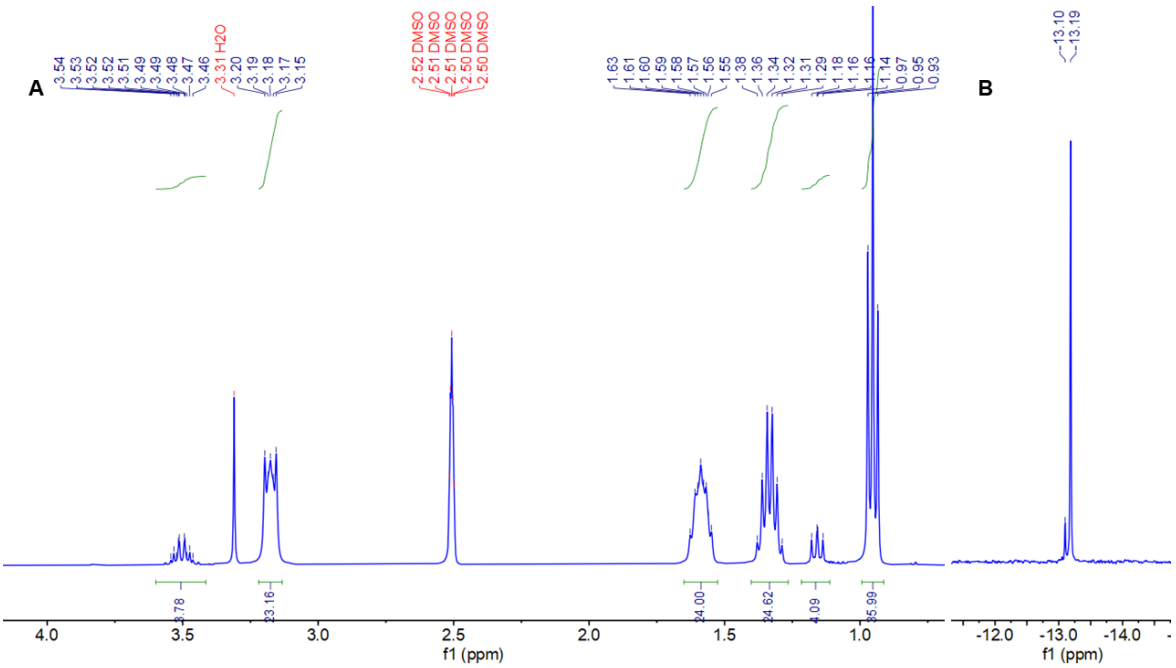

*Figure 3-41 The ^{1}H NMR (A) and ^{31}P NMR (B) of (**$K_{Si}[N_3]$-2**) in DMSO.*

Synthesis of $(TBA)_3[PW_{11}O_{39}O\{SiCH_2CH_2\text{-}N_3CCH\text{-}CH_2N(CH_2Py)_2\}_2]$ (**$K_{Si}[N_3DPA]$-2**)

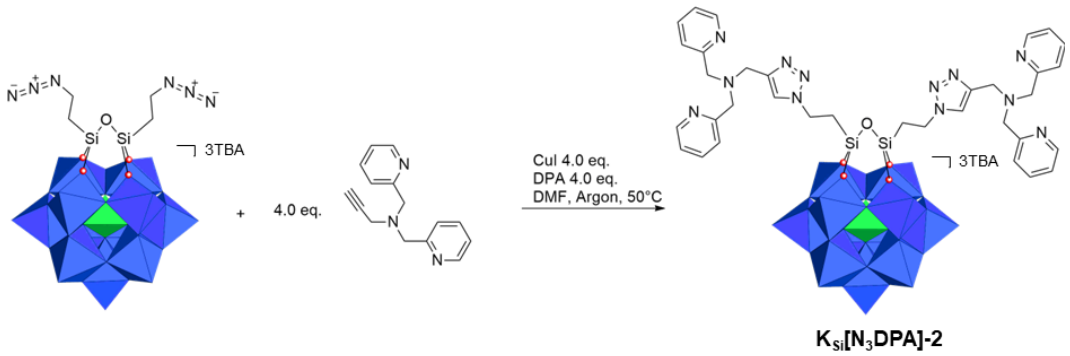

Scheme 3-12 The synthesis of ***$K_{Si}[N_3DPA_3]$-2***

The mixture of 38.3 mg, 0.16 mmol propargyl-DPA, 34.4 mg, 0.16 mmol DPA and 30.5 mg, 0.16 mmol CuI was dissolved in 1.5 mL anhydrous DMF under argon resulting brown-greenish solution after 20 mins stirring, followed by the addition of 1.5 mL **$K_{Si}[N_3]$-2** (150 mg, 0.04 mmol) anhydrous DMF solution. The resulting dark green solution was stirred under room temperature. The doublet peak at 8.13 ppm in ^{1}H NMR indicated the formation of the triazole, coupled with the shift of the silane chain and the appearance of the pyridine peaks and the diminish of azido absorption at 2090 cm^{-1} in IR spectrum (Figure 3-41). In the meantime, there was an unnormal shift of the phosphate signals from -13.19 ppm to – 8.93 ppm in line with the

significant absorption variation of the POM skeleton in IR spectrum compared to the precursor **$K_{Si}[N_3]$-2**, which indicated the structure of the POM might be changed. The "click" functionalization of DPA onto the POM skeleton through short spacer need to be further investigated.

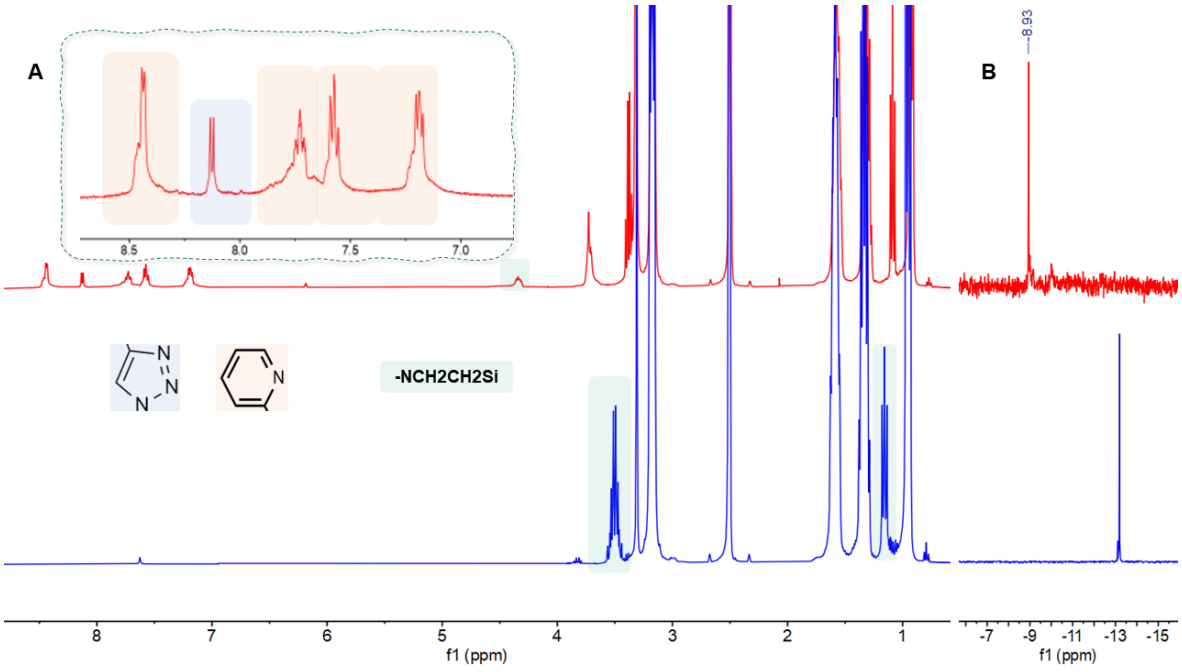

*Figure 3-42 The ^{1}H NMR (A) and ^{31}P NMR (B) of (**$K_{Si}[N_3DPA]$-2**) (red) in DMSO.*

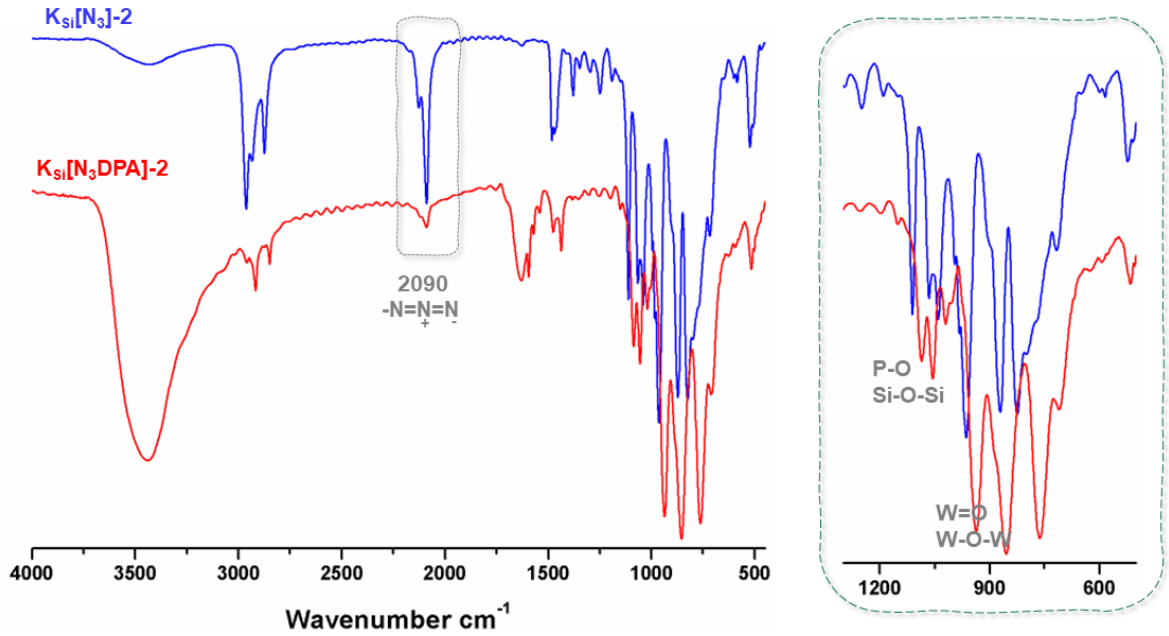

*Figure 3-43 The IR spectrum of **$K_{Si}[N_3]$-2** (blue) and **$K_{Si}[N_3DPA]$-2** (red).*

Reference:

(1) Duffort, V.; Thouvenot, R.; Afonso, C.; Izzet, G.; Proust, A. Straightforward Synthesis of New Polyoxometalate-Based Hybrids Exemplified by the Covalent Bonding of a Polypyridyl Ligand. *Chemical Communications* **2009**, *0* (40), 6062–6064.

(2) Zhu, Y.; Wang, L.; Hao, J.; Yin, P.; Zhang, J.; Li, Q.; Zhu, L.; Wei, Y. Palladium-Catalyzed Heck Reaction of Polyoxometalate-Functionalised Aryl Iodides and Bromides with Olefins. *Chemistry – A European Journal* **2009**, *15* (13), 3076–3080.

(3) Kang, J.; Xu, B.; Peng, Z.; Zhu, X.; Wei, Y.; Powell, D. R. Molecular and Polymeric Hybrids Based on Covalently Linked Polyoxometalates and Transition-Metal Complexes. *Angewandte Chemie* **2005**, *117* (42), 7062–7065.

(4) Xu, B.; Lu, M.; Kang, J.; Wang, D.; Brown, J.; Peng, Z. Synthesis and Optical Properties of Conjugated Polymers Containing Polyoxometalate Clusters as Side-Chain Pendants. *Chem. Mater.* **2005**, *17* (11), 2841–2851.

(5) He, T.; He, J.; Lu, M.; Chen, B.; Pang, H.; Reus, W. F.; Nolte, W. M.; Nackashi, D. P.; Franzon, P. D.; Tour, J. M. Controlled Modulation of Conductance in Silicon Devices by Molecular Monolayers. *J. Am. Chem. Soc.* **2006**, *128* (45), 14537–14541.

(6) Bareyt, S.; Piligkos, S.; Hasenknopf, B.; Gouzerh, P.; Lacôte, E.; Thorimbert, S.; Malacria, M. Efficient Preparation of Functionalized Hybrid Organic/Inorganic Wells−Dawson-Type Polyoxotungstates. *J. Am. Chem. Soc.* **2005**, *127* (18), 6788–6794.

(7) Micoine, K.; Hasenknopf, B.; Thorimbert, S.; Lacôte, E.; Malacria, M. A General Strategy for Ligation of Organic and Biological Molecules to Dawson and Keggin Polyoxotungstates. *Organic Letters* **2007**, *9* (20), 3981–3984.

(8) Harriman, A.; Elliott, K. J.; Alamiry, M. A. H.; Pleux, L. L.; Séverac, M.; Pellegrin, Y.; Blart, E.; Fosse, C.; Cannizzo, C.; Mayer, C. R.; Odobel, F. Intramolecular Electron Transfer Reactions Observed for Dawson-Type Polyoxometalates Covalently Linked to Porphyrin Residues. *The Journal of Physical Chemistry C* **2009**, *113* (14), 5834–5842.

(9) Joo, N.; Renaudineau, S.; Delapierre, G.; Bidan, G.; Chamoreau, L.-M.; Thouvenot, R.; Gouzerh, P.; Proust, A. Organosilyl/-Germyl Polyoxotungstate Hybrids for Covalent Grafting onto Silicon Surfaces: Towards Molecular Memories. *Chemistry – A European Journal* **2010**, *16* (17), 5043–5051.

(10) Ren, T. Peripheral Covalent Modification of Inorganic and Organometallic Compounds through C−C Bond Formation Reactions. *Chem. Rev.* **2008**, *108* (10), 4185–4207.

(11) Izzet, G.; Abécassis, B.; Brouri, D.; Piot, M.; Matt, B.; Serapian, S. A.; Bo, C.; Proust, A. Hierarchical Self-Assembly of Polyoxometalate-Based Hybrids Driven by Metal Coordination and Electrostatic Interactions: From Discrete Supramolecular Species to Dense Monodisperse Nanoparticles. *Journal of the American Chemical Society* **2016**, *138* (15), 5093–5099.

(12) Matt, B.; Moussa, J.; Chamoreau, L.-M.; Afonso, C.; Proust, A.; Amouri, H.; Izzet, G. Elegant Approach to the Synthesis of a Unique Heteroleptic Cyclometalated Iridium(III)-Polyoxometalate Conjugate. *Organometallics* **2012**, *31* (1), 35–38.

(13) Matt, B.; Renaudineau, S.; Chamoreau, L.-M.; Afonso, C.; Izzet, G.; Proust, A. Hybrid Polyoxometalates: Keggin and Dawson Silyl Derivatives as Versatile Platforms. *The Journal of Organic Chemistry* **2011**, *76* (9), 3107–3112.

(14) Feng, G.; Zhang, C.-J.; Lu, X.; Liu, B. Zinc(II)-Tetradentate-Coordinated Probe with Aggregation-Induced Emission Characteristics for Selective Imaging and Photoinactivation of Bacteria. *ACS Omega* **2017**, *2* (2), 546–553.

(15) Knoth, W. H.; Domaille, P. J.; Farlee, R. D. Anions of the Type (RMOH2)3W18P2O689- and [H2OCo]3W18P2O6812-. A Reinvestigation of “B,.Beta.-W9PO349-.” *Organometallics* **1985**, *4* (1), 62–68.

(16) Xin, F.; Pope, M. T. Polyoxometalate Derivatives with Multiple Organic Groups. 1. Synthesis and Structures of Tris(Organotin) .Beta.-Keggin and .Alpha.-Dawson Tungstophosphates. *Organometallics* **1994**, *13* (12), 4881–4886.

(17) *Hussain, F.; Kortz, U.; Clark, R. J. The Bis-Phenyltin-Substituted, Lone-Pair-Containing Tungstoarsenate $[(C_6H_5Sn)_2As_2W_{19}O_{67}(H_2O)]^{8-}$. Inorg. Chem.* ***2004****, 43 (10), 3237–3241*.

(18) Matt, B.; Xiang, X.; L. Kaledin, A.; Han, N.; Moussa, J.; Amouri, H.; Alves, S.; L. Hill, C.; Lian, T.; G. Musaev, D.; Izzet, G.; Proust, A. Long Lived Charge Separation in Iridium(Iii)-Photosensitized Polyoxometalates: Synthesis, Photophysical and Computational Studies of Organometallic–Redox Tunable Oxide Assemblies. *Chemical Science* **2013**, *4* (4), 1737–1745.

(19) Blanchard, S.; Rager, M.-N.; Duprat, A. F.; Reinaud, O. A Novel Calix[6]Arene-Based Mononuclear Copper(I) Complex That Exhibits Chirality at Low Temperature. *New J. Chem.* **1998**, *22* (11), 1143–1146.

(20) Solomon, E. I.; Heppner, D. E.; Johnston, E. M.; Ginsbach, J. W.; Cirera, J.; Qayyum, M.; Kieber-Emmons, M. T.; Kjaergaard, C. H.; Hadt, R. G.; Tian, L. Copper Active Sites in Biology. *Chem. Rev.* **2014**, *114* (7), 3659–3853.

(21) Quist, D. A.; Diaz, D. E.; Liu, J. J.; Karlin, K. D. Activation of Dioxygen by Copper Metalloproteins and Insights from Model Complexes. *J Biol Inorg Chem* **2017**, *22* (2), 253–288.

(22) Nakamoto, K. *Infrared and Raman Spectra of Inorganic and Coordination Compounds*, 4th edition.; Wiley-Interscience: New York, 1986.

(23) Stephenson, T. A.; Wilkinson, G. Acetato Complexes of Palladium (II). *Journal of Inorganic and Nuclear Chemistry* **1967**, *29* (8), 2122–2123.

(24) Crutchley, R. J.; Hynes, R.; Gabe, E. J. Five- and Four-Coordinate Copper(II) Complexes of 2,2’-Bipyridine and Phenylcyanamide Anion Ligands: Crystal Structures, Cyclic Voltammetry, and Electronic Absorption Spectroscopy. *Inorg. Chem.* **1990**, *29* (24), 4921–4928.

(25) Bard, A. J.; Faulkner, L. R. *Electrochemical Methods: Fundamental and Applications*, 2nd edition.; John Wiley & Sons: Hoboken: New York, 2001.

(26) Cosby, K.; Partovi, K. S.; Crawford, J. H.; Patel, R. P.; Reiter, C. D.; Martyr, S.; Yang, B. K.; Waclawiw, M. A.; Zalos, G.; Xu, X.; Huang, K. T.; Shields, H.; Kim-Shapiro, D. B.; Schechter, A. N.; Cannon, R. O.; Gladwin, M. T. Nitrite Reduction to Nitric Oxide by Deoxyhemoglobin Vasodilates the Human Circulation. *Nat Med* **2003**, *9* (12), 1498–1505.

(27) Jin, Y.; Veiga, M. C.; Kennes, C. Bioprocesses for the Removal of Nitrogen Oxides from Polluted Air. *Journal of Chemical Technology & Biotechnology* **2005**, *80* (5), 483–494.

(28) Inoue, T.; Gotowda, M.; Deligeer; Kataoka, K.; Yamaguchi, K.; Suzuki, S.; Watanabe, H.; Gohow, M.; Kai, Y. Type 1 Cu Structure of Blue Nitrite Reductase from Alcaligenes

Xylosoxidans GIFU 1051 at 2.05 Å Resolution: Comparison of Blue and Green Nitrite Reductases1. *The Journal of Biochemistry* **1998**, *124* (5), 876–879.

(29) Cioncoloni, G.; Roger, I.; Wheatley, P. S.; Wilson, C.; Morris, R. E.; Sproules, S.; Symes, M. D. Proton-Coupled Electron Transfer Enhances the Electrocatalytic Reduction of Nitrite to NO in a Bioinspired Copper Complex. *ACS Catalysis* **2018**, *8* (6), 5070–5084.

(30) Bencini, A.; Bertini, I.; Gatteschi, D.; Scozzafava, A. Single-Crystal ESR Spectra of Copper(II) Complexes with Geometries Intermediate between a Square Pyramid and a Trigonal Bipyramid. *Inorg. Chem.* **1978**, *17* (11), 3194–3197.

(31) Garribba, E.; Micera, G. The Determination of the Geometry of Cu(II) Complexes: An EPR Spectroscopy Experiment. *J. Chem. Educ.* **2006**, *83* (8), 1229.

(32) Worrell, B. T.; Malik, J. A.; Fokin, V. V. Direct Evidence of a Dinuclear Copper Intermediate in Cu(I)-Catalyzed Azide-Alkyne Cycloadditions. *Science* **2013**, *340* (6131), 457–460.

(33) Macdonell, A.; Johnson, N. A. B.; Surman, A. J.; Cronin, L. Configurable Nanosized Metal Oxide Oligomers via Precise “Click” Coupling Control of Hybrid Polyoxometalates. *J. Am. Chem. Soc.* **2015**, *137* (17), 5662–5665.

(34) Odobel, F.; Séverac, M.; Pellegrin, Y.; Blart, E.; Fosse, C.; Cannizzo, C.; Mayer, C. R.; Elliott, K. J.; Harriman, A. Coupled Sensitizer–Catalyst Dyads: Electron-Transfer Reactions in a Perylene–Polyoxometalate Conjugate. *Chemistry – A European Journal* **2009**, *15* (13), 3130–3138.

(35) Jia, H.; Li, Q.; Bayaguud, A.; Huang, Y.; She, S.; Chen, K.; Wei, Y. Diversified Polyoxovanadate Derivatives Obtained by Copper(I)-Catalysed Azide–Alkyne Cycloaddition Reaction: Their Synthesis and Structural Characterization. *Dalton Trans.* **2018**, *47* (2), 577–584.

(36) Li, D.-D.; Tian, J.-L.; Gu, W.; Liu, X.; Yan, S.-P. A Novel 1,2,4-Triazole-Based Copper(II) Complex: Synthesis, Characterization, Magnetic Property and Nuclease Activity. *Journal of Inorganic Biochemistry* **2010**, *104* (2), 171–179.

(37) Parrot, A.; Izzet, G.; Chamoreau, L.-M.; Proust, A.; Oms, O.; Dolbecq, A.; Hakouk, K.; El Bekkachi, H.; Deniard, P.; Dessapt, R.; Mialane, P. Photochromic Properties of Polyoxotungstates with Grafted Spiropyran Molecules. *Inorg. Chem.* **2013**, *52* (19), 11156–11163.

Chapter 4

Functionalization of $[P_2V_3W_{15}O_{62}]^{9-}$ with tridentate amine ligands

Chapter 4 Functionalization of $[P_2V_3W_{15}O_{62}]^{9-}$ with tridentate amine ligands

4.1 Direct functionalization of $[P_2V_3W_{15}O_{62}]^{9-}$ with aromatic tripodal ligand

In order to introduce a bioinspired tripodal ligand onto the surface of the POM and with a shorter link, an alternative direct functionalization relying on the use of tris(hydroxymethyl)aminomethane (**H_3Tris**) was sought. In this approach, the tris moiety is first modified to incorporate the organic function of interest, and then grafted onto the surface of the POM.

4.1.1 Synthesis of H_3Tris-DPA

Tris(hydroxymethyl)aminomethane (**H_3Tris**) and 2-picolylchloride were associated here according to the synthesis route, which was published by Zhao,[1] (Scheme 4-1). **H_3Tris** reacted with 1.0 eq. of 2-picolylchloride in dry acetonitrile in the presence of potassium carbonate and potassium iodide.

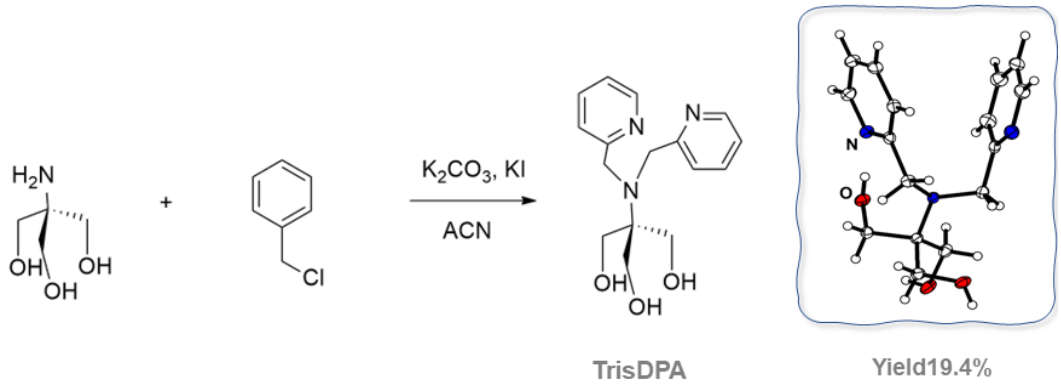

*Scheme 4-1 The synthesis route of 2-(bis(pyridin-2-ylmethyl)amino)-2-(hydroxymethyl)propane -1,3-diol (**H_3Tris-DPA**) and its crystal structure representation.*

After chromatography using methanol/ethyl acetate mixture as eluent, crystallization of the product occurred in a moderate total yield (19.4%). The ^{1}H NMR and ^{13}C NMR are in agreement with the formation of the doubly substituted tris(hydroxymethyl)-aminomethane compound, **H_3-TrisDPA**.

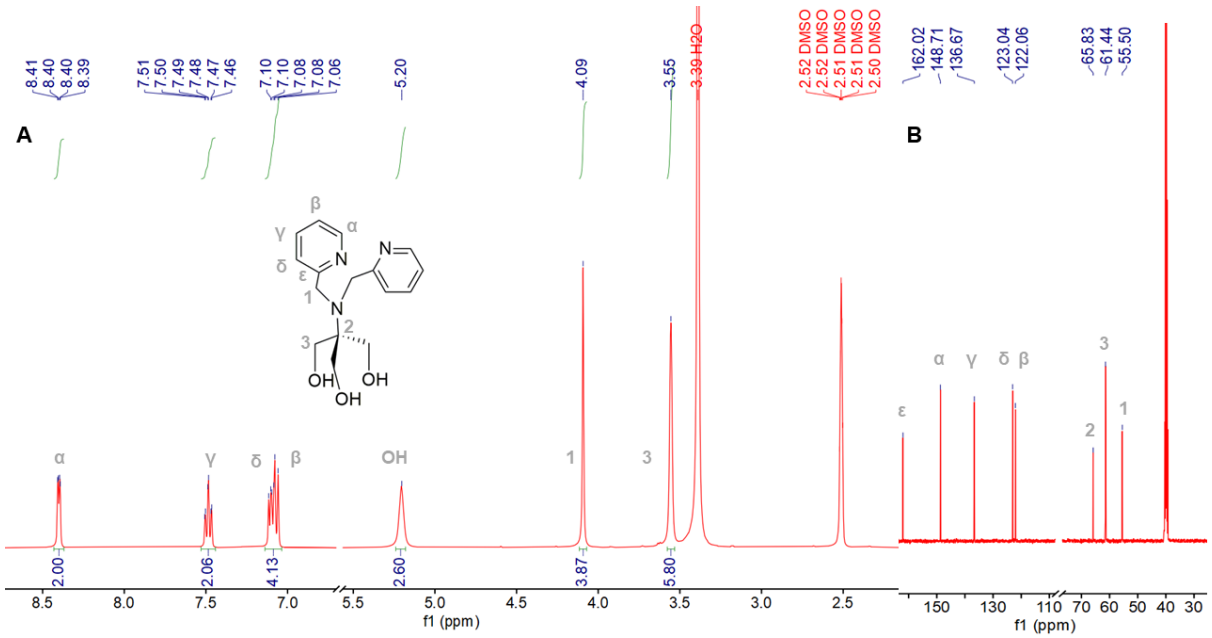

*Figure 4-1 A) ^{1}H NMR and B) ^{13}C NMR of **H_3Tris-DPA** (in DMSO).*

Furthermore, single crystal X-ray diffraction was performed on the colorless crystal and confirmed the nature of the product (insert Scheme 4-1): the two pyridines are indeed coupled with the tris(hydroxymethyl)aminomethane skeleton to regenerate a DPA type moiety.

4.1.2 Direct functionalization of $[P_2V_3W_{15}O_{62}]^{9-}$ with H_3Tris-DPA

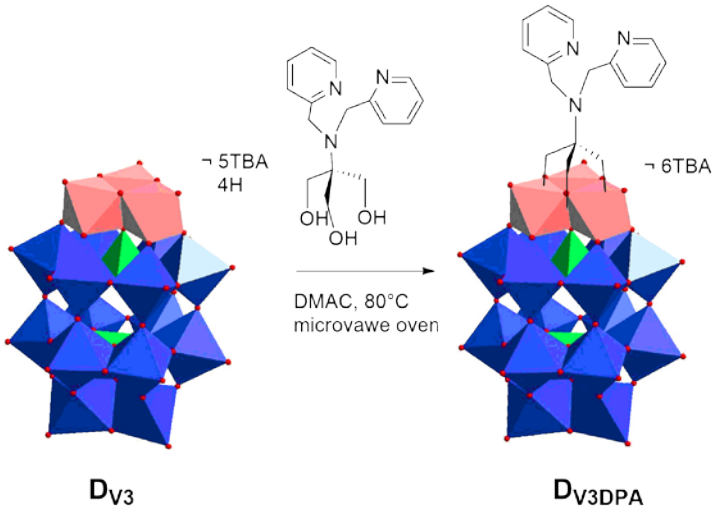

*Scheme 4-2 The synthesis route of TBA_6 $[P_2V_3W_{15}O_{62}$(Tris-DPA)] (abbreviated **D_{V3DPA}**).*

Subsequent reaction of the obtained **H_3Tris-DPA** with trivanadate cap-substituted Dawson POM $TBA_5H_4[P_2V_3W_{15}O_{62}]$ (abbreviated **D_{V3}** hereafter, which was obtained

according to Finke's publication[2]) was carried out through modified conditions of Lacôte's and Thorimbert' s work.[3] A mixture of 1.0 eq. **D_{V3}** and 1.2 eq. **H_3Tris-DPA** was dissolved in dimethylacetamide (DMAc), the resulting orange solution was heated with microwave at 80℃. After 1 hour, the olive-green solution was precipitated in diethyl ether and a brown solid was obtained. The crude product was characterized with NMR.

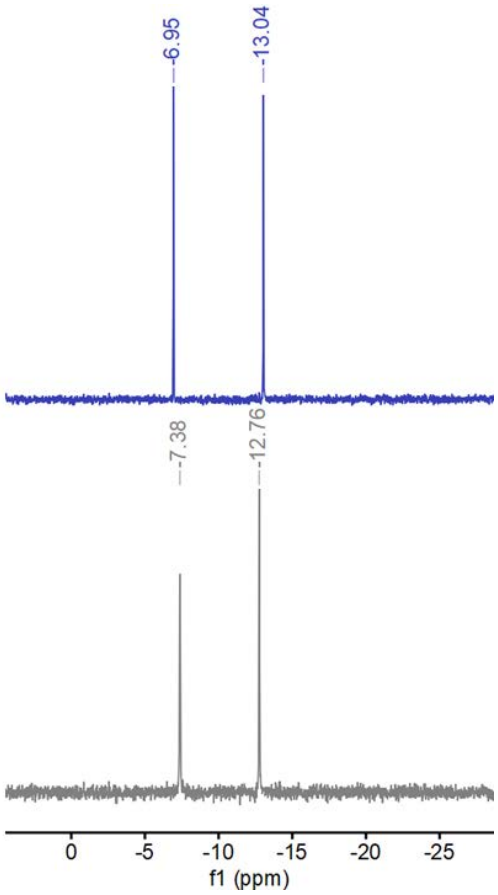

*Figure 4-2 Comparison of the ^{31}P NMR (CD_3CN) in the synthesis of **D_{V3DPA}** (blue) from **D_{V3}** (gray).*

The only two sharp characteristic Well-Dawson peaks in the ^{31}P NMR indicated that only one kind of POM skeleton existed. In agreement with Hill's previous work,[4] upon the formation of the hybrid, the two characteristic peaks in ^{31}P NMR are shifted from -7.38 ppm and -12.76 ppm[2] to -6.95 ppm and -13.04 ppm respectively, attesting the formation of the triester onto the POM surface. In ^{1}H NMR, we observed the presence of the pyridine peaks, attesting successful grafting, however they are broad and ill-defined, which, in hybrid-POM chemistry, is classical of the organic moiety being protonated. Therefore, the brown solid was

re-dissolved in acetonitrile, and precipitated with a mixture of diethyl ether / ethanol (V/V = 30/10) containing 10 mM TBAOH (~ 4.0 eq. to the POM) with a final yield 55.9%.

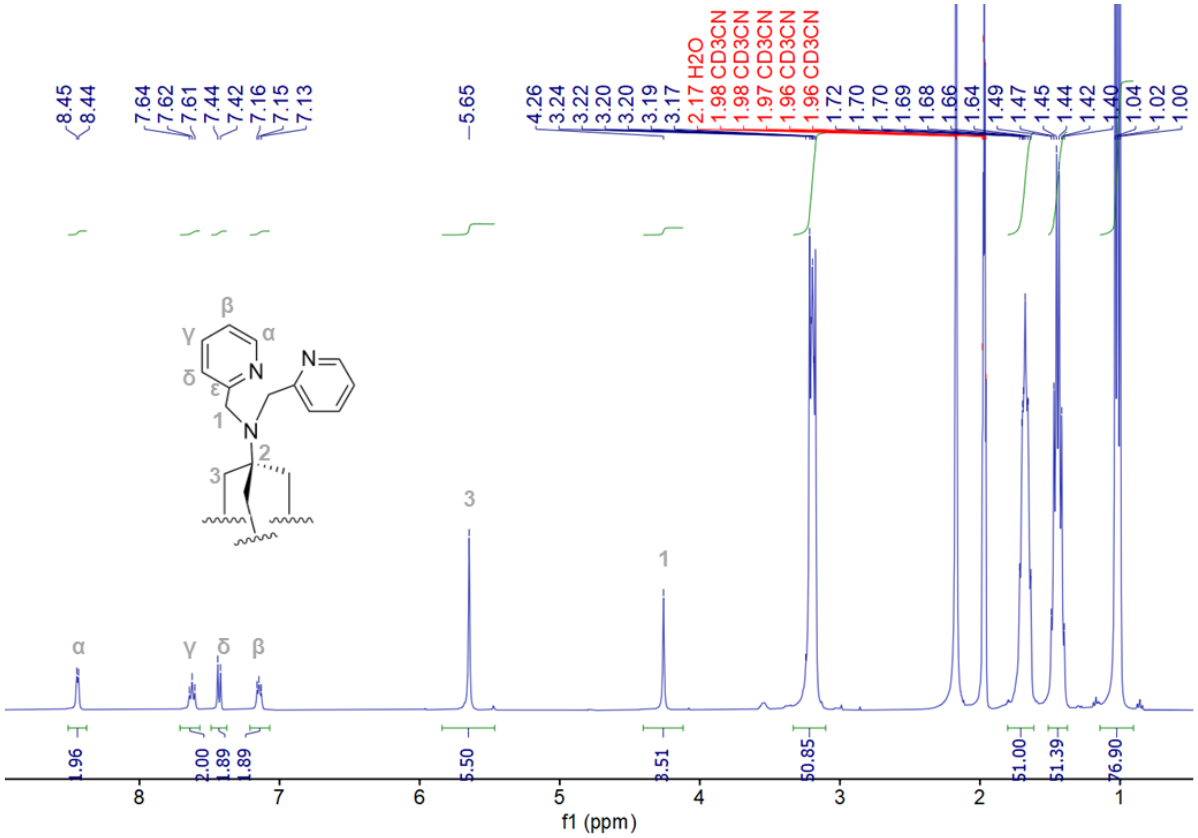

*Figure 4-3: ^1H NMR in CD_3CN of **D_{V3DPA}** after treatment*

Indeed, the ^1H NMR of the isolated brown product displays much sharper peaks characteristic of two equivalents pyridine ring in the aromatic part, together with the expected two types of methylene (NCH_2O and NCH_2Py) and the 6 eq. TBA signature (compared to the grafted organic moiety). Small changes, notably in the relative intensities, of the W-O and V-O stretching region in IR spectrum (700-1100 cm^{-1}) confirm the preservation of the Dawson structure. (Figure 4-11, navy blue).

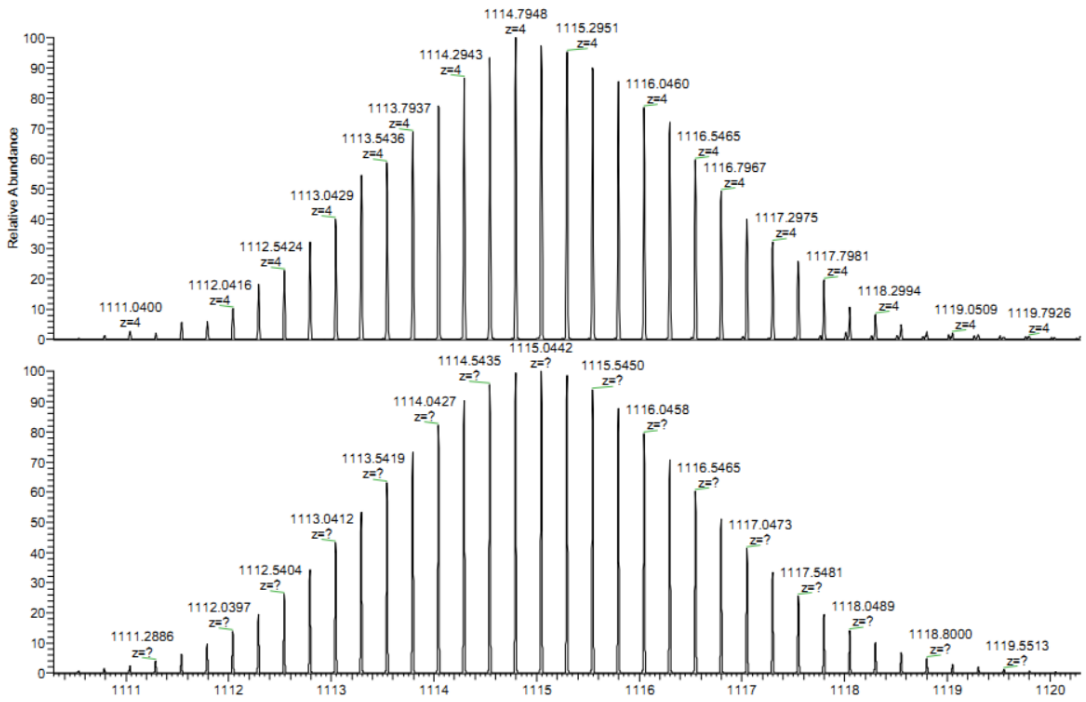

Figure 4-4 The ESI-MS of ***D*** $_{V3DPA}$ *which gives the formular {TBAH[*$P_2V_3W_{15}O_{62}$*(Tris-DPA)]}*$^{4-}$

The isotopic pattern of the adduct $\{TBAH[P_2V_3W_{15}O_{62}(TrisDPA)]\}^{4-}$ at m/z = 1114.79 (z = 4) was detected in HR ESI-Mass and further confirmed the successful grafting, while elemental analysis confirms the purity of the product as $TBA_6[P_2V_3W_{15}O_{62}(TrisDPA)]$ (abbreviated $\mathbf{D}_{V3DPA}$).

The single crystal was obtained via the diffussion of ethyl acetate into the $\mathbf{D}_{V3DPA}$ acetonitrile solution. The preliminary crystal structure analysis (Figure 4-5) confirmed the grating mode and revealed that the regioselectivity of the substitution, as expected, at the three V-O-V bridging positions in the V_3 cap of the POM. And the full structure including the counter ions need to be further dissolved.

Table 4-1 Crystal data and structure refinement for ***D*** $_{V3}$

Empirical formula	$C_{86.5}N_6O_{62}P_2V_3W_{15}H_{0.12}$
Formula weight	5087.56
Temperature/K	200.15
Crystal system	orthorhombic
Space group	Pbcn
a/Å	58.129(7)
b/Å	19.830(2)

c/Å	30.818(4)
α/°	90
β/°	90
γ/°	90
Volume/Å^3	35524(7)
Z	8
ρ_{calc}g/cm^3	1.903
μ/mm^{-1}	9.899
F(000)	18129
Radiation	MoKα (λ = 0.71073)
2Θ range for data collection/°	2.992 to 50.698
Index ranges	-69 ≤ h ≤ 70, -23 ≤ k ≤ 23, -26 ≤ l ≤ 37
Reflections collected	181433
Independent reflections	32473 [R_{int} = 0.0929, R_{sigma} = 0.0736]
Data/restraints/parameters	32473/0/1254
Goodness-of-fit on F^2	1.192
Final R indexes [I>=2σ (I)]	R_1 = 0.1001, wR_2 = 0.2097
Final R indexes [all data]	R_1 = 0.1567, wR_2 = 0.2400
Largest diff. peak/hole / e Å^{-3}	3.07/-2.80

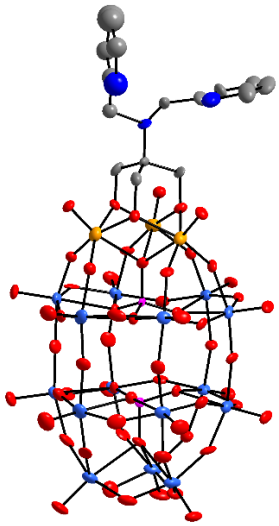

Figure 4-5 Molecular structure of $[P_2V_3W_{15}O_{62}(TrisDPA)]^{6-}$. Ball and stick: gray C, blue N, red O. pink P, orange V, pale blue W.

4.2 Functionalization of $[P_2V_3W_{15}O_{62}]^{9-}$ with aliphatic tripodal ligand

In order to be able to tune the redox potential of the coordinated metal ion and thus tune its reactivity, we decided to synthesize an analogue of the TrisDPA POM by replacing the aromatic pyridine moieties with aliphatic amines.

4.2.1 Synthesis of H_3Tris-DA-Boc

We first tried a direct functionalization of **H_3-Tris**. However, all reactivities were hampered by the insolubility of the latter in most of the organic solvents. Thus, the aliphatic tripodal ligand was synthesized according to the route in Scheme 4-3.

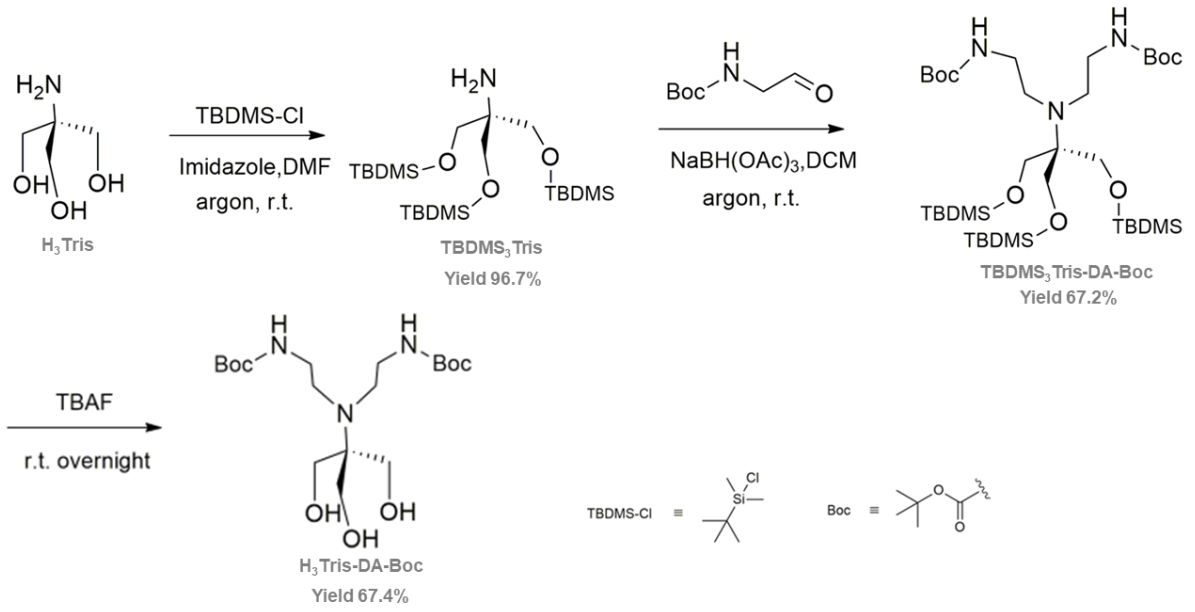

*Scheme 4-3 The synthesis route of the di-tert-butyl (((1,3-dihydroxy-2-(hydroxymethyl)propan-2-yl)azanediyl)bis(ethane-2,1-diyl))dicarbamate **(H_3Tris-DA-Boc)**.*

In order to improve the solubility for the following reductive amination in dichloromethane, the hydroxide groups of **H_3Tris** are protected with tert-butyldimethylsilyl chloride (TBDMS-Cl) in the presence of imidazole,[5] resulting in 6-(((tert-butyldimethylsilyl)oxy)methyl)-2,2,3,3,9,9,10,10-octamethyl-4,8-dioxa-3,9-disilaundecan-6-amine (**$TBDMS_3$Tris**, yield 96.7%). Then we slightly modified the procedure by Shah et al[6] to perform the reductive amination. First, 1.0 eq. of **$TBDMS_3$Tris** and 2.5 eq. of tert-butyl (2-oxoethyl)carbamate, were mixed in dichloromethane for 0.5 h, followed by the gradually addition of 8.0 eq. sodium triacetoxyborohydride ($NaBH(OAc)_3$), monitoring the reaction both by thin layer chromatography (TLC) and ^{1}H NMR of aliquots. The reaction was quenched with saturated sodium bicarbonate aqueous solution after overnight stirring at room temperature. The resulting colorless oil was purified via silica gel column with cyclohexane/ethyl acetate as eluent, yielding 67.2% of a colorless oil. The TBDMS was removed by reaction with TBAF in

THF, followed by silica gel column chromatography using chloroform/methanol as eluent to give 67.4% of the H_3Tris-DA-Boc moiety. This colorless oil was redissolved in acetonitrile and crystallized out, to yield 73.2% of crystalline powder which was characterized by ^{1}H NMR in DMSO (Figure 4-6). X-ray single crystal structure analysis could be performed on one of these and confirmed the nature of the synthesized product (Figure 4-7).

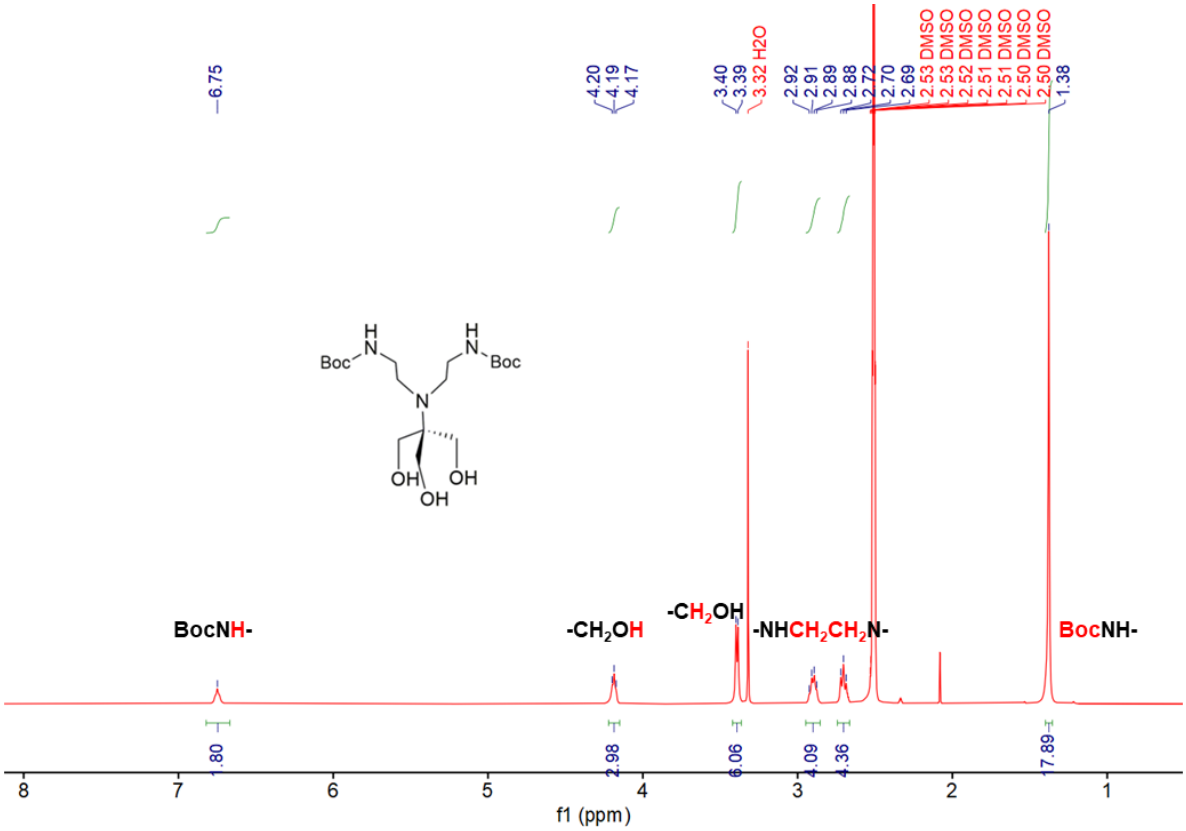

*Figure 4-6 ^{1}H NMR of **H_3Tris-DA-Boc** in DMSO.*

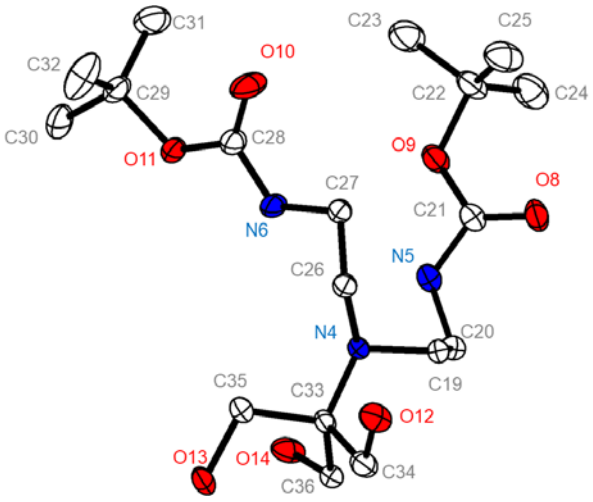

*Figure 4-7 Crystal structure of the molecular **H_3Tris-DA-Boc***

4.2.2 Functionalization of $[P_2V_3W_{15}O_{62}]^{9-}$ with H_3Tris-DA

The grafting of **H_3Tris-DA-Boc** onto the $[P_2V_3W_{15}O_{62}]^{9-}$ followed the same procedure as for the synthesis of **D_{V3DPA}**.

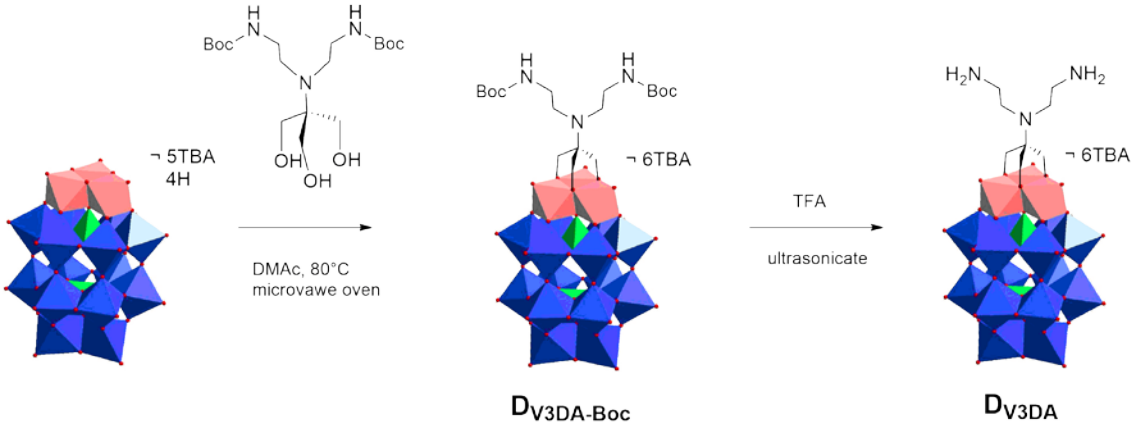

*Scheme 4-4 The synthesis route of $TBA_6[P_2V_3W_{15}O_{62}$(Tris-DA-Boc)] (abbreviated **$D_{V3DA\text{-}Boc}$**) and $TBA_6[P_2V_3W_{15}O_{62}$(Tris-DA)] (abbreviated **D_{V3DA}**).*

A mixture of 1.0 eq. **D_{V3}** and 1.2 eq. **H_3Tris-DA-Boc** were dissolved in DMAc and degassed with argon. The resulting orange solution was heated with microwave oven under 80℃. After 1 hour, the olive-green solution was precipitated in diethyl ether and a brown solid was obtained (**$D_{V3DA\text{-}Boc}$**), which was characterized with NMR (Figure 4-8 black) after being treated with TBAOH (~1.0 eq.). The ^{1}H NMR shows two well-defined peaks at 3.05 and 2.85 ppm attributed to two CH_2 of $BocNHCH_2CH_2N$-, the characteristic POM grafted triester peak at 5.53 ppm and the TBA^+ peaks. The two sets of peaks in ^{31}P NMR indicates there are two kinds of POM skeleton, probably due to the protonation as in the following de-Boc treatment, the ^{31}P NMR is much cleaner.

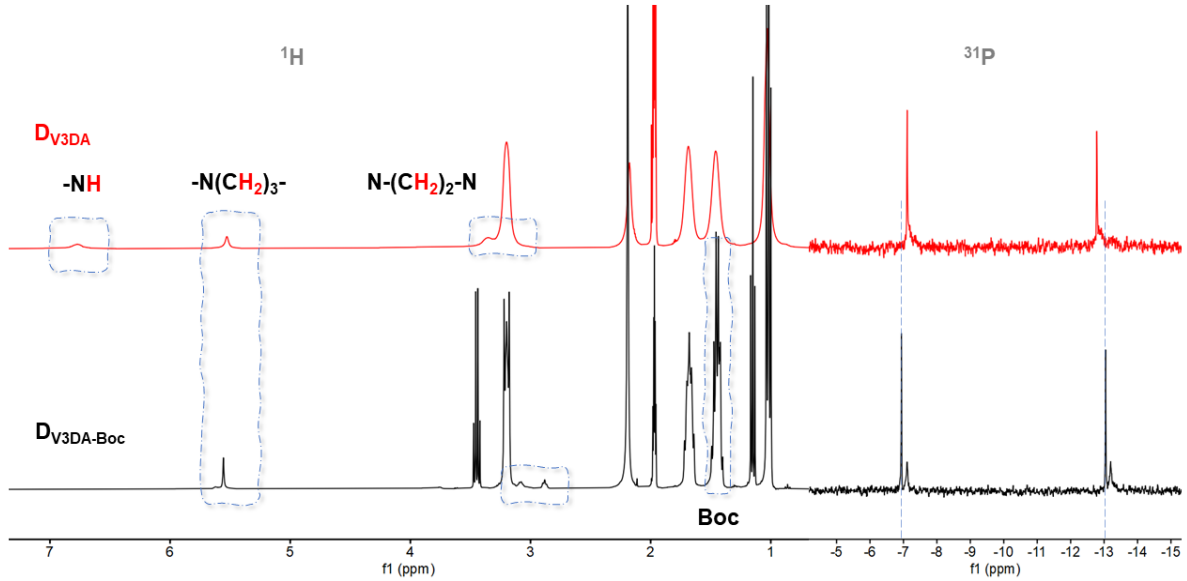

Figure 4-8 The ^{1}H NMR (left) and ^{31}P NMR (right) of the $\boldsymbol{D_{V3DA\text{-}Boc}}$ *treated with TBAOH (~1.5 eq.) from crude product (black) and* $\boldsymbol{D_{V3DA}}$ *(red).*

The brown solid was redissolved in acetonitrile and treated with trifluoroacetate acid (TFA) under ultrasonication for 2 hours. The brown solution turned from brown to green-yellow, combined with the precipitation of a brown powder, which was separated. The powder was suspended in acetonitrile and was redissolved with the gradual addition of TBAOH. The resulting brown solution was precipitated in diethyl ether led to a brown precipitate which was characterized by NMR (Figure 4-8 red). The clear shift in ^{1}H NMR of the -$NHCH_2CH_2N$- and the disappearance of the Boc signal indicate the successful deprotection of the amines, which is further confirmed with the shift of the main peaks in ^{31}P NMR from - 6.94 and -13.05 ppm to - 7.11 and -12.78 ppm.

These preliminary results on the functionalization of $\boldsymbol{D_{V3}}$ with aliphatic tripodal moieties need to be further explored in a future work.

4.3 Complexation of the D_{V3DPA}

4.3.1 Copper (II) acetate

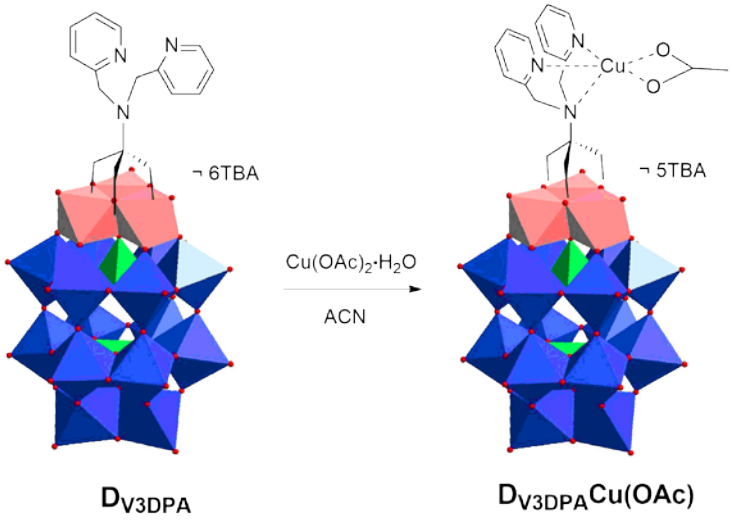

Scheme 4-5 Complexation of copper acetate with D_{V3DPA}.

The complexation of copper (II) acetate ($Cu(OAc)_2$) with D_{V3DPA} was carried out in acetonitrile. Upon addition of $Cu(OAc)_2$, the POM solution turned gradually from brown to olive-green. In order to better follow this process, titration of the POM with the copper salt was monitored by UV-vis spectroscopy. Upon gradual addition of Cu(II), one can observe a diminution of the intensity around 550 nm while a new broad band around 700 nm is growing, with an isosbestic point at 642 nm (Figure 4-9). Plot of the evolution of the absorbance at 540 nm and 690 nm (insert, black and red respectively) clearly show a change in the slope of the linear adjustment in agreement with the formation of a 1:1 complex.

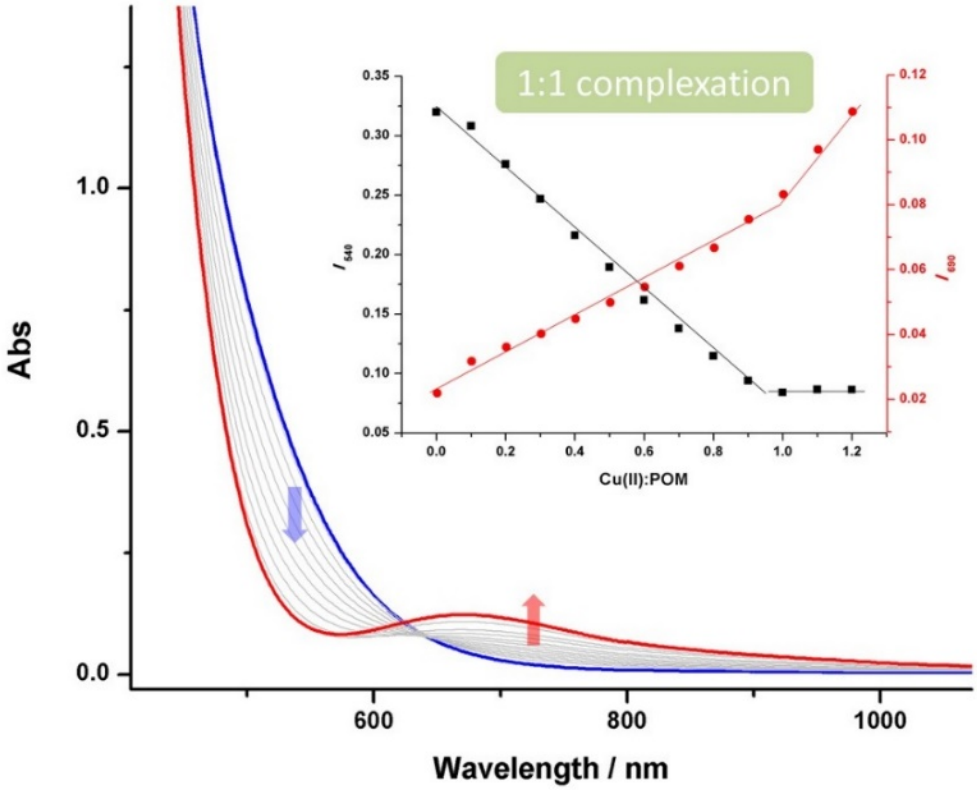

Figure 4-9: UV vis titration of ***D*** $_{V3DPA}$ *(1.0 mM) with increasing amount of* $Cu(OAc)_2$*. Insert: evolution of the absorbance at 540 nm and 690 nm with the number of equivalents of added copper ion.*

A 1:1 $Cu(OAc)_2$ / $\mathbf{D}_{V3DPA}$ olive-green solution in acetonitrile was thus precipitated with diethyl ether affording a green-yellow powder which was first characterized with ESI-MS spectrum (Figure 4-10). The large number of naturally abundant W isotopes, combined with various counter ion, yield to very specific and characteristic, though quite complicated, isotopic patterns.[7,8] Notably, the spectrum shown in Figure 4-10 displays several signals of - 3 charge anions corresponding to the association of the $\{Cu(II)\text{-}D_{V3DPA}\}^{4-}$ with either one H^+ or a TBA cation, and with or without acetate coordinated. For example, the peak at m/z 1427.63 corresponds quite nicely to $\{H[D_{V3DPA}(Cu^{II})]\}^{3-}$ (calc. m/z = 1427.35). Attribution of the other peaks is summarized in the table 4-1.

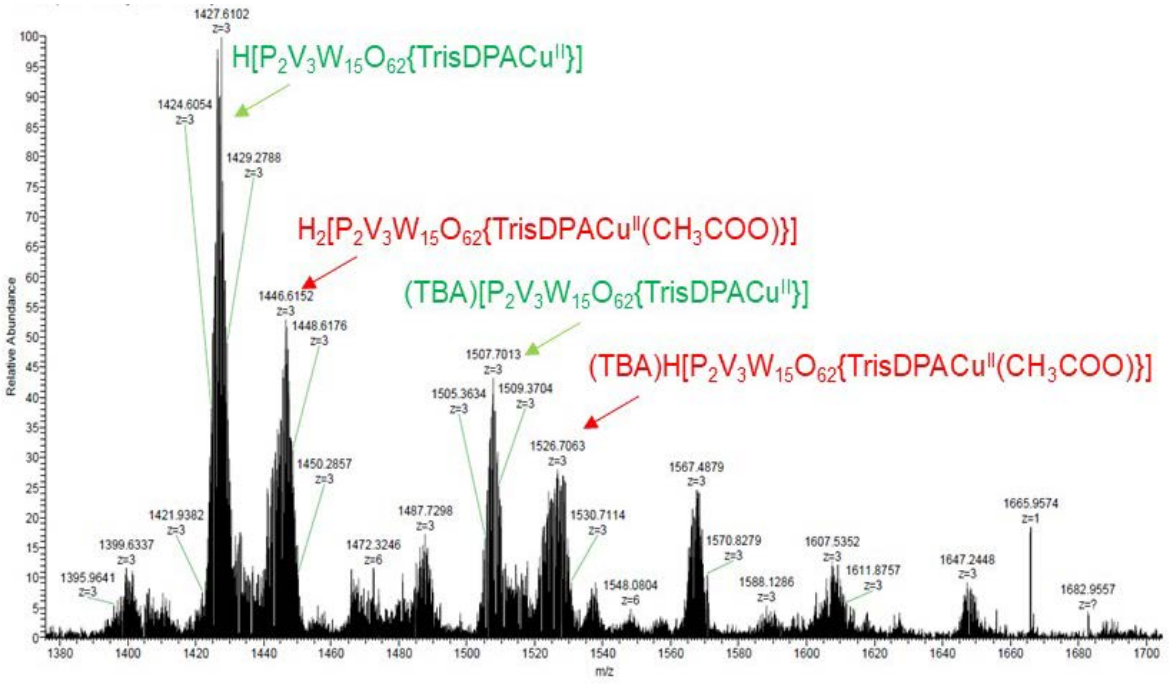

Figure 4-10: ESI-MS spectrum and attribution of various peaks of trianionic species derived from the ***$D_{V3DPA}Cu(OAc)$*** *anion*

Table 4-1 The main peaks of trianionic species derived from the $[D_{V3DPA}Cu^{II}]^{4-}$ anion

entry	formular	Found (m/z)	Calculate (m/z)
1	$H[P_2V_3W_{15}O_{62}\{TrisDPACu^{II}\}]$	1427.63	1427.35
2	$H_2[P_2V_3W_{15}O_{62}\{TrisDPACu^{II}(CH_3COO)\}]$	1446.61	1447.27
3	$TBA[P_2V_3W_{15}O_{62}\{TrisDPACu^{II}\}]$	1507.70	1507.67
4	$TBAH[P_2V_3W_{15}O_{62}\{TrisDPACu^{II}(CH_3COO)\}]$	1526.70	1527.67

Elemental analysis in agreement with the formula $TBA_{4.8}H_{0.2}[P_2V_3W_{15}O_{62}\{TrisDPACu^{II}(OAc)\}]$ was also obtained, while the IR spectrum (Figure

4-11, red) showed little variations compared to the free ligand, with essentially two new bands at 1572 cm^{-1} and 1447 cm^{-1} that correspond to the acetate stretching frequencies.

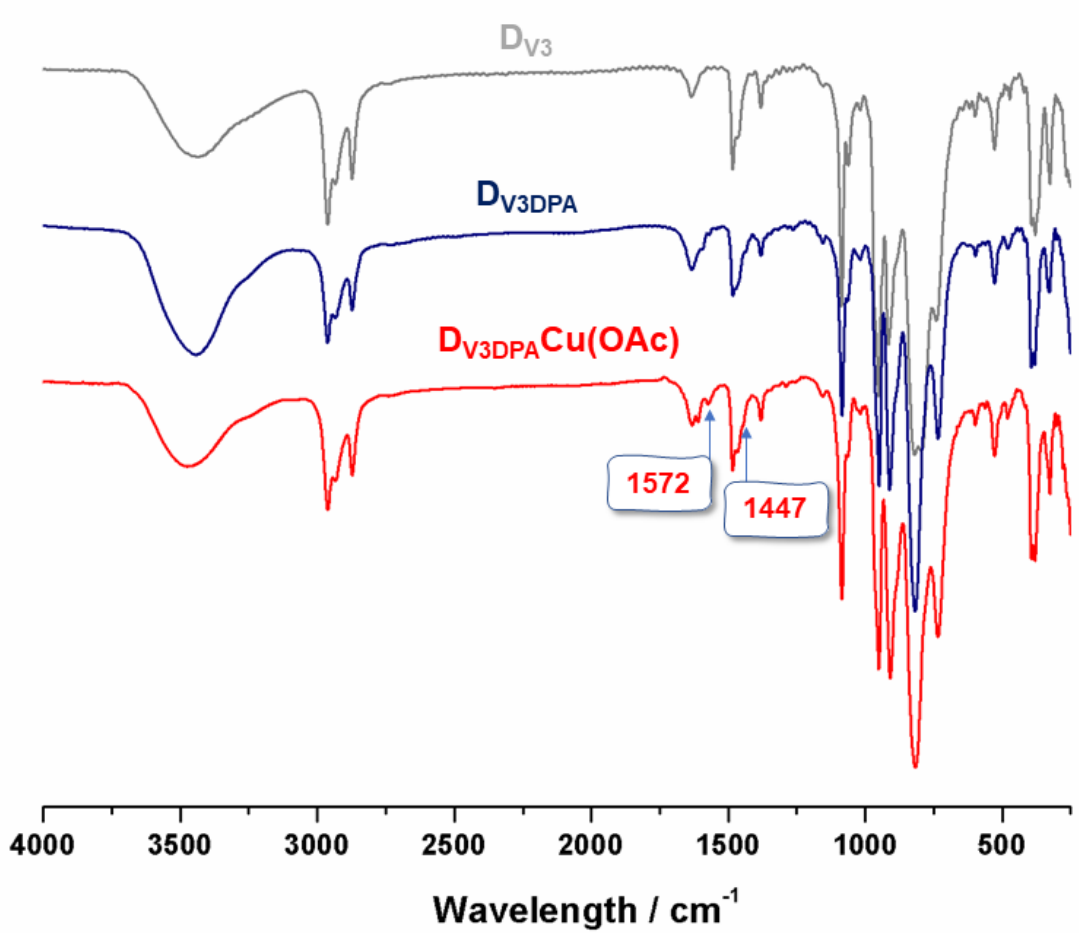

Figure 4-11 the IR of ***D_{V3}*** *(gray),* ***D_{V3DPA}*** *(navy blue) and* ***$D_{V3DPA}Cu(OAc)$*** *(red). The arrowss point out the absorption of acetate 1572 cm^{-1} and 1447 cm^{-1}*

For the isolated complex, only two peaks at - 5.93 ppm and - 12.61 ppm are present in the ^{31}P NMR spectrum, slightly shifted compared to the free ligand, confirming the formation of a single product. The dipicolylamine peaks in ^{1}H NMR are much more affected, as can be expected with the coordination to a paramagnetic Cu(II) ion. Indeed, as can be seen Figure 4-12, both the 4 aromatic peaks and the CH_2 of the free ligand, originally around 8 ppm and 4.3 ppm respectively, completely vanished, and are replaced by broad peaks with paramagnetic chemical shift at 15.30 ppm, 12.81 ppm, 12.23 ppm and -1.15 ppm. All these information is in favor of the successful isolation of **$D_{V3DPA}Cu(OAc)$**.

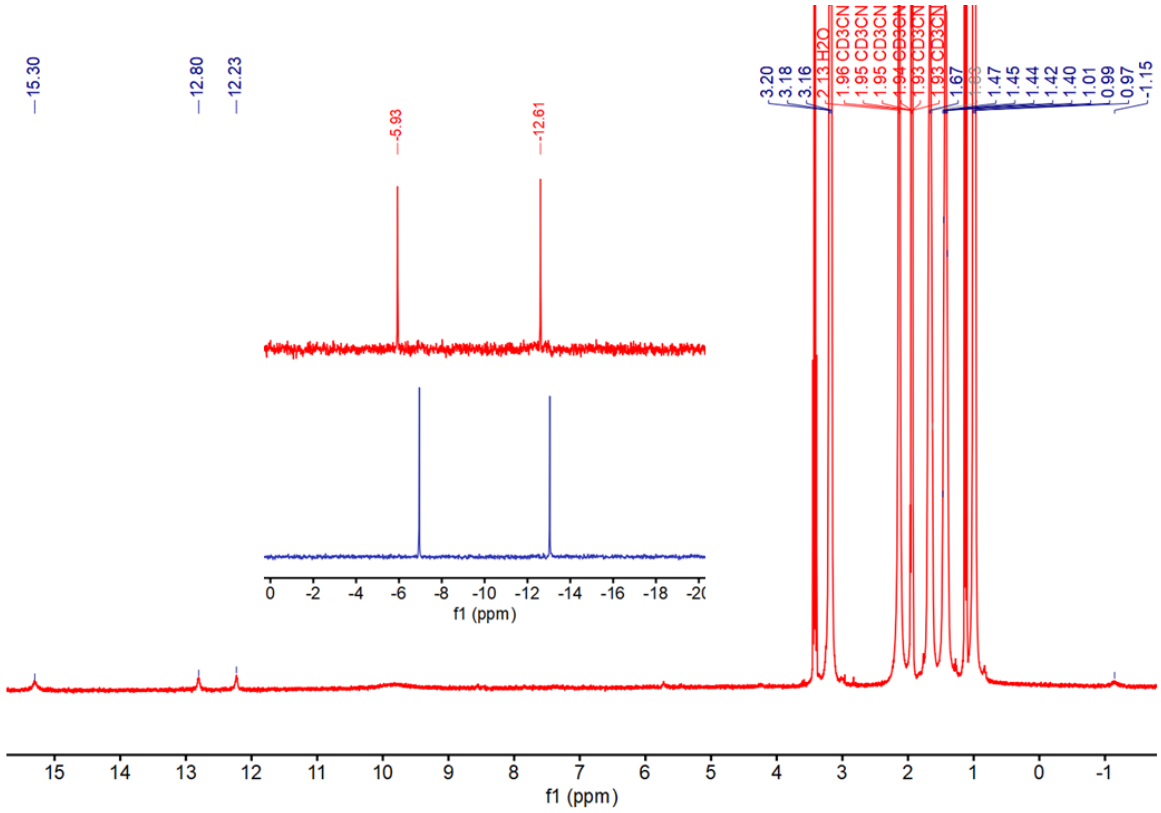

*Figure 4-12 The ^{1}H NMR (CD_3CN) of the **$D_{V3DPA}Cu(OAc)$**; insert: The variation of the ^{31}P NMR (CD_3CN) in the synthesis of **$D_{V3DPA}Cu(OAc)$** (red) from **D_{V3DPA}** (navy blue).*

4.3.2 Tetrakis(acetonitrile) copper(I) hexafluorophosphate

Cu(I) complex (**$D_{V3DPA}Cu^{I}$**) was generated in situ by the addition of 1.0 eq. of tetrakis(acetonitrile) copper(I) hexafluorophosphate ($[Cu(NCMe)_4]PF_6$) into the ligand CD_3CN solution in NMR tube under inert atmosphere without further purification. The ^{1}H NMR displays a clear low-field chemical shift of the grafted organic moiety compared to the free ligand. In the meantime, the ^{31}P NMR shows a slightly shift from - 6.95 and - 13.04 ppm to - 6.92 and - 12.98 ppm.

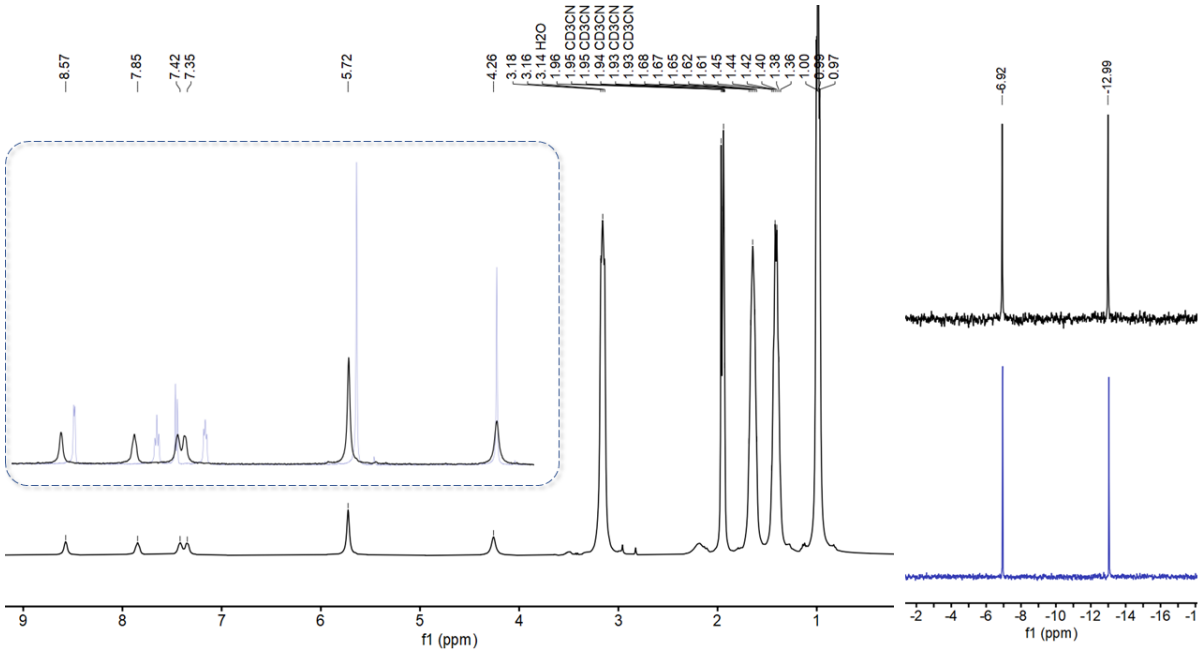

Figure 4-13 A) The ^{1}H NMR (CD_3CN) of the ***$D_{V3DPA}Cu^{I}$****, insert: the variation of the ^{1}H NMR from* ***D_{V3DPA}*** *(blue) to* ***$D_{V3DPA}Cu^{I}$*** *(black); B) The variation of the ^{31}P NMR (CD_3CN) from* ***D_{V3DPA}*** *(blue) to* ***$D_{V3DPA}Cu^{I}$*** *(black).*

To gain more insight into this coordination, a variable temperature ^{1}H NMR study was carried out. As the temperature decreased from 298 K to 233 K, the signals of the pyridine and triester are almost unchanged, while the signal of the CH_2 linked to pyridine became more and more broad and seems to split into two symmetric peaks at 233K. This is classical of a diastereotopic differentiation of the two protons of the methylene of the DPA ligand at low temperature, while, when the temperature is high, a fast exchange of the two positions due to coordination and decoordination makes the two protons on the CH_2 pseudo equivalent. This phenomenon is a clear indication that the Cu^{I} is, as expected, coordinated to the tripodal site.

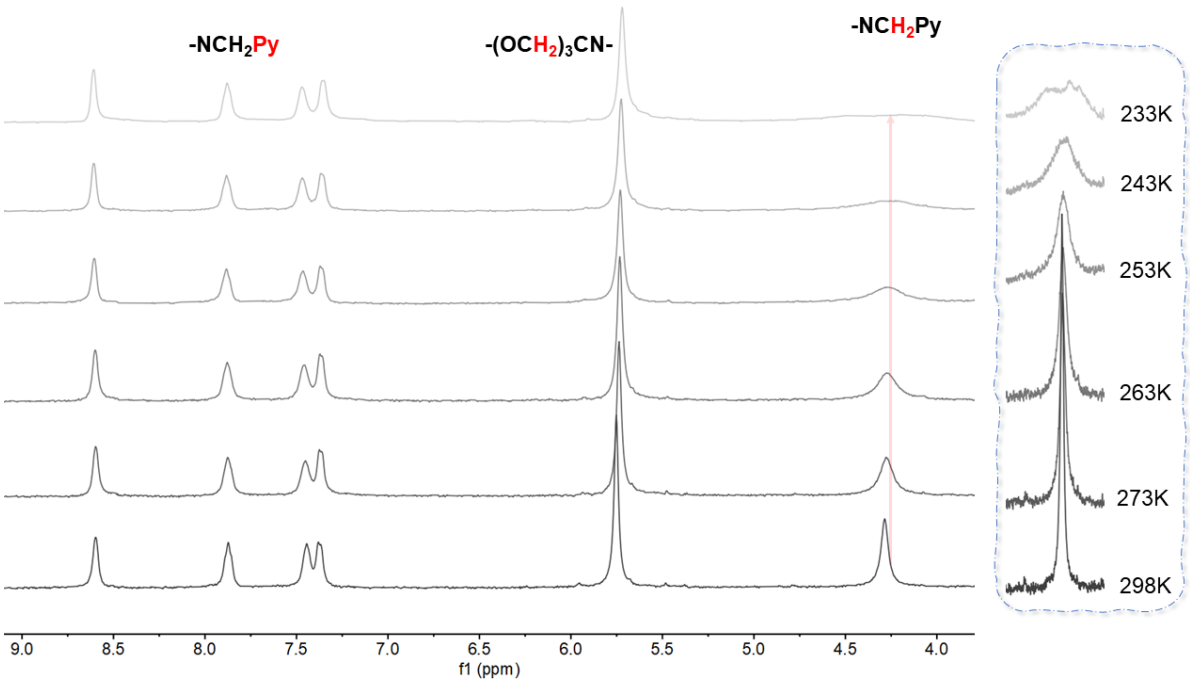

*Figure 4-14 Evolution of the ^{1}H NMR of **$D_{V3DPA}Cu^I$** in CD_3CN with temperature.*

4.4 Electrochemical investigation of D_{V3DPA} and $D_{V3DPA}Cu(OAc)$

4.4.1 Redox properties of D_{V3DPA} and $D_{V3DPA}Cu(OAc)$

Cyclic voltammetry (CV) of both the ligand and the complex were performed in acetonitrile containing tetrabutylammonium hexafluorophosphate ($TBAPF_6$) as electrolyte. As can be observed in Figure 4-15, in the case of the **D_{V3DPA}** ligand alone, in the reduction process, two quasi-reversible waves at -0.090 V/SCE and -0.452 V/SCE are displayed, followed by a less well-defined process at -0.761 V/SCE. By analogy with Ruhlmann's work,[9,10] these three processes correspond quite nicely to the three waves of the hybrid POM—tvb3.3 (- 0.11 V/SCE, - 0.48V/SCE and - 0.85 V/SCE), which also derives from the trivanadate substituted Dawson POM,[10] and are thus similarly attributed to the successive one electron reduction of each of the three V(V) into V(IV). This is also in agreement with the UV-vis signature of these reduced species (vide infra). At much more negative potentials (< - 1.8 V/SCE, data not shown), additional processes corresponding to either the Pyridine rings reduction or W(VI) to W(V) reduction are observed.

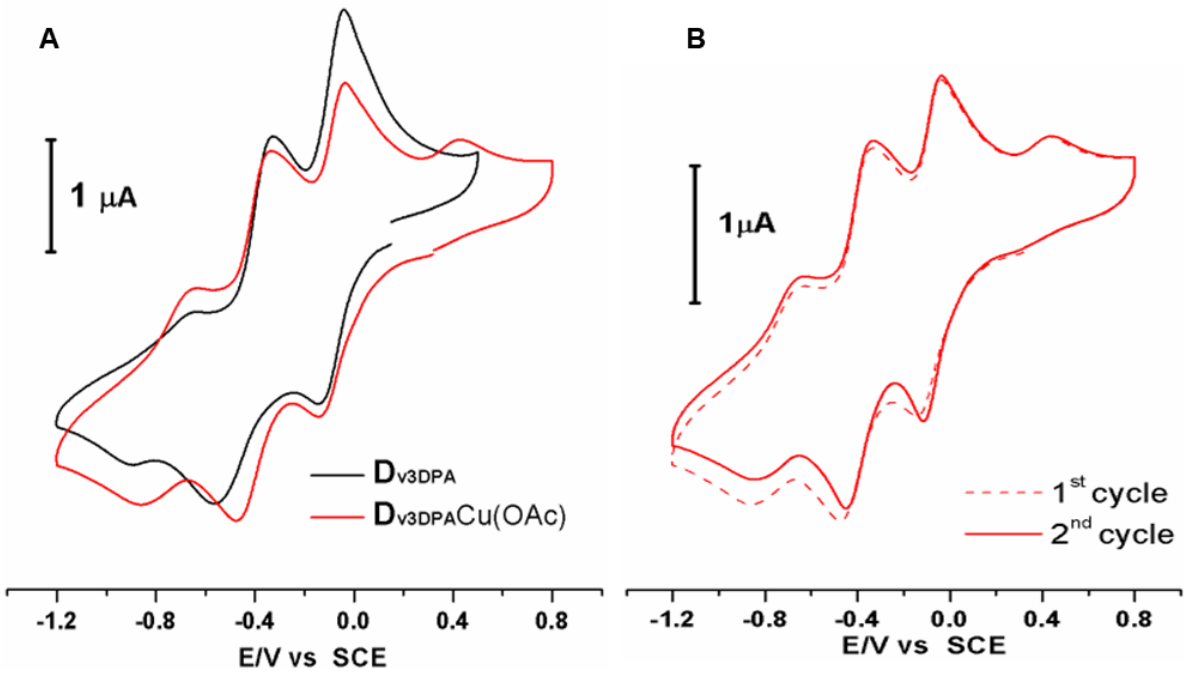

Figure 4-15: A) Cyclic voltammograms of ***D_{V3DPA}*** *(black) and* ***D_{V3DPA}Cu(OAc)*** *(red) at 1.0 mmol.L^{-1} in CH_3CN containing 0.1 mol.L^{-1} $TBAPF_6$ and v = 100 mV s^{-1}. B) Cyclic voltammograms of* ***D_{V3DPA}Cu(OAc)*** *first cycle (dash) and second cycle (solid).*

In the case of the **D_{V3DPA}Cu(OAc)**, very similar waves are present in the CV when going to negative potentials, that we again associate with V centered redox processes. Besides, a new and quite broad redox process appears at 0.435 V/SCE when going back in oxidation. As the only change is the presence of the copper ion, it is associated with Cu(I) to Cu(II) process. The initial wave associated with Cu(II) to Cu(I) reduction is very broad and hard to attribute, being already started at the resting potential of 0.34 V/SCE (the product in solution seems to be already partially reduced from Cu(II) to Cu(I) during the preparation of the experiment, which will be explained in the following section **4.5**). Indeed, when a second cycle is recorded in the same CV (Figure 4-15 B), no obvious change occurs except for the observation of broad reduction wave starting at 0.46V/SCE and merging with the first V(V) reduction wave. The poor electrochemical reversibility of this process is quite common in copper chemistry and is related to the very different requirements in term of preferred geometries between Cu(I) and Cu(II). The redox potentials and peak to peak separation are summarized table 4-2.

Table 4-2: Potentials of the waves in V versus SCE. Half-wave potentials $E_{1/2} = (E_p^{ox} + E_p^{red})/2$. In brackets: $\Delta Ep = E_p^{ox} - E_p^{red}$, in mV.

Product	Cu(II)/Cu(I)			V(V)/V(IV)								
				1st			2nd			3rd		
	E_p^{ox}	E_p^{red}	$E_{1/2}$	E_p^{ox}	E_p^{red}	$E_{1/2}$	E_p^{ox}	E_p^{red}	$E_{1/2}$	E_p^{ox}	E_p^{red}	$E_{1/2}$
D_{V3DPA}				-0.044	-0.136	-0.090 (92)	-0.328	-0.576	-0.452 (148)	-0.640	-0.882	-0.761 (242)
D_{V3DPA} Cu(OAc)	0.435	*		-0.035	-0.145	-0.090 (90)	-0.321	-0.461	-0.391 (140)	-0.634	-0.850	-0.742 (216)

*ill-defined

4.4.2 Spectroelectrochemical studies of D_{V3DPA}Cu(OAc)

The attributions in the CV are further confirmed by spectroelectrochemical studies performed on the complex. Upon stepwise reduction of the **D_{V3DPA}Cu(OAc)** at more and more negative potentials, from 0.2 V/SCE down to -1.5 V/SCE applied potentials, various new signatures are observed. The first reduction process, associated with an electrolysis at about - 0.65 V/SCE (resting potential at 0.21 V/SCE) corresponds to a progressive disappearance of the very weak transition at 690 nm associated with the Cu(II) d-d transition, and the apparition of an isosbestic point at 575 nm: this agrees with an initial reduction of Cu(II) to Cu(I).

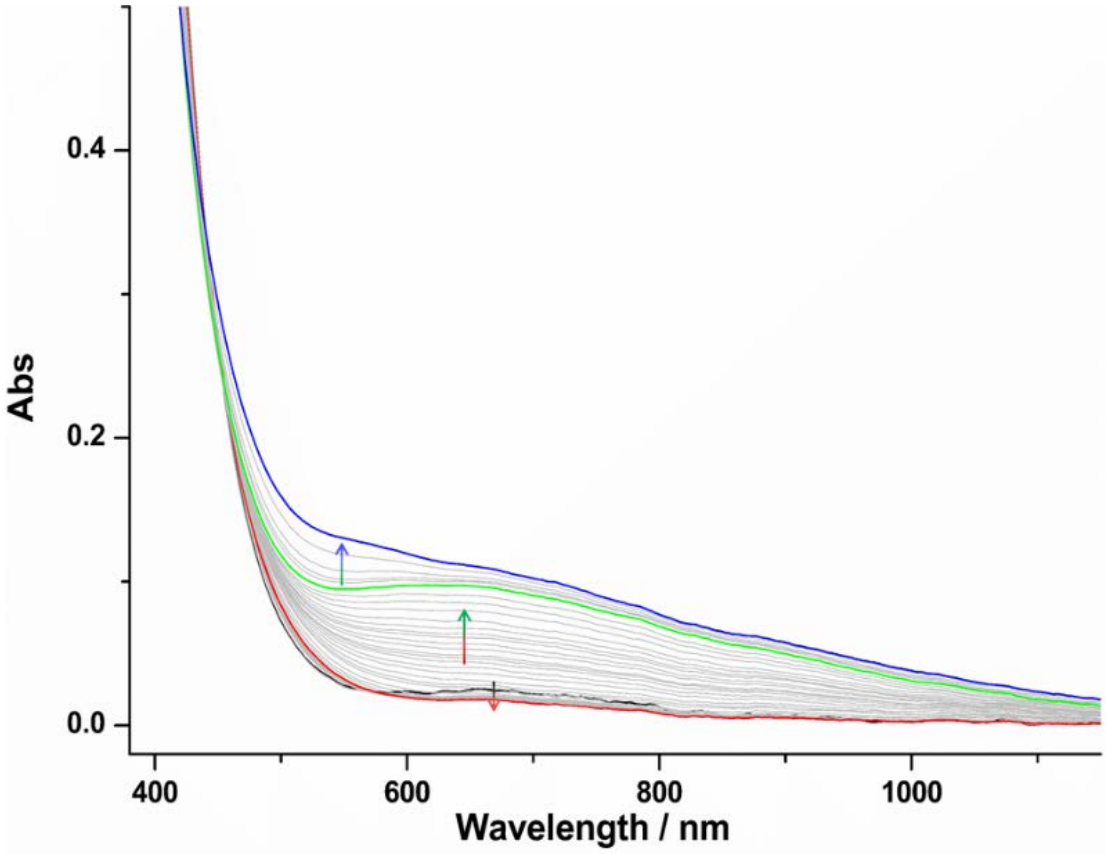

Figure 4-16 : UV-vis evolution upon electrochemical reduction of a 0.2 mmol^{-1} solution of ***D_{V3DPA}Cu(OAc)*** *in CH_3CN /0.1M $TBABF_4$ electrolyte from 0.2 V/SCE to -1.5 V/SCE. The arrows describe the successive evolutions upon change in the signature of the reduced species, with stationary forms highlighted in red (1e$^-$ reduced signature), green (2e$^-$), blue (3e$^-$).*

This is followed by a second evolution when reducing at – 1.2 V/SCE, where a very broad and panchromatic (from 400 nm up to 1200 nm) absorption grows, associated with the detection of a second isosbestic point at 455 nm. Finally, a new species is generated when fixing the potential at -1.5 V/SCE, with essentially a growth around 500 nm this change is associated with an isosbestic point at 423 nm. Concerning these last three processes, reduction could either occur at the W or V centers. However, the first W(VI) to W(V) reduction in Dawson POMs is classically associated with metal to metal charge transfer bands and d-d transitions leading to a broad absorption growth around 850 nm with ε values of several hundreds, while the second process leads to a new band arising around 700 nm, with ε values of a few thousand.[11,12] Moreover, in mixed W/V oxoclusters, V(V) to V(IV) is usually observed

at less negative potentials compared to W(VI) to W(V) processes.[10] Thus, and as proposed previously in agreement with the literature, we attribute the last two processes to V(V) to V(IV) reductions.

4.5 Photocatalytic activities investigation

4.5.1 Photo-redox property of $D_{V3DPA}Cu(OAc)$

NMR evolution

Interestingly, an evolution of the NMR signatures is observed with time. While two new peaks are observed at - 6.89 ppm and - 12.99 pm in ^{31}P NMR, suggesting the formation of a new species, re-appearance in the proton NMR of the 6 peaks of the Tris-dipicolylamine organic moiety indicates the formation of a diamagnetic species (Figure 4-17 c). As some POMs, like the metatungstate ion or some polyoxovanadate, were known in some instances to possess photoredox properties,[13–15] we wondered if photoreduction could have occurred. Indeed, when irradiating the NMR tube with a more powerful light source, full conversion of the Cu(II)-complex into a diamagnetic species was observed within 60 minutes (Figure 4-17 d). In parallel, addition of one equivalent of cobaltocene as chemical reducing agent into a freshly prepared solution of the **$D_{V3DPA}Cu(OAc)$** anion resulted in the same ^{1}H NMR (Figure 4-17 e) and ^{31}P NMR signature, thus confirming the reduction of the complex, presumably from Cu(II) paramagnetic, to Cu(I) diamagnetic. These signatures are also similar to those of the Cu(I) complex previously generated in situ under inert atmosphere, (§ **4.3.2** and Figure 4-17, g).

Addition of a second equivalent of cobaltocene led to the disappearance of the two peaks in ^{31}P NMR, while the ^{1}H NMR shows a slight shift of the peak in the aromatic region, with some line broadening. Thus, and in agreement with the electrochemical studies, the second reduction most likely occurs on one of the V(V) of the polyoxometalate framework: the para-magnetism of the V(IV) formed would explain the disappearance of the ^{31}P NMR signals, while the organic moiety, situated further away from the paramagnetic center, would be less affected (see below for more evidences).

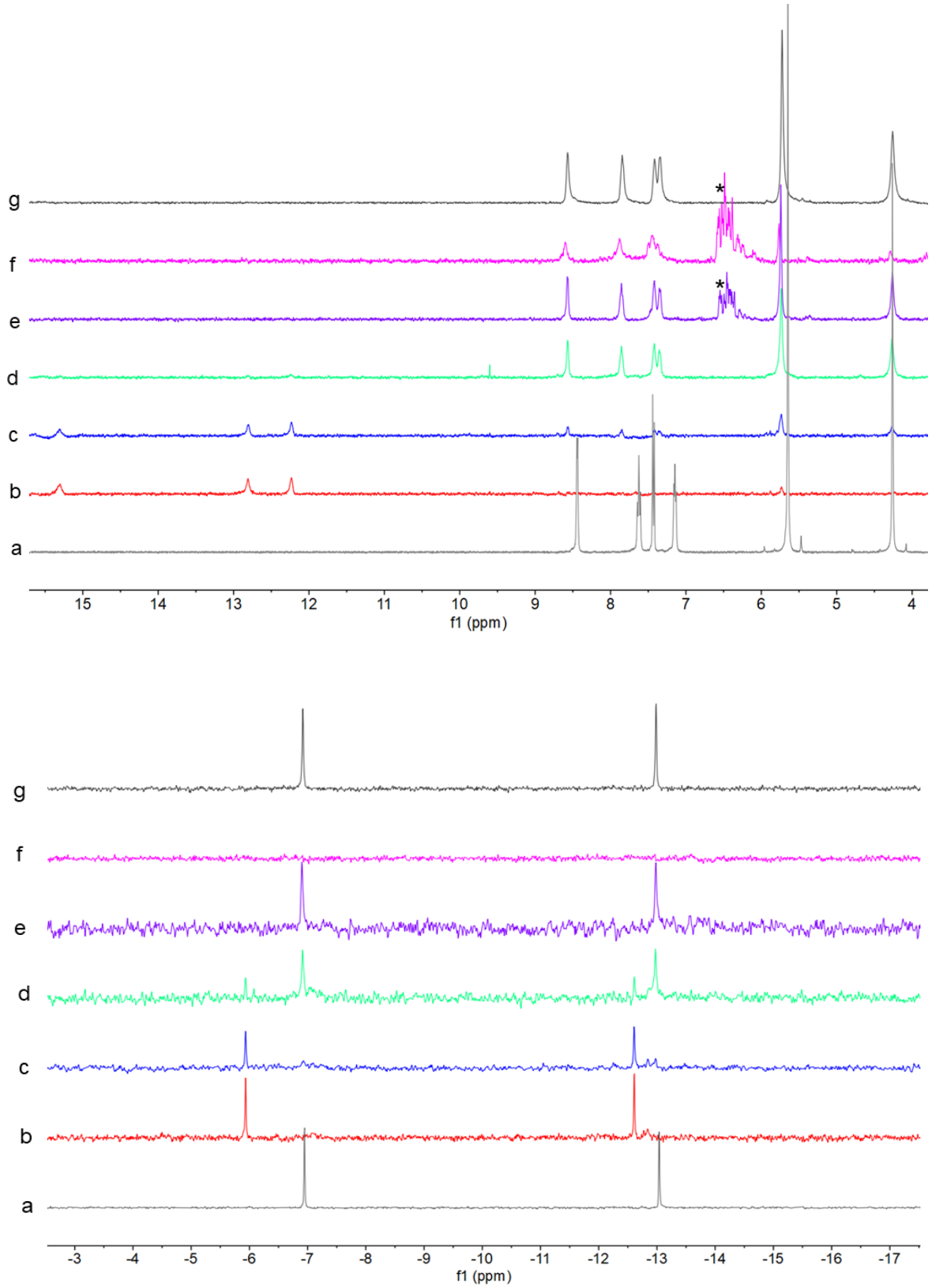

*Figure 4-17: A) ^{1}H NMR spectra and B) ^{31}P NMR of a) ligand **D_{V3DPA}** (gray), b) freshly synthesized **D_{V3DPA}Cu(OAc)** (red), c) after evolution in the NMR tube (blue), d) after irradiation with a Xenon lamp (>385nm, 75 μWcm^{-1}) (green), e) upon reduction with 1.0 eq.*

*[$CoCp_2$] (purple), and f) 2.0 eq. [$CoCp_2$] (pink), g) in situ generated Cu(I) complex (black). *: ^{1}H NMR signature the of $[Co(Cp)_2]^+$ cation.*

Peracetic acid reoxidation

In order to get the analytic characterization of the fully oxidized species, peracetic acid (CH_3COOOH) was used as an oxidant. Progressive addition of CH_3COOOH on a solution of **D_{V3DPA}Cu(OAc)** in ACN led to an increase of the band around 680 nm which is attributed to the d-d transition of the Cu^{II} complex.

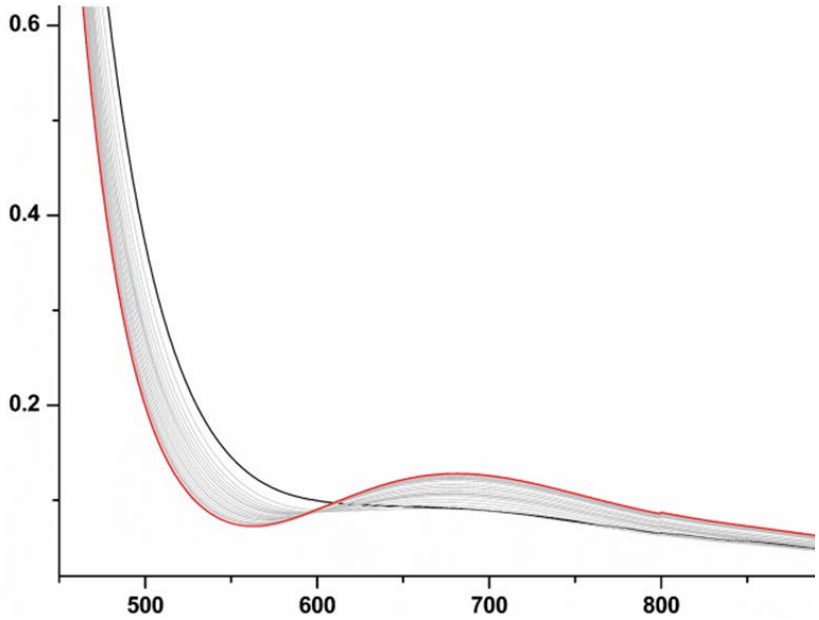

*Figure 4-18 UV-vis spectrum of the **D_{V3DPA}Cu(OAc)** (1.0 mM) with the titration of peracetate acid from 0 to 2.2 eq.*

In the meantime, the peaks at – 6.92 & - 13.01 ppm in ^{31}P NMR are fully converted to – 5.96 & - 12.63 ppm, with disappearance in the ^{1}H NMR of the diamagnetic peaks and increase of the paramagnetic peaks. This confirmed that the isolated complex is partially reduced, presumably due to light exposure upon treatment.

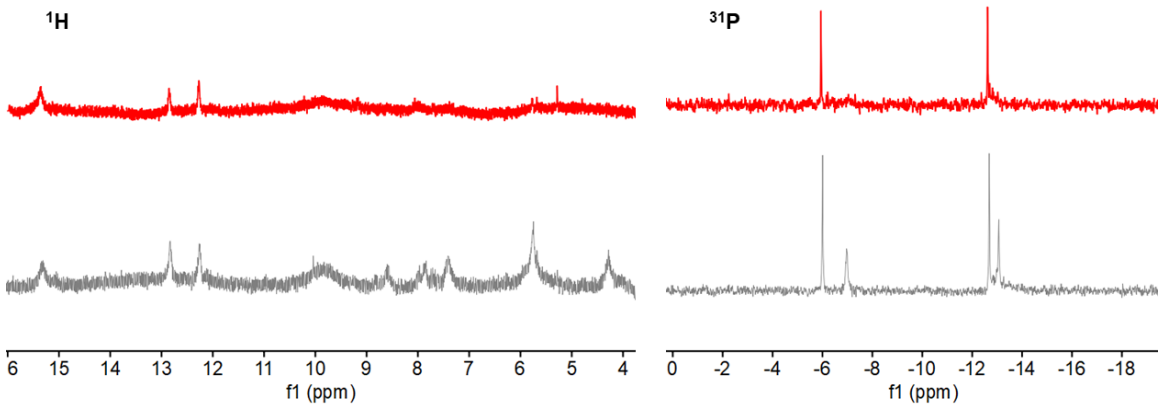

Figure 4-19 ^{1}H NMR and ^{31}P NMR of ***D_{V3DPA}Cu(OAc)*** *before (gray) and after (red) being oxidized by peracetate acid 2.0 eq.*

4.5.2 Spectrophotochemistry of D_{V3DPA}Cu(OAc)

UV-vis spectroscopy

This photoreduction was further studied by UV-vis spectroscopy. Upon visible-light irradiation of the **D_{V3DPA}Cu(OAc)** anion in acetonitrile, a global evolution reminiscent to that of the spectroelectrochemistry experiment is observed. However, slight changes of the profile probably result from different solvatation effects of the electrolyte (spectroelectrochemistry) compared to pure acetonitrile (photochemistry).

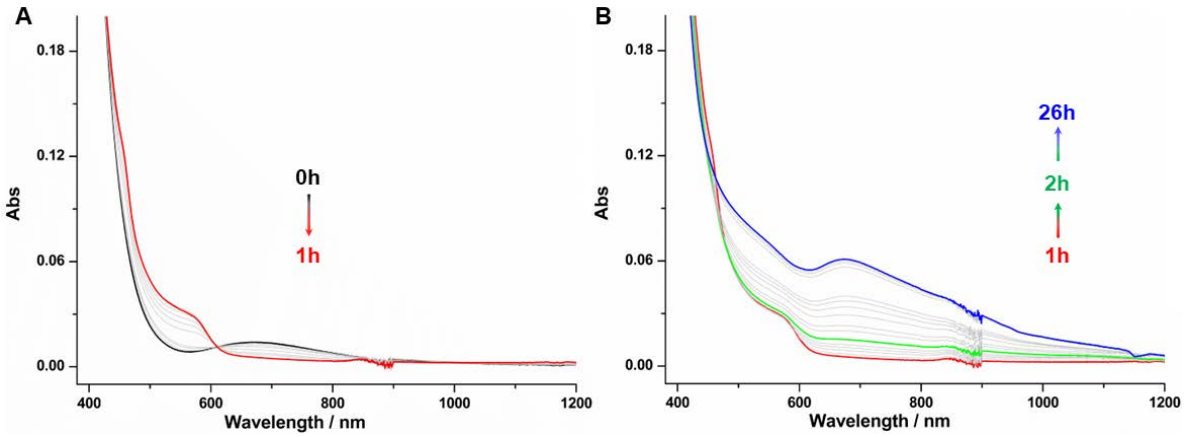

Figure 4-20: Evolution of the UV-VIS signature of a 0.2 mM solution of ***D_{V3DPA}Cu(OAc)*** *in acetonitrile upon visible light irradiation. Arrows highlight the successive changes of species associated with photoreduction of the complex by 1, 2 or 3 electrons.*

In a first step, the band at 680 nm, assigned to the Cu(II) d-d transition (Figure 4-20 A), progressively decreases, in agreement with the reduction of Cu(II) to Cu(I) and the formation of the diamagnetic complex observed by NMR. At the same time, one can observe an increase around 550 nm, and a first isosbestic point at 609 nm.

Longer irradiation (over about one hour) lead to a second process (red to green evolution, Figure 4-20 B) where the absorption at 550 nm stays constant while an overall though modest increase from 600 nm to 1200 nm appears, with this change of species associated with the observation of an isosbestic point at 480 nm. This would correspond to the reduction of one V(V) to V(IV).

Finally, after 26h, a last major change, notably with a very important increase of the absorption around 700 nm, is observed and keeps on growing with overnight irradiation and new isosbestic point at 442 nm (green to blue evolution, Figure 4-20 B). We propose that the latter originates from a second V(V) to V(IV) photoreduction.

EPR spectroscopy

In parallel, the oxidation states of the isolated, oxidized and irradiated products were studied by X-band EPR spectroscopy in frozen acetonitrile at 30 K. The spectrum of isolated fully oxidized $\mathbf{D_{V3DPA}Cu(OAc)}$ anion can be reasonably simulated with a rhombic g-matrix (g_x = 2.245, g_y = 2.10, g_z = 2.03) with hyperfine coupling of A_x = 485 MHz only detectable on the highest g-value, which is in agreement with a five coordinated Cu(II) ion in an intermediate geometry between bipyramid trigonal and square planar.[16,17] Upon irradiation of the sample, a diminution of the Cu(II) signal is observed, while in the meantime apparition of a new pattern, associate with an axial S = 1/2, I = 7/2 spin system with ($g_\perp$ = 1.97, $A_\perp$ = 180 MHz) and ($g_{//}$ = 1.92, $A_{//}$ = 500 MHz), and characteristic of the formation of an axial V(IV) species[18] arises. The simultaneous observation of the Cu(II) and V(IV) signals of the synthesized one agrees with the overlap of the Cu(II)/Cu(I) and V(V)/V(IV) reduction waves in the CV, whereby the vanadium starts to be reduced before all the Cu(II) has been converted to Cu(I). Finally, further irradiation leads to the progressive disappearance of the Cu(II) signal and concomitant increase of the V(IV) signals.

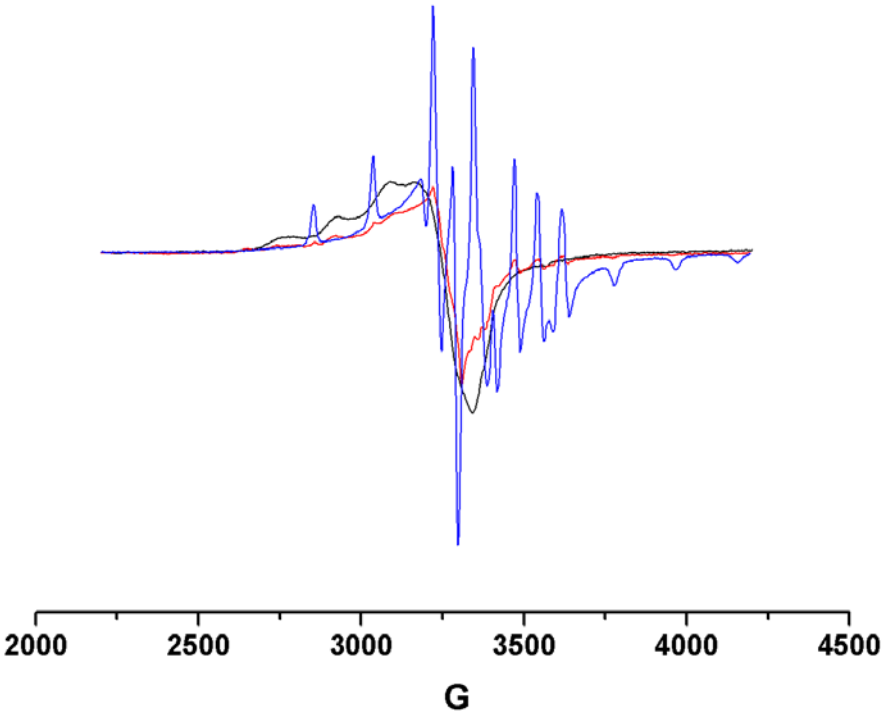

Figure 4-21: The EPR spectrum of 0.2 mM ***D_{V3DPA}Cu(OAc)*** *in acetonitrile: oxidized with 2.0 eq. of peracetate acid (black); synthesized one (red) and irradiated with visible light for 1h (blue).*

Combining the NMR, UV-vis and EPR results clearly show that upon irradiation, **D_{V3DPA}Cu(OAc)** is successively photoreduced by up to three electrons, with a first Cu(II) to Cu(I) reduction process followed by two vanadium-centered processes. Although electrochemical storage of up to 2 electrons has been proposed on polyoxometalates photoaccumulation of three charges has seldom been observed[19,20] and, to the best of our knowledge, three electron photoreduction on a POM-hybrid has so far not been described.

4.5.3 Photo-reduction of nitrite (NO_2^-)

As we can photo-accumulate electrons on the **D_{V3DPA}Cu(OAc)** through visible light irradiation, we wonder if these electrons could be further transferred to some substrates in a photocatalytic process. As in chapter 3, a possible target could be NO_2^- reduction to nitric oxide.[21]

In a preliminary study, we added $TBANO_2$ into a an acetonitrile solution of partially reduced **D_{V3DPA}Cu(OAc)** and followed the evolution of the ^{31}P NMR: upon addition of NO_2^-,

the relative intensity of the signals characteristic of the Cu(I) form at – 6.92 ppm & - 13.01 ppm decreased while those of the Cu(II) form at – 5.96 ppm & - 12.63 ppm increased (Figure 4-15), indicating that the Cu(I) species was oxidized to Cu(II) in the presence of NO_2^-, in the meantime, the NO_2^- might get reduced. However, when this solution is subsequently irradiated with visible light, the signal of Cu(II) species diminished again. These encouraging results suggest that **D_{V3DPA}Cu(OAc)** could indeed be a potential catalyst to photoreduce the nitrite.

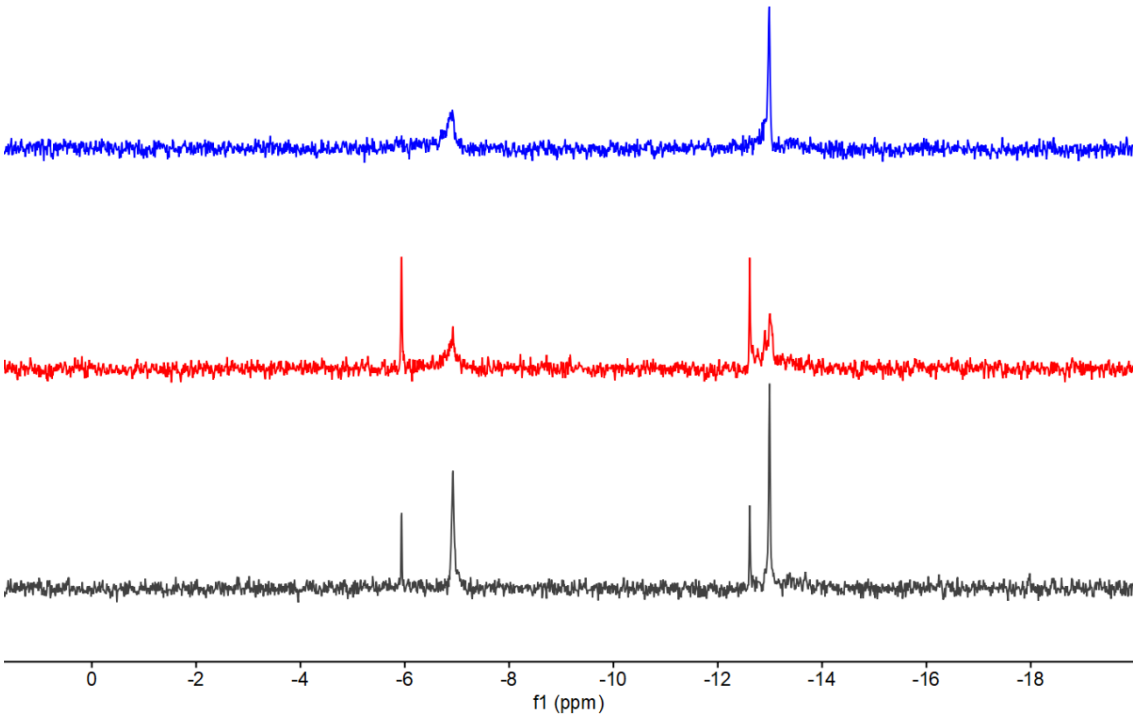

*Figure 4-15 The ^{31}P NMR of the partly photo-reduced **D_{V3DPA}{Cu^{II}(OAc)}** (black), after addition of $TBANO_2$ (red) and following irradiation (blue).*

When using POMs like decatungstate (the most used one) as photosensitizer, as the proposed mechanism is that the excited POM is able to abstract a hydrogen atom. In the presence of reactive species able to trap the generated radical, this can be further used for hydrogen atom transfer (HAT) reactionin organic synthesis.[22] For example, as described in eqn (1) and (2), the photoexcited decatungstate catalyst ($W_{10}O_{32}^{4-*}$) abstracts a hydrogen atom from the alkane (RH), producing an alkyl radical (R$^\bullet$) and the protonated reduced catalyst $W_{10}O_{32}^{5-}H^+$. The resulting alkyl radical is subsequently trapped by an unsaturated substrate

(C=C), yielding a new radical intermediate. This radical intermediate is then converted to the final product by reductive $H^{\cdot}$ donation from $W_{10}O_{32}^{5-}H^{+}$ (eqn (4)), in which the reduced catalyst is reoxidized to complete the catalytic cycle.

$$W_{10}O_{32}^{4-} + h\nu \rightarrow W_{10}O_{32}^{4-*} \quad (1)$$

$$RH + W_{10}O_{32}^{4-*} \leftrightharpoons W_{10}O_{32}^{5-}H^{+} + R^{\bullet} \quad (2)$$

$$R^{\bullet} + C{=}C \rightarrow R{-}C{-}C^{\bullet} \quad (3)$$

$$R{-}C{-}C^{\bullet} + W_{10}O_{32}^{5-}H^{+} \rightarrow R{-}C{-}C{-}H + W_{10}O_{32}^{4-} \quad (4)$$

For nitrite reduction, we are instead interested in using the electron stored on the POM without interference of the electron source, and thus envisioned the using of a sacrificial electron donor. As POMs have been shown to photooxidize alcohols to ketone,[23] we choose isopropanol as an electron source.

We tried to photocatalysis of the 40 eq. $TBANO_2$ with **D_{V3DPA}Cu(OAc)** in the presence of 40 eq. of isopropanol in deuterium acetonitrile solution containing 40 eq. benzoic acid (PhCOOH)[21] as the proton source in inert atmosphere. After 14 hours irradiation, we can observe a quite intense acetone peaks (2.08 ppm in CD_3CN) accounting for a turnover number (TON) up to 28.

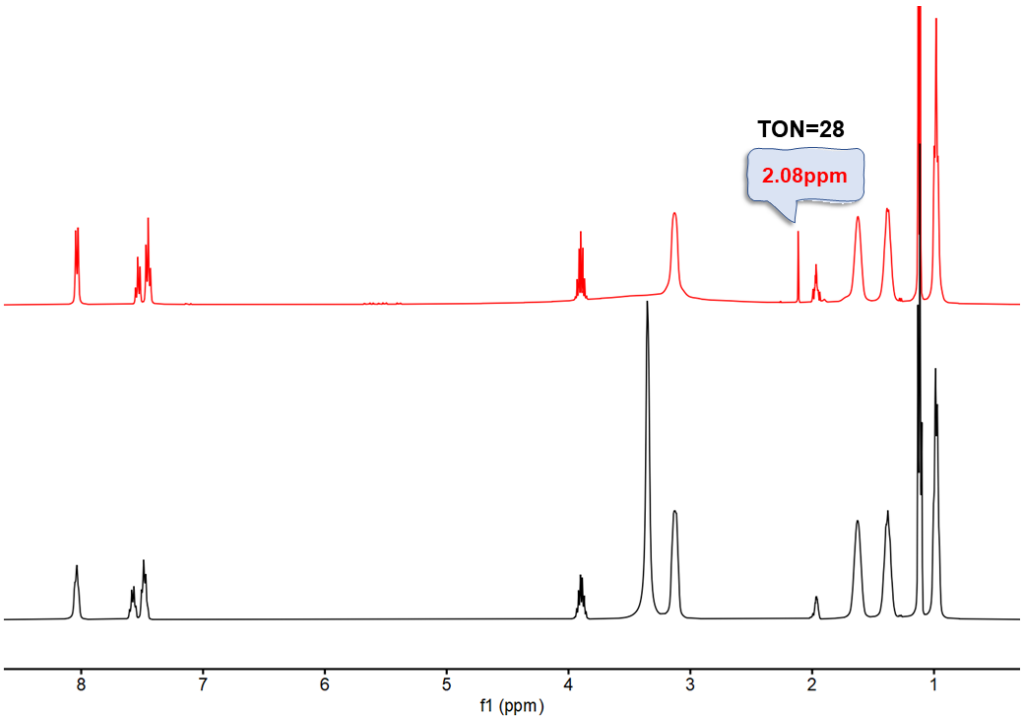

*Figure 4-16 The ^{1}H NMR of **D_{V3DPA}Cu(OAc)** (1.0 mM) in the presence of 40 mM of $TBANO_2$, PhCOOH and isopropanol before and after irradiation with visible light (>382 nm).*

In order to determine if any NO was produced during this photoreduction process, we use the known NO complexation agent cobalt(II) meso-tetraphenylporphyrin (Co-TPP) which undergoes a highly characteristic shift in the position of its visible absorption band (λ_{max} ~ 530 nm) upon NO binding.[24,25] The photolysis are carried out in an airtight vial containing 2.0 mL acetonitrile dissolved 0.5 mM **D_{V3DPA}Cu(OAc)** , 40 mM PhCOOH and $TBANO_2$ under argon. The vial containing Co-TPP in dichloromethane is left open at the top of the headspace, so that the produced NO gas could diffuse into the Co-TPP solution without mixing with the reaction solution. The absorption around 530 nm shifts from 527 nm to 539 nm, which strongly indicates the production of NO.

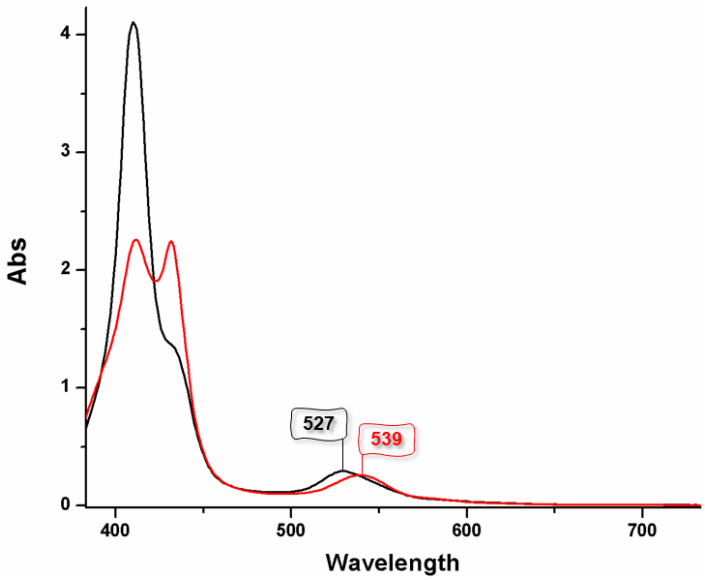

*Figure 4-17 The UV-vis spectrum of 0.08mM Co-TPP to detect the production of NO in the photoreduction of $TBANO_2$ (40 mM) with **D_{V3DPA}Cu(OAc)** (0.5 mM) in the presence of PhCOOH (40 mM).*

In order to quantitatively detect the amount of NO with gas chromatography (GC), a calibration curve was constructed with the reduction of sodium nitrite with ascorbic acid in glacial acetic acid/H_2O as a NO source.[26] Then, in an airtight vial, $TBANO_2$ (40eq.) was photo-irradiated in the present of PhCOOH (40 eq.) and isopropanol (40 eq. electron donner) with 0.004 mmol **D_{V3DPA}Cu(OAc)** or **D_{V3DPA}** as catalysts in 1.5 mL argon purged acetonitrile.

From the curve, at the beginning, the rate of the NO production of two systems are almost the same until around 90 mins. But with longer irradiation, **D_{V3DPA}Cu(OAc)** was much faster than **D_{V3DPA}**, and finally the yield of NO for the former was 2 times than with the later.

Surprisingly, the control group with only $TBANO_2$, benzoic acid and isopropanol inside proved also able to produce NO, even at a more moderate rate and with almost no variation after 90 mins. From these photolysis results, **D_{V3DPA}Cu(OAc)** seems to accelerate the nitrite photoreduction.

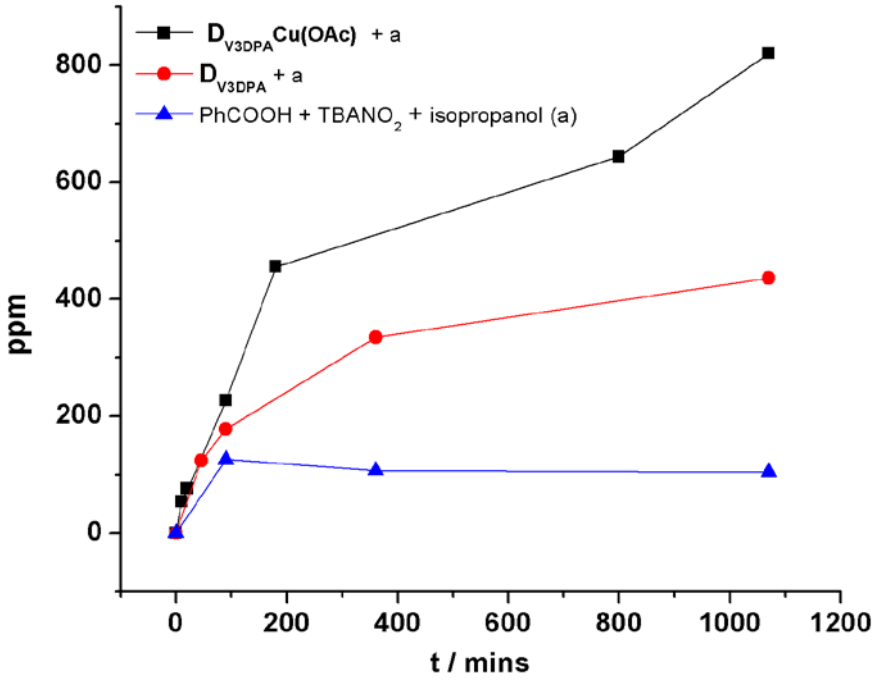

*Figure 4-18 Amount of photo-produced NO from $TBANO_2$ (108 mM) in 1.5 mL acetonitrile with or without the catalyst **D_{V3DPA}Cu(OAc)** (2.67 mM) or **D_{V3DPA}** (2.67 mM) in the presence of benzoic acid (40eq. 108 mM) and isopropanol (40eq. 108 mM) in function of irradiation time.*

In order to furtherly investigate the influence of the copper coordination in the process of photoreduction, we synthesized tris-methyl grafted POM $TBA_6[P_2V_3W_{15}O_{62}(TrisMe)]$ (**D_{V3Me}**) and applied it as a photosensitizer in the presence of $Cu(OAc)_2$ in the nitrite photoreduction.

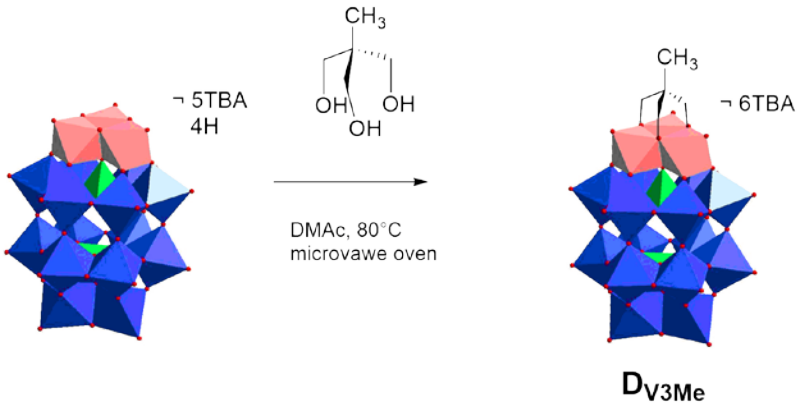

*Scheme 4-6 The synthesis of $TBA_6[P_2V_3W_{15}O_{62}(TrisMe)]$ (**D_{V3Me}**)*

Unfortunately, not only the rate of the photoreduction, but also the yield for both the covalently grafted POM complex and the noncovalent system were almost the same: thus, also the POM can act as a photosensitizer for this reaction, the covalent link does not seem to be a requisite.

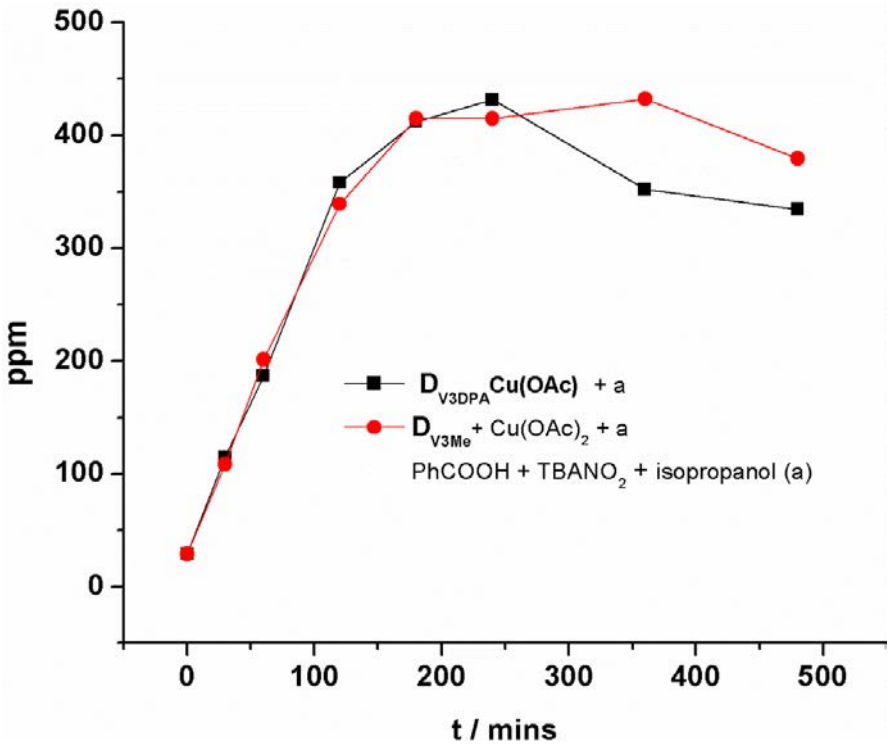

*Figure 4-19 Amount of photo-produced NO from $TBANO_2$ (160eq., 110 mM) in 1.5 mL acetonitrile with the catalyst **$D_{V3DPA}Cu(OAc)$** (0.67 mM) or the mixture of [**D_{V3Me}** +$Cu(OAc)_2$] (0.67 mM) in the presence of benzoic acid (160 eq., 110mM) and isopropanol (160 eq., 110 mM) in function of irradiation time.*

In parallel, these reactions were monitored by ^{1}H NMR to determine the amount of acetone produced: surprisingly it was almost the same in all three cases, even without POM involved (Figure 4-20). It indicates the POM is probably not necessary in the process of photo reduction of the nitrite. Indeed, the amount of NO (data vacu) produced with $Cu(OAc)_2$ salt as catalyst was almost the same with **D_{V3DPA}Cu(OAc)** or the mixture of **D_{V3Me}** and free $Cu(OAc)_2$.

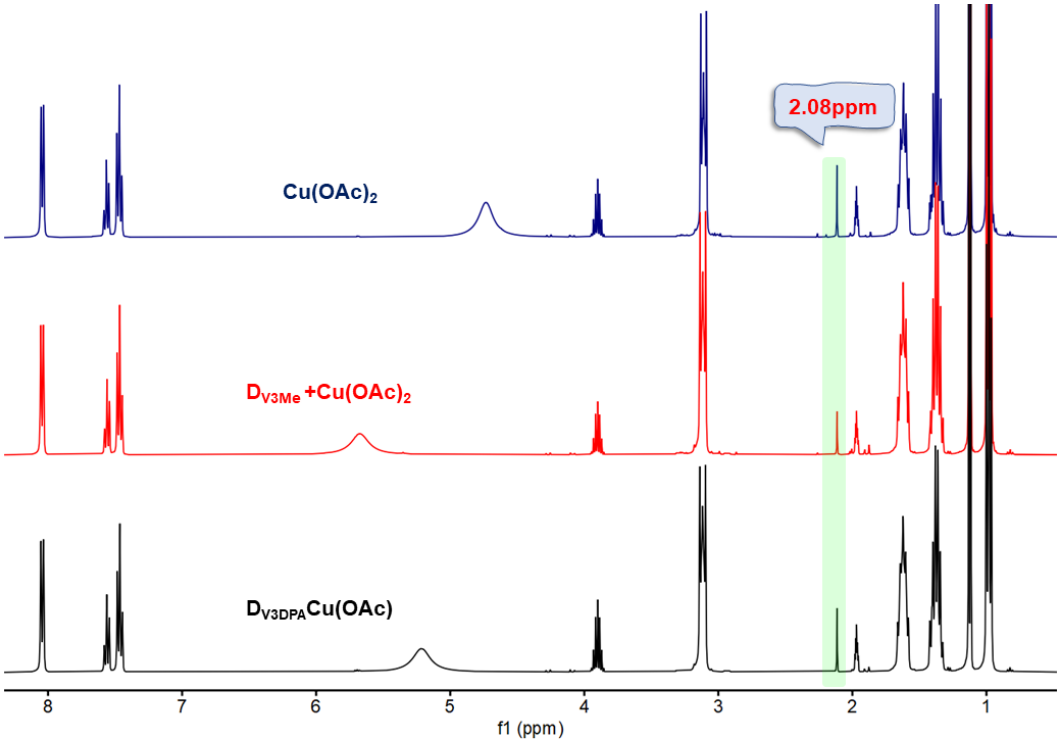

*Figure 4-20 The ^{1}H NMR of **D_{V3DPA}Cu(OAc)** (black), the mixture of **D_{V3Me}** and free copper acetate (red) and the copper acetate alone (navy blue) in the presence of benzoic acid and isopropanol after 1.5 hours irradiation with visible light.*

Overall, these first results indicates that the POM is able to slightly accelerate the reaction, in a very moderate fashion while the isopropanol oxidation may process via different mechanism, I the presence or absence of POM. The exact role of the POM, as well of trying to optimize the reaction (changing the electron donor source for example) will require further investigation.

4.5.4 Photo-reduction of CF_3^+

Incorporation of fluorine or fluorinated groups into molecules can greatly improve their efficiency in a variety of applications, ranging from drugs to material science. In particular, trifluoromethylation has proven an chosen way to improve the efficiency of agrochemicals such as pesticides or plant growth regulators as well as the pharmacokinetic and stability properties of medicinal molecules, or even to introduce Positron Emission Tomography radiotracers.[27–31] This has led to an intensive research on the incorporation of the CF_3 moiety onto organic molecules, and especially of late to the catalysis of the direct C-CF_3 bond formation, starting from halogenated C-X derivatives or even via direct activation of C-H bond.[32] A wide range of electrophilic, nucleophilic or even radical source of trifluoromethylation sources has allowed this field to blossom.[33–35] Several metals have shown great efficiency to catalyze this reaction, among which palladium,[36,37] nickel[38–40] and copper[41–43] play a significant role. Among the various proposed methodologies, MacMillan applied in 2019 copper/photoredox dual catalysis to achieve the trifluoromethylation of alkylbromides.[44] Taking advantage of the well documented ability of the decatungstate $[W_{10}O_{32}]^{4-}$ polyanion (DT) upon irradiation to abstract hydrogen atoms and thus generate carbon centered radicals,[45–47] the same team successfully replaced the noble metal based iridium photosensitizer by DT, thus developing an approach relying on more abundant metal ions.[48]

We thus tried to use the complex $\mathbf{D_{V3DPA}Cu(OAc)}$ in the photoreduction of CF_3^+ to CF_3 radical. To easily observe photogeneration of CF_3 radical, we first tried to trap it with TEMPO radical (2,2,6,6-tetramethylpiperidine-N-oxyl radical).

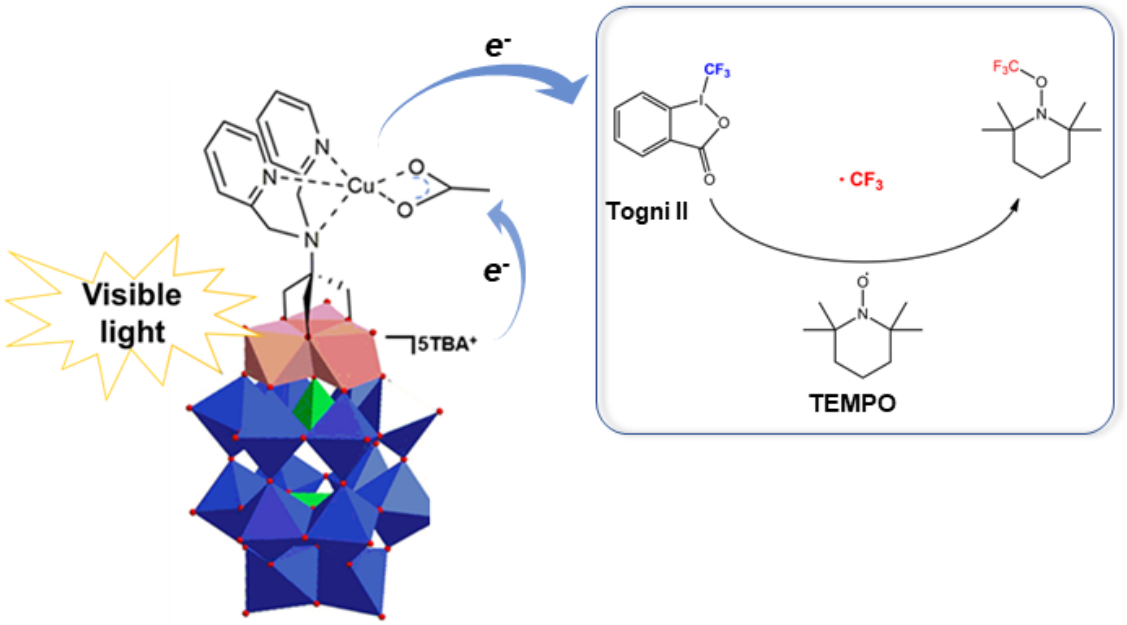

Scheme 4-7 The proposal process of the visible light introduced Cu(II) reduction. TEMPO trapping for the generation of CF_3 radicals

While no reaction occurred in the dark, visible light irradiation of a mixture of Togni (II) reagent as a trifluoromethyl cation source and **$[D_{V3DPA}\{Cu^{II}(OAc)]^{5-}$** anion (1.0 eq.) in the presence of TEMPO radical led, in ^{19}F NMR in CD_3CN, to the disappearance of the Togni (II) signal at 37.5 ppm and the apparition of a single peak at δ = - 55.7 ppm characteristic of the TEMPO-CF_3 adduct (Figure 4-21).[43]

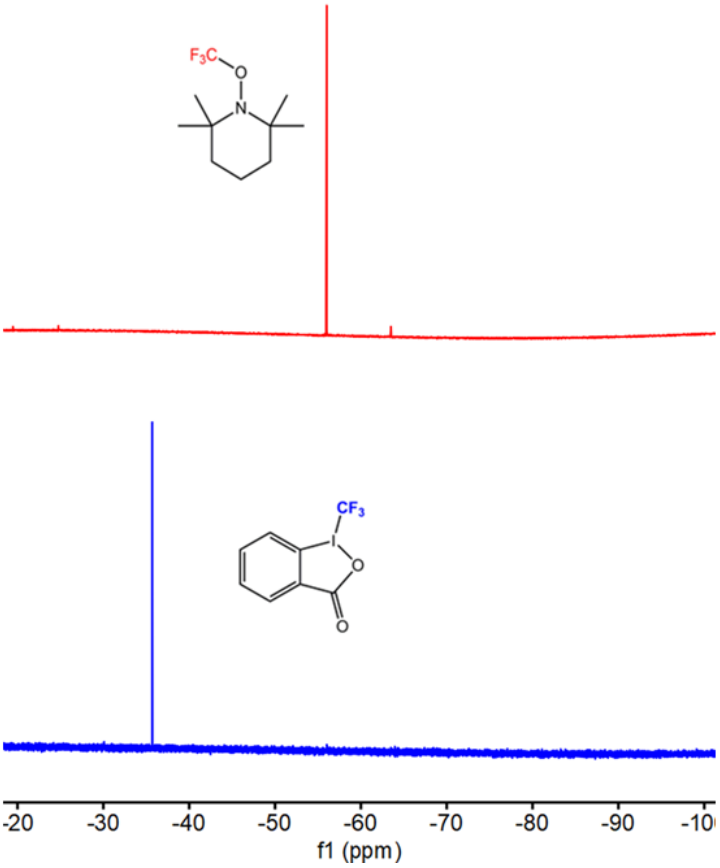

Figure 4-21 ^1H NMR spectrum in CD_3CN of TEMPO trapping experiments for the generation of CF_3 radicals with the ***D_{V3DPA}Cu(OAc)*** *: TEMPO: Togni II = 1: 1: 1.*

Following the same reaction by EPR, the initial triplet signal of TEMPO at g= 2 was replaced by the signature of the **D_{V3DPA}Cu(OAc)** anion (Figure 4- 22). Further irradiation led, as previously observed, to the diminution of the Cu(II) signature and the progressive apparition of the V(IV) signal, indicating that the POM did retain its integrity.

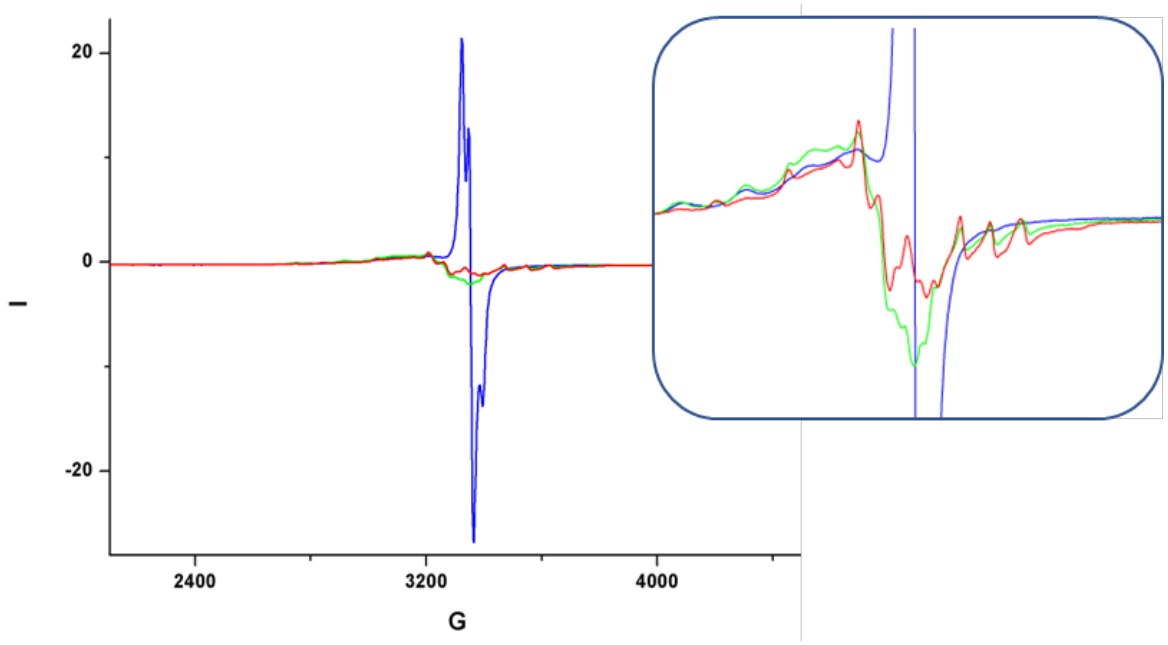

Figure 4-22 EPR spectrum (X-band 9.4GHz 30K) in acetonitrile of TEMPO trapping experiments for the generation of CF_3 radicals with the ***D_{V3DPA}Cu(OAc)*** *: TEMPO : Togni II = 1: 1: 2 after 0- (blue), 0.5- (green) and 1-hour (red) irradiation with visible light (> 382 nm).*

The obvious next step was thus to study the catalytic ability of this hybrid POM to photogenerate CF_3-radicals. Indeed, when using only 5 mol % of POM complex to perform the same reaction, evolution of the ^{19}F NMR clearly indicates an almost full consumption (~92%) of Togni II and being converted into TEMPO-CF_3 within 7 hours (Figure 4-23). Various control experiment where thus performed. When the same reaction was performed either in the presence of the POM ligand (**D_{V3DPA}**) alone or the triester[49] $[CH_3C(CH_2O)_3V_3P_2W_{15}O_{59}]^{6-}$ (**D_{V3Me}**), almost no reaction did occur. However, adding $Cu(OAc)_2$ and DPA to the reaction medium in the latter case allowed for the formation of about 15% TEMPO-CF_3 after 7 hours irradiation. The latter experiment stresses the importance of the covalent link between the POM and the Cu-moiety, that allows for efficient electronic communication between the photoactive POM skeleton and the copper ion and thus improved efficiency.

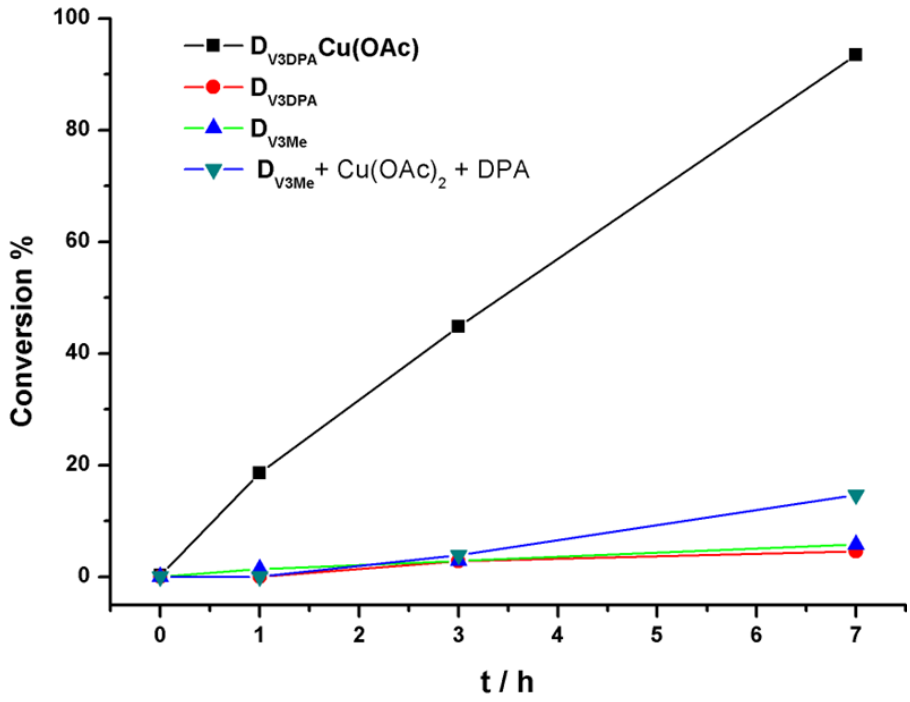

Figure 4-23 Evolution of the conversion of Togni reagent to TEMPO-CF_3 followed by ^{19}FNMR in the presence of ***D_{V3DPA}Cu(OAc)*** *anion (black),* ***D_{V3DPA}*** *(red),* ***D_{V3Me}*** *(bright green), and* ***D_{V3Me}*** *with the mixture of $Cu(OAc)_2$ and DPA (green)*

4.5.5 Trifluoromethylation of styrene

Olefins are versatile synthons for the synthesis of various commodity chemicals. Consequently, numerous catalytic methodologies have been developed allowing olefins to engage into efficient carbon–carbon or carbon–heteroatom bond forming reactions. One specific example that received a lot of attention in recent years is the trifluoromethylation. But direct trifluoromethylation of olefin is still a challenge. As we have proved that the POM complex **D_{V3DPA}Cu(OAc)** could photoreduce CF_3^+ to CF_3 radical, we wonder if it could be trapped by a double bond. Here we use styrene as model substrate to perform trifluoromethylation.

First, a stochiometric reaction was carried out. Visible light irradiation of a mixture of Togni II reagent and **D_{V3DPA}Cu(OAc)** in the presence of styrene in CD_3CN led to a progressive decrease of the signal of Togni II in ^{19}F NMR at - 37.5 ppm which concomitant increase of a triplet signal at - 63.1 ppm, together with the appearance of a new set of new signals at 7.97ppm , 7.69 ppm, 7.55 ppm and 4.04 ppm in ^{1}HNMR. Comparing with literature, the newly

formed product could be identified as 3,3,3-trifluoro-1-phenylpropan-1-one.[43] Additional tiny peaks are also observed at -63.8 ppm, -63.9 ppm & -64.1ppm in ^{19}F NMR that we could not identify.

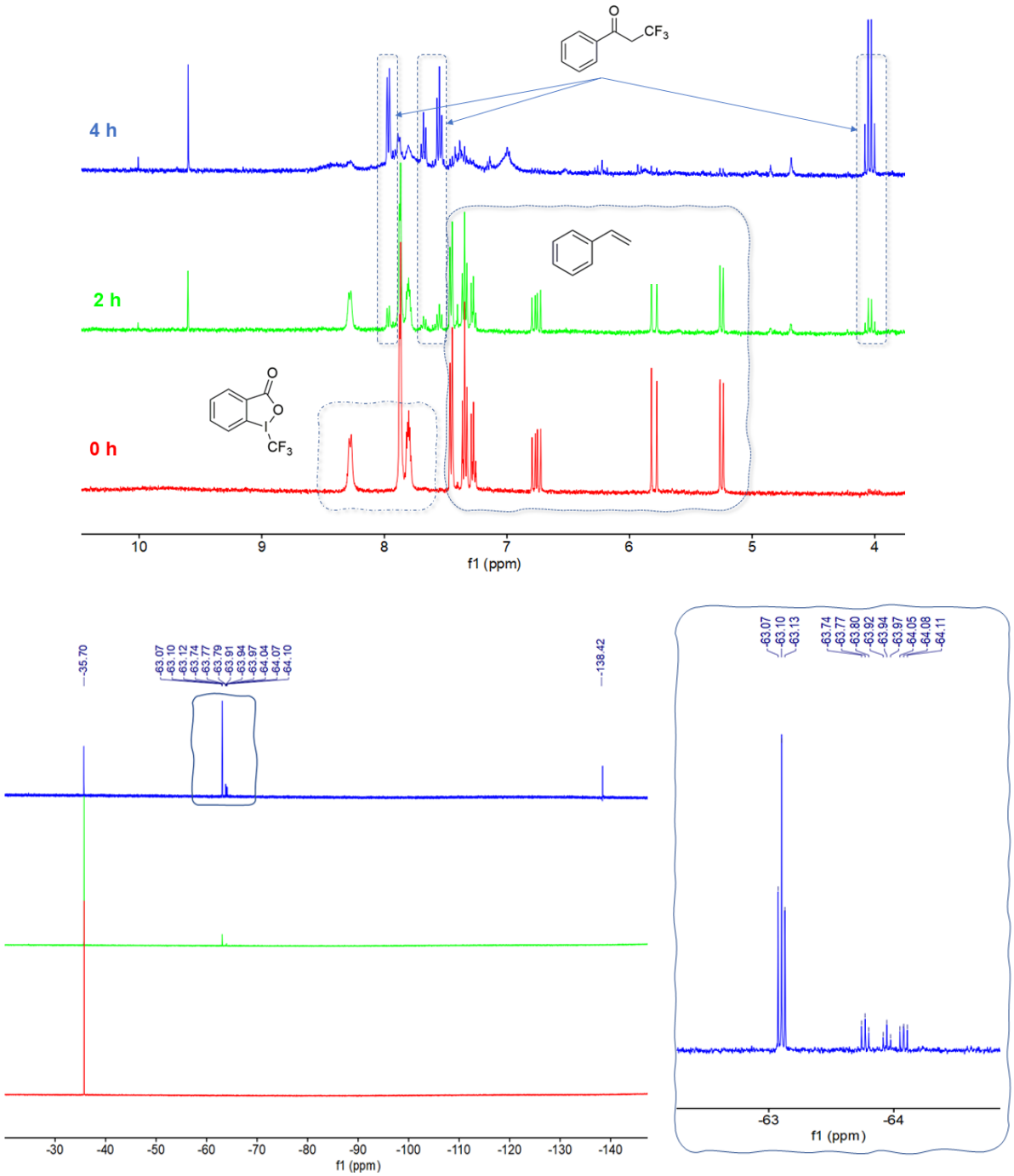

Figure 4-24 ^{1}H NMR and ^{19}F NMR of the reaction of trifluoromethylation of styrene in the ratio of ***D_{V3DPA}Cu(OAc):*** *styrene: CF_3^+ = 1: 1 :4 in CD_3CN after 0-, 2- and 4-hour irradiation with visible light (> 382 nm).*

We tried to change the ratio of reactants in order to see the evolution of the reaction. When we fix the amount of **D_{V3DPA}Cu(OAc)**, an increase of the amount of styrene compared to Togni II yielded an increase in the proportion of the species at -63.8 ppm and -64.1 ppm, both from ~4% to ~35% (ratio of the integration by NMR, in Figure 4-25).

Table 4-3 Different trails of the styrene trifluoromethylation

Condition (Ratio=**D_{V3DPA}Cu(OAc):** styrene: CF_3^+)	**^{19}F NMR** ppm (%) (Crude)	**Styrene consumption** (%)	
Ratio = **1:1:1**, CD_3CN, λ > 380 nm, hv 4h	**-63.1 (25%)** -138.4 (75%)	25	
Ratio = **1:1:4**, CD_3CN, λ > 380 nm, hv 4h	-37.5 (35.5%), **-63.1 (31.3%)**, **-63.8 (4.6%)**, -63.9 (3.8%), **-64.1 (4.2%)**, -138.4 (20.7%)	100	
Ratio = **1:1:4**, CD_3CN, isopropanol λ > 380 nm, hv 4h	**-63.1 (43.5%)**, **-63.8 (12.4%)**, -63.9 (4.8%), **-64.1 (12.6%)**, -80.0 (CF_3H, 3.9%), -138.4 (22.8%)	100	acetone
Ratio= **1:10:10**, CD_3CN, λ > 380 nm, hv 12h	**-63.1 (19.6%)**, **-63.8 (25.1%)**, -63.9 (6.0%), **-64.1 (29.4%)**, -64.2 (8.9%), -66.7 (7.2%), -67.1 (1.2%), -138.4 (1.4%)	60	
Ratio = **1:10:10**, CD_3CN, isopropanol, λ > 380 nm, hv 12h	**-63.1 (16.9%)**, **-63.8 (24.5%)**, -63.9 (6.1%), **-64.1 (28.4%)**, -64.2 (9.8%) -66.7 (7.6%), -67.1 (1.6%), -138.4 (4.5%)	70	acetone
Ratio = **1:4:2,** CD_3CN, λ > 380 nm, hv 4h	**-63.1 (9.6%)**, **-63.8 (31.6%)**, **-64.1 (35.0%)**, -64.2 (12.4%), -66.7 (11.4%)	50	

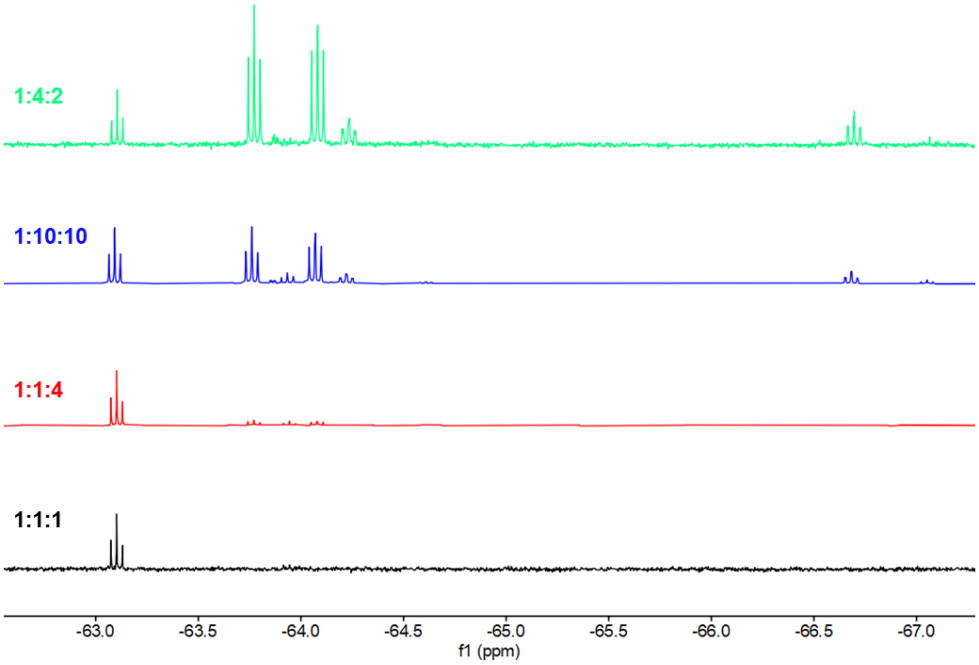

Figure 4-25 Evolution of the ^{19}F NMR as a function of the ratio styrene to Togni II 1:1, 1:4 (red), 10:10 (green), 4:2 (blue).

The preliminary results above have proved that **D_{V3DPA}Cu(OAc)** could be applied in the direct trifluoromethylation of styrene, not only stoichiometrically but also catalytically. Although the resulting products and the mechanism of the process need to be further investigated, it is possible for the system to be applied with some more valuable substrates. This study will need to be continued.

4.5.6 Electron source investigation

One question that arises from the former studies is the sacrificial source of electrons. Indeed, while in some studies, isopropanol was added to the system and some acetone detected after the irradiation the amount of the latter did not correlate well with the observed reactivity. Moreover, several experiments did work even without intentionally added electron donor. Whatever the conditions, we always observed an intriguing singlet at 9.6 ppm in ^1H NMR after the irradiation (e.g., Figure 4-24): we hypothesized that this could belong to hydrogen peroxide (H_2O_2) which could originate from H_2O being oxidized and thus playing the role of electron donor.

In order to verify this, H_2O_2 (4.0 eq.) was added in the NMR tube after irradiation and a first NMR analysis, in order to see if the signal at 9.6 ppm would increase, thus confirming the identification. Unfortunately, in this case, the signal at 9.6 ppm completely vanished once the H_2O_2 was added. Based on that, we wondered if H_2O_2 was also consumed by the complex itself, so that we tested the stability of the H_2O_2 in the presence of $\mathbf{D_{V3DPA}Cu(OAc)}$.

Under dark, 20 eq. of H_2O_2 was mixed with $\mathbf{D_{V3DPA}Cu(OAc)}$ in CD_3CN and monitored with ^1H NMR in function of incubation time. After 3 hours, the signal of H_2O_2 at 8.58 ppm was almost gone (Figure 4-33, A), which indicated the POM complex can decompose the H_2O_2 quite efficient even in the dark. Interestingly, this process is accelerated under irradiation, as the H_2O_2 signal vanished completely within 1 hour. In contrast, in the presence of $\mathbf{D_{V3Me}}$ without copper (Figure 4-33, B), there was no disappearance of the H_2O_2 peak. And also in the $[Cu(OAc)_2$+DPA] case (Figure 4-33, c), there was no significant diminish (~15%).

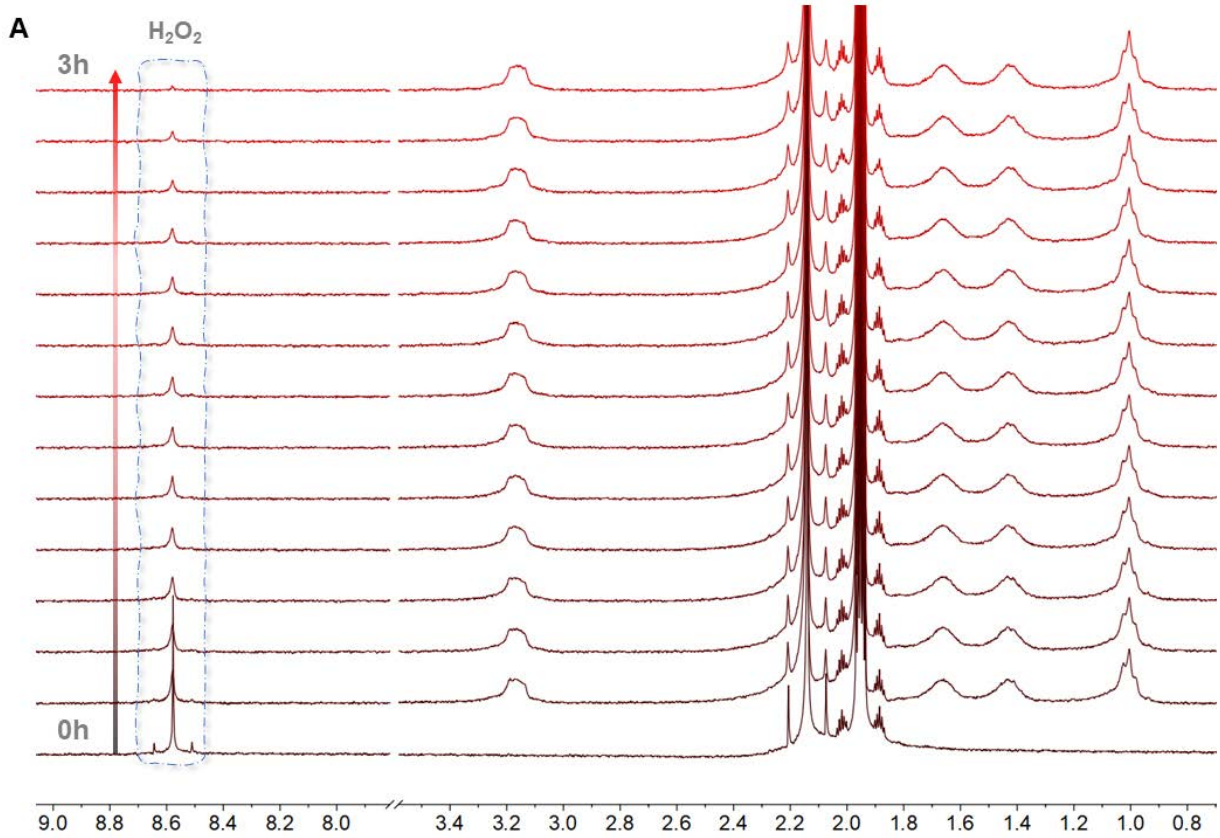

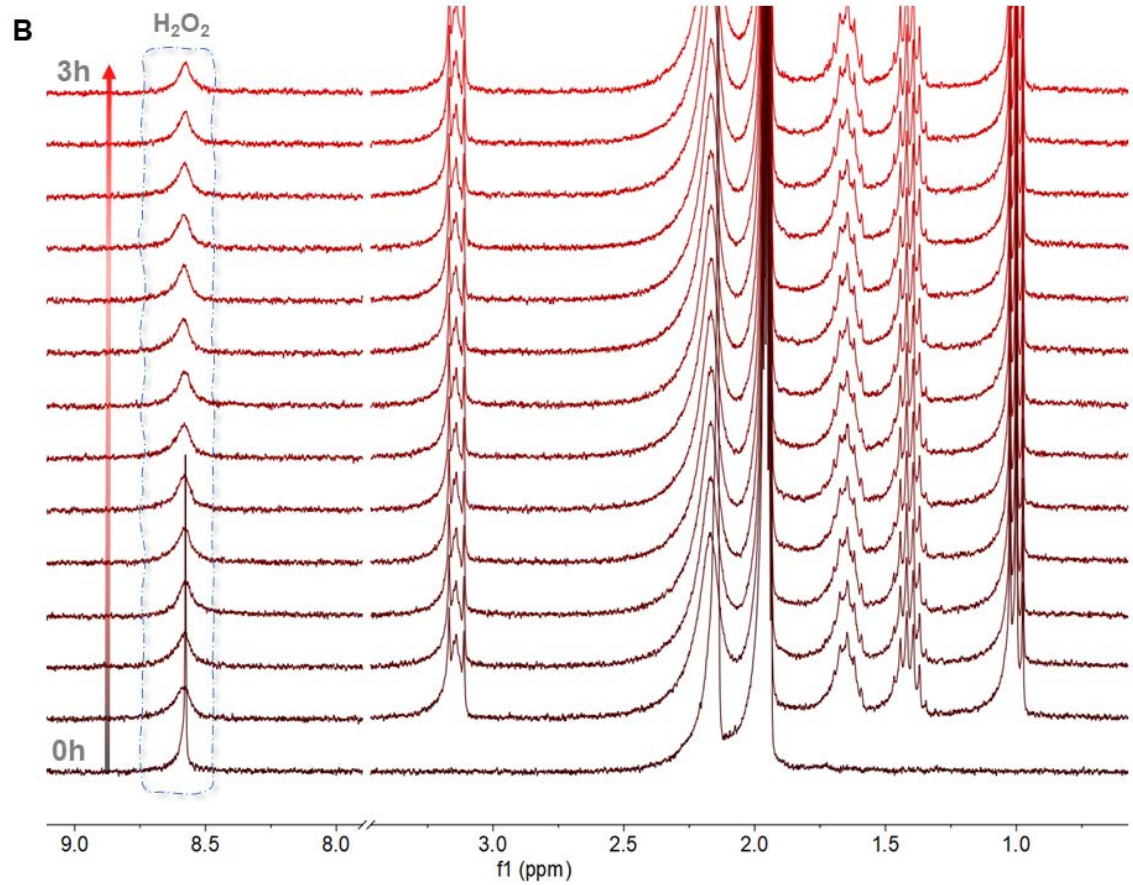
B
H2O2
3h
0h
9.0
8.5
8.0
3.0
2.5
2.0
1.5
1.0
f1 (ppm)

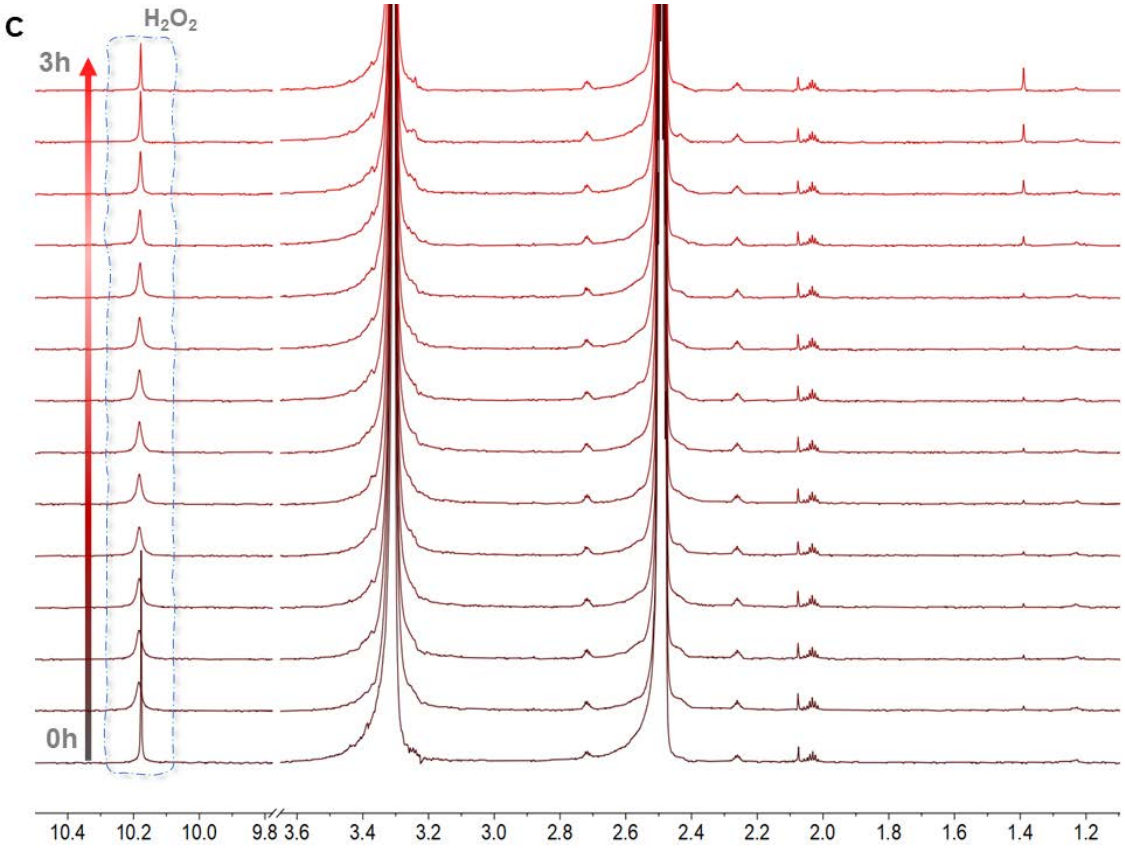
C
H2O2
3h
0h
10.4
10.2
10.0
9.8
3.6
3.4
3.2
3.0
2.8
2.6
2.4
2.2
2.0
1.8
1.6
1.4
1.2

*Figure 4-33 ^1H NMR monitoring the incubation processes of 20 eq. H_2O_2 and A) **D_{V3DPA}Cu(OAc)** (0.4 mM); B) **D_{V3Me}** (0.4 mM) in CD_3CN and C)[$Cu(OAc)_2$+DPA] (0.4 mM) in DMSO from 0- to 3-hour*

4.6 Conclusion and perspective

In this Chapter, we have successfully covalently grafted aromatic tripodal and aliphatic tripodal ligands onto the trivanadate cap substitute Dawson POM, $(TBA_5H_4)[P_2V_3W_{15}O_{62}]$ (**D_{V3}**) to form **D_{V3DPA}** and **D_{V3DA}**. Both of them are characterized by NMR, ESI-Mass to confirm the structures. We have prepared the Cu complex **D_{V3DPA}Cu(OAc)**, which has been well characterized through UV, NMR, ESI-Mass and elemental analysis to verify the successful coordination and its purity.

During this study, we noticed the existence of photoactivity of **D_{V3DPA}Cu(OAc)** from the NMR evolution, and further confirmed by EPR not only the reduction of the Cu(II) to Cu(I), but that a second photoreduction could occur with the formation of V(IV) upon longer time irradiation. Indeed, the cyclic voltammetry shows that the reduction potential of the Cu(II)/Cu(I) is quite close to the first V(V)/V(IV) reduction potential. Through monitoring with the UV-vis spectrum while irradiating **D_{V3DPA}Cu(OAc)** in acetonitrile, we can observe diminution of the d-d transition absorption of the Cu(II) complex first, following the two processes of the V(V) reduction with longer irradiation, which indicates a rare three electrons accumulation on the POM complex.

Then, the **D_{V3DPA}Cu(OAc)** was applied to catalytically photoreduce CF_3^+, which was proved to form CF_3 radical that could be trapped by TEMPO. In this case, the importance of a covalent bond between the POM and the Cu complex has been clearly evidenced. This complex is thus a potential photocatalyst for trifluoromethylation of some more valuable substrates, as confirmed by preliminary results on the trifluoromethylation of styrene which need to be further investigated. A pending question remains the source of the electron in these processes.

In parallel, **D_{V3DPA}Cu(OAc)** was applied to mimic the CuNIR to photoreduce nitrite (NO_2^-). While the POM could accelerate a bit the reaction, the activity of the POM complex

was almost the same with the mixture of $\mathbf{D_{V3Me}}$ and $Cu(OAc)_2$ in the presence of benzoic acid, and a covalent link did in this case not bring beneficial effects.

These first studies have revealed a photoactivity of the hybrid POM and shown some promising results, with possible synergy between the POM skeleton and the bioinspired complex through covalent grafting, For the next step, we would like to prepare the Cu complex with the aliphatic amine functionalized POM, $\mathbf{D_{V3DA}}$, to tune the redox properties of the POM complex, and study the effect of the coordination shell on this synergy and the reactivity.

Experimental section:

Synthesis of 2-(Bis-pyridin-2-ylmethyl-amino)-2-hydroxymethyl-propane-1,3-diol **H_3TrisDPA**

2-(Bis-pyridin-2-ylmethyl-amino)-2-hydroxymethyl-propane-1,3-diol (**H_3TrisDPA**) was synthesized according to the modified protocol published by Zhao.[49] 1.21 g, 10 mmol 2-amino-2-hydroxymethyl-propane-1,3-diol, 3.28 g 10 mmol 2-picolyl chloride hydrochloride, 5.52 g, 40 mmol K_2CO_3 and 1.66 g KI was mixed under argon followed by the addition of 100 mL dry acetonitrile. The resulting orange solution was filtered after 48 hours, and the filtrate was rotary evaporated. The dark brown oil was spread in 20 mL chloroform to remove the K_2CO_3 and KI residue and the filtrate was rotary evaporated. The resulting 3.0 g dark brown oil was further purified through chromatography with methanol/ethyl acetate (1:9) as the eluent. The resulting eluent solution was crystallized out and crystals suitable for X-ray diffraction were obtained. Yield, 587 mg, 19.4% The colorless crystal was analyzed by ^{1}H NMR (400 MHz, DMSO) δ 8.40 (dd, J = 5.0, 1.7 Hz, 2H), 7.48 (td, J = 7.7, 1.8 Hz, 2H), 7.14 – 7.04 (m, 4H), 5.21 (s, 2H), 4.09 (s, 4H), 3.55 (s, 6H); ^{13}C NMR (101 MHz, DMSO) δ 162.02, 148.71, 136.67, 123.04, 122.06, 65.83, 61.44, 55.50.

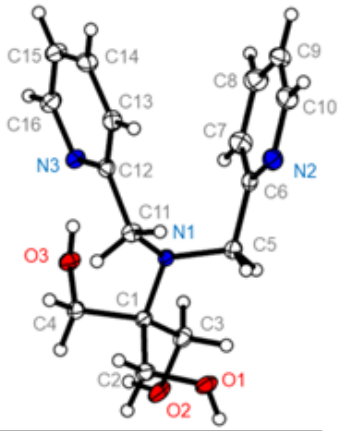

Bond:

N1	C11	1.4683(14)
N1	C1	1.4830(13)
N2	C6	1.3374(15)
N2	C10	1.3439(17)
N3	C16	1.3395(15)
N3	C12	1.3408(14)
C1	C2	1.5340(15)
C1	C4	1.5364(14)
C1	C3	1.5387(15)
C5	C6	1.5078(16)
C6	C7	1.3859(18)
C7	C8	1.3809(19)
C8	C9	1.377(2)
C9	C10	1.369(2)
C11	C12	1.5131(15)
C12	C13	1.3879(16)
C13	C14	1.3817(18)
C14	C15	1.3789(19)
C15	C16	1.3787(18)

Angle:

C5	N1	C11	109.99(9)
C5	N1	C1	118.21(8)
C11	N1	C1	115.57(8)
C6	N2	C10	117.16(11)
C16	N3	C12	118.33(10)
N1	C1	C2	113.98(9)
N1	C1	C4	107.63(8)
C2	C1	C4	108.25(9)
N1	C1	C3	109.02(9)
C2	C1	C3	109.69(9)
C4	C1	C3	108.09(9)
O1	C2	C1	112.16(9)
O2	C3	C1	112.09(9)
O3	C4	C1	112.44(9)
N1	C5	C6	110.66(9)
N2	C6	C7	122.19(11)
N2	C6	C5	117.12(11)
C7	C6	C5	120.69(10)
C8	C7	C6	119.60(12)
C9	C8	C7	118.48(13)
C10	C9	C8	118.49(12)
N2	C10	C9	124.08(12)
N1	C11	C12	112.80(9)
N3	C12	C13	121.63(10)
N3	C12	C11	116.65(9)
C13	C12	C11	121.67(10)
C14	C13	C12	119.29(11)
C15	C14	C13	119.22(11)
C16	C15	C14	118.16(11)
N3	C16	C15	123.35(12)

Synthesis of **D_{V3DPA}**

$TBA_6[P_2V_3W_{15}O_{62}(trisDPA)]$ (**D_{V3DPA}**) was synthesized according to a modified procedure published by Hasenknopf. [50] A mixture of 495 mg $TBA_4H_5[P_2V_3W_{15}O_{62}]$ (**D_{V3}**) which was synthesized according to the procedure published by Finke[51] and 36.6 mg (1.2 eq) **H3L** were dissolved in 5 mL DMAc in a Schlenk tube under argon. The orange solution was heated with microwave at 80℃ for 1 hour. The resulting olive solution was precipitated in 40mL diethyl ether. The brown precipitate was redissolved in 2 mL acetonitrile and then the resulting brown

solution was precipitated with 40 mL ethanol/diethyl ether (v/v=10/30) containing 10 mM TBAOH. Yield, 55.9%. ^{1}H NMR (400 MHz, CD3CN) δ 8.44 (d, *J* = 4.9 Hz, 2H), 7.62 (t, *J* = 7.7 Hz, 2H), 7.43 (d, *J* = 7.9 Hz, 2H), 7.15 (t, *J* = 6.2 Hz, 2H), 5.65 (s, 6H), 4.26 (s, 4H), 3.27 – 3.15 (m, 48H), 1.68 (dq, *J* = 15.7, 7.5 Hz, 48H), 1.44 (h, *J* = 7.4 Hz, 48H), 1.02 (t, *J* = 7.3 Hz, 72H). ^{31}P NMR (162 MHz, CD_3CN) δ -6.95, -13.04. Elemental analysis: found% C 23.7, H 4.25, N 2.16; Calculate% C 23.72, H 4.16, N 2.22.

Synthesis of $\mathbf{D_{V3Me}}$

$TBA_6P_2V_3W_{15}O_{62}$(trisMe) ($\mathbf{D_{V3Me}}$) was synthesized according to the same procedure as $\mathbf{D_{V3DPA}}$. A mixture of 243 mg $TBA_4H_5P_2V_3W_{15}O_{62}$ ($\mathbf{D_{V3}}$) and 6.6 mg (1.2 eq) 2-(hydroxymethyl)-2-methylpropane-1,3-diol were dissolved in 3 mL DMAc in a Schlenk tube under argon. The orange solution was heated with microwave at 80℃ for 1 hour. The resulting yellow-greenish solution was precipitated in 40 mL diethyl ether, the yellow-greenish precipitate was washed with ether (20mL*2). ^{1}H NMR (400 MHz, CD_3CN) δ 5.45 (s, 6H) δ 3.22 – 3.13 (m, 48H), 1.73 – 1.61 (m, 48H), 1.44 (h, *J* = 7.4 Hz, 482H), 1.02 (t, *J* = 7.3 Hz, 72H). ^{31}P NMR (162 MHz, CD_3CN) δ -7.34, -12.53.

Synthesis of $\mathbf{D_{V3DPA}Cu(OAc)}$

226.8 mg, 0.04 mmol $\mathbf{D_{V3DPA}}$ was dissolved in 6mL acetonitrile, the resulting slight brown solution was added gradually into 4 mL acetonitrile solution containing 8.0 mg, 0.04 mmol $Cu(OAc)_2$ under dark with stirring. The resulting yellow-green solution was precipitate with 60 mL diethyl ether resulting 198 mg green-yellowish solid. Yield 89.2%. ^{1}H NMR (400 MHz, CD_3CN) δ 15.31, 12.81, 12.23, δ 3.22 – 3.13 (m), 1.73 – 1.61 (m), 1.44 (h, *J* = 7.4 Hz), 1.02 (t, *J* = 7.3 Hz). ^{31}P NMR (162 MHz, CD_3CN) δ -5.93, -12.61.

Oxidation investigation of $\mathbf{D_{V3DPA}Cu^I}$

There is still some Cu^I species left after the addition of air saturated solution or bubbling air inside the solution, indicates the oxidation of $\mathbf{D_{V3DPA}Cu^I}$ is quite slow and the oxygen could

not oxidize it completely. But once the addition of H_2O_2, the diamagnetic signals completely vanished.

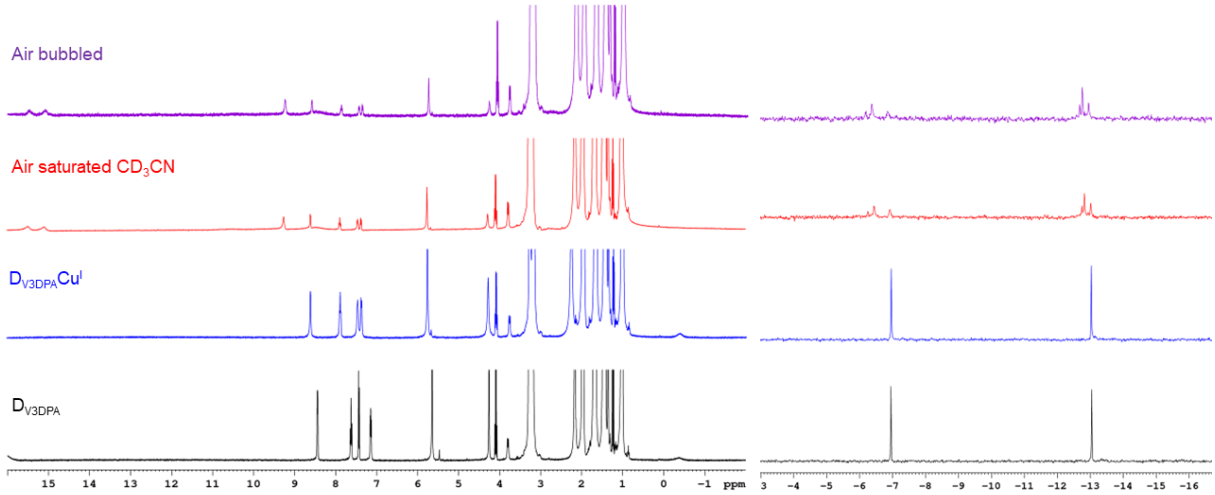

Figure 4-34 The oxidation of $D_{V3DPA}Cu^{I}$ *with air.*

UV-vis titration of $\mathbf{D_{V3DPA}}$ and $\mathbf{D_{V3}}$ with $Cu(ClO_4)_2$

10 mM $Cu(ClO_4)_2$ was gradually added into 1.0 mM $\mathbf{D_{V3DPA}}$ or $\mathbf{D_{V3}}$ acetonitrile solution and monitored with UV-vis spectrum. For the $\mathbf{D_{V3DPA}}$ case (left), shows the appearance of an isosbestic point at 608 nm and the plot of the evolution of the absorption at 530 nm and 647 nm clearly show a change in the slope of the linear adjustment in agreement with the formation of a 1: 1 complex. While in the titration of $\mathbf{D_{V3}}$, there is no isosbestic point indicating the electronic interaction process of $\mathbf{D_{V3}}$ and $Cu(ClO_4)_2$.

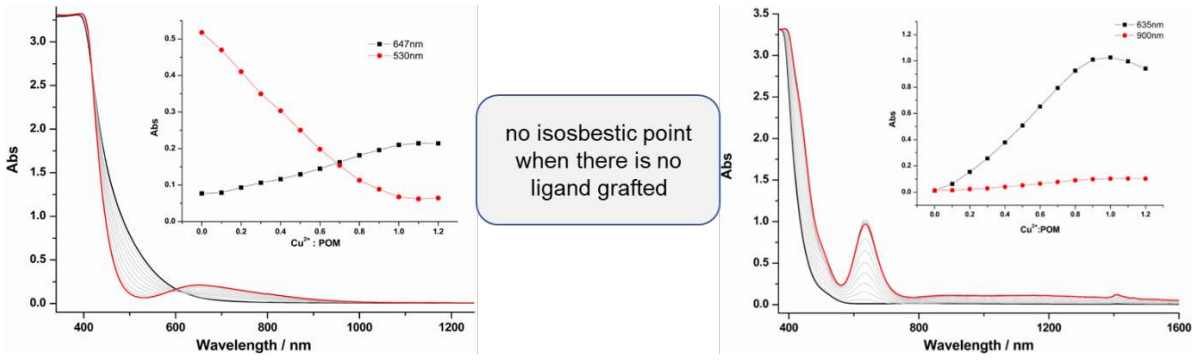

Figure 4-35 UV-vis titration of D_{V3DPA} *and* D_{V3} *with* $Cu(ClO_4)_2$

Nitric oxide (NO) GC calibration

A 10 mL Schlenk vessel filled with 1.5 mL of a 50 mM solution of ascorbic acid in glacial acetic acid/H_2O (respectively 1.35 mL/0.15 mL) was purged with argon, which is known to generate NO stoichiometrically from nitrite. Known aliquots of sodium nitrite (as a solution in water) were then added to this solution with stirring for 10 mins (until there were no obvious bubbles appearing). The amount of the NO in the headspace was detected with GC, for every spot injected 50 μL with syringe.

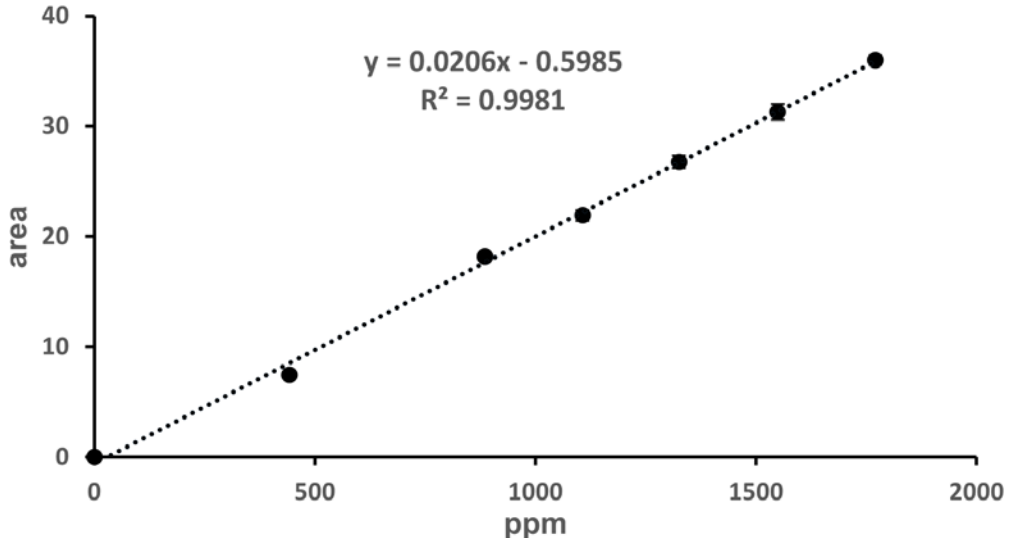

Figure 4-36 The GC calibration curve of NO produced from the reduction of sodium nitrite with ascorbic acid in the presence of glacial acetate acid.

Synthesis of 6-(((tert-butyldimethylsilyl)oxy)methyl)-2,2,3,3,9,9,10,10-octamethyl-4,8-dioxa-3,9-disilaundecan-6-amine (**$TBDMS_3$Tirs**)

3.35 g, 22.3 mmol Tert-butyldimethylsilyl chloride and 3.15 g, 46.5 mmol imidazole were dissolved in 4 mL dry DMF followed by the addition of 0.75 g tris(hydroxymethyl)methylamine under argon. The resulting slightly yellow solution was washed with H_2O and extracted dichloromethane. The organic phase was dry with anhydrous Na2SO4, followed by the removement of solvent with rotary evaporate, resulting in a colorless solid. Yield 2.97 g, 96.7%. ^{1}H NMR (400 MHz, $CDCl_3$) δ 3.48 (s, 6H), 0.91 (s, 27H), 0.06 (s, 18H).

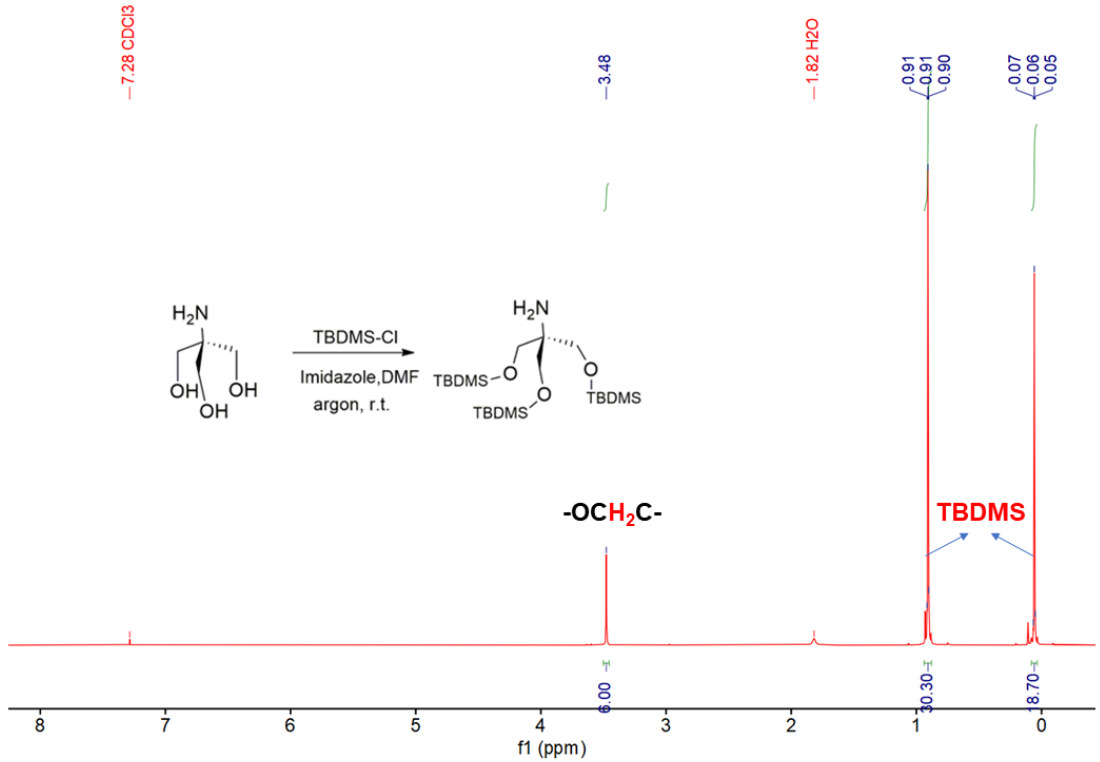

*Figure 4-37 ^{1}H NMR of **TBDMS$_3$Tris** in $CDCl_3$.*

Synthesis of di-tert-butyl (((6-(((tert-butyldimethylsilyl)oxy)methyl)-2,2,3,3,9,9,10,10-octamethyl-4,8-dioxa-3,9-disilaundecan-6-yl)azanediyl)bis(ethane-2,1-diyl))dicarbamate (**TBDMS$_3$Tris-DA-Boc**)

1.51 g, 3.35 mmol of **TBDMS$_3$Tirs** and 0.54 g, 3.35 mmol of aldehydes tert-butyl (2-oxoethyl)carbamate, was dissolved in 40mL dry dichloromethane, stirred under argon for 15 mins at room temperature, followed by the addition of 2.81 g, 13.4 mmol sodium triacetoxyborohydride ($NaBH(OAc)_3$). The reaction was monitored with ^{1}H NMR and thin layer chromatography (TLC) after being stirring for 1.0 h, and then add another 1.62 g, 10.0 mmol tert-butyl (2-oxoethyl)carbamate followed the addition of 2.81 g, 13.4 mmol $NaBH(OAc)_3$ after 1.0 h. The reaction was quenched with 100mL saturated sodium bicarbonate aqueous solution after overnight stirring at room temperature. The resulting colorless oil was purified via silica gel column with cyclohexane/ethyl acetate (15/1) as eluent, yield 1.64 g, 67.2%. ^{1}H NMR (300 MHz, $CDCl_3$) δ 5.18 (s, 1H), 3.63 (s, 6H), 3.09 (q, *J* = 5.9 Hz, 4H), 2.90 (t, *J* = 6.2 Hz, 4H), 1.46 (s, 18H), 0.91 (s, 27H), 0.07 (s, 18H).

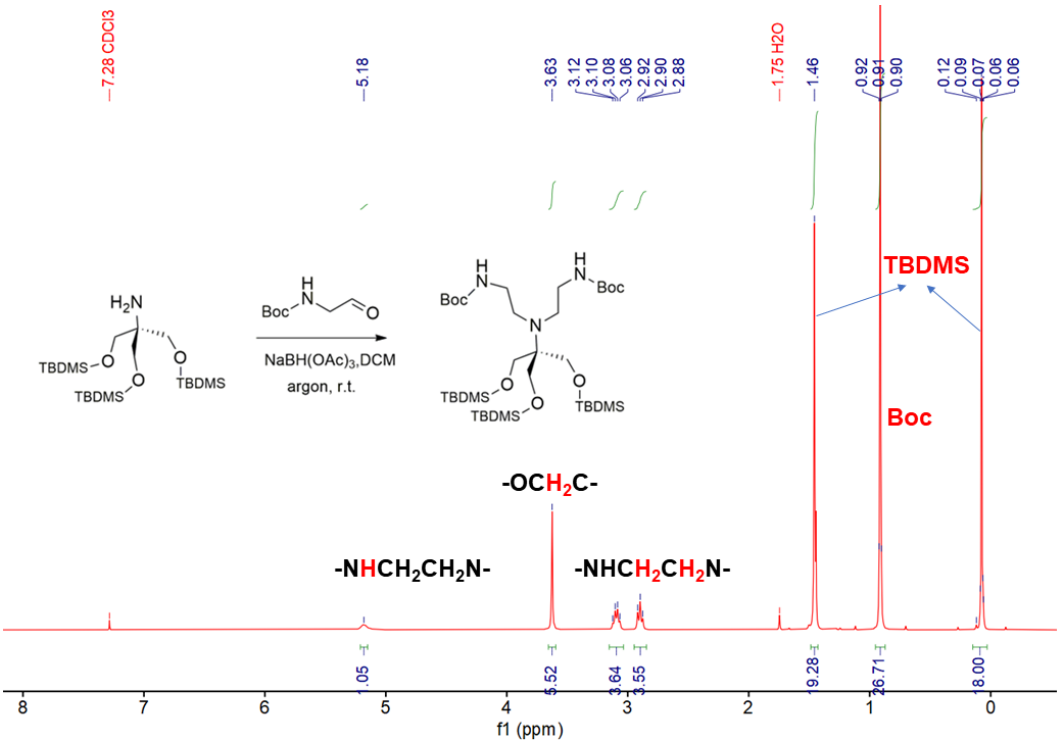

*Figure 4-38 ^1H NMR of **TBDMS₃Tris-DA-Boc** in $CDCl_3$.*

Synthesis of di-tert-butyl (((1,3-dihydroxy-2-(hydroxymethyl)propan-2-yl)azanediyl)bis(ethane-2,1-diyl))dicarbamate (**H₃Tris-DA-Boc**)

1.6 g **TBDMS₃Tris-DA-Boc** was dissolved in 10 mL THF and followed by the addition of 6.5 mL 1.0 M tetrabutylammonium fluoride (TBAF) in THF. After overnight stirring, the resulting slightly brown solution was rotary evaporated to remove THF to get a slightly brown oil which was washed with 2*5 mL water. The water phase was collected, and rotary evaporated to remove water. The resulting pale-yellow oil was chromatographed with silica gel column eluted with chloroform/methanol (50/3). The collected colorless oil (yield 600 mg, 67.4%) was dissolved in 1 mL acetonitrile and crystallized overnight (yield 439.2 mg, 73.2%). The obtained colorless of crystal was suitable for the single crystal XRD, which indicates us that two Boc protected amines are connected to the tris(hydroxymethyl)aminomethane through ethyl forming **H₃Tris-DA-Boc**. ^1H NMR (400 MHz, DMSO) δ 6.75 (s, 2H), 4.19 (t, *J* = 5.1 Hz, 3H), 3.39 (d, *J* = 5.2 Hz, 6H), 2.90 (q, *J* = 6.5 Hz, 4H), 2.70 (t, *J* = 6.9 Hz, 4H), 1.38 (s, 18H).

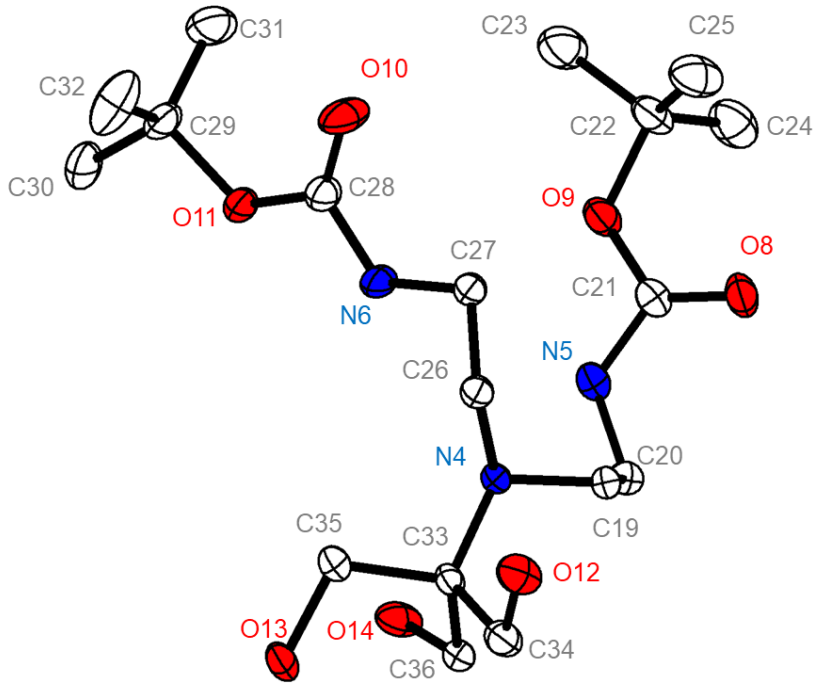

Bond:

O1	C3	1.225(5)	N1	C8	1.474(5)	C8	C9	1.506(7)
O2	C3	1.342(5)	N1	C1	1.486(5)	C11	C13	1.504(8)
O2	C4	1.473(5)	N1	C15	1.488(5)	C11	C14	1.515(8)
O3	C10	1.192(5)	N2	C3	1.340(5)	C11	C12	1.517(7)
O4	C10	1.358(5)	N2	C2	1.449(5)	C15	C18	1.503(7)
O4	C11	1.461(5)	N3	C10	1.336(6)	C15	C16	1.524(6)
O5	C16	1.366(6)	N3	C9	1.447(6)	C15	C17	1.558(6)
O6	C17	1.442(6)	N4	C19	1.469(5)	C19	C20	1.519(6)
O7	C18	1.417(5)	N4	C26	1.477(5)	C22	C24	1.508(8)
O8	C21	1.225(5)	N4	C33	1.486(5)	C22	C23	1.509(7)
O9	C21	1.342(5)	N5	C21	1.335(5)	C22	C25	1.526(7)
O9	C22	1.475(5)	N5	C20	1.450(5)	C26	C27	1.508(6)
O10	C28	1.198(5)	N6	C28	1.342(5)	C29	C31	1.499(7)
O11	C28	1.355(5)	N6	C27	1.459(5)	C29	C32	1.517(8)
O11	C29	1.479(5)	C1	C2	1.528(6)	C29	C30	1.519(7)
O12	C34	1.412(5)	C4	C5	1.506(6)	C33	C34	1.534(6)
O13	C35	1.432(5)	C4	C7	1.511(6)	C33	C36	1.535(6)
O14	C36	1.425(5)	C4	C6	1.524(7)	C33	C35	1.535(6)

Angle:

C3	O2	C4	121.9(3)	O2	C4	C5	102.0(3)	C18	C15	C16	115.0(4)	N6	C27	C26	112.2(3)
C10	O4	C11	119.4(3)	O2	C4	C7	110.6(4)	N1	C15	C17	107.1(4)	O10	C28	N6	124.5(4)
C21	O9	C22	121.9(3)	C5	C4	C7	110.7(4)	C18	C15	C17	107.3(3)	O10	C28	O11	125.0(4)
C28	O11	C29	119.5(3)	O2	C4	C6	109.2(4)	C16	C15	C17	102.7(4)	N6	C28	O11	110.6(3)
C8	N1	C1	109.5(3)	C5	C4	C6	110.7(4)	O5	C16	C15	115.9(4)	O11	C29	C31	109.8(4)
C8	N1	C15	114.3(3)	C7	C4	C6	113.0(4)	O6	C17	C15	107.6(4)	O11	C29	C32	109.2(4)
C1	N1	C15	115.9(3)	N1	C8	C9	112.7(4)	O7	C18	C15	109.4(3)	C31	C29	C32	113.7(5)
C3	N2	C2	122.5(3)	N3	C9	C8	112.5(4)	N4	C19	C20	114.5(3)	O11	C29	C30	102.7(4)
C10	N3	C9	121.0(4)	O3	C10	N3	124.6(4)	N5	C20	C19	113.8(3)	C31	C29	C30	109.7(4)
C19	N4	C26	110.5(3)	O3	C10	O4	125.1(4)	O8	C21	N5	123.7(4)	C32	C29	C30	111.2(5)
C19	N4	C33	114.8(3)	N3	C10	O4	110.3(4)	O8	C21	O9	125.5(4)	N4	C33	C34	115.9(3)
C26	N4	C33	116.1(3)	O4	C11	C13	110.1(4)	N5	C21	O9	110.7(4)	N4	C33	C36	109.7(3)
C21	N5	C20	122.4(4)	O4	C11	C14	110.3(4)	O9	C22	C24	109.0(4)	C34	C33	C36	103.2(3)
C28	N6	C27	120.9(3)	C13	C11	C14	113.3(5)	O9	C22	C23	102.3(4)	N4	C33	C35	108.7(3)
N1	C1	C2	114.6(3)	O4	C11	C12	102.3(4)	C24	C22	C23	111.4(5)	C34	C33	C35	110.6(4)
N2	C2	C1	112.5(3)	C13	C11	C12	109.1(5)	O9	C22	C25	109.9(4)	C36	C33	C35	108.6(3)
O1	C3	N2	124.1(4)	C14	C11	C12	111.2(5)	C24	C22	C25	113.5(4)	O12	C34	C33	111.9(3)
O1	C3	O2	125.4(4)	N1	C15	C18	110.7(4)	C23	C22	C25	110.2(5)	O13	C35	C33	109.3(3)
N2	C3	O2	110.5(3)	N1	C15	C16	113.3(3)	N4	C26	C27	112.3(3)	O14	C36	C33	110.3(3)

Synthesis of $\mathbf{D_{V3DA}}$

A mixture of 495 mg $\mathbf{D_{V3}}$ and 36.6 mg (1.2 eq) $\mathbf{H_3}$**Tris-DA-Boc** were dissolved in 5 mL DMAc in a Schlenk tube under argon. The orange solution was heated with microwave at 80℃ for 1 hour. The resulting olive solution was precipitated in 40mL diethyl ether. The brown precipitate was redissolved in 10 mL acetonitrile followed by the addition of 1.5 mL TFA and ultrasonication for 2 hours. The resulting yellow-green solution was precipitated in 40 mL diethyl ether and wash with 2*20 mL diethyl ether. The obtained ~400 mg brown solid was dispersed in 10 mL acetonitrile followed by the addition of TBAOH (~240 μL 1.0 M in methanol) to make the solid dissolved. The resulting brown-greenish solution was precipitate with 30 mL diethyl ether and washed 2*20 mL diethyl ether, yield 232.4 mg, 53.3%. ^{1}H NMR (400 MHz, CD3CN) δ 6.77 (NH), 5.53 (O-CH_2-C-), 3.35 (-NH-CH_2CH_2-N-),3.20 (-NH-CH_2CH_2-N-, overlapped by TBA signal), 3.20, 1.67, 1.60, 1.03 (TBA). ^{31}P NMR (162 MHz, CD_3CN) δ -7.12, -12.79.

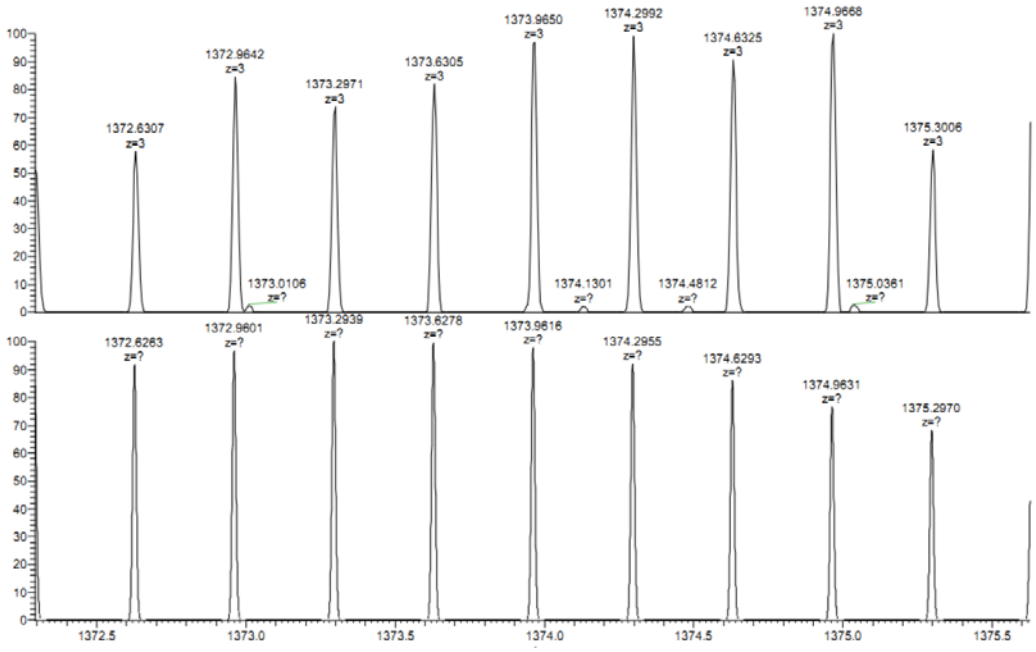

Figure 4-39 The ESI-MS of $\boldsymbol{D_{V3DA}}$ *which gives the formular* $\{H_3[P_2V_3W_{15}O_{62}(\text{Tris-DA})]\}^{3-}$

Reference

(1) Li, Q.; Peng, Y.; Qian, J.; Yan, T.; Du, L.; Zhao, Q. A Family of Planar Hexanuclear CoII4LnIII2 Clusters with Lucanidae-like Arrangement and Single-Molecule Magnet Behavior. *Dalton Trans.* **2019**, *48* (34), 12880–12887.

(2) Finke, R. G.; Rapko, Brian.; Saxton, R. J.; Domaille, P. J. Trisubstituted Heteropolytungstates as Soluble Metal Oxide Analogs. III. Synthesis, Characterization, Phosphorus-31, Silicon-29, Vanadium-51, and 1- and 2-D Tungsten-183 NMR, Deprotonation, and Proton Mobility Studies of Organic Solvent Solute Forms of $H_xSiW_9V_3O_{40}^{x-7}$ and $H_xP_2W_{15}V_3O_{62}^{x-9}$. *J. Am. Chem. Soc.* **1986**, *108* (11), 2947–2960.

(3) Li, J.; Huth, I.; Chamoreau, L.-M.; Hasenknopf, B.; Lacôte, E.; Thorimbert, S.; Malacria, M. Insertion of Amides into a Polyoxometalate. *Angew. Chem. Int. Ed.* **2009**, *48* (11), 2035–2038.

(4) Hou, Y.; Hill, C. L. Hydrolytically Stable Organic Triester Capped Polyoxometalates with Catalytic Oxygenation Activity of Formula $[RC(CH_2O)_3V_3P_2W_{15}O_{59}]^{6-}$ (R = CH_3, NO_2, CH_2OH). *J. Am. Chem. Soc.* **1993**, *115* (25), 11823–11830.

(5) Otis, F.; Voyer, N.; Polidori, A.; Pucci, B. End Group Engineering of Artificial Ion Channels. *New J. Chem.* **2006**, *30* (2), 185–190.

(6) Abdel-Magid, A. F.; Carson, K. G.; Harris, B. D.; Maryanoff, C. A.; Shah, R. D. Reductive Amination of Aldehydes and Ketones with Sodium Triacetoxyborohydride. Studies on Direct and Indirect Reductive Amination Procedures1. *J. Org. Chem.* **1996**, *61* (11), 3849–3862.

(7) Wilson, E. F.; Miras, H. N.; Rosnes, M. H.; Cronin, L. Real-Time Observation of the Self-Assembly of Hybrid Polyoxometalates Using Mass Spectrometry. *Angew. Chem. Int. Ed.* **2011**, *50* (16), 3720–3724.

(8) Debela, A. M.; Ortiz, M.; Beni, V.; Thorimbert, S.; Lesage, D.; Cole, R. B.; O'Sullivan, C. K.; Hasenknopf, B. Biofunctionalization of Polyoxometalates with DNA Primers, Their Use in the Polymerase Chain Reaction (PCR) and Electrochemical Detection of PCR Products. *Chem. – Eur. J.* **2015**, *21* (49), 17721–17727.

(9) Allain, C.; Schaming, D.; Karakostas, N.; Erard, M.; Gisselbrecht, J.-P.; Sorgues, S.; Lampre, I.; Ruhlmann, L.; Hasenknopf, B. Synthesis, Electrochemical and Photophysical Properties of Covalently Linked Porphyrin –Polyoxometalates. *Dalton Trans.* **2013**, *42* (8), 2745–2754.

(10) Azcarate, I.; Ahmed, I.; Farha, R.; Goldmann, M.; Wang, X.; Xu, H.; Hasenknopf, B.; Lacôte, E.; Ruhlmann, L. Synthesis and Characterization of Conjugated Dawson-Type Polyoxometalate–Porphyrin Copolymers. *Dalton Trans.* **2013**, *42* (35), 12688–12698.

(11) Cameron, J. M.; Wales, D. J.; Newton, G. N. Shining a Light on the Photo-Sensitisation of Organic–Inorganic Hybrid Polyoxometalates. *Dalton Trans.* **2018**, *47* (15), 5120–5136.

(12) Matt, B.; Fize, J.; Moussa, J.; Amouri, H.; Pereira, A.; Artero, V.; Izzet, G.; Proust, A. Charge Photo-Accumulation and Photocatalytic Hydrogen Evolution under Visible Light at an Iridium(Iii)-Photosensitized Polyoxotungstate. *Energy Environ. Sci.* **2013**, *6* (5), 1504.

(13) Papaconstantinou, E.; Hiskia, A. Photochemistry and Photocatalysis by Polyoxometalates. In *POLYOXOMETALATED MOLECULAR SCIENCE*; BorrasAlmenar,

JJ and Coronado, E and Muller, A and Pope, M, Ed.; NATO SCIENCE SERIES, SERIES II: MATHEMATICS, PHYSICS AND CHEMISTRY; NATO Adv Study Inst; NATO, Sci Affairs Div; Spain Minist Ciencia Tecnol, 2003; Vol. 98, pp 381–416.

(14) Li, C.; Suzuki, K.; Mizuno, N.; Yamaguchi, K. Polyoxometalate LUMO Engineering: A Strategy for Visible-Light-Responsive Aerobic Oxygenation Photocatalysts. *Chem. Commun.* **2018**, *54* (52), 7127–7130.

(15) Anjass, M.; Lowe, G. A.; Streb, C. Molecular Vanadium Oxides for Energy Conversion and Energy Storage: Current Trends and Emerging Opportunities. *Angew. Chem. Int. Ed.* **2021**, *60* (14), 7522–7532.

(16) Bencini, A.; Bertini, I.; Gatteschi, D.; Scozzafava, A. Single-Crystal ESR Spectra of Copper(II) Complexes with Geometries Intermediate between a Square Pyramid and a Trigonal Bipyramid. *Inorg. Chem.* **1978**, *17* (11), 3194–3197.

(17) Garribba, E.; Micera, G. The Determination of the Geometry of Cu(II) Complexes: An EPR Spectroscopy Experiment. *J. Chem. Educ.* **2006**, *83* (8), 1229.

(18) Zhang, T.; Solé-Daura, A.; Hostachy, S.; Blanchard, S.; Paris, C.; Li, Y.; Carbó, J. J.; Poblet, J. M.; Proust, A.; Guillemot, G. Modeling the Oxygen Vacancy at a Molecular Vanadium(III) Silica-Supported Catalyst. *J. Am. Chem. Soc.* **2018**, *140* (44), 14903–14914.

(19) Matt, B.; Fize, J.; Moussa, J.; Amouri, H.; Pereira, A.; Artero, V.; Izzet, G.; Proust, A. Charge Photo-Accumulation and Photocatalytic Hydrogen Evolution under Visible Light at an Iridium(III)-Photosensitized Polyoxotungstate. *Energy Environ. Sci.* **2013**, *6* (5), 1504–1508.

(20) Cameron, J. M.; Fujimoto, S.; Wei, R.-J.; Newton, G. N.; Oshio, H. Post-Functionalization of a Photoactive Hybrid Polyoxotungstate. *Dalton Trans.* **2018**, *47* (31), 10590–10594.

(21) Cioncoloni, G.; Roger, I.; Wheatley, P. S.; Wilson, C.; Morris, R. E.; Sproules, S.; Symes, M. D. Proton-Coupled Electron Transfer Enhances the Electrocatalytic Reduction of Nitrite to NO in a Bioinspired Copper Complex. *ACS Catal.* **2018**, *8* (6), 5070–5084.

(22) Tzirakis, M. D.; Lykakis, I. N.; Orfanopoulos, M. Decatungstate as an Efficient Photocatalyst in Organic Chemistry. *Chem. Soc. Rev.* **2009**, *38* (9), 2609.

(23) Richter-Addo, G. B.; Hodge, S. J.; Yi, G.-B.; Khan, M. A.; Ma, T.; Van Caemelbecke, E.; Guo, N.; Kadish, K. M. Synthesis, Characterization, and Spectroelectrochemistry of Cobalt Porphyrins Containing Axially Bound Nitric Oxide. *Inorg. Chem.* **1996**, *35* (22), 6530–6538.

(24) Kumar, M.; Dixon, N. A.; Merkle, A. C.; Zeller, M.; Lehnert, N.; Papish, E. T. Hydrotris(Triazolyl)Borate Complexes as Functional Models for Cu Nitrite Reductase: The Electronic Influence of Distal Nitrogens. *Inorg. Chem.* **2012**, *51* (13), 7004–7006.

(25) Nagababu, E.; Rifkind, J. M. Measurement of Plasma Nitrite by Chemiluminescence. In *Free Radicals and Antioxidant Protocols*; Uppu, R. M., Murthy, S. N., Pryor, W. A., Parinandi, N. L., Eds.; Methods in Molecular Biology; Humana Press: Totowa, NJ, 2010; pp 41–49.

(26) Meanwell, N. A. Fluorine and Fluorinated Motifs in the Design and Application of Bioisosteres for Drug Design. *J. Med. Chem.* **2018**, *61* (14), 5822–5880.

(27) General Discussion of Organic Fluorine Chemistry. In *Fluorine in Organic Chemistry*; John Wiley & Sons, Ltd, 2004; pp 1–22.

(28) Applications of Organofluorine Compounds. In *Modern Fluoroorganic Chemistry*; John Wiley & Sons, Ltd, 2004; pp 203–277.

(29) Berger, R.; Resnati, G.; Metrangolo, P.; Weber, E.; Hulliger, J. Organic Fluorine Compounds: A Great Opportunity for Enhanced Materials Properties. *Chem. Soc. Rev.* **2011**, *40* (7), 3496–3508.

(30) Young, N. J.; Pike, V. W.; Taddei, C. Rapid and Efficient Synthesis of [11C]Trifluoromethylarenes from Primary Aromatic Amines and [11C]CuCF3. *ACS Omega* **2020**, *5* (31), 19557–19564.

(31) Alonso, C.; Martínez de Marigorta, E.; Rubiales, G.; Palacios, F. Carbon Trifluoromethylation Reactions of Hydrocarbon Derivatives and Heteroarenes. *Chem. Rev.* **2015**, *115* (4), 1847–1935.

(32) Charpentier, J.; Früh, N.; Togni, A. Electrophilic Trifluoromethylation by Use of Hypervalent Iodine Reagents. *Chem. Rev.* **2015**, *115* (2), 650–682.

(33) Liu, X.; Xu, C.; Wang, M.; Liu, Q. Trifluoromethyltrimethylsilane: Nucleophilic Trifluoromethylation and Beyond. *Chem. Rev.* **2015**, *115* (2), 683–730.

(34) Xiao, H.; Zhang, Z.; Fang, Y.; Zhu, L.; Li, C. Radical Trifluoromethylation. *Chem. Soc. Rev.* **2021**, *50* (11), 6308–6319.

(35) Natte, K.; Jagadeesh, R. V.; He, L.; Rabeah, J.; Chen, J.; Taeschler, C.; Ellinger, S.; Zaragoza, F.; Neumann, H.; Brückner, A.; Beller, M. Palladium-Catalyzed Trifluoromethylation of (Hetero)Arenes with CF_3Br. *Angew. Chem. Int. Ed.* **2016**, *55* (8), 2782–2786.

(36) Trost, B. M.; Gholami, H.; Zell, D. Palladium-Catalyzed Asymmetric Allylic Fluoroalkylation/Trifluoromethylation. *J. Am. Chem. Soc.* **2019**, *141* (29), 11446–11451.

(37) Bour, J. R.; Camasso, N. M.; Sanford, M. S. Oxidation of Ni(II) to Ni(IV) with Aryl Electrophiles Enables Ni-Mediated Aryl–CF_3 Coupling. *J. Am. Chem. Soc.* **2015**, *137* (25), 8034–8037.

(38) Jacquet, J.; Cheaib, K.; Ren, Y.; Vezin, H.; Orio, M.; Blanchard, S.; Fensterbank, L.; Desage-El Murr, M. Circumventing Intrinsic Metal Reactivity: Radical Generation with Redox-Active Ligands. *Chem. - Eur. J.* **2017**, *23* (60), 15030–15034.

(39) Deolka, S.; Govindarajan, R.; Khaskin, E.; Fayzullin, R. R.; Roy, M. C.; Khusnutdinova, J. R. Photoinduced Trifluoromethylation of Arenes and Heteroarenes Catalyzed by High-Valent Nickel Complexes. *Angew. Chem. Int. Ed.* **2021**, *60* (46), 24620–24629.

(40) Karuo, Y.; Hayashi, T.; Tarui, A.; Sato, K.; Kawai, K.; Omote, M. Copper-Catalyzed Oxidative Trifluoromethylation of Terminal Alkenes Using AgCF3. *J. Org. Chem.* **2020**, *85* (7), 5104–5108.

(41) Chen, Y.; Ma, G.; Gong, H. Copper-Catalyzed Reductive Trifluoromethylation of Alkyl Iodides with Togni's Reagent. *Org. Lett.* **2018**, *20* (15), 4677–4680.

(42) Jacquet, J.; Blanchard, S.; Derat, E.; Murr, M. D.-E.; Fensterbank, L. Redox-Ligand Sustains Controlled Generation of CF_3 Radicals by Well-Defined Copper Complex. *Chem. Sci.* **2016**, *7*, 2030–2036.

(43) Kornfilt, D. J. P.; MacMillan, D. W. C. Copper-Catalyzed Trifluoromethylation of Alkyl Bromides. *J. Am. Chem. Soc.* **2019**, *141* (17), 6853–6858.

(44) Combs-Walker, L. A.; Hill, C. L. Use of Excited-State and Ground-State Redox Properties of Polyoxometalates for Selective Transformation of Unactivated Carbon-Hydrogen

Centers Remote from the Functional Group in Ketones. *J. Am. Chem. Soc.* **1992**, *114* (3), 938–946.

(45) Schultz, D. M.; Lévesque, F.; DiRocco, D. A.; Reibarkh, M.; Ji, Y.; Joyce, L. A.; Dropinski, J. F.; Sheng, H.; Sherry, B. D.; Davies, I. W. Oxyfunctionalization of the Remote C−H Bonds of Aliphatic Amines by Decatungstate Photocatalysis. *Angew. Chem. Int. Ed.* **2017**, *56* (48), 15274–15278.

(46) Ravelli, D.; Fagnoni, M.; Fukuyama, T.; Nishikawa, T.; Ryu, I. Site-Selective C–H Functionalization by Decatungstate Anion Photocatalysis: Synergistic Control by Polar and Steric Effects Expands the Reaction Scope. *ACS Catal.* **2018**, *8* (1), 701–713.

(47) Sarver, P. J.; Bacauanu, V.; Schultz, D. M.; DiRocco, D. A.; Lam, Y.; Sherer, E. C.; MacMillan, D. W. C. The Merger of Decatungstate and Copper Catalysis to Enable Aliphatic C(Sp3)–H Trifluoromethylation. *Nat. Chem.* **2020**, *12* (5), 459–467.

(48) Hou, Y.; Hill, C. L. Hydrolytically Stable Organic Triester Capped Polyoxometalates with Catalytic Oxygenation Activity of Formula $[RC(CH_2O)_3V_3P_2W_{15}O_{59}]^{6-}$ (R = CH_3, NO_2, CH_2OH). *J. Am. Chem. Soc.* **1993**, *115* (25), 11823–11830.

(49) Li, Q.; Peng, Y.; Qian, J.; Yan, T.; Du, L.; Zhao, Q. A Family of Planar Hexanuclear CoIII4LnIII2 Clusters with Lucanidae-like Arrangement and Single-Molecule Magnet Behavior. *Dalton Trans.* **2019**, *48* (34), 12880–12887.

(50) Li, J.; Huth, I.; Chamoreau, L.-M.; Hasenknopf, B.; Lacôte, E.; Thorimbert, S.; Malacria, M. Insertion of Amides into a Polyoxometalate. *Angew. Chem. Int. Ed.* **2009**, *48* (11), 2035–2038.

(51) Finke, R. G.; Rapko, Brian.; Saxton, R. J.; Domaille, P. J. Trisubstituted Heteropolytungstates as Soluble Metal Oxide Analogs. III. Synthesis, Characterization, Phosphorus-31, Silicon-29, Vanadium-51, and 1- and 2-D Tungsten-183 NMR, Deprotonation, and Proton Mobility Studies of Organic Solvent Solute Forms of $H_xSiW_9V_3O_{40}^{x-7}$ and $H_xP_2W_{15}V_3O_{62}^{x-9}$. *J. Am. Chem. Soc.* **1986**, *108* (11), 2947–2960.

General conclusion

General conclusion

Inspired by the catalytic mechanisms of metalloenzymes, POM was introduced to supply electrons and protons for the metal complexes. The covalent linker strategy is applied, in order to enhance the communication between the POMs and the metal complexes expecting the enhancement of catalytic properties. In this thesis, we first tried to covalently graft the organic moieties onto the POM surface to form the POM hybrid ligands followed by the complexation, and then to investigate the synergy between the skeletons and the metal complexes as well as the resulting catalytic activities.

First, various POM skeletons, here lacunary Keggin $[PW_{11}O_{39}]^{3-}$ and trivanadate cap substituted Well Dawson $[P_2W_{15}V_3O_{62}]^{9-}$, have been chosen for covalent functionalization with the tripodal ligands using post-functionalization or direct-functionalization strategies. We have not only obtained the tripodal ligand functionalized hybrid POM which would be further applied to coordinated with metal ions, but also, we have expanded the methodology to functionalize the POM with polyamine including the synthesis and the purification process.

In chapter 2, in order to introduce two coordination sites onto the POM surface which could coordinate to two metals to form “diamond” complexes, we built a Keggin type platform, **K_{Si}[I]-1** containing two iodo-groups which could be potential leaving groups to perform nucleophilic substitution with tripodal ligand, **DPA**. Although there were indeed some variations of the spectroscopic signatures upon reaction, DOSY NMR experiment proved decisive to show that no substitution, but rather ion pairing, did occur.

We have several hypotheses for the failure of the nucleophilic substation and the corresponding improvements: 1) Steric hindrance: the short methylene spacers result in the substitution sites quite near to the POM framework, that lead to the DPA could not get close to the sites. To overcome the steric hindrance, we need to prolong the spacers to ethylene or propylene or change it to other types of linkers. 2) Protonation of DPA: it results in the decrease of nucleophilic capability and being electrostatically attracted by the reduced POM.

In the very recent work of Parac-Vogt, they successfully performed nucleophilic substitution of the doubly iodide-functionalized Wells−Dawson-type $[P_2W_{17}O_{62}]^{10-}$ with various primary and secondary amines. They have proved that organosilyl-inserted $[\alpha_2\text{-}P_2W_{17}O_{61}]^{10-}$ could be

stable in the nucleophilic substitution reaction. It encourages us to do further investigation on the nucleophilic substitution methodology of POM post-functionalization.

In chapter 3, we have used two different coupling reactions to perform the post-functionalization of Keggin polyoxometalates with the tripodal organic ligand propargyl-**DPA**. The first POM-ligand relies on “Sonogashira” coupling and has afforded POM ligand (**K_{Sn}[DPA]**) successfully which has been well characterized, and a corresponding Cu complex (**K_{Sn}[DPA]**@$Cu(OAc)_2$) has been prepared. This route can be easily extended with the “propargyl approach” to numerous N based ligands. Unfortunately, the first reactivity trial, nitrite reduction, has not given the expected results, but this exploration of hybrid POM complexes and reactivity has opened a lot of perspectives.

In order to investigate the “click” reaction on POM functionalization, we have prepared a new azido-functionalized precursor, **K_{Si}[N_3]-3**. Through optimizing the “click” conditions, we have successfully obtained a bi-DPA functionalized POM ligand, **K_{Si}[DPA]-3**. First complexation studies suggest that the triazole ring might interfere with the coordination process. The multi-potential coordinate sites could be applied to mimic multi-metal sites enzymes.

In chapter 4, we have directly grafted the aromatic tripodal ligand onto the trivanadate cap substitute Dawson POM, $TBA_5H_4[P_2V_3W_{15}O_{62}]$ (**D_{V3}**) to form **D_{V3DPA}** which is characterized by NMR, ESI-Mass. We have prepared the corresponding Cu complex **D_{V3DPA}Cu(OAc)** with **D_{V3DPA}** and $Cu(OAc)_2$, which has been well characterized through UV, NMR, ESI-Mass and elemental analysis.

During the exploration, we observe the existence of photoactivity of **D_{V3DPA}Cu(OAc)** from the NMR evolution. We hypothesis that the V(V) is reduced by the irradiation and then one electron is transfer to the Cu(II) center resulting the formation of Cu(I). Indeed, the cyclic voltammetry shows the reduction potential of the Cu(II)/Cu(I) is quite close to the first V(V)/V(IV) reduction potential. Through monitoring with the UV-vis spectrum while irradiating **D_{V3DPA}Cu(OAc)** in acetonitrile, we did conclude that not only was Cu(II) reduced to Cu(I), but also up to two more electrons could be stored via V(V) to V(IV) reductio processes, which correspond to a rare three electrons photoaccumulation on a POM derivative.

Furthermore, the **D_{V3DPA}Cu(OAc)** was applied to catalytically photoreduce CF_3^+, which was proved to form CF_3 radical. This opens the road to potential photocatalysis for trifluoromethylation of some more valuable substrates, and the encouraging preliminary results on the trifluoromethylation of styrene have been obtained, that need to be further investigated. In the meantime, the electron source of the catalytic process still confuses us, although we hypothesis that the electron could come from H_2O based on some undirected evidence.

Anyway, the photoactivity of the POM and bioinspired complex hybrid through covalent connecting, is proved to have electron communication between each other which is quite encouraging. The explorations of preparation of POM complexes and reactivity have opened a lot of perspectives. Such as aliphatic tripodal ligands functionalized **D_{V3}**, **D_{V3DA}** has been synthesized preliminary, with which we would like to prepare the Cu complex, **D_{V3DA}Cu(OAc)** , and to see if the redox properties of the POM complex comparing to **D_{V3DPA}Cu(OAc)** could be tuned or not, and then hopefully to introduce some more interesting properties and applications.

One of our initial targets was to graft the “diamond core” onto the surface of the POM. The obtained **K_{Si}[DPA]-3** through “click” reaction has, at the end of the day, provided us with three potential coordination sites instead of the only two expected, which did complicate its complexation studies. But its successful synthesis inspires us the potential grafting of some other ligands, such as bipyridine or its derivatives to form potential bi-coordinating sites ligands.

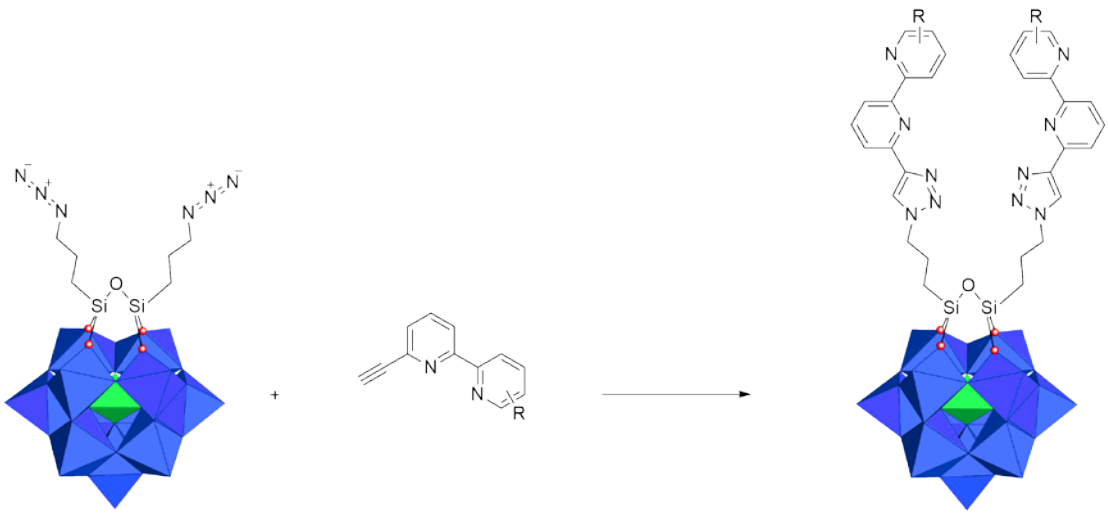

Scheme: Perspective of the bi-coordinate site POM ligand synthesized through "Click" reaction.

This thesis has thus opened up a lot of new avenues in this burgeoning field of bioinspired polyoxometalate hybrid systems, and will I think give birth to very exciting new projects.

Résumé :

"Catalyseurs bio-inspirés à base d'hybrides de POMs : synthèse et activité catalytique"

Cette thèse porte sur la synthèse de dérivés hybrides de polyoxométallates fonctionalisés par des ligands polydentes azoté et de l'études des complexes formés comme catalyseurs bioinspirés. Après un premier chapitre qui introduit le contexte et les objectifs de ce travail, une première approche reposant sur la fonctionnamisation par une approche "substitution nucléophile" est résumée. Le troisième chapitre de cette thèse porte sur la synthèse des hybrides par des voies plus classiques, que ce soit par couplage de Sonogashira ou par chimie click. Dans le premier cas, une étude des propriétés catalytiques des complexes de cuivre obtenus en réduction des nitrites est décrite. Enfin, le dernier chapitre, avant une conclusion sur l'ensemble de ces travaux, décrit la fonctionnalisation d'u dérivé $[P_2V_3W_{15}O_{62}]^{9-}$ par un ligand tripodal azoté porteur d'un groupement de greffage triol, des complexes obtenus et d'une première étude très prometteuse en trifluorométhylation photocatalytique.

Chapitre 1 : Introduction

Les polyoxométalates (POMs) présentent d'excellentes propriétés redox et sont de bons candidats pour travailler comme réservoirs d'électrons et de protons. De plus, ces polyanions peuvent être fonctionnalisés avec des parties organiques ou organométalliques, permettant d'en améliorer les propriétés physiques et chimiques et ainsi d'étendre leur champ d'application. Divers travaux de la littérature ont démontré qu'il existe une communication électronique entre le squelette polyanionique et les centres métalliques au sein de ces POMs hybrides.

Le but de cette thèse est de construire des structures hybrides de complexes métalliques bioinspirés associés à des POMs pour mimer les métalloenzymes puis d'étudier la synergie entre les deux partenaires, en vue d'améliorer la réactivité du complexe modèle de site actif.

Le premier chapitre de cette thèse s'efforce de faire une courte présentation des sites actifs des métalloenzymes, en particulier sur l'importance des interactions de seconde sphère,

puis sur les POMs et leur fonctionnalisation, en relation avec mon projet de doctorat "Catalyseurs bio-inspirés à base d'hybrides de POMs : synthèse et activité catalytique".

Les métalloenzymes sont une variété de biocatalyseurs importants, impliqués dans des transformations chimiques impliquant comme substrats des molécules biologiques et souvent comme réactifs de petites molécules telles que l'oxygène moléculaire, l'hydrogène, l'azote ou l'eau. Un large éventail de cations métalliques ou de clusters métalliques sont observés au niveau des sites actifs dans les structures cristallines de métalloprotéines et se sont avérés être la partie la plus essentielle des métalloenzymes, ce qui a incité de nombreux chercheurs à synthétiser des complexes pour reproduire la première sphère de coordination de ces sites actifs.

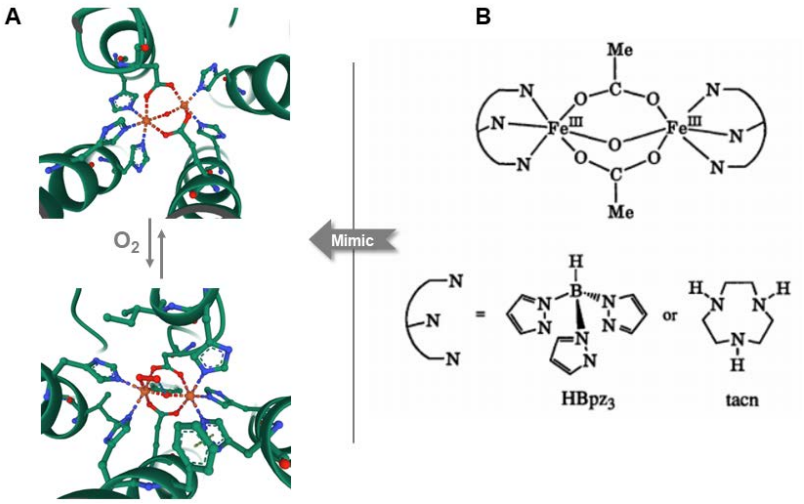

Figure 1-1 A) Structure de la désoxyhémérythrine et de l'oxyhémérythrine [PDB ID : 1HMD & 1HMO], B) complexes modèles correspondants.

Comme l'indique l'étude approfondie de ces métalloenzymes, le milieu environnant, appelé sphère secondaire, est également essentiel pour que la métalloenzyme fonctionne efficacement, notamment par le biais de relais pour transférer les électrons ou les protons nécessaires à la réaction catalysée.

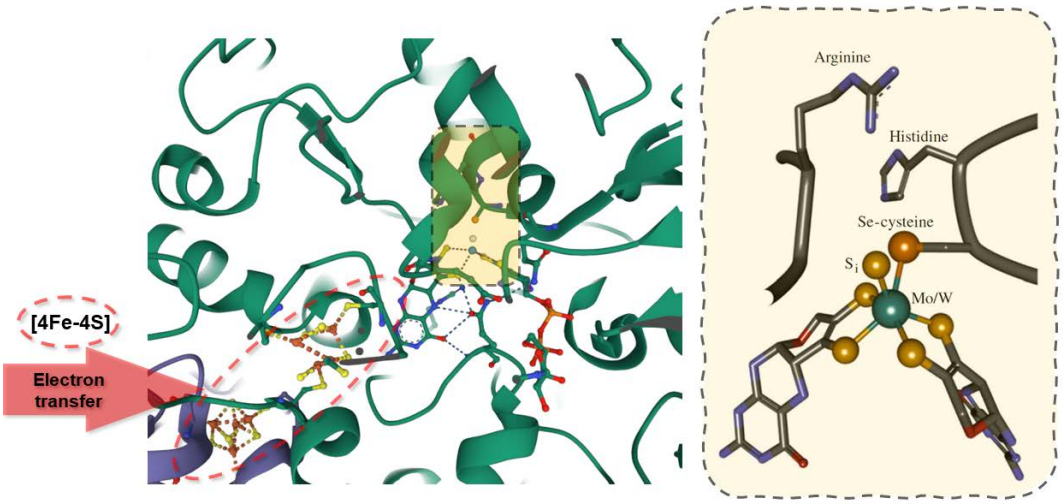

Figure1-2 Zoom de la structure cristalline de la formate déshydrogénase (Fdhs) oxydée contenant du molybdène/tungstène [PDB ID : 1H0H]; Entouré en rouge : relais électroniques.

Au cours des dernières décennies, grâce aux études spectroscopiques couplées au développement de la cristallographie des protéines et des technologies de calcul, la structure et le mécanisme de certaines métalloenzymes ont été révélés. Inspiré par cela, un grand nombre de complexes métalliques synthétiques ont été développés pour imiter les métalloenzymes, non seulement les sites métalliques mais aussi leur environnement. En conséquence, la bio-inspiration a largement amélioré les propriétés catalytiques telles que la sélectivité et l'efficacité et a ainsi élargi les applications des complexes métalliques. Par exemple, le groupe de Symes a récemment synthétisé deux complexes de cuivre avec deux ligands tripodes N-donneurs, l'un portant un ester et l'autre un acétate. Ces deux complexes ont été appliqués à l'électroréduction de NO_2^-. D'après les données d'électrocatalyse, l'activité de réduction du nitrite du complexe contenant un acétate était 2 fois plus élevée que celle du complexe contenant un ester. Elle est en accord avec la structure cristalline du CuNIR qui indique que la liaison H dans le site actif est essentielle aux réactions catalytiques.

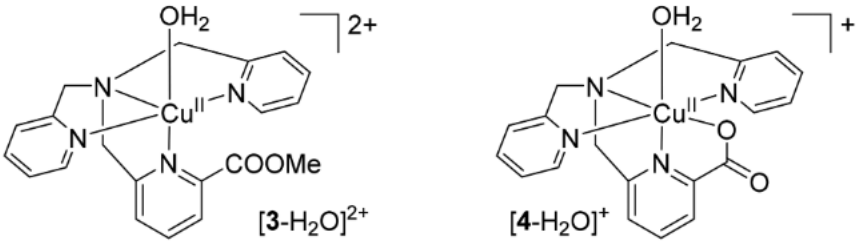

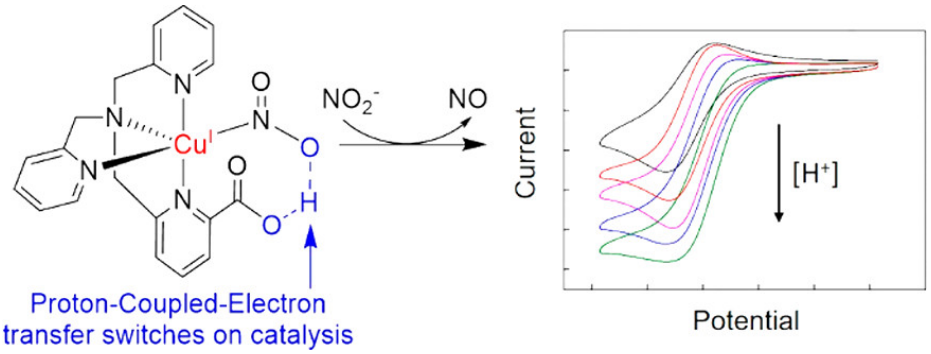

Figure 1-5 Les deux complexes tripodes de Cu donneurs de N bioinspirés et la proposition de mécanisme de transfert de protons couplés à des électrons pour le processus de réduction électrocatalytique du nitrite.

Les polyoxométalates (POM) représentent un groupe important de nanoclusters métal-oxo qui sont formés par condensation acide d'oxoanions en solution (généralement dans l'eau), dans diverses conditions de pH et de température. De nombreuses expériences ont démontré que les polyoxométalates ont de riches propriétés redox.

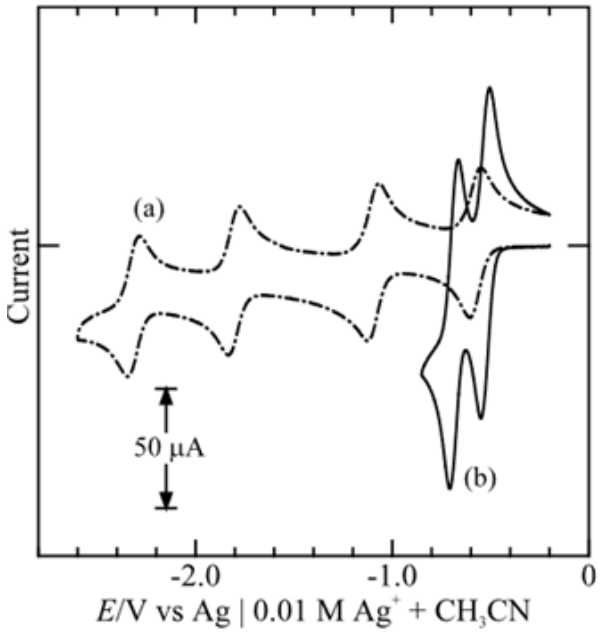

Figure 1-8 Voltammogrammes cycliques d'une solution 0.50 mM $[PW_{12}O_{40}]^{3-}$ dans CH_3CN contenant 0.1 M n-Bu_4NClO_4., $[CF_3SO_3H]$ (a) 0 mM ; (b) 5.0 mM

Ainsi Himeno a étudié les propriétés rédox du $[PW_{12}O_{40}]^{3-}$, anion de type Keggin, par voltammétrie cyclique et a constaté qu'en présence de protons, les quatre vagues réversible de réduction à un électron observées sur une gamme de 0 $V_{/(Ag+/Ag)}$ à -2.6 $V_{/(Ag+/Ag)}$ se transformaient, en présence de protons, en deux vagues de réduction réversibles

biélectroniques rassemblées sur des potentiels moins négatifs -0$V_{/(Ag+/Ag)}$ à -1$V_{/(Ag+/Ag)}$), ce qui indique que les POM pourraient être dans ce cas stocker de manière réversible de 4 protons et 4 électrons à des potentiels aisément accessibles.

Les processus redox multi-électroniques des POMs en font des candidats idéaux, tant pour les POMs complets que pour les dérivés fonctionnalisés, pour le développement de systèmes redox multi-étapes. Ces propriétés sont très intéressantes à la fois en photocatalyse et en électro-catalyse.

Les POM, notamment les dérivés lacunaires, présentent des atomes d'oxygène très nucléophiles qui peuvent être utilisés soit comme ligands pour former des complexes de cations de métaux de transition soit être fonctionnalisés de manière covalente avec des groupements organiques. Un grand nombre d'hybrides organiques-inorganiques ont ainsi été développés au cours des dernières décennies, avec différents groupes fonctionnels en fonction des applications recherchées. Pour y parvenir, deux stratégies différentes ont été développées en fonction des groupes fonctionnels recherchés : la fonctionnalisation directe et la post-fonctionnalisation. Dans le premier cas, les dérivés organiques ou les fragments organométalliques sont liés de manière covalente aux unités de greffage, qui sont ensuite mises en interaction directement avec les oxygènes à la surface des POM selon des protocoles bien définis. Dans le cas de la post-fonctionnalisation, un premier greffage direct d'un groupe porteur d'une fonction réactive est d'abord effectué sur le POM pour former une plateforme, puis la fonction réactive est utilisée, selon des réactions classiques avec des protocoles adaptés aux POMs pour fonctionnaliser ces derniers avec d'autres molécules organiques ou coordonnés à des cations métalliques ou avec des clusters contenant des métaux. Pour la post-fonctionnalisation des hybrides POM, la première étape consiste à synthétiser les plateformes appropriées. Au cours des dernières décennies, de nombreux précurseurs avec des groupes spéciaux (halogénure d'aryl, amine, alcyne...) ont été synthétisés, qui pourraient être impliqués dans des réactions ultérieures telles que :

1. Réaction de condensation

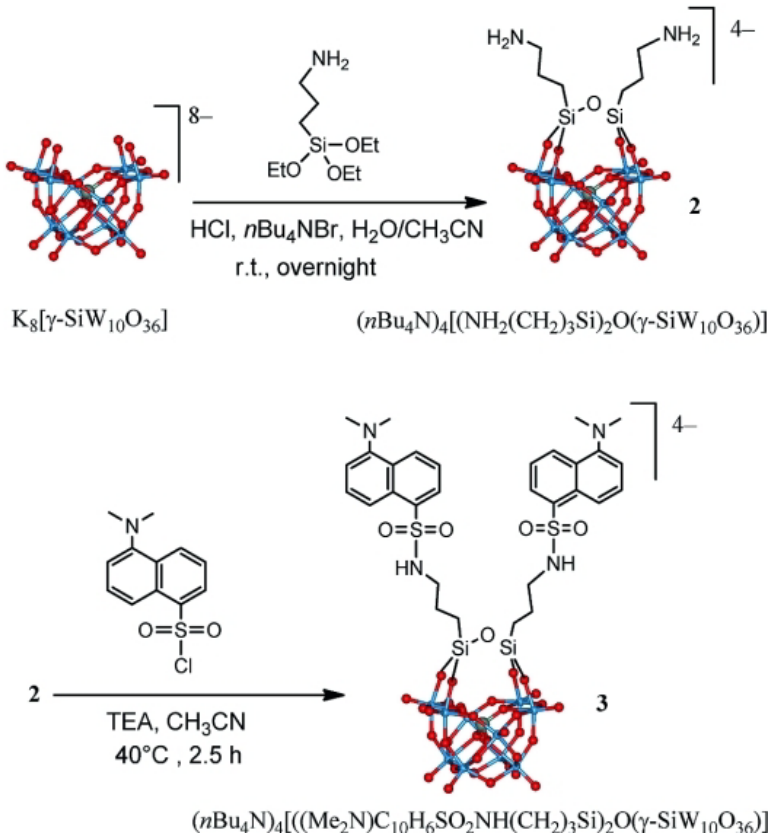

Figure 1-12 Etape 1 : synthèse de la plateforme à terminaison amine [γ-$SiW_{10}O_{36}\{O(Si(CH_2)_3NH_2)_2\}]^{4-}$. Etape 2 sa post-sulfonamidation.

2. Couplage "Sonogashira"

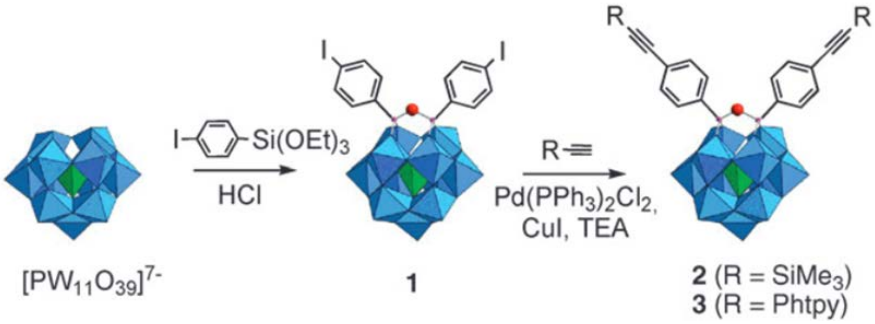

Figure 1-14 Voie de synthèse d'hybrides organo-silylés.

3. reaction “Click”

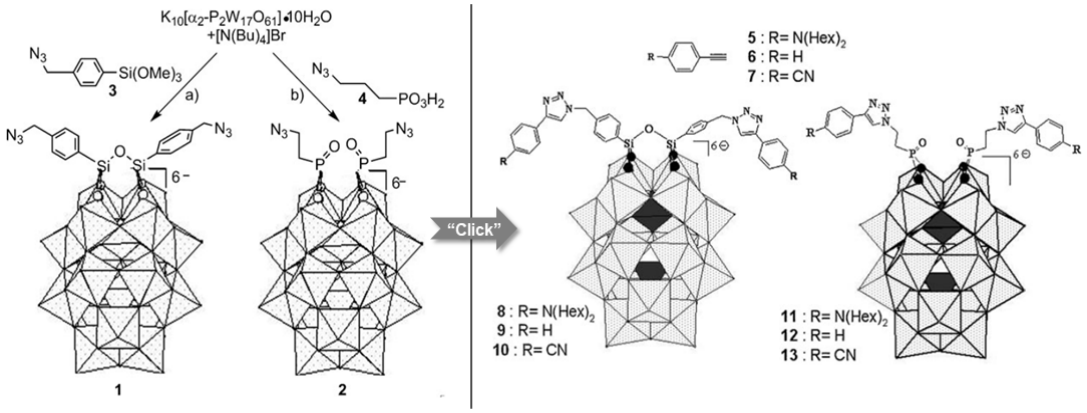

Figure 1-15 La voie de préparation des plates-formes de Well-Dawson fonctionnalisées par des di-azido et la réaction "Click" ultérieure avec des fragments organiques à terminaison alcyne.

4. Réaction de substitution nucléophile

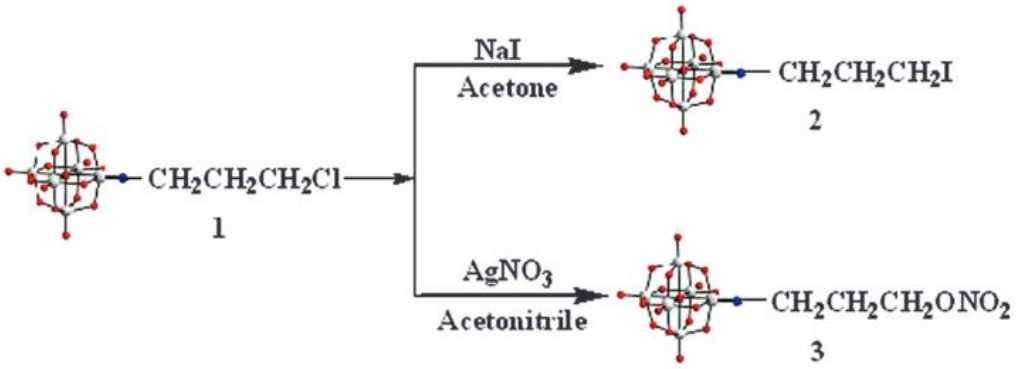

Figure 1-17 Substitution nucléophile d'hexamolydate fonctionnalisé par du chloropropyle.

La classe émergente des POM hybrides post-fonctionnalisés permet le couplage de POM présentant des propriétés redox riches avec différentes fonctionnalités organiques et des cations métalliques, élargissant ainsi les propriétés physico-chimiques clés qui sont pertinentes pour des applications telles que la catalyse et la science des matériaux.

1. L'auto-assemblage supramoléculaire

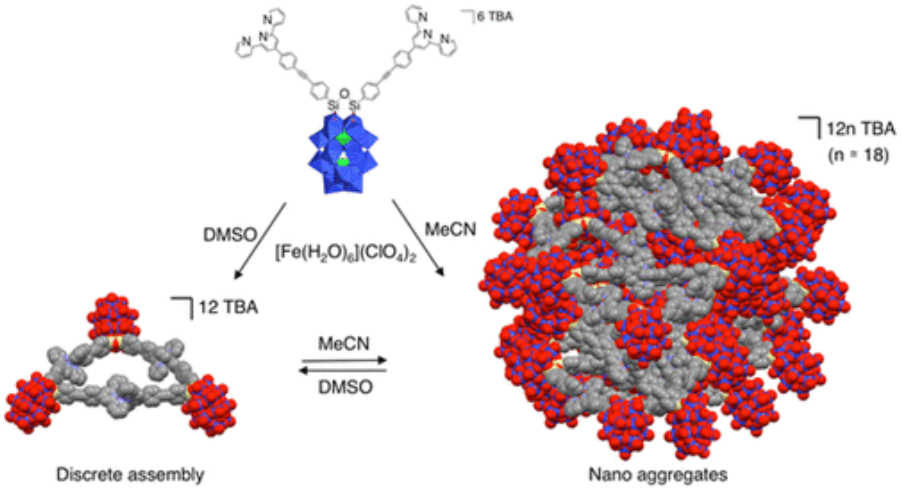

Figure1-20 Représentation de la formation des agrégats nanométriques par auto-assemblage hiérarchique de ***D*** $_{Si}$ ***[tpy]*** *lors de sa complexation avec* Fe^{2+}.

2. Catalyseurs organométalliques

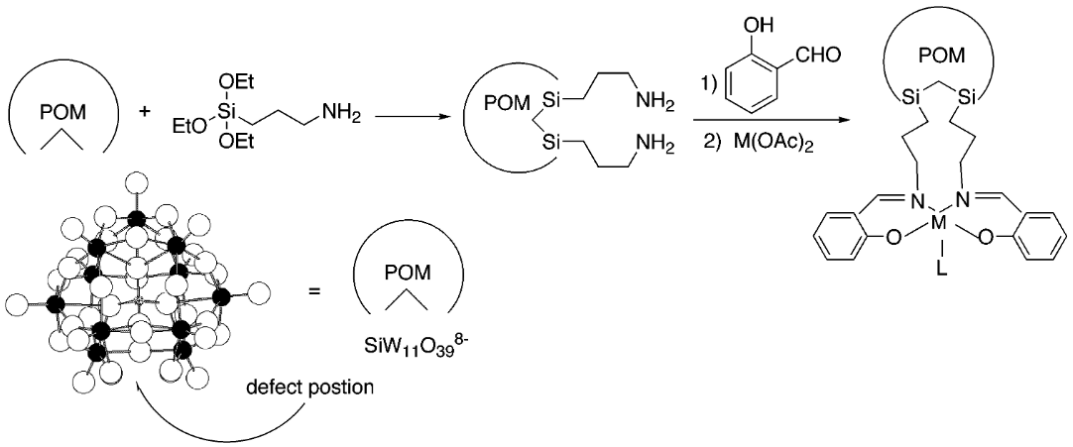

Figure 1-21 Voie de synthèse pour la préparation des composés M-Salen-POM, M= Mn, Co, Ni et Pd.

3. Transferts d'électrons intramoléculaires

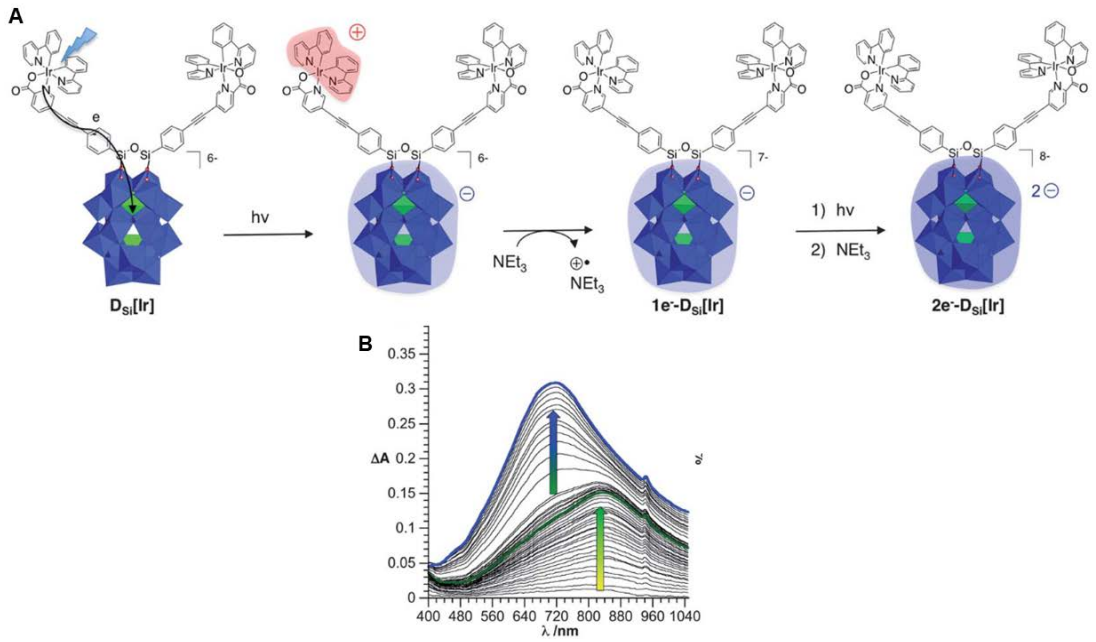

Figure 1-23 Hybride de POM de type Well-Dawson fonctionnalisé par un complexe d'iridium (III) et sa photoactivité dans l'évolution de l'hydrogène. A) Photo-accumulation de charges se produisant dans la dyade ***D_{Si}[Ir]*** *; B) évolution du spectre d'absorption différentielle dans le visible d'une solution de* ***D_{Si}[Ir]*** *(0,2 mM) dans du DMF contenant Et_3N (1 M) pendant la photo-irradiation sous lumière visible.*

Dans cette thèse, l'objectif est de synthétiser des hybrides présentant une forte communication entre le POM, source d'interaction de seconde sphère et des complexes bioinspirés mimes de sites actifs. Dans un premier temps, je décrirai notre stratégie pour la synthèse des ligands, puis lorsque ceux-ci ont été obtenus la coordonner d'ions métalliques, Cu^{2+}, $Fe^{2+/3+}$ et Co^{2+}, pour reproduire le site actif de métalloenzymes dans l'espoir d'améliorer les propriétés catalytiques. Une fois les hybrides synthétisés, nous étudierons ensuite la synergie entre les squelettes et les complexes métalliques ainsi que les activités catalytiques qui en résultent.

Chapitre 2 Voie "Substitution nucléophile"

Une première vois de synthèse de ligands à base de POM reposant sur une post-fonctionnalisation par des réactions de substitution nucléophile, a été envisagée.

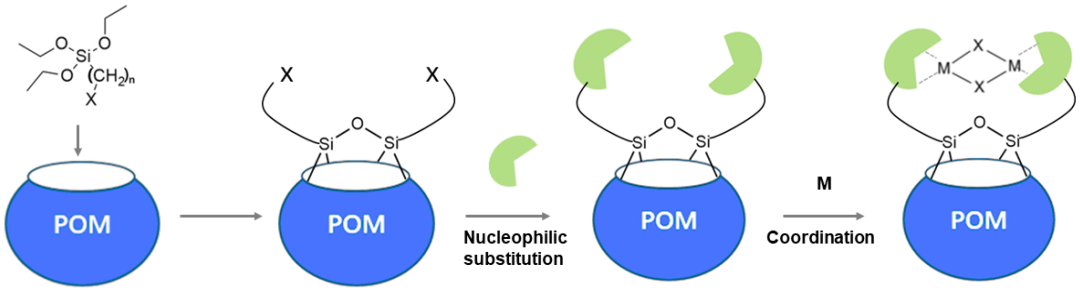

Schéma 2-2 La stratégie vers les complexes bimétalliques à base de polyoxométalate.

La première étape a consisté en la synthèse d'une plateforme porteuse d'une fonction iodure d'alkyle, l'anions iodure étant considéré comme un bon groupe partant.

Pour ce faire, un précurseur triéthoxy(iodométhyl)silane a été préparé :

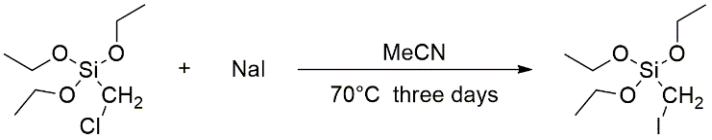

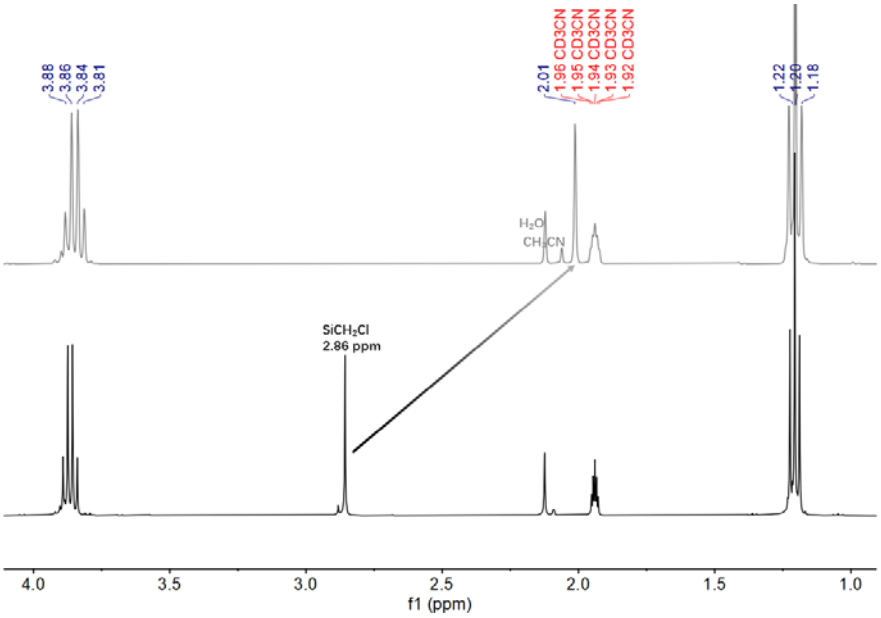

Figure 2-1 Spectre RMN ^{1}H du triéthoxy(iodométhyl)silane (gris) et du triéthoxy(chlorométhyl)silane (noir) dans CD_3CN.

La seconde étape a permis d'obtenir la plateforme POM hybride **K_{Si}[I]-1**

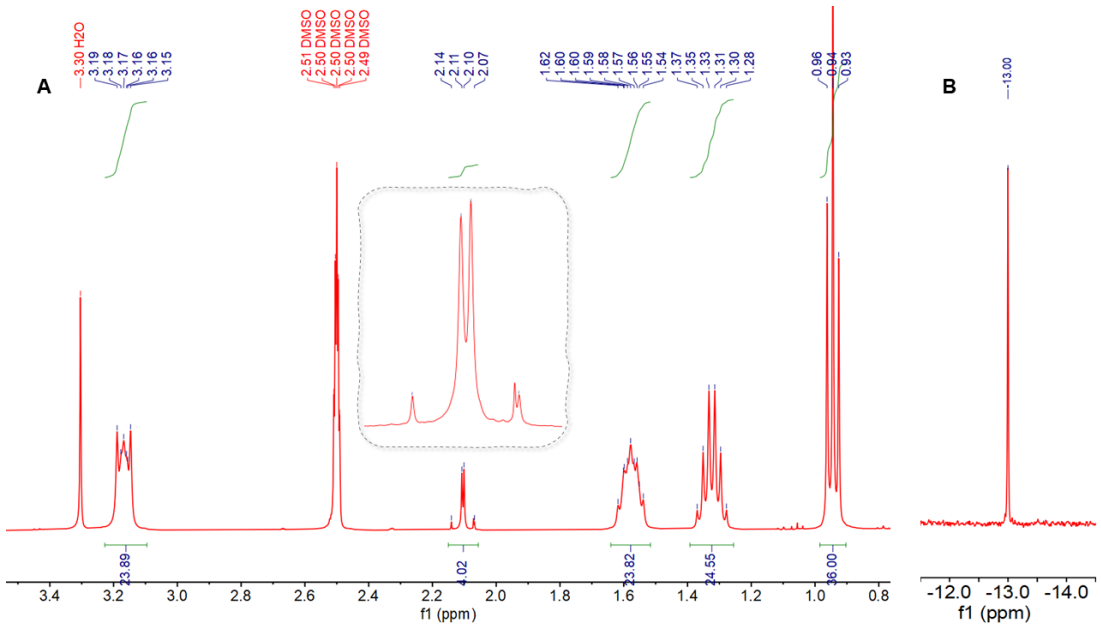

*Figure 2-2 A) RMN ^{1}H et B) RMN ^{31}P de **K_{Si}[I]-1** dans du DMSO-d6*

Cette dernière a alors été utilisée pour réaliser la réaction de substitution nucléophile de **K_{Si}[I]-1** avec la di(2pyridylméthyl) amine DPA, ligand classiquement utilisé en chimie bioispirée.

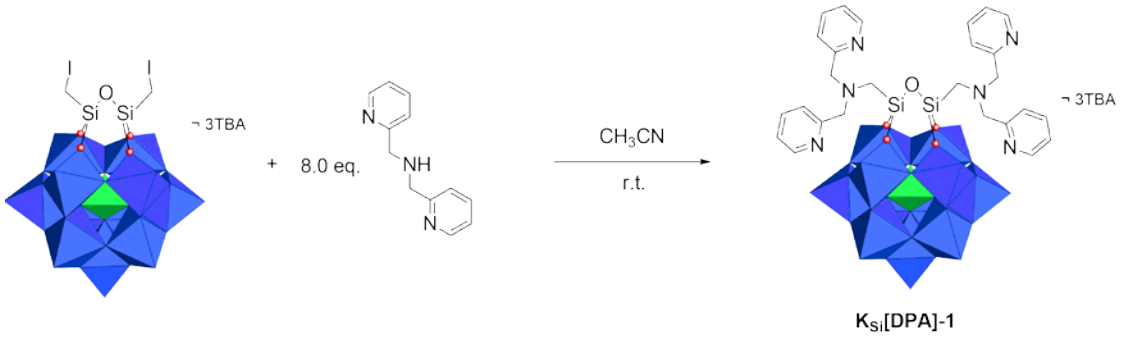

Schéma 2.1 : voie de greffage envisagée

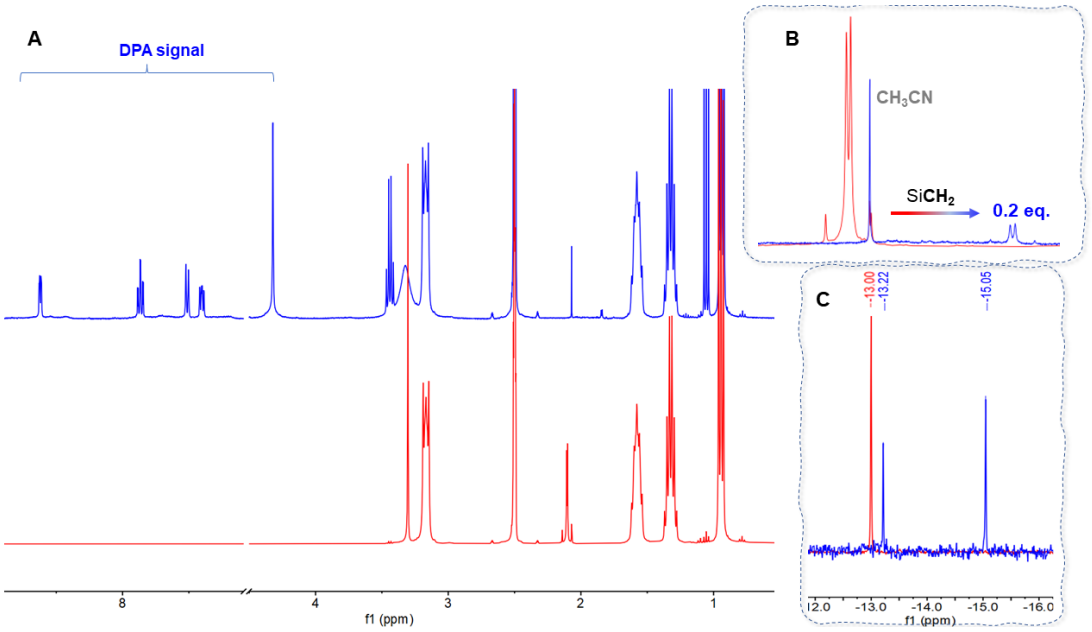

Figure 2-6 La gamme complète (A) et le zoom du $SiCH_2$ (B) du spectre ^{1}H NMR et ^{31}P NMR(C) du précurseur ***K_{Si}[I]-1*** *(rouge) et du* ***K_{Si}[DPA]-1*** *synthétisé(bleu).*

Après réaction, la présence en RMN ^{1}H des pics de la DPA est assez encourageant, mais nous n'avons pas pu identifier le signal associé aux groupements $SiCH_2$, qui doit être modifié par rapport à celui du précurseur. Si celui du précurseur a bien disparu, seul un pic peu intense à 1,86 ppm pourrait être associé à ce signal, mais avec une intégration beaucoup trop faible, quelles que soient les conditions utilisées pour essayer d'améliorer cette réaction (température, choix de la base, …). Par ailleurs, le spectre RMN ^{31}P du produit présente, outre un pic pouvant être associé au produit cible, un second pic à -15,05 ppm, caractéristique du POM complet et donc d'une certaine dégradation.

A de nombreux essais d'optimisation, la faisabilité de cette réaction de greffage par SN s'est posée. Afin de vérifier qu'il existait bien un lien covalent entre la DPA et le POM, nous nous sommes tournés vers la spectroscopie RMN de diffusion ordonnée (DOSY). Et malheureusement, le spectre DOSY montre que le coefficient de diffusion du DPA (~2,50×10^{-10} m^2/s) est presque le même que celui des cations tétrabutylammonium TBA^+ (~2,40×10^{-10} m^2/s), ce qui a clairement indiqué que la DPA n'était pas du tout greffée de manière covalente sur le POM mais agit simplement sous sa forme protonée comme u contre-ion du POM, à l'instar des TBA^+.

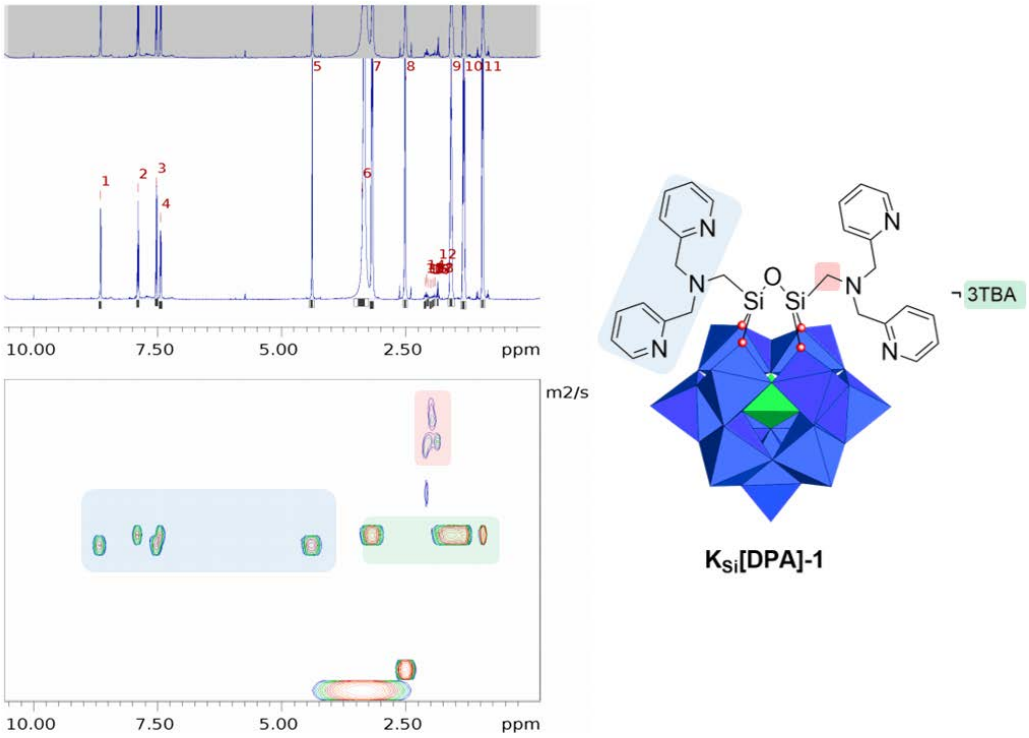

*Figure 2-10 RMN DOSY (dans DMSO-d6) du **K$_{Si}$[DPA]-1** synthétisé*

Des essais de synthèse par voie directe de ce même dérivé ayant également été infructueux, de nouvelles voies de synthèse d'hybrides, reposant sur des voies mieux établies, ont été envisagées.

Chapitre 3 : Post-fonctionnalisation des polyoxométalates de type Keggin et la complexation

3.1 Mono-fonctionnalisation de la [PW$_{11}$O$_{39}$]$^{7-}$ de Keggin par couplage "Sonogashira"

Une première approche a utilisé la réaction de couplage de Sonogashira en un iodure d'aryle et un alcyne vrai, approche développée par G. Izzet au sein de l'équipe E-POM ces dernières années. Elle repose dans un premier temps sur la synthèse de la plateforme porteuse de la fonction iodoaryle :

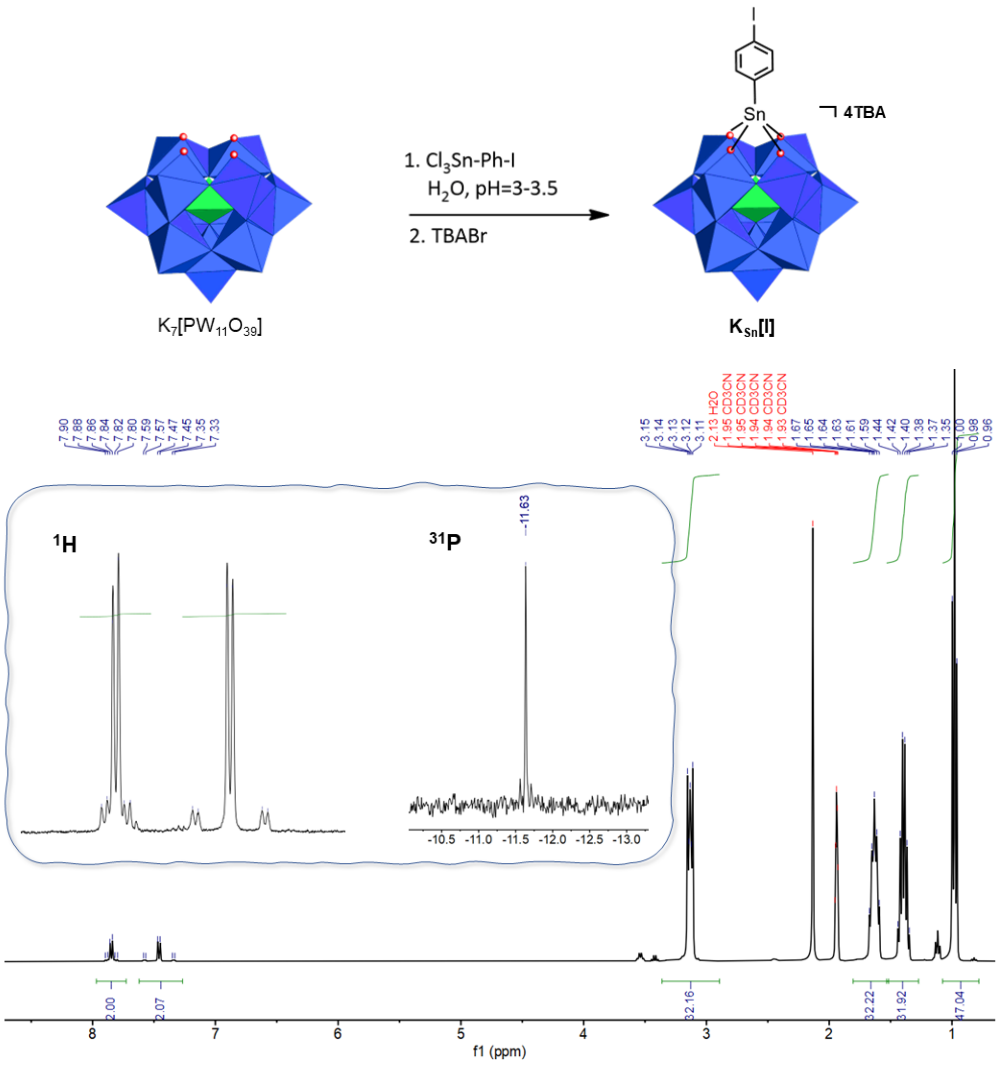

*Figure 3-4 ^{1}H NMR et ^{31}P NMR (insert) de **K_{Sn}[I]** dans CD_3CN.*

Une fois la plateforme obtenue, nous avons pu la faire réagir avec un dérivé propargyl-DPA que nous avons synthétisé en parallèle. Ceci nous a permis d'obtenir, après optimisation de la synthèse, le dérivé **K_{Sn}[DPA],** comme en atteste notamment les spectres RMN ^{1}H et ^{31}P.

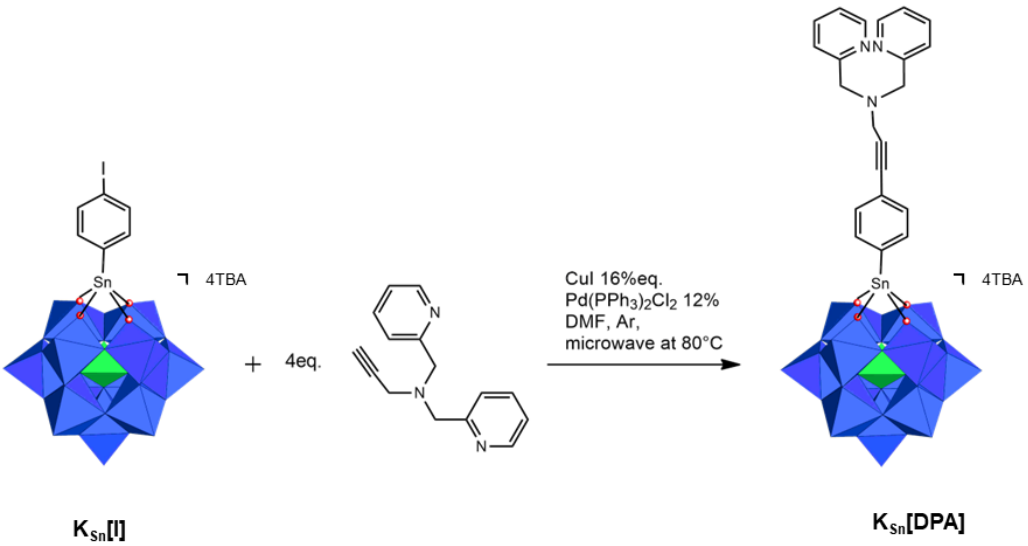
Sn
4TBA
4eq.
CuI 16%eq.
Pd(PPh3)2Cl2 12%
DMF, Ar,
microwave at 80°C
Sn
4TBA

K_{Sn}[I] K_{Sn}[DPA]

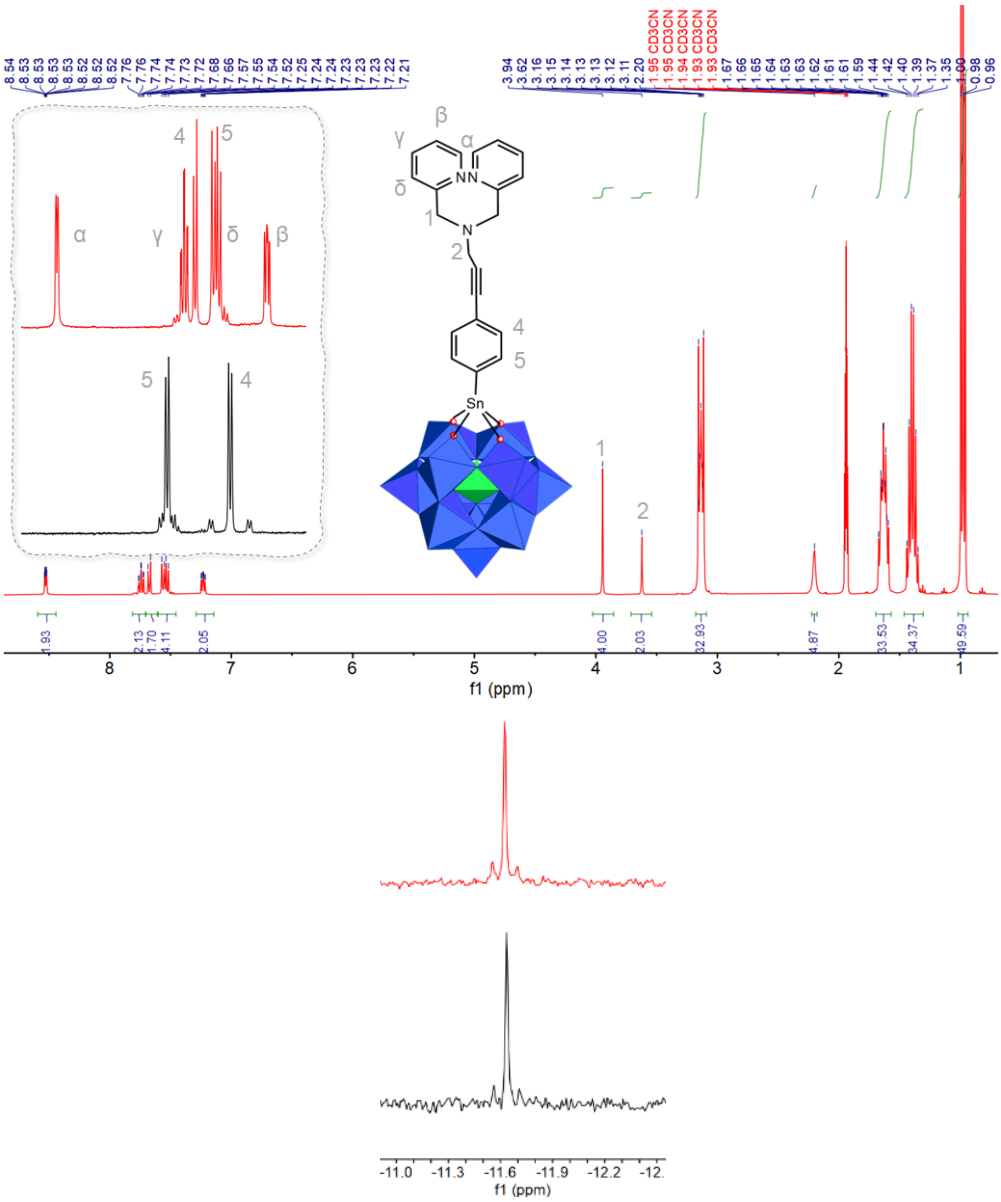
f1 (ppm)
-11.0 -11.3 -11.6 -11.9 -12.2 -12.
f1 (ppm)

*Figure 3-7 RMN ^{1}H et RMN ^{31}P de **K_{Sn}[DPA]** après purification dans CD_3CN.*

L'étape suivante a reposé sur l'étude de la complexation d'ions métalliques, et notamment de l'acétate de cuivre (II) $Cu(OAc)_2$ avec le ligand **K_{Sn}[DPA]**. Afin de déterminer la stœchiométrie de cette réaction, dosage, suivi par spectroscopie UV visible, a permis de mettre en évidence une modification du spectre de l'acétate de cuivre par ajout successifs d'aliquotes d'une solution de POM, évolution observée jusqu'à l'ajout d'un équivalent de POM par ion cuivrique, et donc conduisant à un adduit 1 :1 au final.

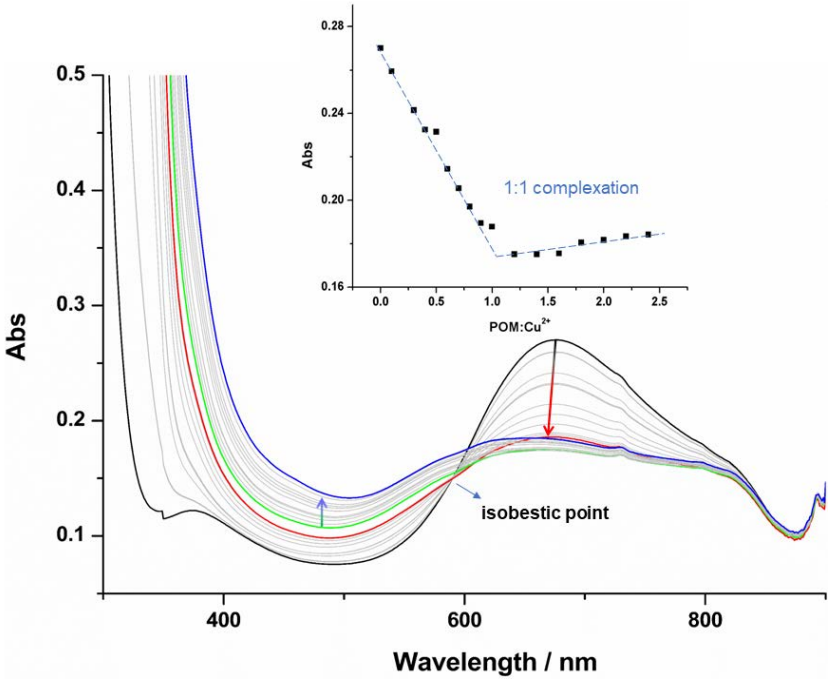

*Figure 3-11 Titrage UV-vis de la complexation de 1.0 mM $Cu(OAc)_2$ avec **K_{Sn}[DPA]**. Insert : évolution de l'absorbance à 664 nm en fonction du ratio POM/Cu*

Le complexe cuivrique correspondant a été isolé, et caractérisé notamment par spectroscopie IR et par RPE, mais aussi par voie électrochimique.

Le cyclovoltammogramme du complexe POM-DPACu dans le DMF possède trois processus monoélectroniques réversibles en réduction. La première vague est associée à la réduction du Cu(II) en Cu(I), alors que les deux suivantes sont centrées sur les tungstène du polyanion (réduction d'ions W(VI) en W(V).

Afin de déterminer si le complexe hybride POM pouvait avoir une efficacité plus élevée ou non que son dérivé précurseur, la même étude sur la capacité de ces complexes à catalyser l'électroréduction des nitrites a été réalisée avec le complexe propargyl cuivre seul

ou greffé sur le POM. Malheureusement, si un processus de type électrocatalytique est bien observé pour les deux complexes, avec des vagues irréversibles de forte intensité à -1.14 V et - 1.60 V ont été obtenues lors de l'ajout de $TBANO_2$, avec un accroissement de l'intensité à chaque ajout jusqu'à 150 éq., ce processus et identique pour les deux complexes.

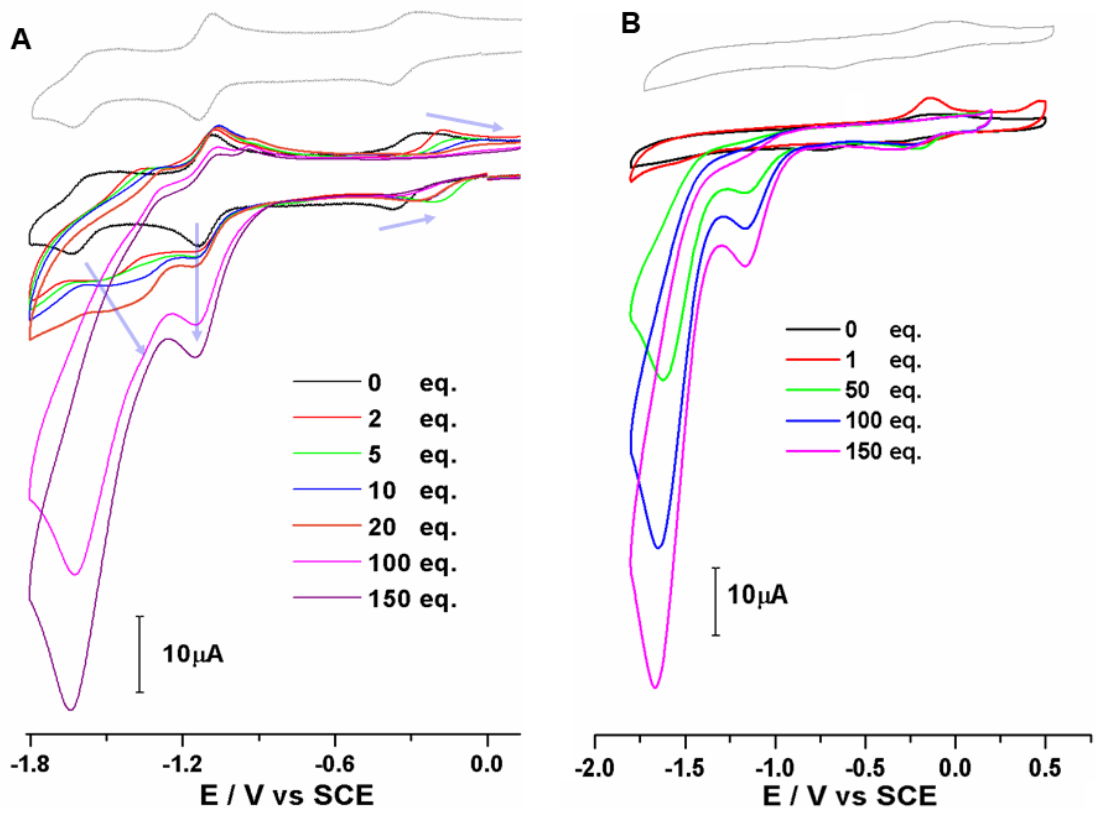

Figure 3-21 Voltammogramme cyclique de A) solution 0,45 mM de ***K_{Sn}[DPA]***@$Cu(OAc)_2$ *en présence de (0, 2, 5, 10, 20, 100, 150 éq.) $TBANO_2$; B) solution 0,45 mM de propargyl DPA@$Cu(OAc)_2$ en présence de (0, 1, 50, 100, 150 éq.) $TBANO_2$ dans du DMF dégazé contenant 0,1 M de $TBAPF_6$, vitesse de balayage : 100 mV/s, électrode de travail : carbone vitreux, électrode de référence : ECS.*

Ainsi, dans ce cas, aucun effet synergique n'a pu être observé et a présence du POM n'améliore donc pas le processus.

3.2 Di-fonctionnalisation du $[PW_{11}O_{39}]^{7-}$ de Keggin par réaction "Click"

En parallèle, une seconde famille d'hybride, présentant à nouveau potentiellement deux sites de coordination, a été mise en œuvre en utilisant des réactions de type "Click" entre un dérivé triazoture et un alcène fonctionnalisé.

La première étape consiste en la synthèse de la plateforme **$K_{Si}[N_3]$-3**, qui a été caractérisée par spectroscopie RMN et par spectrométrie de masse.

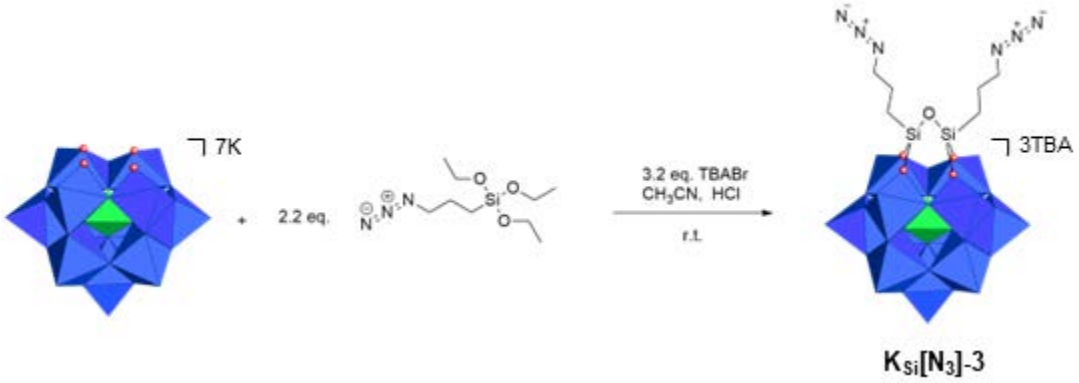

Schéma de synthèse de **$K_{Si}[N_3]$-3**

Une fois le dérivé azoture obtenu, la synthèse de **$K_{Si}[N_3DPA]$-3** par chimie click a été réalisée. Après optimisation des conditions de synthèse et de purification, le produit cible a été obtenu avec un rendement de l'ordre de 49%. Le pic caractéristique de la formation du cycle triazole est observé a 8,12ppm, tandis que la signature IR de la fonction azoture du précurseur à 2092 cm^{-1} a complètement disparu. Le greffage est par ailleurs confirmé par le spectre DOSY, sur lequel les pics des groupements alkyles de la plateforme ont les mêmes coefficients de diffusion que les pics des pyridines.

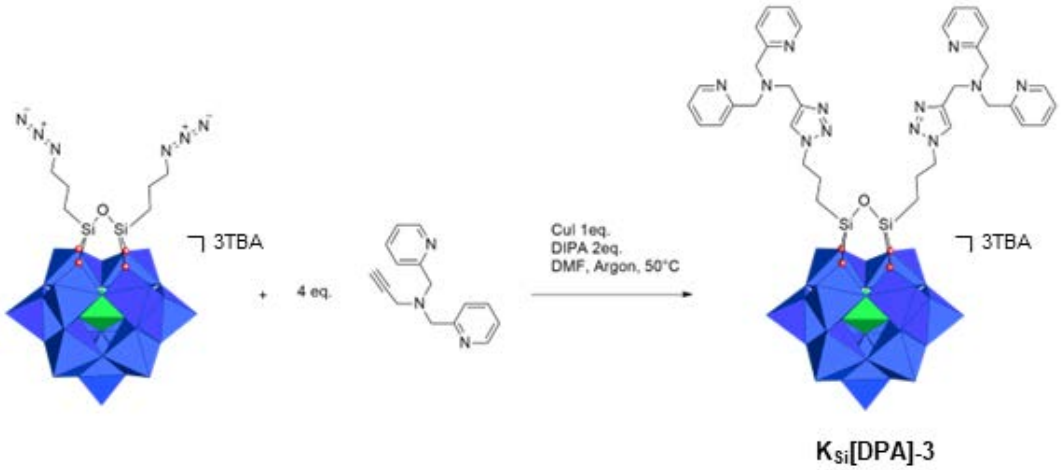

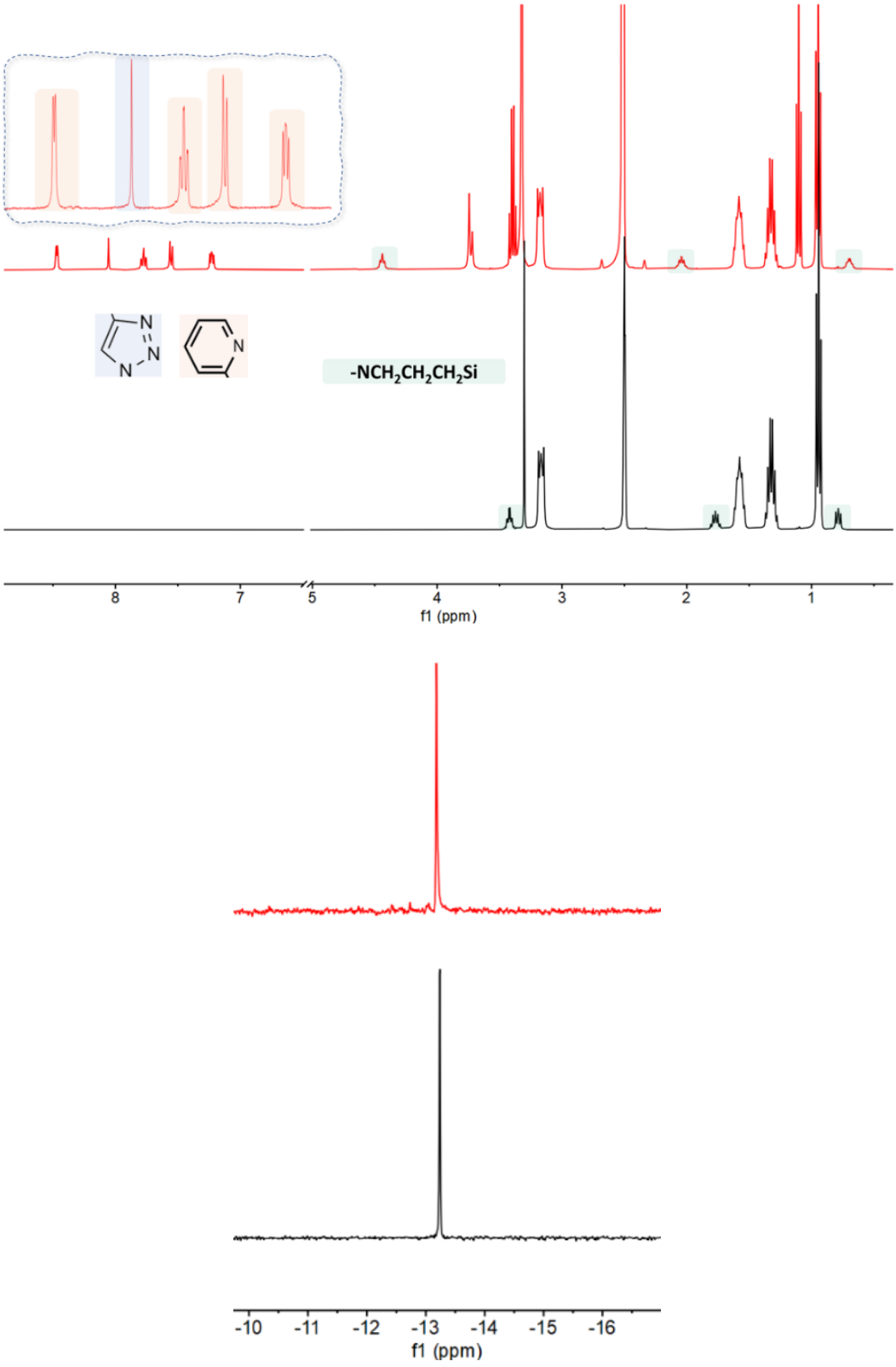

*Figure 3-34 Comparaison de la RMN ^{1}H et de la RMN ^{31}P des **$K_{Si}[N_3DPA]$-3** (noir) et **$K_{Si}[N_3]$-3** (rouge) purifiés.*

Une fois l'hybride synthétisé, des études de complexation ont été réalisées.

Une solution d'acétate de cuivre acétonitrile a été titrée avec **K_{Si}[N_3DPA]-3** et suivie par spectroscopie UV-vis. Quatre points isosbestiques à 376, 471, 566 et 803 nm peuvent être simultanément observés lors d'ajout de 0 éq. A 0,60 éq.de **K_{Si}[N_3DPA]-3** sur une solution d'acétate de cuivre. Cependant, la pente (Figure 3-36 B) montre que le processus de complexation est terminé après l'ajout de 0,35 éq. de **K_{Si}[N_3DPA]-3**, ce qui suggère qu'un ligand **K_{Si}[N_3DPA]-3** peut coordonner 3 ions cuivriques. C'est assez inattendu, car cela suggère des sites de coordination supplémentaires en plus des deux fragments DPA : ce pourraient être dû à la présence des azotes des deux triazoles.

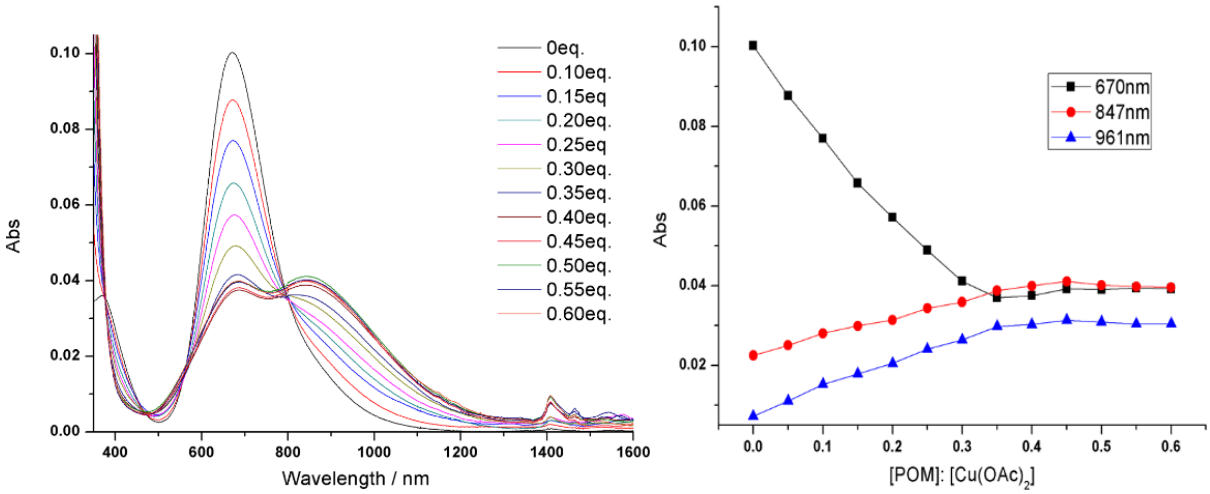

*Figure 3-36 Le titrage UV-vis de 0,50 mM $Cu(OAc)_2$ avec **K_{Si}[N_3DPA]-3** dans l'acétonitrile et la pente à 670, 847 et 961nm.*

Nous proposons donc un modèle de coordination possible (Figure 3-37), mais ceci devra être étudié de manière plus approfondie. Quoi qu'il en soit, de tels sites de coordination multiples pourraient être appliqués pour imiter les sites métalliques des enzymes présentant des sites actifs polymétalliques.

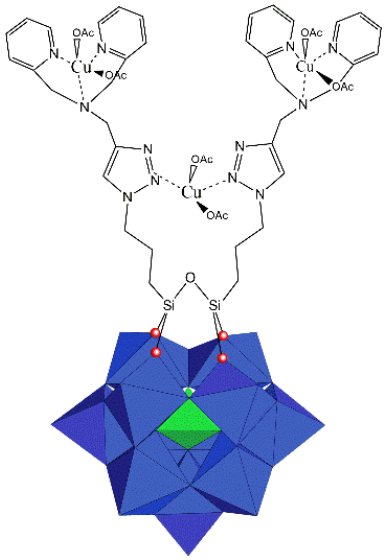

Figure 3-37 Une structure de coordination possible de ***K_{Si}[N_3DPA]-3***@$Cu(OAc)_2$.

Ainsi, en utilisant cette réactivité, nous avons ouvert la voie au greffage de deux ligands polyamines identiques sur des squelettes POM de manière contrôlée.

Chapitre 4 Fonctionnalisation de $[P_2V_3W_{15}O_{62}]^{9-}$ avec des ligands amine tridentés

L'absence de synergie entre le POM et le complexe de cuivre dans l'exemple précédent pourrait s'expliquer par la longueur du bras entre le POM et le tripode azoté. Afin de pallier cet inconvénient, une approche différente, reposant sur une fonctionnalisation directe à partir d'un ligand DPA associé par un lien court avec un groupement triol comme fonction de greffage, a été développée.

Dans un premier temps, la synthèse de **H_3Tris-DPA** a été réalisée.

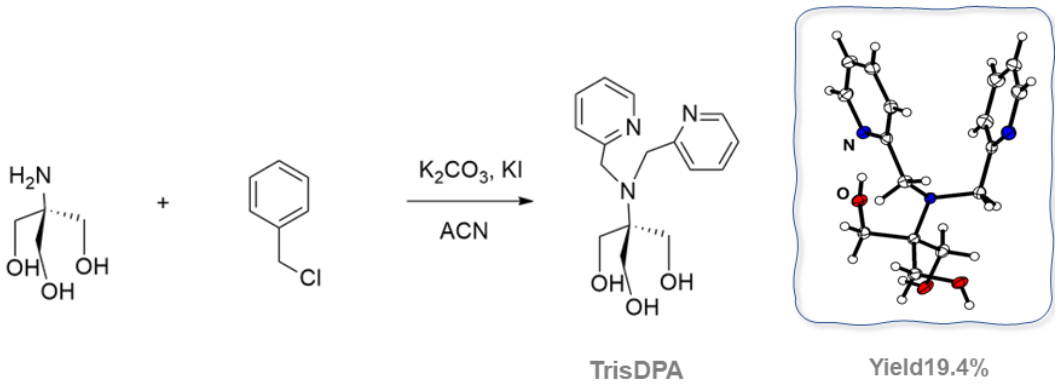

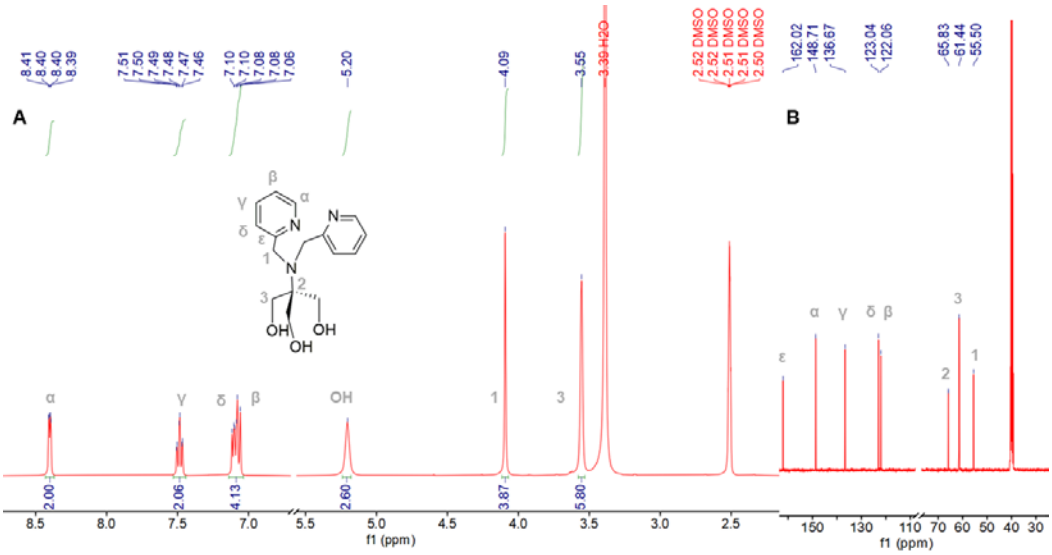

*Figure 4-1 A) RMN ^{1}H et B) RMN ^{13}C de **H_3Tris-DPA** (dans le DMSO).*

Une fois ce fragment obtenu, comme en atteste en particulier la structure obtenue par diffraction des rayons X sur monocristal, ce dernier a été utilisé pour réaliser un couplage direct sur **$[P_2V_3W_{15}O_{62}]^{9-}$** pour générer le ligand D_{V3DPA} :

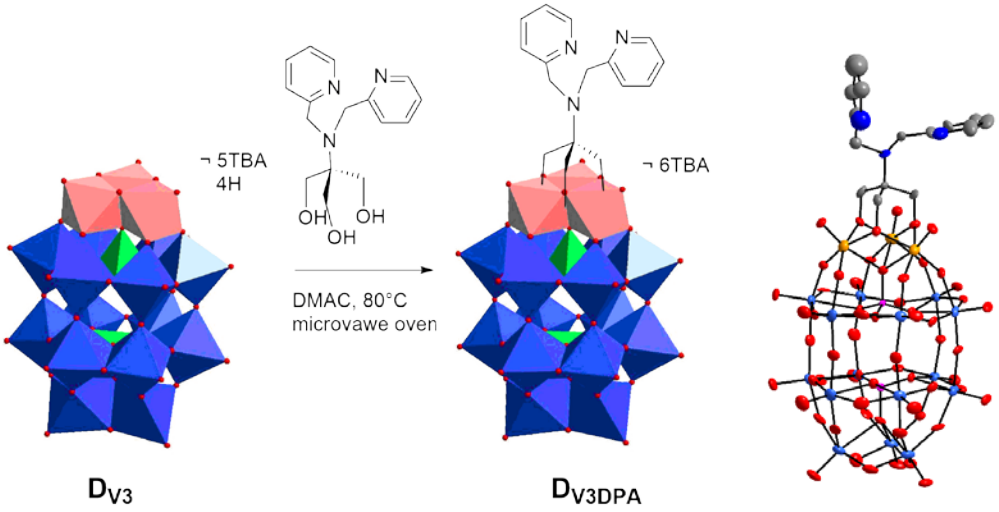

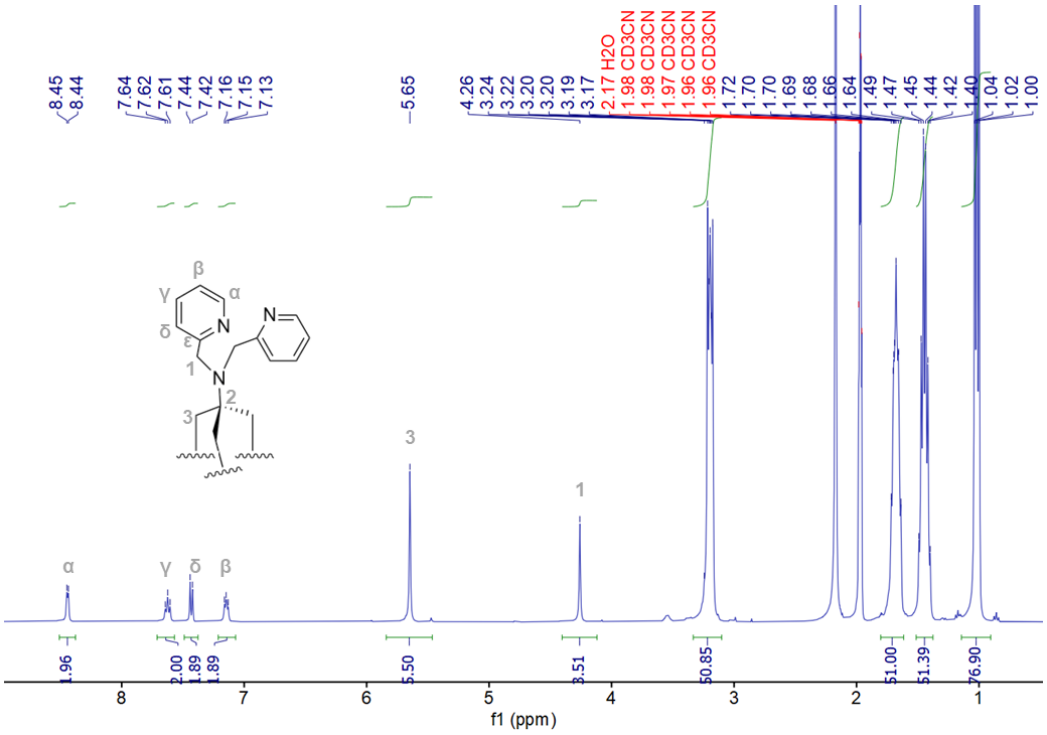

Figure 4-3 RMN ^{1}H dans le CD_3CN du ***D*** $_{V3DPA}$ *après traitement et la structure cristal.*

Ce dernier a été parfaitement caractérisé, que ce soit par diverses spectroscopies (RMN multinoyaux, IR...) mais aussi par spectrométrie de masse et analyse élémentaire. Enfin, une structure par diffraction des rayons X sur monocristal permet sans ambiguïté la présence du groupement DPA greffé sur le POM, avec une distance courte entre le site de coordination et la surface du polyanion.

La complexation de l'acétate de cuivre (II) ($Cu(OAc)_2$) avec le $\mathbf{D}_{V3DPA}$ a été réalisée dans l'acétonitrile. Après l'ajout de $Cu(OAc)_2$, la solution de POM est passée progressivement du brun au vert olive. Afin de mieux suivre ce processus, le titrage du POM avec le sel de cuivre a été suivi par spectroscopie UV-vis. Les graphiques de l'évolution de l'absorbance à 540 nm et 690 nm (encart, noir et rouge respectivement) montrent clairement un changement de la pente de l'ajustement linéaire en accord avec la formation d'un complexe 1 :1.

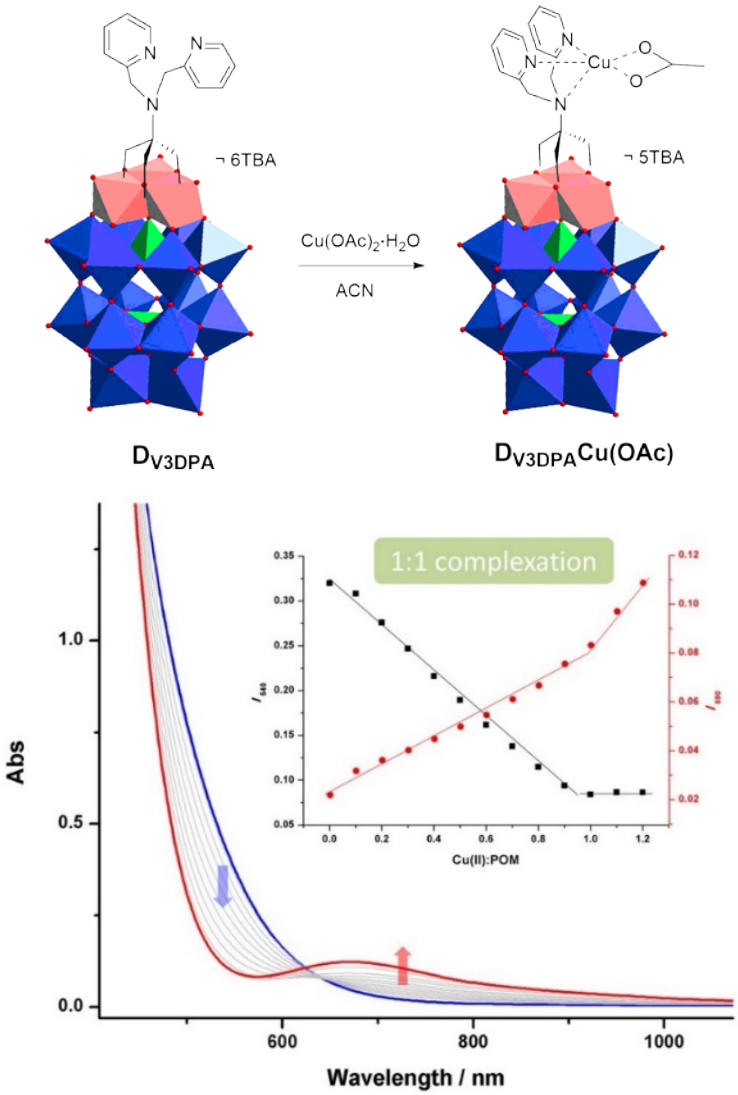

Figure 4-9 Titrage UV vis du ***D****V3DPA (1,0 mM) avec une quantité croissante de Cu(OAc)₂. Encart : évolution de l'absorbance à 540 nm et 690 nm avec le nombre d'équivalents de l'ion cuivre ajouté.*

En RMN ^{1}H, on observe notamment la disparition des pics de la DPA du ligand dans la zone aromatique classique, mais aussi l'apparition à des déplacements inhabituels 5(> 12 ppm et < 0 ppm) de pics pouvant être attribués à la DPA liée au Cu(II), ion paramagnétique.

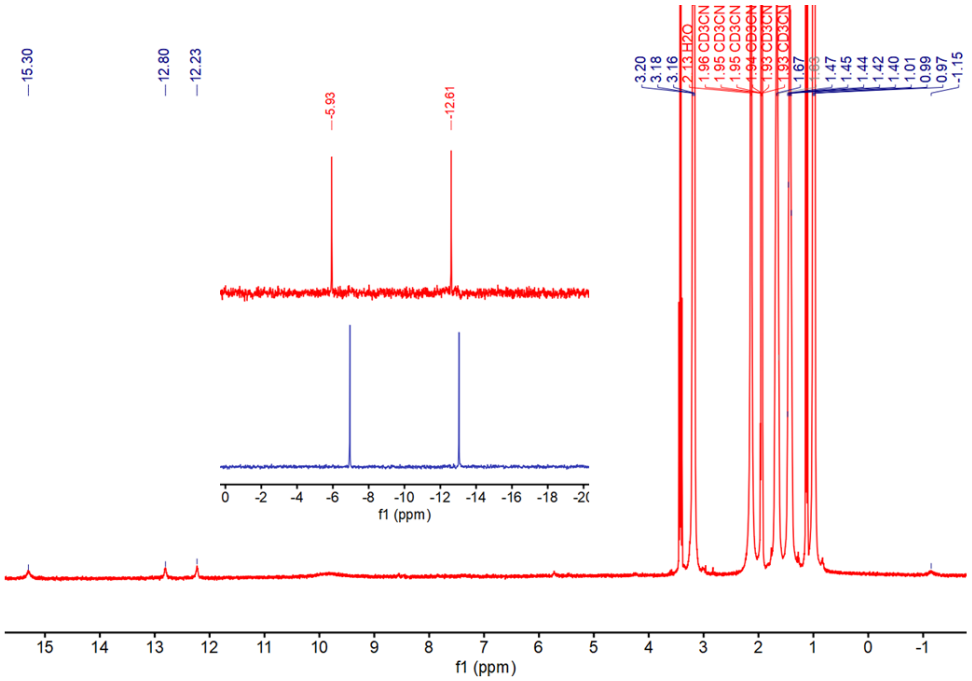

*Figure 4-12 The ^{1}H NMR (CD_3CN) of the **$D_{V3DPA}Cu(OAc)$**; insert: The variation of the ^{31}P NMR (CD_3CN) in the synthesis of **$D_{V3DPA}Cu(OAc)$** (red) from **D_{V3DPA}** (navy blue).*

Les propriétés rédox du ligand **D_{V3DPA}** et du complexe de cuivre **$D_{V3DPA}Cu(OAc)$** ont ensuite été étudiée par électrochimie. La Voltammogrammes cycliques (CV) du ligand et du complexe a été réalisée dans de l'acétonitrile contenant de l'hexafluorophosphate de tétrabutylammonium ($TBAPF_6$) comme électrolyte. Dans le cas du ligand D_{V3DPA} seul, dans le processus de réduction, deux vagues quasi-réversibles à -0,090 V/ECS et -0,452 V/ECS sont affichées, suivies d'un processus moins bien défini à -0,761 V/ECS. Toutes ces vagues sont attribuées à la réduction successive d'un électron de chacun des trois V(V) en V(IV).

Dans le cas du **$D_{V3DPA}Cu(OAc)$**, des vagues similaires sont présentes dans le CV lorsque l'on scan vers les potentiels négatifs, que l'on associe à nouveau à des processus redox centrés sur V. De plus, un nouveau processus redox assez large apparaît à 0.435 V/ECS en retournant en oxydation. Celui-ci est associé au processus de réoxydation du Cu(I) en Cu(II). La vague initiale associée à la réduction de Cu(II) en Cu(I) est très large et est plus aisément attribuée en examinant le second cycle. On constate que cette vague très large démarre vers 0.6 V et se confond ensuite avec la première vague de réduction de V(V). Le potentiel de repos est donc caractéristique d'u mélange de la forme tout oxydée (Cu(II) et d'une fraction de forme réduite (Cu(I))

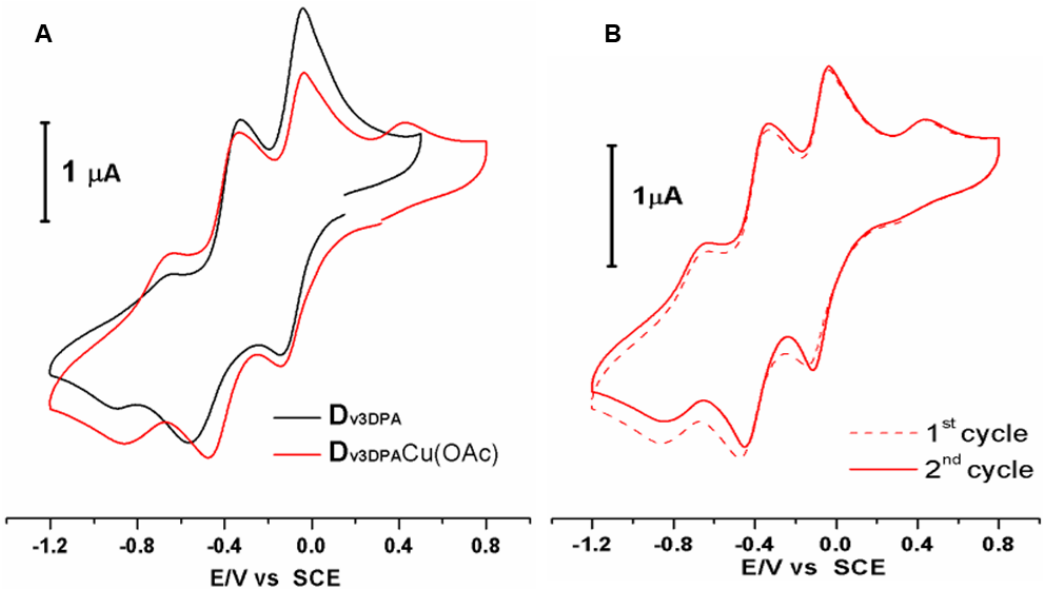

Figure 4-15 A) Voltammogrammes cycliques de D_{V3DPA} (noir) et de ***D_{V3DPA}Cu(OAc)*** *(rouge) à 1,0 mmol•L^{-1} dans CH_3CN contenant 0,1 mol•L^{-1} $TBAPF_6$ et v = 100 mV•s^{-1}. B) Voltammogrammes cycliques de* ***D_{V3DPA}Cu(OAc)*** *premier cycle (tiret) et second cycle (solide).*

Ce complexe cuivrique s'est révélé photoactif et son évolution sous irradiation a donc été étudiée en détail. Ceci a initialement été remarqué en RMN, où une évolution des spectres est observée avec le temps. Pour vérifier que l'évolution observée était liée à la lumière, le tube RMN a été irradié avec une source lumineuse plus puissante, qui a conduit à une conversion complète du complexe Cu(II) en une espèce diamagnétique en 60 minutes environ. Parallèlement, l'ajout d'un équivalent de cobaltocène comme agent réducteur chimique dans une solution fraîchement préparée de l'anion **D_{V3DPA}Cu(OAc)** a donné lieu à un spectre RMN ^{1}H similaire à celui obtenu sous irradiation, confirmant ainsi la photoréduction du complexe, d'une espèce de Cu(II) paramagnétique en un complexe de Cu(I) diamagnétique. Ce complexe de Cu(I) a également pu être généré par synthèse directe sous atmosphère inerte.

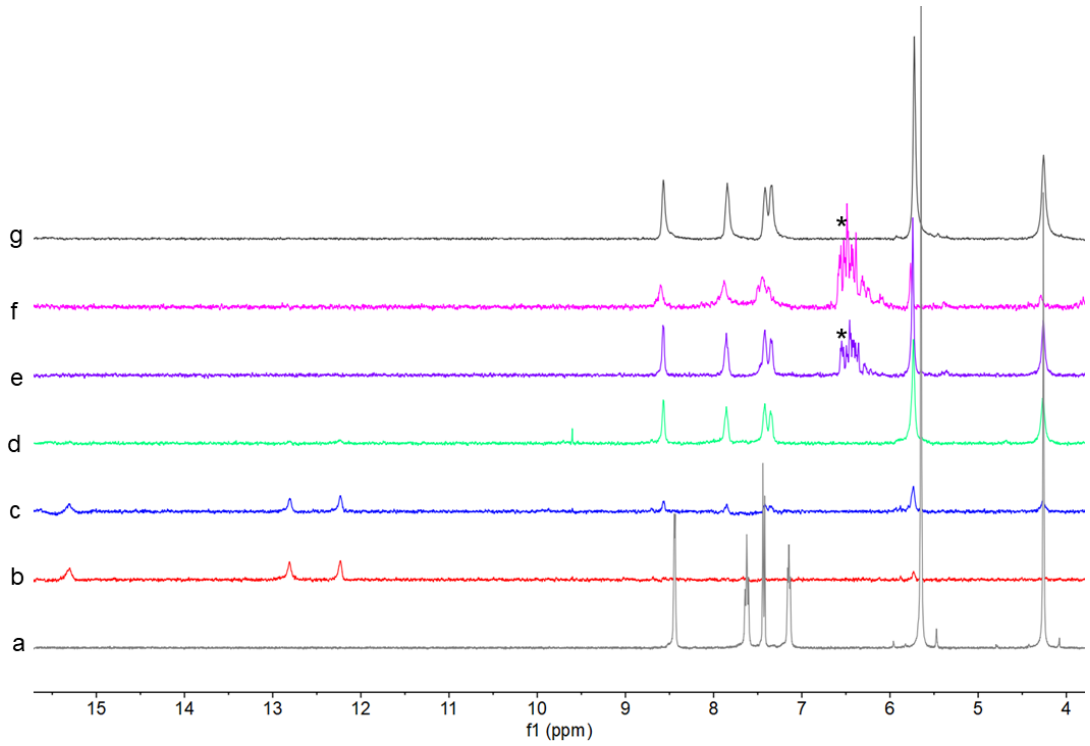

Figure 4-17 Spectres RMN ^{1}H de a) ligand ***D*** $_{V3DPA}$ *(gris), b)* ***D*** $_{V3DPA}$***Cu(OAc)*** *fraîchement synthétisé (rouge), c) après évolution dans le tube RMN (bleu), d) après irradiation avec une lampe à Xénon (>385nm, 75 µWcm-1) (vert), e) après réduction avec 1,0 éq. [CoCp$_2$](violet), et f) 2,0 éq. [CoCp$_2$] (rose), g) complexe Cu(I) généré in situ (noir). * : Signature RMN ^{1}H du cation [Co(Cp)$_2$]$^+$.*

En parallèle, les états d'oxydation des produits isolés, oxydés à l'acide peracétique et après irradiation ont été étudiés par spectroscopie RPE en bande X dans l'acétonitrile congelé à 30 K. Le spectre de l'anion **D$_{V3DPA}$Cu(OAc)** isolé, puis réoxydé sous sa forme la plus oxydée par l'ajout d'un oxydant puissant (CH_3COOOH) peut être raisonnablement simulé avec une matrice g rhombique (g_x = 2. 245, g_y = 2.10, g_z = 2.03) avec un couplage hyperfin de A_x = 485 MHz détectable uniquement sur la valeur g la plus élevée, ce qui est en accord avec un ion Cu(II) pentacoordiné dans une géométrie intermédiaire entre la bipyramide trigonale et le plan carré. Lors de l'irradiation, une diminution du signal Cu(II) est observée, ave e même temps l'apparition d' un nouveau profil RPE, associé à un système de spin axial S = 1/2, I = 7/2 avec (g = 1,97, A = 180 MHz) et ($g_{//}$ = 1,92, $A_{//}$ = 500 MHz), et caractéristique de la formation d'une espèce V(IV) axiale. L'observation simultanée des signaux Cu(II) et V(IV) indique que la forme la plus oxydée et la forme réduite à deux électrons peuvent coexister, en accord avec le chevauchement des vagues de réduction Cu(II)/Cu(I) et V(V)/V(IV) observés en voltammétrie, le vanadium commençant à être réduit avant que tout le Cu(II) n'ait été converti en Cu(I). Enfin,

une irradiation prolongées conduit à la disparition progressive du signal Cu(II) et à l'augmentation concomitante des signaux V(IV).

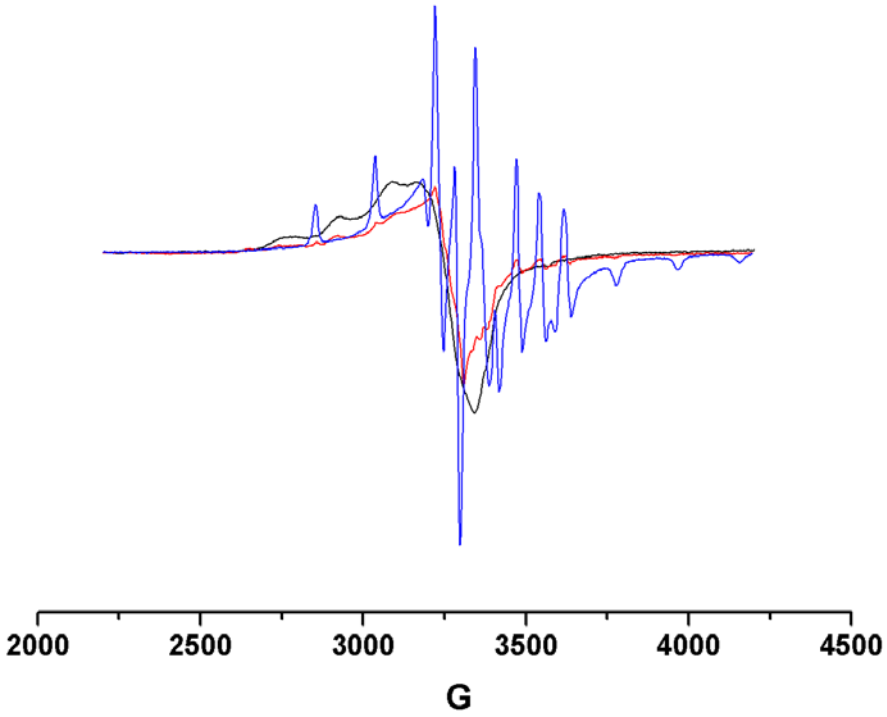

Figure 4-21 Le spectre RPE de 0,2 mM de ***D_{V3DPA}Cu(OAc)*** *dans l'acétonitrile : oxydé avec 2,0 éq. d'acide peracétate (noir) ; synthétisé (rouge) et irradié avec de la lumière visible pendant 1h (bleu).*

Cette photoréduction a par ailleurs été suivie par spectroscopie UV-vis, et comparée à des expériences de spectroélectrochimie. Lors de, Une évolution globale du spectre UV-Vis est obtenu, que ce soit par irradiation à la lumière visible de l'anion **D_{V3DPA}Cu(OAc)** dans l'acétonitrile o ensuivant sa réductions à l'électrode.

Après une heure d'irradiation, la bande attribuée à une transition d-d du Cu(II) à 680 nm diminue progressivement, en accord avec la réduction de Cu(II) en Cu(I). Une irradiation plus longue (plus d'une heure environ) conduit à un second processus (du spectre rouge à vert, figure ci-dessous), qui correspondrait à la réduction d'un premier V(V) en V(IV). Enfin, après une irradiation prolongée de 26h, un dernier changement majeur, notamment avec une augmentation très importante de l'absorption autour de 700 nm, est observée. En accord avec le suivi électrochimique, ce processus correspond à une la photoréduction d'un deuxième atome de V(V) en V(IV).

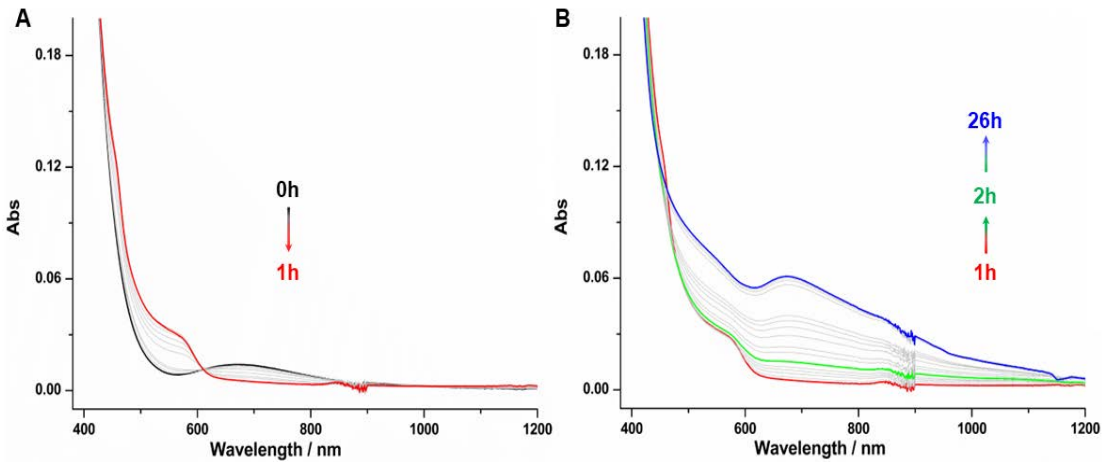

Figure 4-20 Évolution de la signature UV-VIS d'une solution 0,2 mM de ***D_{V3DPA}Cu(OAc)*** *dans l'acétonitrile lors de l'irradiation par la lumière visible. Les flèches mettent en évidence les changements successifs d'espèces associés à la photoréduction du complexe par 1, 2 ou 3 électrons.*

Globalement, ces études suggèrent qu'il est possible de photo-accumuler jusqu'à 3 électrons sur l'anion **D_{V3DPA}Cu(OAc)**, ce qui illustre les capacités de réservoirs d' électrons de ces molécules.

L'utilisation de ces propriétés a ensuite été envisagée pour des applications en photocatalyse. Des résultats ont notamment été obtenus dans la photoconversion de donneurs de " CF_3^+ " en radical $CF_3^{\bullet}$.

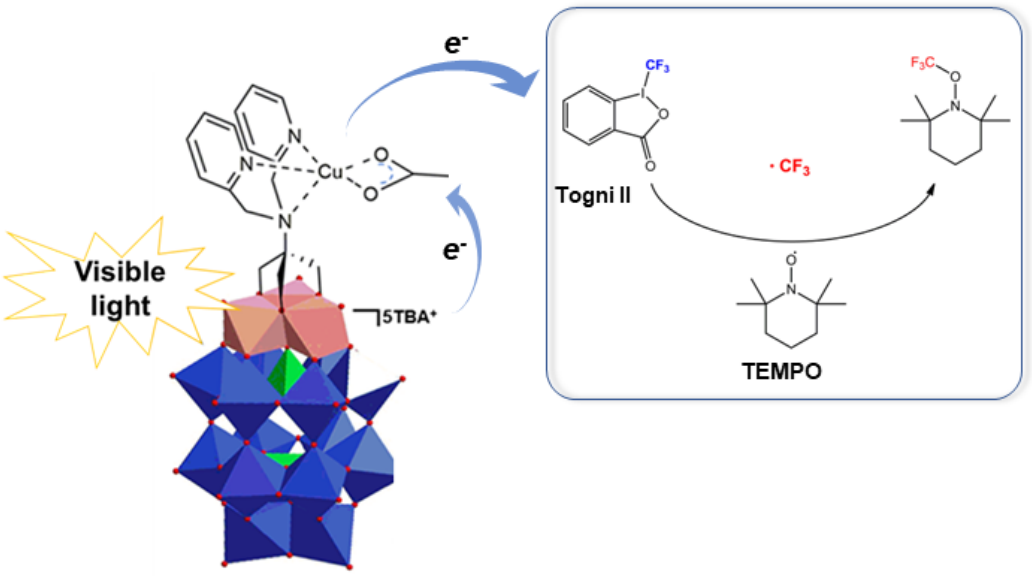

Ainsi, alors qu'aucune réaction ne se produit dans l'obscurité, l'irradiation à la lumière visible d'un mélange stœchiométrique de réactif de Togni (II) comme source de cation trifluorométhyle et d'anion **D_{V3DPA}Cu(OAc)** (1,0 éq.) en présence du radical TEMPO a conduit,

en RMN ^{19}F dans CD_3CN, à la disparition du signal de Togni (II) à 37,5 ppm et à l'apparition d'un pic unique à = - 55,7 ppm caractéristique de l'adduit TEMPO-CF_3 (Figure 4-21).

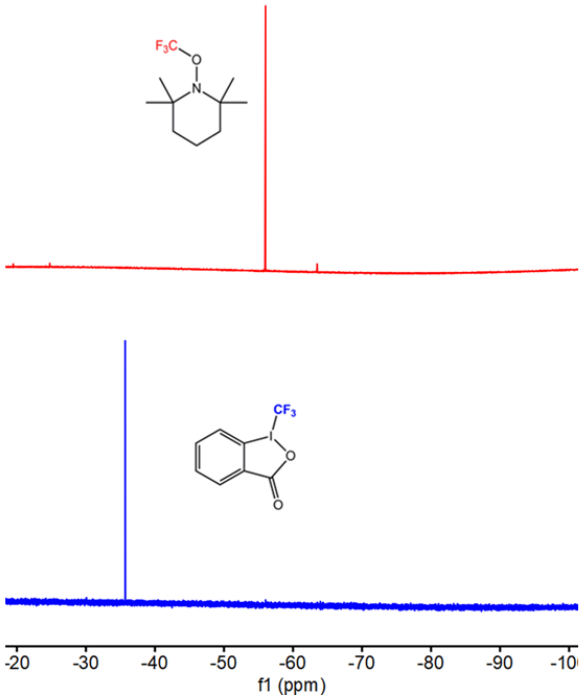

Figure 4-21 Spectre RMN ^1H dans CD_3CN d'expériences de piégeage TEMPO pour la génération de radicaux CF_3 avec le ***$D_{V3DPA}Cu(OAc)$*** *: TEMPO : Togni II = 1 : 1 : 1.*

En suivant la même réaction par RPE, le signal triplet initial de TEMPO à g= 2 a été remplacé par la signature de l'anion **$D_{V3DPA}Cu(OAc)$** (Figure 4-22). Une irradiation supplémentaire conduit, comme observé précédemment, à la diminution de la signature Cu(II) et à l'apparition progressive du signal V(IV), indiquant que le POM a conservé son intégrité.

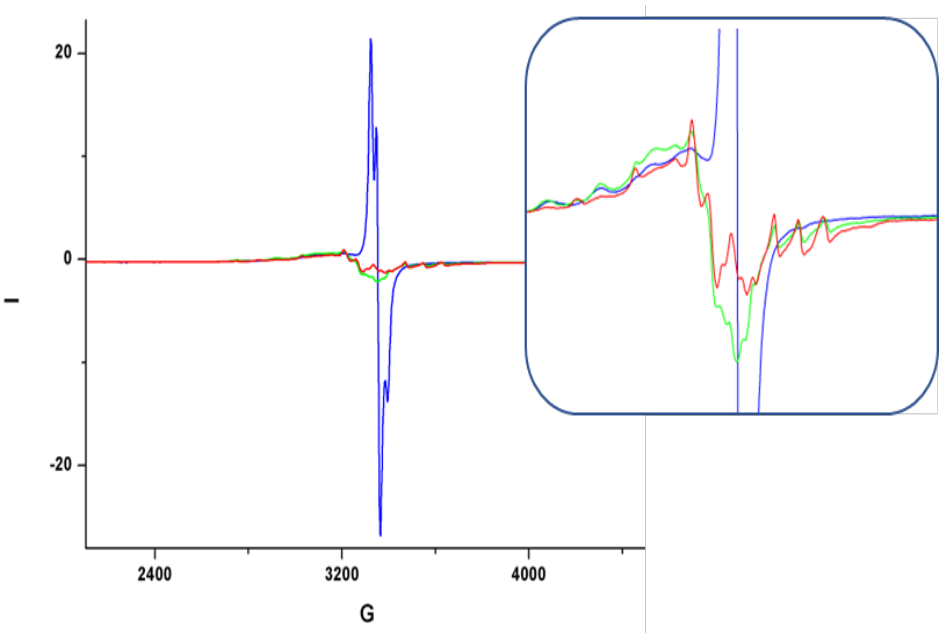

Figure 4-22 Spectre RPE (bande X 9,4GHz 30K) dans l'acétonitrile d'expériences de piégeage de TEMPO pour la génération de radicaux CF_3 avec le ***$D_{V3DPA}Cu(OAc)$*** *: TEMPO : Togni II = 1 : 1 : 2 après une irradiation de 0- (bleu), 0,5- (vert) et 1 heure (rouge) avec de la lumière visible (> 382 nm)*

L'étape suivante a consisté à étudier la capacité de ce POM hybride à photogénérer de manière catalytique ces radicaux CF_3. En utilisant seulement 5 mol % du complexe POM pour réaliser la même réaction, l'évolution de la RMN ^{19}F indique clairement une consommation presque totale (~92%) de Togni II et sa conversion en TEMPO-CF_3 en 7 heures (Figure 4-23). Plusieurs expériences de contrôle ont été réalisées. Lorsque la même réaction a été réalisée en présence du ligand POM (**D_{V3DPA}**) seul ou du triester $[CH_3C(CH_2O)_3V_3P_2W_{15}O_{59}]^{6-}$ (**D_{V3Me}**), analogue ne portant pas la fonction tripode azotée, presque aucune réaction ne s'est produite. Cependant, l'ajout de $Cu(OAc)_2$ et de DPA au milieu réactionnel en présence de **D_{V3Me}** a permis la formation d'environ 15% de TEMPO-CF_3 après 7 heures d'irradiation. Cette dernière expérience souligne l'importance du lien covalent entre le POM et la partie Cu, qui permet une communication électronique efficace entre le squelette photo actif du POM et l'ion cuivre et donc une meilleure efficacité.

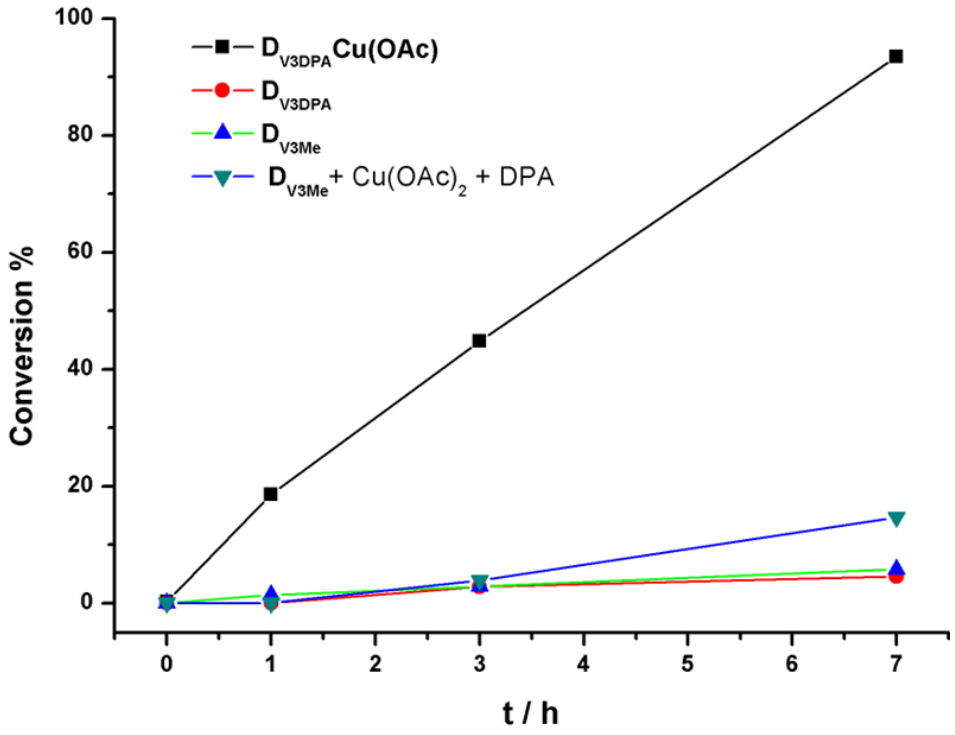

Figure 4-23 Evolution de la conversion du réactif de Togni en TEMPO-CF_3 suivie par ^{19}F RMN en présence de l'anion ***D*** *V3DPA* ***Cu(OAc)*** *(noir),* ***D*** *V3DPA (rouge),* ***D*** *V3Me (vert clair), et* ***D*** *V3Me avec le mélange de $Cu(OAc)_2$ et DPA (vert)*

Conclusion

Les travaux réalisés au cours de cette thèse ont conduit à l'élaboration de nouveaux hybrides qui viennent enrichir cette famille de POM. Ainsi, une nouvelle plateforme alkyl-iodée dérivé de $[PW_{11}O_{39}]^{7-}$ a été obtenue, mais son utilisation pour une fonctionnalisation avec des dérivés aminés par substitution nucléophile n'a malheureusement pas aboutie. En revanche, cette fonctionnalisation de polyanions par la propargyl-DPA que ce soit par couplage de Sonogashira ou par réaction Click a conduit à l'obtention de deux ligands POM porteur de DPA. Toutefois, dans le premier cas, aucune synergie entre le POM et le complexe de cuivre greffé 'a pu être mise en évidence. Dans le second cas, la présence des fonctions triazoles issues de la chimie click ont rendu les études de complexation un peu plus compliquée : ces dernières devront être approfondies. Finalement, l'approche directe à partir de dérivés trialcoxo de DPA a permis la synthèse d'un complexe **D_{V3DPA}Cu(OAc)**. Ce dernier présente des propriétés photophysiques intéressantes qui ont été mises à profit pour des réactions de trifluorométhylatio photocatalysées.

Abbreviations

Abbreviations

POM	Polyoxometalate
NMR	Nuclear Magnetic Resonance
DOSY	Diffusion Ordered Spectroscopy
EPR	Electron Paramagnetic Resonance
ESI-MS	Electrospray Ionization Mass Spectrometry
IR	Infra-Red
UV-vis	Ultra-violet visible
XRD	X-Ray Diffraction
CV	Cyclic voltammetry
SCE	Saturated Calomel Electrode
$TBAPF_6$	Tetra(butyl)ammonium hexafluorophosphate
TBA	Tetrabutylammonium
TBAB**r**	Tetrabutylammonium bromide
$TBABr_3$	Tetrabutylammonium t**ri**bromide
DMAc	Dimethylacetamide
DMF	Dimethylformamide
DMSO	Dimethyl Sulfoxide
DCM	Dichloromethane
THF	Tetrahydrofuran
Et_2O	Diethyl ether
DIPEA	Diisopropylethylamine
DIPA	Diisopropylamine
TEA	Triethylamine
ACN	Acetonitrile
BTPP	*Tert*-butylimino-tri(pyrrolidino)phosphorane
eq.	Equivalent
r.t.	Room Temperature

N**uc**	Nucleophile
DPA	bis(pyridin-2-ylmethyl)amine
Propargyl DPA	N,N-bis(pyridin-2-ylmethyl)prop-2-yn1-amine
MP	Methyl Propiolate
NMI	1-methyl-1H-imidazole
K_{Si}[Cl]-1	$TBA_3[PW_{11}O_{39}\{O(SiCH_2Cl)_2\}]$
K_{Si}[I]-1	$TBA_3[PW_{11}O_{39}\{O(SiCH_2I)_2\}]$
K_{Si}[DPA]-1	$TBA_3[PW_{11}O_{39}\{O(SiCH_2DPA)_2\}]$
K_{Si}[DPA]-3	$TBA_3[PW_{11}O_{39}\{O(SiCH_2CH_2CH_2DPA)_2\}]$
K_{Si}[NMI]-3	$TBA_3[PW_{11}O_{39}\{O(SiCH_2CH_2CH_2NMI)_2\}]$
K_{Sn}[I]	$TBA_4[PW_{11}O_{39}\{SnC_6H_4I\}]$
K_{Sn}[DPA]	$TBA_4[PW_{11}O_{39}\{SnC_6H_4CCCH_2DPA\}]$
K_{Si}[N_3]-2	$TBA_3[PW_{11}O_{39}\{O(SiCH_2CH_2N_3)_2\}]$
K_{Si}[N_3DPA]-2	$TBA_3[PW_{11}O_{39}\{O(SiCH_2CH_2N_3CHCCH_2DPA)_2\}]$
K_{Si}[N_3]-3	$TBA_3[PW_{11}O_{39}\{O(SiCH_2CH_2CH_2N_3)_2\}]$
K_{Si}[N_3DPA]-3	$TBA_3[PW_{11}O_{39}\{O(SiCH_2CH_2CH_2N_3CHCCH_2DPA)_2\}]$
K_{Si}[N_3MP]-3	$TBA_3[PW_{11}O_{39}\{O(SiCH_2CH_2CH_2N_3CHCCH_2MP)_2\}]$
H_3Tris	Tris(hydroxymethyl)aminomethane
H_3Tris-DPA	2-(bis(pyridin-2-ylmethyl)amino)-2-(hydroxymethyl)propane -1,3-diol
D_{V3}	$TBA_5H_4[P_2V_3W_{15}O_{62}]$
D_{V3DPA}	TBA_6 $[P_2V_3W_{15}O_{62}$(Tris-DPA)]
D_{V3Me}	TBA_6 $[P_2V_3W_{15}O_{62}$(Tris-Me)]
TBDMSCl	Tert-Butyldimethylsilyl Chloride
$TBDMS_3$Tris	6-(((tert-butyldimethylsilyl)oxy)methyl)-2,2,3,3,9,9,10,10-octamethyl-4,8-dioxa-3,9-disilaundecan-6-amine
$TBDMS_3$Tris-DA-Boc	di-tert-butyl (((6-(((tert-butyldimethylsilyl)oxy)methyl)-2,2,3,3,9,9,10,10-octamethyl-4,8-dioxa-3,9-disilaundecan-6-yl)azanediyl)bis(ethane-2,1-diyl))dicarbamate

H_3Tris-DA-Boc	di-tert-butyl (((1,3-dihydroxy-2-(hydroxymethyl)propan-2-yl)azanediyl)bis(ethane-2,1-diyl))dicarbamate
$D_{V3DA-Boc}$	TBA_6 [$P_2V_3W_{15}O_{62}$(Tris-DA-Boc)]
D_{V3DA}	TBA_6 [$P_2V_3W_{15}O_{62}$(Tris-DA)]
TON	Turn over numbers
Togni II	1-(Trifluoromethyl)-1λ^3,2-benziodoxol-3(1*H*)-one
TEMPO	(2,2,6,6-Tetramethylpiperidin-1-yl)oxyl

Appendix

Appendix

IR spectra were collected in the 250-4000 cm^{-1} range. Measurements were carried out on Jasco FT/IR 4100 spectrometer with KBr pellets (with a 2 cm^{-1} resolution).

NMR spectra were recorded on Bruker Avance 300, 400 and 600 spectrometers at room temperature: For broad ^{1}H NMR signals, the full-width-at-half-maximum values are given in Hz.

Mass spectrometric analyses (ESI mode) were performed on a quadrupole-Orbitrap Q Exactive mass spectrometer from Thermo Scientific.

Elemental analyses (C, H, N) were carried out in INSTITUT DES SCIENCES ANALYTIQUES in Lyon.

Electrochemical studies. CVs were performed on an Autolab PGSTAT 100 workstation. A standard three electrode cell was used, which consisted of a working vitrous carbon electrode, an auxiliary platinum electrode and an aqueous saturated calomel electrode (SCE) equipped with a double junction.